SUPPRESSION AND AVOIDANCE OF SSR IN SYNCHRONOUS GENERATORS

Mithqal M. Sartawi, B.Sc., (Iraq), M.Eng., (Sheffield)

SUPPRESSION AND AVOIDANCE OF SUBSYNCHRONOUS RESONANCE IN SYNCHRONOUS GENERATORS

by

Mithqal M. Sartawi, B.Sc. (Iraq), M.Eng. (Sheffield)

A thesis submitted to the Faculty of Graduate Studies and Research in partial fulfillment of the requirements for the degree of Doctor of Philosophy.

Department of Electrical Engineering,
McGill University,
Montreal, Canada.

June, 1978.

ABSTRACT

The suppression of the subsynchronous resonance (SSR) phenomenon that occurs in synchronous generators connected to series capacitor compensated transmission lines has been investigated. The synchronous machine field winding has been considered as a means of controlling this phenomenon. The physical concepts of how the above phenomenon can be suppressed by field current control are introduced, and the properties of the control signal required are explained.

Among the different signals which can be used to suppress the SSR phenomenon, the signal composed of ΔP and ΔQ is adopted in the study. In confirming the physical concepts by a numerical example, the above signal is seen to give a flexible and a robust feedback.

After understanding the principle of SSR suppression and after choosing the control signal, a feedback scheme which passes through the machine excitation system, is designed for the SSR suppression. The small perturbation analysis of a system incorporated with such a feedback scheme has shown the effectiveness of this scheme in eliminating any undesirable SSR oscillation.

After testing the above feedback scheme against small disturbances, it is necessary to see what is the situation under large disturbances. Digital simulations show that ΔP and ΔQ feedback alone is incapable of stabilizing the large unstable SSR oscillations. The reason is that the machine regulator saturation limits (voltage ceilings) prevent the above scheme from injecting a large enough stabilizing signal. To overcome this difficulty, a nonlinear resistor protection scheme connected across the series capacitor is added to the system. Results show that both the nonlinear resistor protection and the above feedback scheme working together are required for ensuring system stability under small and large disturbances.

Next, the torsional resonance of the multi-inertia shaft system, as it is coupled to the SSR of the series capacitor compensated system, is

considered in the analysis. The feedback scheme with ΔP and ΔQ as the control signal is tested against the instability arising from the torsional resonance interaction. Because the ΔP and ΔQ scheme is unable to eliminate the above instability, a power blocking filter is used for this purpose. Its effectiveness under small and large perturbations has been investigated.

Finally,instead of suppression, a fresh approach based on avoiding SSR is introduced. A preliminary small perturbation analysis of a system, which is shunt compensated by a synchronous capacitor, has been included.

RESUME

On a examiné la suppression du phénomène de la résonance sous-synchrone (SRS) qui se produit dans les générateurs synchrones reliés aux lignes de transmission compensées par des condensateurs en série. Pour contrôler ce phénomène, on a pris en considération le bobinage inducteur de la machine synchrone. On a presenté les concepts physiques pour pouvoir supprimer le phénomène ci-haut mentionné par le contrôle du bobinage et on a expliqué les propriétés du signal de contrôle requis.

Parmi les différents signaux qui peuvent être employés pour supprimer le phénomène SRS, on choisit dans cette étude le signal composé ΔP et ΔQ . Afin de confirmer les concepts physiques par un exemple numérique, ce signal semble donner une rétroaction souple et solide.

Après avoir compris le principe de la suppression de SRS et après avoir choisi le signal de contrôle, un arrangement rétroactif qui passe par le système d'amorçage de la machine est construit pour la suppression SRS. L'analyse de la petite perturbation d'un système incorporé à un tel arrangement rétroactif a demontré l'efficacité de cet arrangement en éliminant toute oscillation SRS indésirable.

Après l'expérimentation de l'arrangement rétroactif ci-haut mentionné contre les petites perturbations, il faut étudier la situation contre les grandes perturbations. Les simulations digitales démontrent que la rétroaction de ΔP et ΔQ seulement est incapable de stabiliser les grandes oscillations SRS. Les limites de saturation du régulateur de la machine (limites de voltage) qui empêchent cet arrangement d'injecter un signal stabilisateur assez grand en est la raison. Pour vaincre cette difficulté, on ajoute au système un arrangement de protection de résistance non linéaire rattaché parallèlement aux series du condensateur. Les résultats démontrent que la protection de résistance non linéaire et l'arrangement rétroactif sont tous deux nécessaires pour assurer la stabilité du système contre les petites et les grandes perturbations.

Puis on analyse la résonance de torsion et le système de puits à inerties multiples tel qu'il est associé au SRS du système des séries du condensateur. On vérifie l'arrangement rétroactif avec ΔP et ΔQ comme signal de contrôle contre l'instabilite provenant de l'interaction de la résonance de torsion. Parce que l'arrangement de ΔP et ΔQ est incapable d'éliminer cette instabilité, on se sert d'un filtre bloquant l'énergie. On a étudié son efficacité contre les grands et les petites perturbations.

Enfin, au lieu de la suppression, on introduit un nouvel abord pour éviter le SRS. On a aussi inclus une analyse préliminaire des petites perturbations d'un système de compensation shunt par un condensateur synchrone.

ACKNOWLEDGEMENTS

I am greatly indebted to Dr. B.T. Ooi for his constant supervision and invaluable advice without which this work would not have been accomplished. He has guided and encouraged me with a wise and friendly attitude.

My sincere appreciation to Drs. P. Bélanger, F. Galiana, J. Lemay and H.L. Nakra for the helpful and the fruitful discussions.

The assistance of Mr. R.G. Farmer from Arizona Public Service Company in providing some technical data is greatly acknowledged.

My deep appreciation to Mr. A. Safaai-Jazi specially and Messrs. M. Banakar, J. Jarjis and O.P. Jain for their friendship and good counsel.

I am very thankful to Miss N. Menemenlis and Mr. J. Lazar for translating the abstract and to Mr. J. Mui for the photographic work.

I am grateful to Mrs. P. Hyland for her patience in typing this thesis.

My deepest gratitude to Mrs. D. Pommier for her encouragement and patience in correcting and preparing this manuscript.

TABLE OF CONTENTS

LIST OF ILLUSTRATIONS

LIST OF TABLES

NOMENCLATURE

Matrices

$[A]$	Constant matrix of the homogeneous equation of the linearized mode (equation 4.2).
$[C_{odq}^{abc}]$	Transformation matrix from abc reference frame to odq, reference frame (equation A-1.1).
$[C_{dq}^{DQ}]$	Transformation matrix from D-Q to d-q rotating reference frames (equation 2.39).
$[D]$, $[F]$	Coefficient matrices of the linearized mathematical model of the series capacitor compensated system (equation 4.1).
$\underline{e}_s$, $\underline{e}_r$	Vectors of stator and rotor voltages.
$\underline{i}$, $\underline{\psi}$	General current and flux vectors.
$\underline{I}$, $\underline{E}$	Steady state current and voltage vectors defined in equations 2.49, 2.50.
$[L]$	Inductance matrix in henry.
$[R]$	Resistance matrix in ohm.
$\underline{X}$	Vector of the state variable of the nonlinear differential equation (equation 6.13).
$[\ ]^T$	Transpose.
$\underline{U}$	General input vector.
$[\ ]^{-1}$	Inverse.

Subscripts

a, b, c	Used for quantities in the abc frame.
d, q	Denotes quantities in the d-q reference frame.
e	Denote electrical quantity (equations 2.12, 2.21).
f	Used for power blocking filter (S-ction 7.5).
fd	Field winding quantities.
kd	Direct axis amortisseur winding quantities.
kq	Quadrature axis amortisseur winding quantities.
o	Steady state quantities.
r, s	Denotes rotor and stator quantities.
ssrp	Positive sequence SSR mode.
ssrn	Negative sequence SSR mode.
t	Machine terminal quantities.
B	Used for base values.
C	Used for quantities associated with the series capacitor.
D, Q	Synchronously rotating reference frame quantities.
E	Network and exciter quantities.
G	Generator quantities.
GT	Rotor shaft variables.

T	Water turbine variables.
L	Quantities associated with the line reactance.
ND	Represent the NDS quantities.
0	Infinite bus bar quantities.
P	Power system stabilizer quantities.

Constants

r	Resistance in per-unit.
D	Damping coefficient.
H	Inertia constant in Second.
J	Moment of inertia in Joule.second.second .
K	General constant coefficient.
L	Inductance in Henry.
M	Angular momentum in Joule.second .
X	Reactance in per-unit.
ϕ	Control angle.

Variables

i, e, ψ	Instantaneous current, voltage and flux linkage.
mmf	Magnemotive force phasor.

P	Active power.
Q	Reactive power.
T	Torque.
t	Time.
t'	Per-unit time.
δ	Machine rotor angle.
θ	Instantaneous rotor angular position in electrical radians.
ω	Rotor speed in electrical r / s .
ω_n	Resonant frequency of the L-C circuit in electrical r / s .
ω_m	Mechanical resonant frequency in electrical r / s .
ω_0	Synchronous speed in electrical r / s .
μ	Control signal .

CHAPTER I

INTRODUCTION

1.1 The Use of Series Capacitors

Stability studies have been considered as an essential part of power system planning. The task of achieving acceptable stability performance becomes more difficult as the power system expands and the distance over which the power is transmitted, increases.

Over the history of power system growth, stability was maintained without great difficulty. This is because the centres of consumption were close to the generation stations. Therefore, short transmission lines were satisfactorily used to transmit the necessary power. However, within the last decade the sources of generated electric power became increasingly further removed from the centres of consumption. Thus, long transmission lines are used to connect the sources of generated power with the centres of consumption. Therefore, system stability becomes a serious problem.

From the standpoint of power system stability analysis, the most important function [1] is the power-angle curve as shown in Figure 1.1. Assuming for simplicity a cylindrical synchronous generator connected to an infinite bus bar through a transmission line, the power transmitted (P_e) is sinusoidally varying with the electrical angular displacement between the infinite bus and the generator rotor (δ). Assuming that the

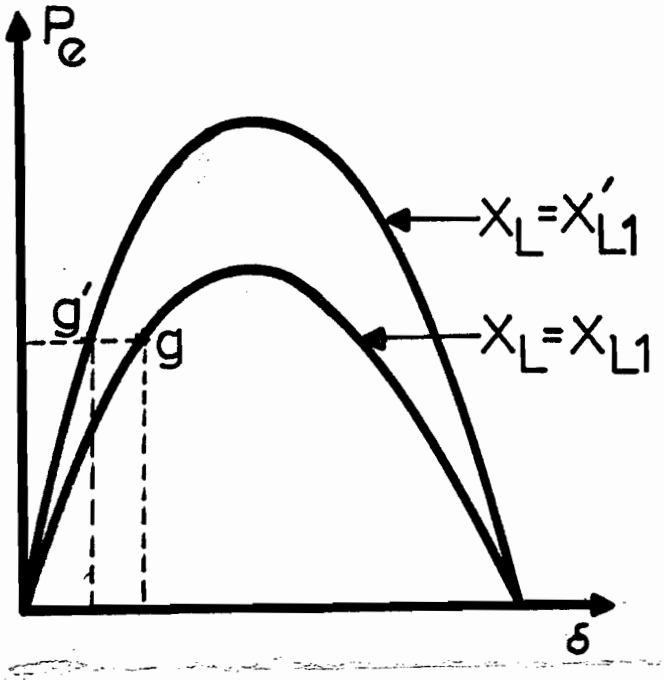

Figure 1.1. Power-angle Curve.

system resistances are neglected, then the peak of the curve in Figure 1.1 is inversely proportional with the net effective reactance in the path of the current flowing between the generator and the infinite bus [2] .

In the context of Figure 1.1 , the system steady state operating point is characterized by the amount of the transmitted power and the angular position of the machine rotor with respect to the infinite bus (e.g., point g in Figure 1.1). The system steady state stability is related to the slope of the power-angle curve at the system operating point [3]. In fact this slope determines the synchronizing torque available on the generator. When the operating point is at point, say g, in which the slope is positive, then the steady state is said to be stable. The

portion of the power-angle curve in which the slope is negative corresponds to the unstable operating angles. As the steepness of the slope is an index of the electromechanical stiffness acting on the rotor during oscillations,it is desirable to operate at increased slope.

However, the system transient stability is discussed on the basis of the equal area criterion [2] where the system is said to be stable following a severe disturbance, if the total energy acting to accelerate the machine is equal to the total energy acting to decelerate the machine .

In the light of the previous paragraph, one can improve the system stability by reducing the inductive reactance in the transmission circuit. This is because the power-angle curve takes the form of $V_1 V_2 \sin \delta / X_L$ where V_1 and V_2 are the magnitudes of the voltages of the generator and the infinite bus and X_L is the inductive reactance between the voltages. Reducing X_L clearly increases the peak of the power-angle curve as shown in Figure 1.1. For the same power delivered, the operating point is shifted from g (for X_{L1}) to g' (for X'_{L1}) . Firstly, we note that the slope of the power-angle curve at g' is greater than that at g, so that the system steady state stability is improved. Secondly, we note that g' is at a smaller operating angle than g. This is combined with the fact that the peak of the curve for X'_{L1} is greater than that for X_{L1} . This implies that the system with reduced reactance can withstand a more severe fault. In brief, the transient stability is improved [4].

The conclusion to be drawn is that in order to improve the stability, it is necessary to reduce the net effective reactance in the path of the current flowing in the transmission line. In systems where short transmission lines are used, the problem is already solved, since these lines have low inductive reactance. Whereas in long transmission lines, series capacitors are installed in series with these lines to compensate for their large inductive reactances [5, 6] .

Series capacitors are the most economical and practical method of improving the system stability [7, 8] and they provide an excellent means of increasing the power transmission [9]. Series capacitors have been extensively used [8, 10, 11, 12] over the last two decades. However, their introduction in the transmission lines has brought about two damaging effects: the subsynchronous resonance (SSR) and the torsional resonance interaction where the latter resulted in the destruction of the two shafts at the same Mohave power station on December 9, 1970 and again on October 26, 1971 [13, 14].

1.2 What is SSR

Although the series capacitor compensation effectively reduces the line reactance, the resonance associated with the L - C circuit may be undesirable. In the first place, the series capacitance is chosen

such that forced oscillation at the supply frequency does not occur. For stability reasons, the resonance is never chosen to be supersynchronous [15] . Consequently, the L - C resonance frequency is always subsynchronous [16] .

1.2.1 L - C Resonance

The natural frequency of oscillation of the inductance and the series capacitor ω_n is [17] :

$$\omega_n = \omega_0 \sqrt{\frac{X_C}{X_2 + X_L}} \quad \text{electrical} \quad r / s \tag{1.1}$$

where X_L , X_C and X_2 are the line inductive, the series capacitive and the generator negative sequence reactances respectively.

Whether the SSR is of any consequence to the system performance depends on whether the resonating mode is negatively or positively damped. Generally, it is expected that the resistance in the system will damp out this mode. However, the amortisseur windings in the rotor of the synchronous generator is effectively a negative resistance to this mode [18]. When this negative resistance dominates, the SSR mode is negatively damped.

1.2.2 Physical Explanation of SSR Oscillation

Under any disturbance, the resonance of the external L - C circuit (network) results in positive and negative sequence currents and consequently rotating mmfs in the stator of the synchronous generator at subsynchronous and supersynchronous frequencies respectively [19]. The negative sequence current acts like a brake on the rotor, dissipating energy and helping to damp this component. This is because the synchronous machine rotor behaves as a positive resistance when viewed by this current, therefore, it is damped out.

The positive sequence current which oscillates at subsynchronous frequency ω_n, sets up a stator magnetic field rotating in the airgap at ω_n which is by design less than the synchronous speed ω_0 electrical r / s [20, 21]. The synchronous generator rotor is rotating at a constant synchronous speed ω_0, thus, currents at a frequency of $\omega_0 - \omega_n$ electrical r / s are induced in the rotor circuits which in turn produce a rotor magnetic field in the airgap stationary with respect to the stator magnetic field produced by the positive sequence current. The interaction between these two subsynchronous fields will result in a time invariant counter torque component associated with this mode.

The SSR positive sequence current oscillation will tend to be damped by the line and transformer resistances. However, the synchronous generator acts as an induction generator to this current, since its rotor is rotating at a higher speed than that of the SSR positive sequence current.

That is, the rotor of the synchronous generator will behave as a negative resistance as viewed by the SSR positive sequence current. If the net resistance in the path of this current is negative, that is, if the energy fed by the rotating machine is more than that absorbed by the resistance loss in the SSR positive sequence current circuit, then the oscillations will build up in time and cause system instability. This is known [19] as the induction generation effect giving rise to the unstable SSR oscillation. However, if under this induction generation effect the net effective resistance is positive, then the SSR oscillation will be damped.

1.3 Torsional Resonance Interaction

The generator shaft system usually has many torsional modes [22] and associated with each mode is the natural frequency of the torsional resonance (in practice the torsional resonance frequencies range from 15 Hz to 45 Hz for steam turbo-generator stations and 10 Hz or below for hydro-generator stations [23, 24]). This arises from the fact that the rotors of the generator and the exciter, the high, the intermediate and the low pressure turbines (in the case of a steam station) may be modelled as a number of inertias interconnected by elastic shafts which may be modelled as torsional springs [22]. The mode oscillations of the rotor of the

generator is of some importance because it carries with it the field excitation. The torsional oscillations of the field coil, therefore, has the possibility of inducing voltages across the stator windings [23]. When the electromechanical torque set up by these torsional induced stator currents is phased so as to reinforce positively the magnitude of the torsional vibration, then an unstable situation exists.

The detailed mechanism by which this electromechanical damping occurs is not yet understood, although the condition at which the unstable situation occurs have been identified. This condition is when the frequency of the L - C resonance ω_n is approximately equal to $\omega_0 - \omega_m$, where ω_m is anyone of the torsional resonance frequencies and ω_0 is the rotor synchronous speed. It is known [23] that at this frequency the electrical system will behave as a negative mechanical damping as viewed by the rotor system. If this negative damping is greater than the machine positive damping, then torque oscillation will build up until the shaft is highly stressed. This is known as the torsional resonance interaction [18, 23].

1.4 Review of Previous Work

Literature available prior to 1970 [5, 6, 25] described the concept of series resonance possible in transmission lines utilizing series capacitor. Some of the references have described the phenomenon

as a form of self-excitation. Reference [25] used the frequency domain method to map the stability boundary on the series capacitive reactance and the line resistance plane. It was found that unstable SSR oscillation is more likely to occur at low line resistance and high series capacitive reactance.

Since the mechanical failure of 1970 at the Mohave power station, a great deal of effort has been concentrated on the study of SSR phenomenon, notably, in the analysis, detection and prevention of this phenomenon. Several mathematical techniques have been developed for large system planning [8, 12, 26, 27, 28, 29, 30].

Reference [26] calculated the negative damping coefficients which resulted from the torsional resonance interaction. The limit at which this negative damping exceeds the machine damping was predicted [26]. This method of calculation was applied in the planning of Kaiparowits power station in U.S.A.

Reference [27] introduced a circuit analysis procedure for the subsynchronous resonance and formulas for calculating the effect of the SSR phenomenon, While References [21, 31] used the Nyquist criterion for investigating the stability conditions in the multi-machine power system. The method of calculating the peaks of the SSR oscillations and the expected system condition of these oscillations was described [20] . Reference [32] used the eigenvalue technique to investigate the

effect of the torsional resonance interaction on the system stability. It was found that an additional region of instability is caused by this interaction. Reference [33] added the machine regulator and governor systems to the analysis of [32]. It was found [33] that the stability region under torsional resonance interaction can be improved by a proper design of electro-hydraulic governors while the regulator system remains ineffective.

The theoretical analysis carried out in [18] for the Mohave power station to explain the cause of the mechanical damage was confirmed by the experimental results conducted in [34] at the same power station. A detailed model of its mechanical system which is useful for the study of the torsional resonance interaction, is introduced in [35].

The other aspect of development consisted of finding protective devices and solutions to prevent any further damages at the Mohave power station. Most of the solutions for the SSR phenomenon were concerned with reducing the peak torque oscillations following system disturbances since the levels of series capacitor compensations were chosen so as not to cause unstable SSR oscillations. A prime concern is finding practical methods to eliminate the most severe case of all viz: the interaction of a shaft system torsional mode whose resonant frequency is coincident with the frequency of the pulsating torque arising from unstable SSR mode.

To eliminate the torsional resonance interaction, Reference [18] proposed a SSR power blocking filter to be installed in series with the series capacitor compensated transmission line. The SSR blocking filter is a L - C tank circuit which is tuned to the SSR frequency. It presents itself as a large resistance to the SSR current and in consequence dominates over the negative resistance associated with the induction generation action of the amortisseur windings. References [36, 37] installed this filter at the Mohave power station as its responses to temperature variations and to levels of series capacitor compensations were reported. Reference [38] introduced a feedback loop through the machine excitation system to control the torsional resonance interaction. It was shown [38] by eigenvalues analysis and analogue simulation that torsional resonance interaction can be eliminated at a point characterized by fixed values of a series capacitive reactance and a transmission line resistance. Reference [39] introduced a feedback loop through the turbine governor and it was demonstrated by eigenvalues analysis and analogue simulation that torsional interaction is totally eliminated. However, it was recognized [39] that the turbine governor system had a time response which was too fast to be realistic.

There are a number of schemes proposed to protect the series capacitor from the overvoltages which would occur under the condition of unstable SSR oscillation. Reference [18] proposed a tripping relay which trips the generator under sustained SSR oscillation. This relay was tested in the field and the results were reported in [40, 41] . A

dual-gap scheme connected across the series capacitor was proposed [18] to protect the series capacitor and to reduce the peak torque oscillation. Reference [42] introduced a nonlinear resistor protection scheme connected across the series capacitor for the same purpose.

To control the unstable SSR oscillation, Reference [18] proposed a redesign of the generator rotor which has a low amortisseur resistance to eliminate the induction generation action. Reference [23] tested a dynamic filter which is added in series with the series capacitor transmission line to solve the unstable SSR oscillation problem. This filter generates a voltage equal in magnitude and opposite in phase to that produced by the rotor oscillation at subsynchronous frequency.

There has been a number of papers on the control of the unstable SSR oscillation through feedback signals to the field current of the synchronous generator. The first attempt was made by Saito et al [17] when he introduced a negative damping stabilizer (NDS) feedback loop which injects current in the synchronous machine field winding to control the unstable SSR oscillation. The experimental and theoretical results reported in [17] demonstrated the possibility of suppressing the SSR oscillations by field winding control.

In this thesis, the ground work of [17] is followed up, and the machine excitation system is used as a means to control the SSR phenomenon. The two aspects of the series capacitors effect are considered and the analysis is carried out for small and large disturbances.

1.5 Outline of the Problem

After the shaft failures at Mohave [13, 14], a number of serious and thorough analyses of the SSR instability began to appear in the literature. Among this extensive work, a number of patchwork remedies exist. Firstly, one considers prevention: that is, designing for the degree of series capacitor compensation which avoids SSR and torsional interaction instabilities for all conceivable transmission network configurations. Then, as discussed in the review (Section 1.4), one considers the many countermeasures which have been proposed to reduce the overvoltages and the torques of stable SSR to values below the ultimate yield or fatigue limits. However, because of the haste in which engineering solutions are conceived and implemented, and perhaps also because of the propriety and confidential nature of the results, complete analyses and evaluations of the effectiveness of the countermeasures have not been disclosed in print.

The large subject of SSR is reduced to a manageable size in this thesis by selectively treating only two aspects of it viz:

(a) SSR suppression by field excitation control.

(b) SSR avoidance by shunt compensated synchronous capacitor.

The bulk of the study is devoted to field excitation control. Much pioneering work on this aspect has been done by Saito,

Mukae and Murotani [17] and this thesis makes advances on their work in asking the following unanswered questions:

(1) What are the underlying principles in SSR suppression using field excitation control?

(2) What feedback signals are the most appropriate?

(3) Is the excitation system which has already a voltage regulator feedback loop and a power system stabilizer feedback loop, capable of taking on the additional duty of SSR suppression without compromising its existing functions?

(4) Does the fact that the excitation system has saturation limits mean that large unstable SSR oscillations cannot be controlled by field excitation?

(5) Is the field excitation capable of controlling instabilities due to shaft torsional resonance interaction with the SSR ?

(6) If large unstable SSR and torsional resonance interaction cannot be controlled from field excitation feedback, then are the protection schemes against series capacitor overvoltages and the SSR power blocking filter capable of suppressing the instabilities?

In the course of answering these questions, one becomes impressed with the adage that "prevention is better than cure". One is attracted to the idea that shunt compensation avoids SSR altogether, and in consequence a chapter is devoted to the concept of voltage support using synchronous capacitor.

1.6 Methodology

The main concern of this thesis is the analysis of the effect of the series capacitor on the system stability under large and small disturbances. For this purpose two sets of equations are used:

(1) Linearized first order differential equations describing the synchronous machine and the electrical network. These equations are necessary for the small perturbation study.

(2) Nonlinear first order differential equations describing the synchronous machine and the electrical network. These are used in the large perturbation study.

A state space form of the linearized equations is obtained and the concept of eigenvalues and eigenvectors technique is used to investigate the system stability under small disturbances. Instability of the system is recognized if one of the real parts of the

eigenvalues is positive. Eigenvectors are used to relate the eigenvalues with the physical system.

Runge Kutta-Gill numerical integration method is used to integrate the nonlinear first order differential equations in the investigation of the system stability under large disturbances. Instability is recognized if the system oscillations are building up with time.

1.7 Physical Interpretation

All the previous work that dealt with the SSR problem lacked the physical interpretation of the system eigenvalues. It was accepted that when the real part of one of the eigenvalues is positive, the system is unstable. Furthermore, the physical interaction between the machine excitation system and the SSR phenomenon was not explained. To remedy this deficiency, a physical interpretation is given to each of the modes of the system studied. With this insight, it is possible to distinguish instabilities as being to the hunting (mechanical) mode, the SSR mode or the torsional mode. Such a detailed picture gives understanding to the problem.

The magnetic field view-point is adopted to provide a physical understanding in the airgap of the synchronous machine. The space vector diagram of the machine airgap magnetomotive force (mmf) phasors

is used to shed light on the condition of unstable SSR oscillation and how to compensate for the induction generation action.

1.8 Contributions to Knowledge

This thesis claims the following contributions as original to the best of the author's knowledge:

Subsynchronous Resonance Problem

(1) A physically based understanding of the principle of field current control of the SSR has been proposed and the theory verified. The usefulness of this theory has been demonstrated in:

(a) establishing the frequency and time phase criteria of the feedback signal,

(b) showing that: shaft speed, rotor currents, real power (Δ P) and reactive power (Δ Q) signals are acceptable candidates as feedback signals because they contain a component which satisfies the frequency criterion. However, their relative effectiveness is determined by their ability to satisfy the phase criterion as well,

(c) proposing a robust feedback based on a combination of ΔP and ΔQ signals,

(d) explaining why, even when small perturbation stability may be secured by feedback, the system is inherently incapable of withstanding large disturbances due to the physical constraint that the machine excitation system saturates.

(2) The merits of the field excitation system to control SSR instabilities have been evaluated for the case of a feedback strategy based on a combination of real (ΔP) and reactive (ΔQ) power signals. This evaluation takes the following factors into account:

(a) the excitation system which has already a voltage regulator feedback loop and a power system stabilizer (PSS) feedback loop,

(b) the gain of the excitation system saturates (this is modelled by voltage ceilings in the block diagrams),

(c) the feedback system should not only be capable of suppressing small perturbation instabilities but also

the instabilities which follow from large disturbances such as three-line-to-ground fault or switching-out-of-phase,

(d) the shaft torsional resonance can interact with the SSR oscillations resulting in the most severe case of instability.

(3) Recognizing the limitation of ΔP and ΔQ feedback to arrest SSR instabilities from large perturbations and shaft torsional resonance interactions, the merits of supplementary counter-measures have been investigated. These are:

(a) the dual level spark gap with nonlinear resistor employed to protect the compensating capacitor from overvoltages,

(b) the SSR power blocking filter.

While these supplementary devices are needed, we found out that the excitation feedback, nevertheless, plays important roles in ensuring that limit cycling does not occur and in providing improved damping.

Synchronous Capacitor Shunt Compensator

(4) Eigenvalue studies of a shunt compensated long transmission line using synchronous capacitor with a high response voltage excitation have shown that SSR can be avoided while maintaining transient stability and comparable power carrying capability.

While not directly germane to the central theme of the thesis, the other contributions consist of:

Synchronization-out-of-Phase Peak Torque

(5) While considering synchronization-out-of-phase as a source of the large perturbation studies, it becomes apparent that the peak torques associated with synchronization-out-of-phase of the series capacitor compensated transmission line have not appeared in the literature before. It is shown in this thesis how the results for series capacitor compensated transmission line can be predicted from those of the uncompensated line provided that the equivalent line reactance is $X_L - X_C$.

Mode Identification

(6) With the help of the weighted elements in each eigenvector, it has been possible to associate each eigenvalue (or com-

plex conjugate pair) with physical mode. For example, each resonant circuit in the armature has a positive sequence mode and a negative sequence mode. The resonant circuit may be the series capacitor compensating, the line reactance, or it may be the parallel L - C tank circuit used as the SSR power blocking filter. For example, the instabilities may be due to the positive sequence SSR mode, the hunting mode, the torsional resonant mode or the PSS feedback circuit mode. It is by recognizing the physical character of these modes that some understanding of the complex system is possible and hopefully sufficient insight can be gained to find solutions to the problems.

1.9 Outline of the Thesis

A step-by-step approach is adopted in this thesis for the purpose of understanding the complicated interactions of a very complicated system consisting of a synchronous generator feeding a series capacitor compensated transmission line. The field excitation system has a voltage regulator feedback and a power system stabilizer. On top of these, an additional feedback loop is installed with the objective of suppression SSR instabilities and shaft torsional resonance interaction.

Rather than modelling the entire system at once, the approach is to start with the mathematical equations modelling a simple basic system where modes have already been identified. From the simple basic system, the complexities are added one by one. By this method, it is possible to identify the mode associated with each addition. Therefore, the thesis is organized as follows:

(1) Chapter II

In Section 1.6, it was mentioned that the study requires mathematical equations to describe the system that consists of a synchronous machine connected to a series capacitor compensated transmission line. Therefore, the basic synchronous machine equations, the machine reference frames and the per-unit quantities are reviewed in this chapter. Moreover, the mathematical models required for large and small disturbance studies are derived.

(2) Chapter III

Since our main concern is the field excitation control of the SSR phenomenon, then a wise beginning is to explain how it is possible to do so. This chapter is devoted to the theoretical explanation of how SSR instability can be suppressed by field excitation control.

(3) Chapter IV

Any engineering study becomes more convincing and practically acceptable if its theoretical background is backed up by numerical and experimental results. Therefore, in this chapter, the theory introduced in Chapter III is confirmed by a numerical example and the experimental results reported in [17].

(4) Chapter V

From the review (Section 1.4), none of the previous workers considered the machine excitation system in eliminating the unstable SSR oscillations. Even Saito et al [17], who made the first trial in this direction, bypassed the machine excitation system. A feedback loop (NDS') which considers the machine excitation system, is proposed in this chapter for SSR suppression. Eigenvalues are used to evaluate the effectiveness of this feedback loop in controlling the SSR instability.

(5) Chapter VI

Chapter V evaluates the NDS' feedback loop suppression when the system is slightly disturbed from its steady state operating point. To have this feedback loop more accepted by power system engineers, it has to be tested against large disturbances.

This chapter examines the capability of the NDS' feedback loop in stabilizing the unstable SSR oscillation when the system is subjected to a severe fault. The NDS' feedback is found to be unable to handle large unstable SSR oscillations due to the machine excitation system limitations. To overcome this obstacle, a nonlinear resistor protection scheme which is now in use [42], is used with the NDS' feedback loop to eliminate the large unstable SSR oscillation.

(6) Chapter VII

So far, the system torsional resonance has not been included in the analysis. However, torsional resonance interaction is known [32] to cause system instability. For a deeper understanding of the problems brought about by the use of series capacitors, the torsional resonance is added to the system. The main topic of this chapter is the analysis of the torsional resonance instability and its elimination by the SSR power blocking filter.

(7) Chapter VIII

Following the idea of avoiding the SSR instabilities by using shunt compensation instead of series compensation, an elementary analysis is performed on the system which is shunt compensated by a synchronous capacitor. The eigenvalues are used in the small perturbation study to investigate the system instability.

CHAPTER II

BASIC SYNCHRONOUS MACHINE THEORY

2.1 Introduction

The purpose of this chapter is to review the synchronous machine equations in the physical abc frame and the d-q rotating reference frame. The synchronously rotating reference frame is also described for further use in the analysis.

Power system engineers used to write the machine equations in terms of per-unit quantities rather than in terms of voltages, amperes, ohms or henries. In this chapter the most commonly used X_{ad} - base is explained and the per-unit equations are derived.

Per-unit time equations are sometimes used by power system engineers. The relation between real time (t) and per-unit time (t') equations was not well explained in the literature. Moreover, the mechanical equations were used in two different confusing forms. In this chapter these two confusing formulations are discussed and the usage of one form or another is explained.

Finally, a mathematical model of the system used throughout this thesis is derived and the resulting nonlinear equations are linearized around the quiescent point and are put in a state space model necessary for subsequent analysis.

In this thesis the following assumptions are made,

(i) Saturation is neglected.

(ii) The synchronous generator does not have a neutral return and in consequence the zero sequence does not exist.

(iii) All harmonics are neglected.

2.2 Machine Equations in the abc Stationary Reference Frame

The synchronous machine equations in the abc stationary reference frame are given by [43, 44]

$$\underline{e} = [R]\,\underline{i} + \frac{d}{dt}\,\underline{\psi} \tag{2.1}$$

where,

$$\underline{e} = [\underline{e}_s^T \mid \underline{e}_r^T]^T = [e_a\ e_b\ e_c \mid e_{fd}\ e_{kd}\ e_{kq}]^T \tag{2.2}$$

$$[R] = \begin{bmatrix} [R_s] & [0] \\ [0] & [R_r] \end{bmatrix}, \quad [R_s] = \begin{bmatrix} -R_a & & \\ & -R_a & \\ & & -R_a \end{bmatrix}, \quad [R_r] = \begin{bmatrix} R_{fd} & & \\ & R_{kd} & \\ & & R_{kq} \end{bmatrix} \tag{2.3}$$

the stator windings are assumed to have equal internal resistances,

$$\underline{i} = [\underline{i}_s^T \mid \underline{i}_r^T]^T = [i_a\ i_b\ i_c \mid i_{fd}\ i_{kd}\ i_{kq}]^T \tag{2.4}$$

$$\underline{\psi} = [\underline{\psi}_s^T \mid \underline{\psi}_r^T]^T = [\psi_a\ \psi_b\ \psi_c \mid \psi_{fd}\ \psi_{kd}\ \psi_{kq}]^T \tag{2.5}$$

The subscripts s, r indicate the stator and the rotor respectively and the amortisseur windings are represented by two windings, one along the d-axis and the other along the q-axis.

$$\underline{\psi} = [L]\,\underline{i} = \begin{bmatrix} -[L_{ss}] & [L_{sr}] \\ -[L_{rs}] & [L_{rr}] \end{bmatrix} \begin{bmatrix} \underline{i}_s \\ \underline{i}_r \end{bmatrix} \tag{2.6}$$

The sign convention used in the above equations is as follows:

(i) The current flows out of the stator.

(ii) The current flows in the rotor.

$$[L_{ss}] = \begin{bmatrix} L_{aa} & L_{ab} & L_{ac} \\ L_{ba} & L_{bb} & L_{bc} \\ L_{ca} & L_{cb} & L_{cc} \end{bmatrix}, \quad [L_{sr}] = \begin{bmatrix} L_{fad} & L_{kad} & L_{kaq} \\ L_{bfd} & L_{bkd} & L_{bkq} \\ L_{cfd} & L_{ckd} & L_{ckq} \end{bmatrix} \tag{2.7}$$

$$[L_{rr}] = \begin{bmatrix} L_{ffd} & L_{fkd} & 0 \\ L_{fkd} & L_{kkd} & 0 \\ 0 & 0 & L_{kkq} \end{bmatrix}, \quad [L_{rs}] = \begin{bmatrix} L_{afd} & L_{fbd} & L_{fcd} \\ L_{akd} & L_{kbd} & L_{kcd} \\ L_{akq} & L_{kbq} & L_{kcq} \end{bmatrix} \tag{2.8}$$

Under the assumption of sinusoidally distributed stator windings, the stator mutual and self inductances are sinusoidally varying, i.e.,

$$\begin{bmatrix} L_{ab} \\ L_{ac} \\ L_{bc} \end{bmatrix} = \begin{bmatrix} L_{ba} \\ L_{ca} \\ L_{cb} \end{bmatrix} = \begin{bmatrix} -L_m \\ -L_m \\ -L_m \end{bmatrix} + L_0 \begin{bmatrix} \cos\ (2\theta - 120) \\ \cos\ (2\theta + 120) \\ \cos\ (2\theta) \end{bmatrix} \quad \text{(Henry)} \qquad (2.9)$$

$$\begin{bmatrix} L_{aa} \\ L_{bb} \\ L_{cc} \end{bmatrix} = \begin{bmatrix} L_{00} \\ L_{00} \\ L_{00} \end{bmatrix} + L_0 \begin{bmatrix} \cos\ 2\theta \\ \cos\ 2\ (\theta - 120) \\ \cos\ 2\ (\theta + 120) \end{bmatrix} \quad \text{(Henry)} \qquad (2.10)$$

$$[L_{rs}] = [L_{sr}]^T = \begin{bmatrix} L_{afd}\cos\theta & L_{akd}\cos\theta & -L_{akq}\sin\theta \\ L_{afd}\cos(\theta-120) & L_{akd}\cos(\theta-120) & -L_{akq}\sin(\theta-120) \\ L_{afd}\cos(\theta+120) & L_{akd}\cos(\theta+120) & -L_{akq}\sin(\theta+120) \end{bmatrix} \text{(Henr}$$

(2.11)

where θ is the instantaneous angular position of the rotor in electrical degrees,

and L_{00}, L_m, L_0, L_{afd}, L_{akd} and L_{akq} are constants in Henries.

The electromechanical torque (T_e) is given by,

$$T_e = \frac{1}{2} n \frac{\partial}{\partial\theta} \underline{i}^T \underline{\psi} \qquad (2.12)$$

where n is the number of pairs of poles.

2.3 Reference Frames

2.3.1 The d-q Rotating Reference Frame

Park [45, 46] introduced a new practical set of equations in which those trigonometric functions in the inductance matrix (Equation 2.6) no longer occur. He assumed that both stator and rotor reference frames are rigidly connected to the rotor and rotate at the same speed as the rotor, Figure 2.1.

The new equations do not have the same form as Equation 2.1, but contain an additional speed term known as the speed voltage. The new set of equations are given by,

$$\begin{bmatrix} e_d \\ e_q \\ e_{fd} \\ 0 \\ 0 \end{bmatrix} = [R] \begin{bmatrix} i_d \\ i_q \\ i_{fd} \\ i_{kd} \\ i_{kq} \end{bmatrix} + \frac{d}{dt} \begin{bmatrix} \psi_d \\ \psi_q \\ \psi_{fd} \\ \psi_{kd} \\ \psi_{kq} \end{bmatrix} + \begin{bmatrix} -\psi_q \\ \psi_d \\ 0 \\ 0 \\ 0 \end{bmatrix} \omega \qquad (2.13)$$

$$\begin{bmatrix} \psi_d \\ \psi_q \\ \psi_{fd} \\ \psi_{kd} \\ \psi_{kq} \end{bmatrix} = \begin{bmatrix} -L_d & 0 & L_{afd} & L_{akd} & 0 \\ 0 & -L_q & 0 & 0 & L_{akq} \\ -\frac{3}{2}L_{afd} & 0 & L_{ffd} & L_{fkd} & 0 \\ -\frac{3}{2}L_{akd} & 0 & L_{fkd} & L_{kkd} & 0 \\ 0 & -\frac{3}{2}L_{akq} & 0 & 0 & L_{kkq} \end{bmatrix} \begin{bmatrix} i_d \\ i_q \\ i_{fd} \\ i_{kd} \\ i_{kq} \end{bmatrix} \qquad (2.14)$$

where

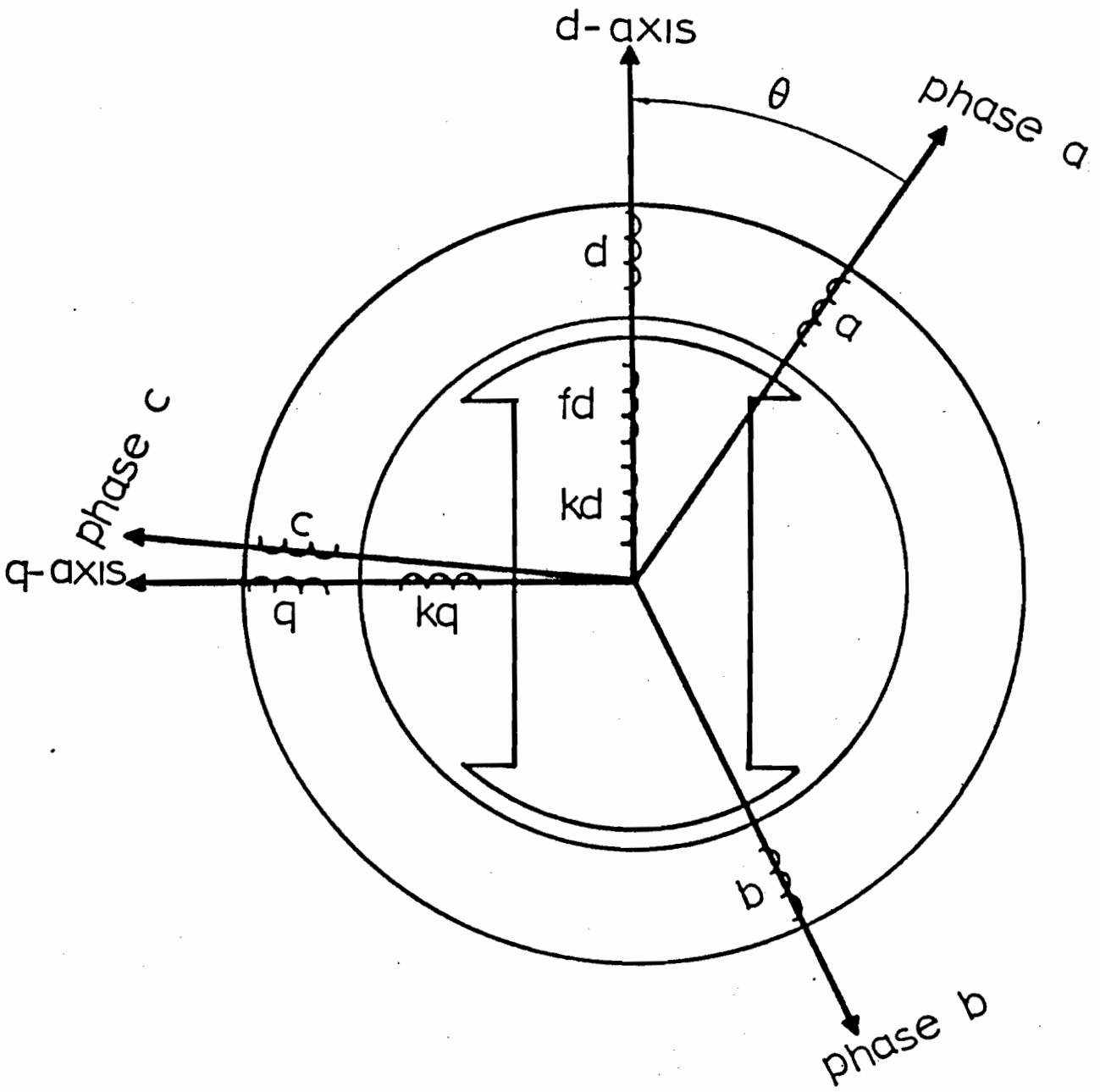

$\theta = \omega t + \theta_0$

ω = rotor speed in electrical r/s

Figure 2.1. Three-phase synchronous machine with two amortisseur windings.

$$L_d = L_{00} + L_m + \frac{3}{2} L_0 \quad \text{(Henry)} \tag{2.15}$$

and

$$L_q = L_{00} + L_m - \frac{3}{2} L_0 \quad \text{(Henry)} \tag{2.16}$$

where the zero sequence does not exist due to the assumption that the machine is not grounded. The electromechanical torque is given by,

$$T_e = i_q \psi_d - i_d \psi_q \tag{2.17}$$

The transformation from the stationary reference frame (abc) to the d-q rotating reference frame is shown in Appendix A-1.

In summary, the following points describe Park's transformation:

(i) The inductance matrix is constant.

(ii) The voltage equation has an additional term called the speed voltage term.

(iii) Park's transformation is not orthogonal (Power invariant) [47].

(iv) The mutual inductances are not reciprocal, i.e., $[L_{rs}] \neq [L_{sr}]^T$ as shown in equation 2.14.

2.3.2 The Synchronously Rotating Reference Frame

The synchronously rotating reference frame is also called the system reference frame. This frame has the following properties:

(i) It rotates at synchronous speed, ω_0 electrical r/s , and it will be described in this thesis by D-Q axis.

(ii) When the rotor of the machine rotates at synchronous speed, the angle between this frame and Park's frame is constant.

(iii) The transformation from the abc stationary reference frame to this frame is carried out in a similar way to that explained in Appendix A-1, except that θ is substituted by $\theta_s = \omega_0 t + \theta_{s0}$, where ω_0 is the synchronous speed.

(iv) If the machine rotor is not rotating at synchronous speed, the machine equations in the synchronously rotating reference frame contain terms of the rotor position.

This frame is very useful when more than one machine is connected to the same network. However, this frame will be used in this thesis in deriving the linearized model necessary for stability analysis and when the synchronous capacitor is used for shunt compensation as will be shown in Chapter VIII.

2.4 Per-Unit System

The knowledge of the machines, transformers and transmission lines parameters are required in the analysis of power systems. Per-unit quantities of impedances, currents, voltages and frequency are commonly used by power engineers due to the following reasons [48] :

(i) The ordinary parameters vary widely with the physical size of the machine. The per-unit quantities do not depend directly on the physical size and their values are of comparable magnitudes.

(ii) In general, the per-unit parameters are small.

(iii) In the 2-axis theory of synchronous machine, a per-unit system is useful in removing those arbitrary numerical values, e.g., $\frac{3}{2}$ in equation 2.14.

(iv) It is a set of dimensionless parameters which help in preventing from converting between different systems of units.

When considering one apparatus, the following base values are usually adopted:

(i) The three-phase volt-ampere rating of the apparatus.

(ii) The rms line to line voltage.

(iii) The nominal frequency.

The base values of currents and voltages and the base impedances of the synchronous machine are not a simple matter to determine. However, the base values of the armature current and voltage are usually determined by the machine rating, hence the armature impedances are automatically defined. But the base values of the rotor currents are chosen so as to make the self inductances of the armature, field and the amortisseur circuits of about the same order of magnitude. The difficulty in determining the turn ratio between stator and rotor circuits due to the complications arising from the distributed nature of the windings has led Rankin [49, 50] to look for alternate approaches of defining the rotor base currents.

The rotor base currents are defined in different ways for different purposes. The choice of the rotor base currents is totally free as long as it makes all the mutual inductances reciprocal and it is used in the calculation of the machine impedances in a consistent way.

One of the definitions of rotor base values commonly used in the X_{ad} - base is derived in Appendix A-2 . This base makes the mutual inductances reciprocal and those between stator and rotor windings on the same axis equal.

2.5 Per-Unit Time (t')

The synchronous machine equations are now written in the d-q axis in terms of per-unit quantities as shown in equation A-2.26 of Appendix A-2. It is sometimes preferable to normalize the time, especially when working with linearized equations, which removes ω_0 from equation A-2.26. Per-unit time has been used quite often in the literature in deriving the synchronous machine equations [17, 28, 32] .

Per-unit time t', is defined as,

$$t' = \omega_0 t$$

In any equation which contains $\sin \omega t$ or $\cos \omega t$, it should be replaced by a similar equation containing $\sin \bar{\omega} t'$ and $\cos \bar{\omega} t'$, ($\bar{\omega}$ is per-unit speed).

For the differential equation, the relations between first and second derivatives in real time t, and per-unit time are derived as follows;

$\frac{d z}{d t}$ is a first derivative in real time of any variable z .

$$\frac{d z}{d t} = \frac{d z}{d t'} \frac{d t'}{d t} = \omega_0 \frac{d z}{d t'} \tag{2.18}$$

and

$$\frac{d^2 z}{d t^2} = \frac{d}{dt} \left(\frac{d z}{d t}\right) = \omega_0 \frac{d}{dt'} \left(\frac{d z}{d t}\right) = \omega_0^2 \frac{d^2 z}{dt'^2} \tag{2.19}$$

Expressions 2.18 and 2.19 indicate that a real time differential equation is changed to a per-unit time differential equation by multiplying the coefficients of the first and second derivatives with ω_0 and ω_0^2 respectively.

2.6 Forms of the Mechanical Equations

Traditionally, the electrical engineers have used different forms of the mechanical equations. One of these forms is used in this thesis. However, it is a matter of clarity to summarize these forms and explain the different use of each of them.

For a generator, the mechanical equations which govern the motion of the machine rotor are,

$$J \frac{d^2 \delta}{d t^2} = T_m - T_e \qquad (2.20)$$

$$\frac{d \delta}{d t} = \omega - \omega_0$$

where J is the moment of inertia of the rotating mass attached to the shaft in Joule. $sec.^2$, T_m is the positive mechanical torque to accelerate the shaft in Joule, T_e is the positive electrical torque acting to decelerate the shaft in Joule, and δ is the rotor angular position in electrical radians.

Equation 2.20 is one of the forms used when the torque is expressed in Joule and the moment of inertia of the machine is given. The other forms of the mechanical equations are:

(1) Using the mechanical and the electrical powers (P_m and P_e respectively) in watts and the angular momentum (M) instead of T_m, T_e and J respectively in equation 2.20. The new mechanical equations can be derived from 2.20 as follows,

$$\begin{aligned} P_m &= \omega_0 T_m \quad \text{watts} \\ P_e &= \omega_0 T_e \quad \text{watts} \\ M &= \omega_0 J \quad \text{Joule. sec.} \end{aligned} \tag{2.21}$$

multiplying the first equation of 2.20 by ω_0, and using 2.21 we obtain:

$$\begin{aligned} M \frac{d^2 \delta}{d t^2} &= P_m - P_e \\ \frac{d \delta}{d t} &= \omega - \omega_0 \end{aligned} \tag{2.22}$$

(2) The third form of the mechanical equations is that which contain per-unit mechanical and electrical torques $\bar{T}_m, \bar{T}_e$ and the inertia constant (H) of the machine. This is simply

the per-unitized form of equation 2.20,

and this can be derived as :

S_B is the base three-phase volt-ampere of the synchronous generator .

T_B is defined as the base torque.

$$T_B = S_B / \omega_0 \quad \text{(KVA.s)} \quad , \quad \omega_0 \text{ electrical r/s}$$

$$\bar{T}_m = \frac{T_m}{T_B} \quad , \quad \bar{T}_e = \frac{T_e}{T_B}$$

Dividing equation 2.20 by $T_B = S_B / \omega_0$, one has,

$$\frac{\omega_0 J}{S_B} \frac{d^2 \delta}{d t^2} = \bar{T}_m - \bar{T}_e \qquad (2.23)$$

and

$$\frac{d \delta}{d t} = \omega - \omega_0 \qquad (2.24)$$

substituting 2.24 into 2.23, we get,

$$\frac{\omega_0}{S_B} J \frac{d \omega}{d t} = \bar{T}_m - \bar{T}_e \qquad (2.25)$$

Using per-unit speed $\bar{\omega} = \frac{\omega}{\omega_0}$ instead of ω in 2.24 and 2.25, we have,

$$\frac{\omega_0^2}{S_B} J \frac{d\bar{\omega}}{dt} = \bar{T}_m - \bar{T}_e \qquad (2.26)$$

$$\frac{d\delta}{dt} = \omega_0 (\bar{\omega} - 1)$$

H is defined as the kinetic energy of the rotor at synchronous speed ω_0 divided by the base volt-ampere of the machine, S_B .

$$H = \frac{1}{2} J \omega_0^2 / S_B \qquad \text{(Joule / KVA)} = \text{(K Watts. sec / KVA)} \qquad (2.27)$$

substituting H instead of J in equation 2.26 we obtain:

$$2H \frac{d\bar{\omega}}{dt} = \bar{T}_m - \bar{T}_e \qquad (2.28)$$

$$\frac{d\delta}{dt} = \omega_0 (\bar{\omega} - 1)$$

We arrive to the three forms of the mechanical equations by assuming that the damping and the stiffness coefficients, D and K respectively, do not exist. However, if damping exists, another torque acting to decelerate the shaft is added and has the form, $D(\omega - \omega_0)$. The existence of the stiffness coefficient will be explained in Chapter VII.

A final remark on the three forms is that the last form (equation 2.28) is widely used by power engineers. This equation is described in real time and it will be used in the following chapters to describe the rotor system of the synchronous machine.

2.7 System Model

The system used in the analysis of the subsynchronous resonance (SSR) is simply a synchronous generator connected to a load, which is represented by an infinite bus bar, through a long transmission line, where a series capacitor is used. The single line diagram of the system is shown in Figure 2.2(a).

The per-unitized synchronous machine equations given in equation A-2.26 of Appendix A-2 will be used. For notational simplicity the per-unitized quantities will be written without the dash on top of the variables except for per-unit speed $\bar{\omega}$. In the present derivations as well as in the forthcoming analysis, real time equations will always be used. From equation A-2.26 of Appendix A-2, the per-unitized synchronous machine equations are,

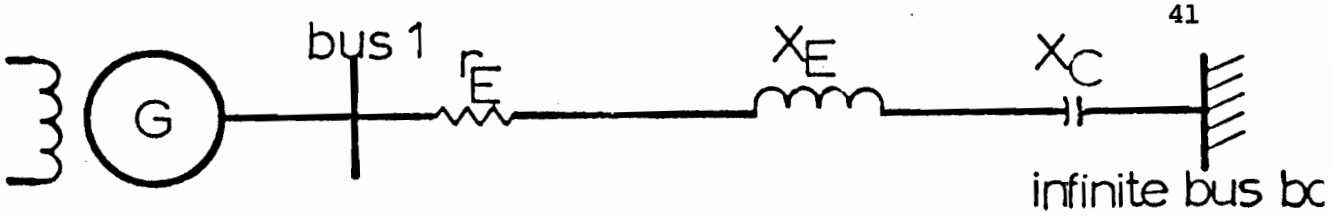

(a) Synchronous generator connected to an infinite bus through a series capacitor compensated transmission line.

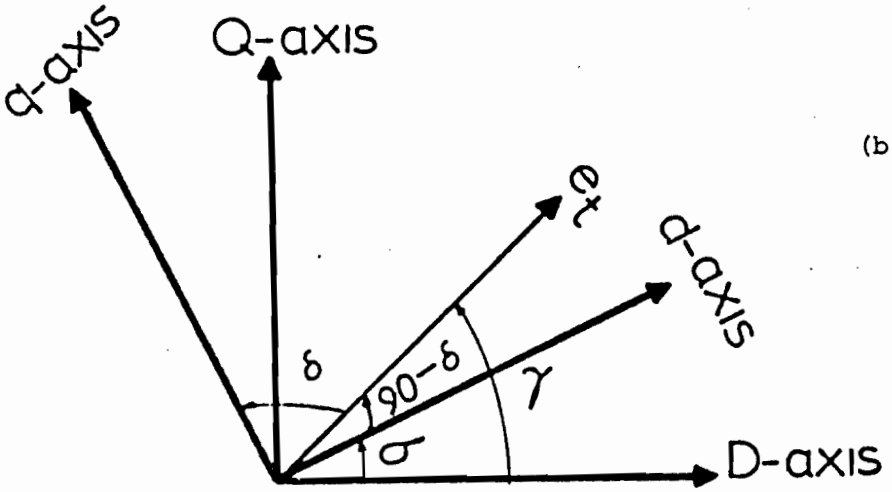

(b) Relation between D-Q synchronously rotating reference frame and Park's rotating reference frame.

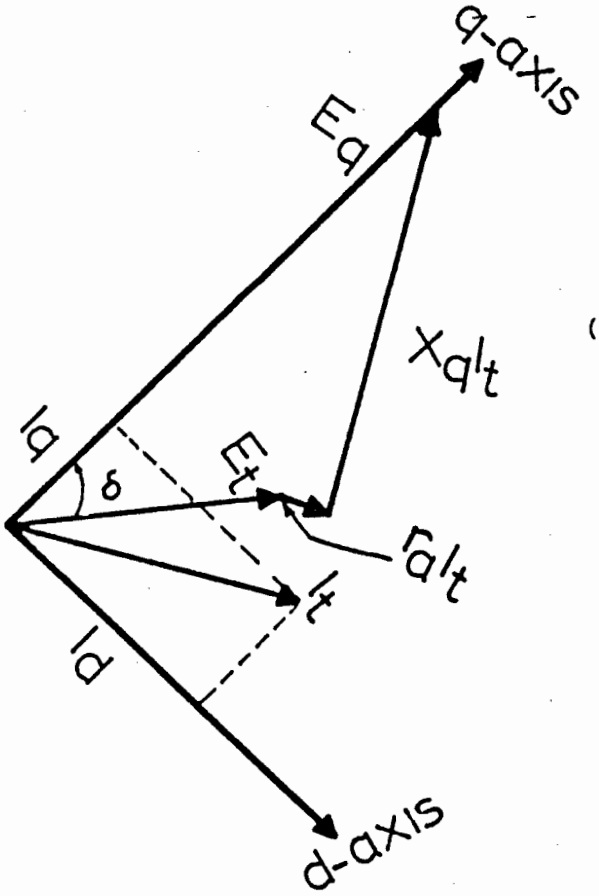

(c) Steady state diagram for calculating generator terminal voltages and currents.

Figure 2.2

$$\begin{bmatrix} e_d \\ e_q \\ e_{fd} \\ 0 \\ 0 \end{bmatrix} = \begin{bmatrix} -r_a & & & & \\ & -r_a & & & \\ & & r_{fd} & & \\ & & & r_{kd} & \\ & & & & r_{kq} \end{bmatrix} \begin{bmatrix} i_d \\ i_q \\ i_{fd} \\ i_{kd} \\ i_{kq} \end{bmatrix} + \frac{1}{\omega_0} \frac{d}{dt} \begin{bmatrix} \psi_d \\ \psi_q \\ \psi_{fd} \\ \psi_{kd} \\ \psi_{kq} \end{bmatrix} + \bar{\omega} \begin{bmatrix} -\psi_q \\ \psi_d \\ 0 \\ 0 \\ 0 \end{bmatrix} \tag{2.29}$$

and

$$\begin{bmatrix} \psi_d \\ \psi_q \\ \psi_{fd} \\ \psi_{kd} \\ \psi_{kq} \end{bmatrix} = \begin{bmatrix} -X_d & 0 & X_{ad} & X_{ad} & 0 \\ 0 & -X_q & 0 & 0 & X_{aq} \\ -X_{ad} & 0 & X_{ffd} & X_{fkd} & 0 \\ -X_{ad} & 0 & X_{fkd} & X_{kkd} & 0 \\ 0 & -X_{aq} & 0 & 0 & X_{kkq} \end{bmatrix} \begin{bmatrix} i_d \\ i_q \\ i_{fd} \\ i_{kd} \\ i_{kq} \end{bmatrix} \tag{2.30}$$

The voltages e_d and e_q in equation 2.29 represent the generator terminal voltage in the d - q rotating reference frame. The network voltage equations viewed from the generator bus are usually written in the D - Q synchronously rotating reference frame. Therefore, to express the generator terminal voltages in terms of the network voltages, a transformation from one reference frame to another should be made.

The one line diagram of the network is shown in Figure 2.2(a). It shows a lumped parameter representation of the transmission line, a per-unit resistance r_E in series with a per-unit inductive reactance X_E

connected to a bus bar. The series capacitive reactance X_C represents the level of the series capacitor compensation in p.u., since our aim is to investigate a system with a series capacitor compensated transmission line.

2.7.1 Transformation

From Figure 2.2(b) the variables in the D - Q and the d - q rotating reference frames are related as follows,

$$\begin{bmatrix} e_d \\ e_q \end{bmatrix} = \begin{bmatrix} \cos\sigma & \sin\sigma \\ -\sin\sigma & \cos\sigma \end{bmatrix} \begin{bmatrix} e_D \\ e_Q \end{bmatrix} \tag{2.31}$$

the inverse relation is:

$$\begin{bmatrix} e_D \\ e_Q \end{bmatrix} = \begin{bmatrix} \cos\sigma & -\sin\sigma \\ \sin\sigma & \cos\sigma \end{bmatrix} \begin{bmatrix} e_d \\ e_q \end{bmatrix} \tag{2.32}$$

The relations between currents and fluxes on both rotating reference frames can be obtained from equations 2.31 and 2.32 by using i and ψ instead of e .

2.7.2 Network Voltage Equations

The voltages at the generator bus (bus 1 in Figure 2.2(a)) can be expressed in the synchronously rotating reference frame D - Q as,

$$e_D = e_{rD} + e_{LD} + e_{CD} + e_{0D} \tag{2.33}$$

and

$$e_Q = e_{rQ} + e_{LQ} + e_{CQ} + e_{0Q} \tag{2.34}$$

where

e_D and e_Q the voltages at bus 1 along the synchronously rotating D and Q axes respectively.

(a) $e_{rD} = r_E\, i_D$ the D - axis voltage across the line resistance r_E .

(b) $e_{rQ} = r_E\, i_Q$ the Q - axis voltage across the line resistance r_E .

(c) $e_{LD} = \frac{1}{\omega_0} X_E \frac{d}{dt} i_D - X_E\, i_Q$ the D - axis voltage across the transmission line inductive reactance X_E .

(d) $e_{LQ} = \frac{1}{\omega_0} X_E \frac{d}{dt} i_Q + X_E\, i_D$ the Q - axis voltage across the transmission line inductive reactance X_E .

(e) $e_{CD} = -\frac{1}{\omega_0}\frac{d}{dt} e_{CQ} + X_C i_Q$ the D - axis voltage across the series capacitive reactance X_C .

(f) $e_{CQ} = \frac{1}{\omega_0}\frac{d}{dt} e_{CD} - X_C i_D$ the Q - axis voltage across the series capacitive reactance X_C .

(g) e_{0D} and e_{0Q} the voltages of the infinite bus bar along the synchronously rotating D and Q axes respectively.

Equations 2.33 and 2.34 can be written as,

$$\begin{bmatrix} e_D \\ e_Q \end{bmatrix} = \begin{bmatrix} r_E & -X_E \\ X_E & r_E \end{bmatrix} \begin{bmatrix} i_D \\ i_Q \end{bmatrix} + \frac{1}{\omega_0} \begin{bmatrix} X_E & \\ & X_E \end{bmatrix} \frac{d}{dt} \begin{bmatrix} i_D \\ i_Q \end{bmatrix} + \begin{bmatrix} e_{CD} + e_{0D} \\ e_{CQ} + e_{0Q} \end{bmatrix} \tag{2.35}$$

and

$$\frac{1}{\omega_0}\frac{d}{dt} \begin{bmatrix} e_{CD} \\ e_{CQ} \end{bmatrix} = \begin{bmatrix} X_C & \\ & X_C \end{bmatrix} \begin{bmatrix} i_D \\ i_Q \end{bmatrix} + \begin{bmatrix} 0 & 1 \\ -1 & 0 \end{bmatrix} \begin{bmatrix} e_{CD} \\ e_{CQ} \end{bmatrix} \tag{2.36}$$

2.7.3 Complete System Equations

So far, the electrical system of the synchronous generator is described in the d - q axis by equation 2.29, and the network equations are described in the D - Q axis by equations 2.35 and 2.36. To obtain

a complete description of the system shown in Figure 2.2(a), one of the forms of the mechanical equations described in Section 2.6 should be added. Since the per-unit quantities are used in the present derivations, then equation 2.28 is used to describe the rotor system of the synchronous generator. Therefore the mechanical equations are,

$$2H \frac{d\bar{\omega}}{dt} = T_m - T_e \tag{2.37}$$

$$\frac{d\delta}{dt} = \omega_0 (\bar{\omega} - 1) \tag{2.38}$$

where T_m, T_e are used for per-unit torques.

The last step in obtaining the system model is to transform all the equations to one reference frame by using the transformation matrix given in equation 2.31, and it is written here as:

$$e_{dq} = [C_{dq}^{DQ}] \; e_{DQ} \quad \text{and} \quad i_{dq} = [C_{dq}^{DQ}] \; i_{DQ}$$

where

$$[C_{dq}^{DQ}] = \begin{bmatrix} \cos\sigma & \sin\sigma \\ -\sin\sigma & \cos\sigma \end{bmatrix} = [C_s] \tag{2.39}$$

2.7.4 The d - q Nonlinear Model

The d - q system model is obtained if the network equations 2.35 and 2.36 are transformed to the d - q axis frame; and this can be done by multiplying equations 2.35 and 2.36 by $[C_s]$ as follows,

$$[C_s]\begin{bmatrix} e_D \\ e_Q \end{bmatrix} = [C_s]\begin{bmatrix} r_E & -X_E \\ X_E & r_E \end{bmatrix}[C_s]^{-1}[C_s]\begin{bmatrix} i_D \\ i_Q \end{bmatrix} + \frac{1}{\omega_0} X_E\,[C_s]\frac{d}{dt}\begin{bmatrix} i_D \\ i_Q \end{bmatrix} + [C_s]\begin{bmatrix} e_{0D} + e_{CD} \\ e_{0Q} + e_{CQ} \end{bmatrix} \tag{2.40}$$

and

$$\frac{1}{\omega_0}[C_s]\frac{d}{dt}\begin{bmatrix} e_{CD} \\ e_{CQ} \end{bmatrix} = X_C\,[C_s]\begin{bmatrix} i_D \\ i_Q \end{bmatrix} + [C_s]\begin{bmatrix} 0 & 1 \\ -1 & 0 \end{bmatrix}[C_s]^{-1}[C_s]\begin{bmatrix} e_{CD} \\ e_{CQ} \end{bmatrix} \tag{2.41}$$

e_{CD} and e_{CQ} are transformed to e_{Cd} and e_{Cq} using relation 2.39 or,

$$\begin{bmatrix} e_{CD} \\ e_{CQ} \end{bmatrix} = [C_s]^{-1}\begin{bmatrix} e_{Cd} \\ e_{Cq} \end{bmatrix}$$

therefore,

$$\frac{d}{dt}\begin{bmatrix} e_{CD} \\ e_{CQ} \end{bmatrix} = \left(\frac{d}{dt}[C_s]^{-1}\right)\begin{bmatrix} e_{Cd} \\ e_{Cq} \end{bmatrix} + [C_s]^{-1}\frac{d}{dt}\begin{bmatrix} e_{Cd} \\ e_{Cq} \end{bmatrix} \tag{2.42}$$

Substituting equation 2.42 for the currents in equation 2.40 we get,

$$\begin{bmatrix} e_d \\ e_q \end{bmatrix} = \begin{bmatrix} r_E & -X_E \\ X_E & r_E \end{bmatrix}\begin{bmatrix} i_d \\ i_q \end{bmatrix} + \frac{1}{\omega_0}\begin{bmatrix} X_E & \\ & X_E \end{bmatrix}\frac{d}{dt}\begin{bmatrix} i_d \\ i_q \end{bmatrix} + \begin{bmatrix} e_{Cd} + e_{0d} \\ e_{Cq} + e_{0q} \end{bmatrix}$$

$$+ \frac{1}{\omega_0} X_E \frac{d\sigma}{dt}\begin{bmatrix} 0 & -1 \\ 1 & 0 \end{bmatrix}\begin{bmatrix} i_d \\ i_q \end{bmatrix} \tag{2.43}$$

similarly, substituting equation 2.42 into equation 2.41 we get,

$$\frac{1}{\omega_0}\frac{d}{dt}\begin{bmatrix} e_{Cd} \\ e_{Cq} \end{bmatrix} = \frac{1}{\omega_0}\frac{d\sigma}{dt}\begin{bmatrix} 0 & 1 \\ -1 & 0 \end{bmatrix}\begin{bmatrix} e_{Cd} \\ e_{Cq} \end{bmatrix} + \begin{bmatrix} X_C & 0 \\ 0 & X_C \end{bmatrix}\begin{bmatrix} i_d \\ i_q \end{bmatrix} + \begin{bmatrix} e_{Cq} \\ -e_{Cd} \end{bmatrix} \tag{2.44}$$

The angle σ is always expressed in terms of δ, e.g., if we assume that the D - axis coincides with the reference voltage (usually the infinite bus voltage), then γ is known and determined by the network parameters (see Figure 2.2(b)), therefore,

$$\sigma = \gamma + \delta - 90^{\circ} \tag{2.45}$$

using equation 2.38 to obtain,

$$\frac{d\sigma}{dt} = \frac{d\delta}{dt} = \omega_0 (\bar{\omega} - 1) \tag{2.46}$$

The time derivative of σ in equations 2.43 and 2.44 are cancelled by using relation 2.46. The resultant network equations in the d - q axis are:

$$\begin{bmatrix} e_d \\ e_q \end{bmatrix} = \begin{bmatrix} r_E & \\ & r_E \end{bmatrix} \begin{bmatrix} i_d \\ i_q \end{bmatrix} + \frac{1}{\omega_0} \begin{bmatrix} X_E & \\ & X_E \end{bmatrix} \frac{d}{dt} \begin{bmatrix} i_d \\ i_q \end{bmatrix}$$

$$+ \bar{\omega} \begin{bmatrix} 0 & -X_E \\ X_E & 0 \end{bmatrix} \begin{bmatrix} i_d \\ i_q \end{bmatrix} + \begin{bmatrix} e_{Cd} + e_{0d} \\ e_{Cq} + e_{0q} \end{bmatrix} \tag{2.47}$$

and

$$\frac{1}{\omega_0} \frac{d}{dt} \begin{bmatrix} e_{Cd} \\ e_{Cq} \end{bmatrix} = \begin{bmatrix} X_C & 0 \\ 0 & X_C \end{bmatrix} \begin{bmatrix} i_d \\ i_q \end{bmatrix} + \bar{\omega} \begin{bmatrix} 0 & 1 \\ -1 & 0 \end{bmatrix} \begin{bmatrix} e_{Cd} \\ e_{Cq} \end{bmatrix} \tag{2.48}$$

The combination of equations 2.29, 2.30, 2.37, 2.38, 2.47 and 2.48, using the stator and the rotor fluxes as the state variables [51], the resultant model will be a set of nine nonlinear first order differential equations. This nonlinear model describes the system shown in Figure 2.2(a) when the per-unit quantities are used. This model is used in Chapter VI for transient stability studies.

2.7.5 Initial Conditions

The steady state operating currents and voltages are assumed to be the initial values throughout this thesis. However, the infinite bus voltage, power and power factor are assumed to be constant and equal to unity.

The steady state currents, voltages and fluxes are defined as:

$$\underline{I}_{s.s} = [I_{d0} \quad I_{q0} \quad I_{fd0} \quad 0 \quad 0]^T \tag{2.49}$$

$$\underline{E}_{s.s} = [E_{d0} \quad E_{q0} \quad E_{fd0} \quad 0 \quad 0]^T \tag{2.50}$$

and

$$\begin{bmatrix} \psi_{d0} \\ \psi_{q0} \end{bmatrix} = \begin{bmatrix} -X_d I_{d0} + X_{ad} I_{fd0} \\ - X_q I_{q0} \end{bmatrix} \tag{2.51}$$

The above steady state values can be calculated from the steady state vector diagram shown in Figure 2.2(c). The detailed calculations are given in [44] .

2.7.6 The D - Q Linearized Model

The linearized model is obtained from the nonlinear one by assuming that the steady state operating point is slightly perturbed. Therefore, the linearized synchronous machine equations in the d - q

axis are obtained from equations 2.29 and 2.30 by taking the first two terms of Taylor series expansion. The linearized equations are,

$$\begin{bmatrix} \Delta e_d \\ \Delta e_q \\ \Delta e_{fd} \\ 0 \\ 0 \end{bmatrix} = [r] \begin{bmatrix} \Delta i_d \\ \Delta i_q \\ \Delta i_{fd} \\ \Delta i_{kd} \\ \Delta i_{kq} \end{bmatrix} + \frac{1}{\omega_0} \frac{d}{dt} \begin{bmatrix} \Delta \psi_d \\ \Delta \psi_q \\ \Delta \psi_{fd} \\ \Delta \psi_{kd} \\ \Delta \psi_{kq} \end{bmatrix} + \begin{bmatrix} -\Delta \psi_q \\ \Delta \psi_d \\ 0 \\ 0 \\ 0 \end{bmatrix} + \begin{bmatrix} -\psi_{q0} \\ \psi_{d0} \\ 0 \\ 0 \\ 0 \end{bmatrix} \Delta \bar{\omega} \tag{2.52}$$

and

$$\begin{bmatrix} \Delta \psi_d \\ \Delta \psi_q \\ \Delta \psi_{fd} \\ \Delta \psi_{kd} \\ \Delta \psi_{kq} \end{bmatrix} = \begin{bmatrix} -X_d & 0 & X_{ad} & X_{ad} & 0 \\ 0 & -X_q & 0 & 0 & X_{aq} \\ -X_{ad} & 0 & X_{ffd} & X_{fkd} & 0 \\ -X_{ad} & 0 & X_{fkd} & X_{kkd} & 0 \\ 0 & -X_{aq} & 0 & 0 & X_{kkq} \end{bmatrix} \begin{bmatrix} \Delta i_d \\ \Delta i_q \\ \Delta i_{fd} \\ \Delta i_{kd} \\ \Delta i_{kq} \end{bmatrix} \tag{2.53}$$

Similarly the linearized mechanical equations are obtained from equations 2.37 and 2.38, and written as;

$$2H \frac{d}{dt} (\Delta \bar{\omega}) = \Delta T_m - \Delta T_e \tag{2.54}$$

$$\frac{d}{dt}(\Delta\delta) = \omega_0 (\Delta\bar{\omega}) \tag{2.55}$$

and from equation 2.17

$$\Delta T_e = \Delta i_q \psi_{d0} + I_{q0} \Delta \psi_d - \Delta i_d \psi_{q0} - I_{d0} \Delta \psi_q \tag{2.56}$$

The linearized D - Q network equations are,

$$\begin{bmatrix} \Delta e_D \\ \Delta e_Q \end{bmatrix} = \begin{bmatrix} r_E & -X_E \\ X_E & r_E \end{bmatrix} \begin{bmatrix} \Delta i_D \\ \Delta i_Q \end{bmatrix} + \frac{1}{\omega_0} \begin{bmatrix} X_E & \\ & X_E \end{bmatrix} \frac{d}{dt} \begin{bmatrix} \Delta i_D \\ \Delta i_Q \end{bmatrix} + \begin{bmatrix} \Delta e_{CD} \\ \Delta e_{CQ} \end{bmatrix} \tag{2.57}$$

and

$$\frac{1}{\omega_0} \frac{d}{dt} \begin{bmatrix} \Delta e_{CD} \\ \Delta e_{CQ} \end{bmatrix} = \begin{bmatrix} X_C & \\ & X_C \end{bmatrix} \begin{bmatrix} \Delta i_D \\ \Delta i_Q \end{bmatrix} + \begin{bmatrix} 0 & 1 \\ -1 & 0 \end{bmatrix} \begin{bmatrix} \Delta e_{CD} \\ \Delta e_{CQ} \end{bmatrix} \tag{2.58}$$

The linearized transformation equation is obtained from 2.31 and has the form :

$$\begin{bmatrix} \Delta e_d \\ \Delta e_q \end{bmatrix} = \begin{bmatrix} \cos\sigma_0 & \sin\sigma_0 \\ -\sin\sigma_0 & \cos\sigma_0 \end{bmatrix} \begin{bmatrix} \Delta e_D \\ \Delta e_Q \end{bmatrix} + \Delta\sigma \begin{bmatrix} -\sin\sigma_0 & \cos\sigma_0 \\ -\cos\sigma_0 & -\sin\sigma_0 \end{bmatrix} \begin{bmatrix} e_{D0} \\ e_{Q0} \end{bmatrix} \tag{2.59}$$

where σ_0 is the steady state angle between the d - q and the synchronously rotating frames D - Q .

e_{D0} and e_{Q0} are the steady state D and Q axes voltages at the generator bus.

Assuming that $\sigma_0 = 0$, which is used throughout this thesis, then,

$$e_{D0} = E_{d0} \quad \text{and} \quad e_{Q0} = E_{q0} \tag{2.60}$$

and from equation 2.45 the following relation is obtained :

$$\Delta \sigma = \Delta \delta \tag{2.61}$$

The D - Q linearized model is obtained by combining equations 2.52, 2.53, 2.54, 2.55, 2.56, 2.57, 2.58, 2.59, 2.60 and 2.61, which results in,

$$\frac{1}{\omega_0}\begin{bmatrix}
-(X_d+X_E) & 0 & X_{ad} & X_{ad} & 0 & 0 & 0 & 0 & 0 \\
0 & -(X_q+X_E) & 0 & 0 & X_{aq} & 0 & 0 & 0 & 0 \\
-X_{ad} & 0 & X_{ffd} & X_{fkd} & 0 & 0 & 0 & 0 & 0 \\
-X_{ad} & 0 & X_{fkd} & X_{kkd} & 0 & 0 & 0 & 0 & 0 \\
0 & -X_{aq} & 0 & 0 & X_{kkq} & 0 & 0 & 0 & 0 \\
 & & & & & 2H\omega_0 & & & \\
 & & & & & & 1 & & \\
 & & & & & & & 1 & \\
 & & & & & & & & 1
\end{bmatrix}\frac{d}{dt}\begin{bmatrix}
\Delta i_D \\ \Delta i_Q \\ \Delta i_{fd} \\ \Delta i_{kd} \\ \Delta i_{kq} \\ \Delta \bar{\omega} \\ \Delta \delta \\ \Delta e_{CD} \\ \Delta e_{CQ}
\end{bmatrix} =$$

$$\begin{bmatrix}
r_a+r_E & -X_q-X_E & & & X_{aq} & A & -B & 1 & \\
X_d+X_E & r_a+r_E & -X_{ad} & -X_{ad} & & B & A & & 1 \\
 & & -r_{fd} & & & X_{ad}I_{q0} & & & \\
 & & & -r_{kd} & & X_{ad}I_{q0} & & & \\
 & & & & -r_{kq} & -X & & & \\
A & B & -X_{ad}I_{q0} & -X_{ad}I_{q0} & X_{aq}I_{d0} & & P_s & & \\
 & & & & & 1 & & & \\
X_C & & & & & & & & 1 \\
 & X_C & & & & & & -1 &
\end{bmatrix}$$

$$\begin{bmatrix} \Delta i_D \\ \Delta i_Q \\ \Delta i_{fd} \\ \Delta i_{kd} \\ \Delta i_{kq} \\ \Delta \bar{\omega} \\ \Delta \delta \\ \Delta e_{CD} \\ \Delta e_{CQ} \end{bmatrix} + \begin{bmatrix} 0 \\ 0 \\ \Delta e_{fd} \\ 0 \\ 0 \\ \Delta T_m \\ 0 \\ 0 \\ 0 \end{bmatrix} \qquad (2.62)$$

where

$$A = \psi_{q0} + X_d I_{q0}$$

$$B = -\psi_{d0} - X_q I_{d0}$$

and

$$P_s = A I_{q0} - B I_{d0}$$

Equation 2.62 is the D - Q linearized model for the system shown in Figure 2.2(a) when per-unit quantities are used. This model will be used in the analysis of the steady state stability in the forthcoming chapters.

Finally, the eigenvalues calculated when the D - Q linearized model is used are the same if the d - q linearized model is used [47]. This is because the real and the imaginary parts of these eigenvalues represent the inverse of the system time constants and the natural frequencies of the same system respectively. These are always unique for a particular system. Moreover, since we are interested in investigating the system stability, therefore, we only assume that the system states are disturbed from their steady state values. This implies that $\Delta T_m = \Delta e_{fd} \equiv 0$ in equation 2.62 .

CHAPTER III

FIELD EXCITATION CONTROL OF UNSTABLE SSR IN SYNCHRONOUS MACHINES

3.1 Introduction

This chapter discusses the feedback loop introduced by Saito et al [17], which suppresses the SSR oscillations via the system field winding. Although, Saito et al [17] have succeeded in solving the problem by field winding control, the principle of how this can be done was not explained.

In this chapter a theory is developed to explain how the SSR can be suppressed by field winding control. Also the use of a control signal formed by a linear combination of the subsynchronous reactive power (Δ Q) and active power (Δ P) instead of that used by [17] (Δ Q only) is explained.

3.2 Synchronous Generator Operation

In synchronous generators [52], the field winding is the source of the magnetic flux. A dc source is connected across the field winding to inject a direct current which creates a constant magnetic flux in the airgap of the machine. The armature windings are connected to the load. When either the armature or the field rotates, voltage is induced

in the armature windings. In synchronous generators,the armature windings are stationary on the stator and the field winding is rotating on the rotor. When current flows in the armature, its windings create a flux component in the airgap. This component interacts with that created by the field winding to produce electromagnetic torque. In a synchronous generator, however, the field and the armature flux components rotate at precisely the same speed (synchronous speed, ω_0). Therefore, the rotating fields of the stator and the rotor are stationary with respect to each other. In this case the resulting torque is time invariant. The torque acts on the rotor in the direction opposite to the rotation of the flux wave in space. In order to keep the rotor revolving in the same direction as the stator flux, an external mechanical torque must be applied to overcome the electromechanical counter torque.

3.3 Rotating Magne-Motive Force (mmf) Phasors

3.3.1 Steady State mmf Phasors

In the steady state operation of synchronous machines, the mmf waves of both the stator and the rotor currents are rotating at synchronous speed in the airgap. These waves are represented in space by phasors characterized by magnitudes and phase angles.

Figure 3.1 shows the mmf phasors of the stator and the rotor currents in the steady state operation of the synchronous machine.

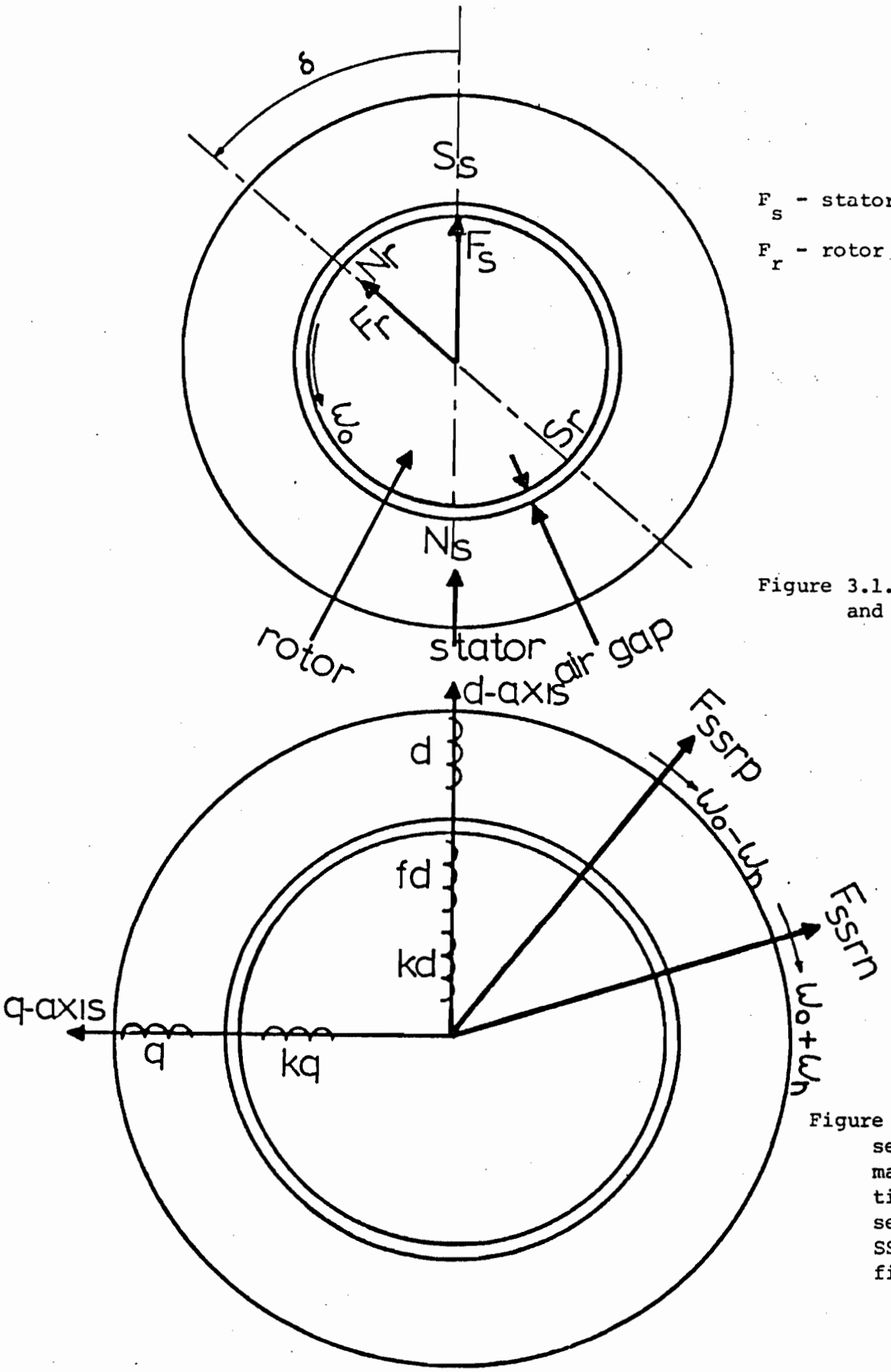

F_s - stator mmf.

F_r - rotor mmf.

Figure 3.1. Steady state stator and rotor mmf phasors.

Figure 3.2. d-q axis representation of synchronou machine showing the pos tive and the negative sequence components of SSR airgap magnetic fields.

The magnitudes of these phasors, at a given instant of time, are proportional to the peaks of the sinusoidally distributed mmf waves. By definition, the angular positions of these phasors coincide with the positions of the positive peaks of the sinusoidally distributed mmf waves. Assuming that the machine is rotating counterclockwise, then the positive direction of the speed ω_0 and the torque angle δ defined in Figure 3.1 are consistent. The electromagnetic counter torque acting on the rotor is given by the vector cross product of the two space phasors in Figure 3.1, or mathematically:

$$T_e = - F_s F_r \sin \delta \tag{3.1}$$

The negative sign comes from the assumption of generator action where the rotor flux is leading the stator flux in the direction of motion due to the application of the mechanical torque before inducing armature current.

The south and north poles are assigned along the mmf phasor axes, as shown in Figure 3.1, due to the fact that the magnetic flux emanates from the north poles. Using the physical notation that unlike magnetic poles attract the attraction of rotor magnetic poles by the stator magnetic poles for the positive torque angle δ , as defined in Figure 3.1, gives rise to a negative countertorque which is consistent with the negative sign in equation 3.1. Thus, interpreting from equation 3.1, the generating and motoring regimes are defined as:

(i) Generating regime corresponds to

$$0^{\circ} < \delta < 180^{\circ} \qquad (3.2)$$

(ii) Motoring regime corresponds to

$$180^{\circ} < \delta < 360^{\circ} \qquad (3.3)$$

3.3.2 Subsynchronous Resonance mmf Phasors

The synchronous generator under consideration is connected to the load through a long transmission line. When series capacitors are used for compensation, under disturbances, currents due to the resonance in the series L - C circuit flow in the stator winding of the generator. The frequency of these currents is ω_n electrical r/s as explained in Section 1.2.1 of Chapter I . In general, these currents are not balanced. When these currents flow in the stator windings of the generator, they produce mmf waves in the airgap. For balanced three-phase stator windings with a pronounced fundamental mmf space harmonic, the magnetic field produced by the unbalanced resonant currents can be resolved into three mmf space phasors, the zero sequence F_{ssro}, the positive sequence F_{ssrp}, and the negative sequence F_{ssrn} . The zero sequence component does not exist. The positive and negative sequence component phasors rotate at ω_n electrical r/s in the forward and backward directions respectively. The series capacitor compensation is designed so that ω_n is always less

than the machine synchronous speed ω_0 electrical r/s, i.e., $\omega_0 > \omega_n$. The d - q axis is fixed on the rotor and rotating at ω_0 in the steady state. Thus, as viewed in the d - q representation of the synchronous machine, the positive and negative sequence phasors F_{ssrp}, F_{ssrn} are rotating backwards at speeds of $\omega_0 - \omega_n$ and $\omega_0 + \omega_n$ respectively as shown in Figure 3.2. The electromagnetic induction action of these mmf phasors with the rotor windings are characterized by their slips as follows:

$$F_{ssrp} \quad \text{slip} \quad s_p = (\omega_n - \omega_0) / \omega_n \tag{3.4}$$

$$F_{ssrn} \quad \text{slip} \quad s_n = (\omega_0 + \omega_n) / \omega_n \tag{3.5}$$

The rotor interaction with the negative sequence mmf F_{ssrn} is one of induction braking, since $s_n > 1.0$. As viewed in the induction machine equivalent circuit, the rotor resistance is (R_2 / s_n), which is positive and in consequence this mode is positively damped. The synchronous machine behaves as an induction generator to the positive sequence component F_{ssrp}, i.e., the rotor looks as a negative resistance when viewed by this component. Therefore, if the net resistance in the path of the positive sequence component is negative, then regeneration action occurs and this component will grow exponentially in time. This is well known as the induction generator action which is the basis for unstable SSR oscillation.

3.4 How SSR can be Suppressed by Field Excitation Control

The positive sequence subsynchronous currents, which flow in the three-phase stator windings, create a magnetic flux wave in the airgap which rotates at an angular velocity ω_n, which is less than the rotor synchronous speed ω_0. Due to the rotation of the machine rotor, currents are induced in the rotor circuits at a slip frequency of $\omega_0 - \omega_n$. These currents, once again, create a rotor flux wave rotating in the airgap at a speed of ω_n. If the rotor is purely inductive, the angle δ, between the two waves, is 180°. When the rotor is both inductive and resistive, as is the practical case, $90^\circ < \delta < 180^\circ$ electrical. The stator and rotor field waves at subsynchronous resonance frequency are stationary in space with respect to each other. Therefore, to construct a phasor diagram of these waves similar to that in Figure 3.1, the induction generation action is assumed to be just sufficient to sustain oscillatory positive SSR mode. Then the positive sequence SSR mmf phasor F_{ssrp}, and the mmf phasor created by the induced rotor currents F_r, can be related in space as shown in Figure 3.3, where the two phasors are rotating backwards at a speed of $\omega_0 - \omega_n$ with respect to the d - q axis and the torque angle between them is a constant obtuse angle ($90^\circ < \delta < 180^\circ$). From equation 3.1, the shaft torque is an electromechanical counter torque and mechanical power is converted to electrical power to sustain the growth of SSR oscillations.

The idea of damping SSR is to reverse the direction of power flow, i.e., the electrical energy should be converted to mechanical power

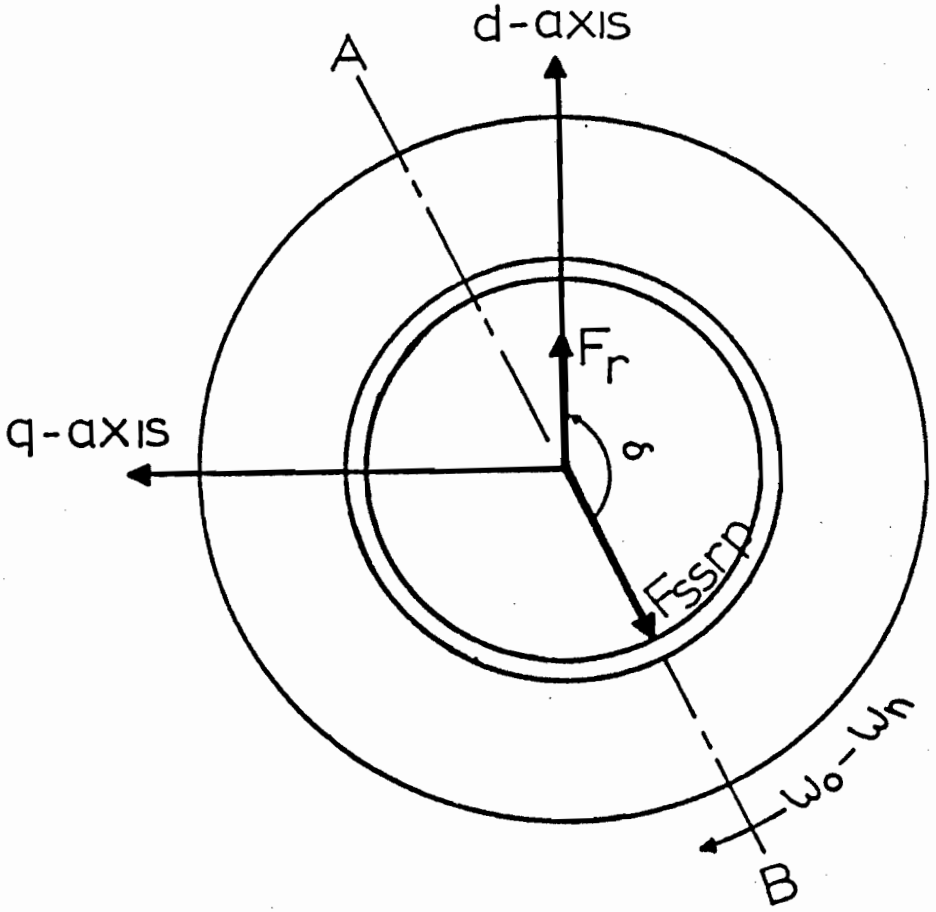

Figure 3.3. Positive sequence SSR mmf diagram showing generating regime where δ is an obtuse angle.

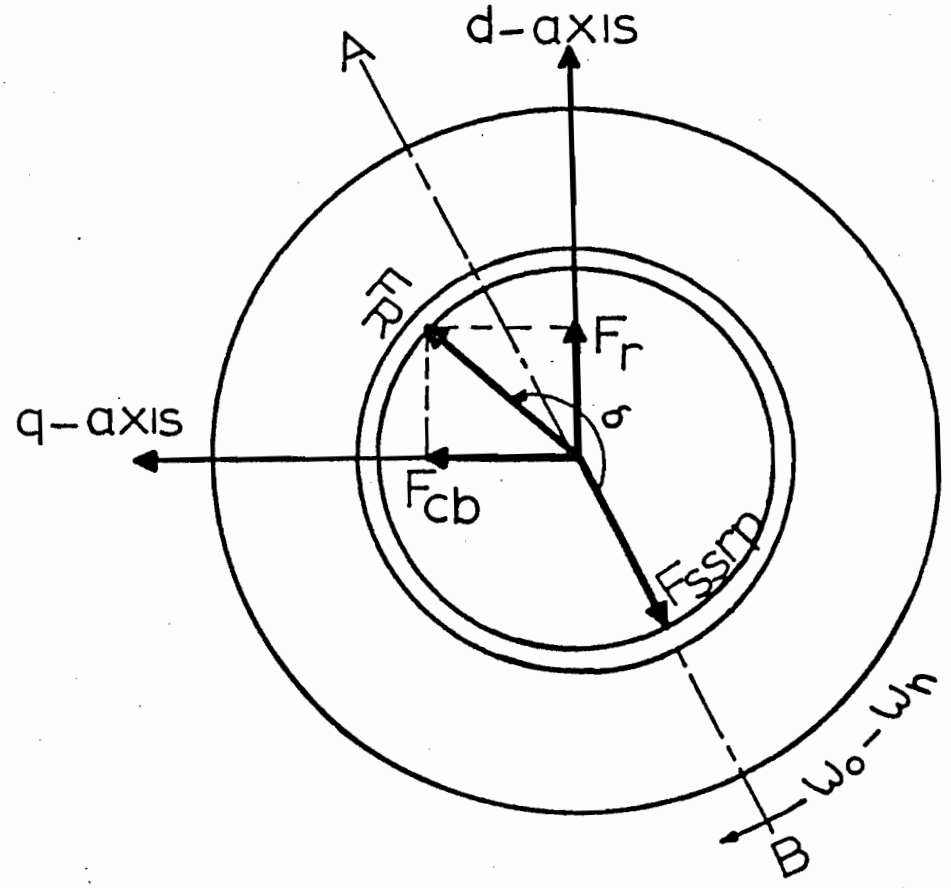

Figure 3.4. The resultant mmf vector diagram after field injection showing motoring regime where δ is a reflex angle.

and absorbed by the shaft. This can be achieved by injecting a rotor flux component F_{cb}, rotating in the airgap at a speed of ω_n. The resultant rotor mmf phasor is F_R, the phasor sum of F_{cb} and F_r as shown in Figure 3.4. This resultant mmf phasor F_R is stationary with respect to the rotating F_{ssrp} and the angle δ, measured from F_{ssrp} in the direction of motion, is $180^o < \delta < 360^o$. The resultant shaft torque is the cross product of F_{ssrp} and F_R (or equivalently the algebraic sum of the cross products of F_{ssrp} with F_r and F_{ssrp} with F_{cb}). If this is a motoring torque, then the electrical power is drawn from the series L - C resonance in the transmission line and converted to mechanical power at the shaft, resulting in the SSR oscillations being positively damped.

3.5 Field Winding Excitation of F_{cb}

As mentioned in Section 3.2, the field winding always has its main dc excitation. However, during SSR the field winding has an additional current that oscillates at a slip frequency of $\omega_0 - \omega_n$. The magnetic field of this additional current is included in F_r of Figure 3.3. We concern ourselves in this section as to how the mmf F_{cb} can be introduced into the airgap so that the resultant F_R from the addition of F_{cb} to F_r, is shifted into the motoring regime. Note that this can be accomplished only when F_{cb} rotates at the same speed as F_r. As the

subsequent paragraph shows, F_{cb} is produced by injecting an ac current at an angular frequency of $\omega_0 - \omega_n$ r/s into the field winding.

The dc excitation current in the field winding creates a time invariant magnetic flux wave in the airgap, which is distributed sinusoidally with space angle around the airgap. When the oscillatory current at an angular frequency of $\omega_0 - \omega_n$ is injected in the field winding, its magnetic flux wave is a standing wave F_c. The mmf phasor representing it is sinusoidally varying with time, but the space angle of the wave is fixed along the d - axis. As is well known in single-phase ac motor theory [52], the mmf phasor F_c can be resolved into two phasors F_{cf} and F_{cb}, rotating forward and backward at absolute speeds of $2\omega_0 - \omega_n$ and ω_n respectively. In the d - q axis representation, the two components are counter rotating at the same speed of $\omega_0 - \omega_n$ as shown in Figure 3.5.

3.5.1 Feedback Signals of F_{cb}

One of the important properties of F_{cb} is that its speed should be ω_n electrical r/s. Hence, the frequency of the excitation current, necessary to produce F_{cb}, should be $\omega_0 - \omega_n$ as shown in Figure 3.4. This can be obtained from any of the following signals:

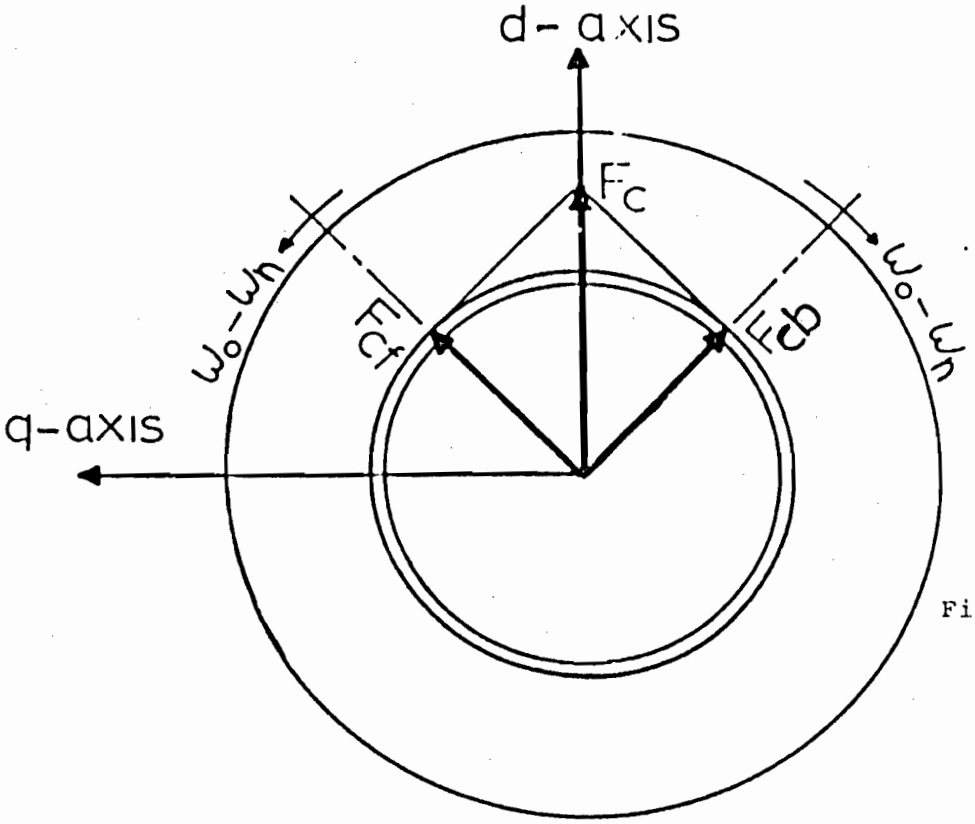

Figure 3.5. Oscillating mmf vector F_c resolved into forward and backward components.

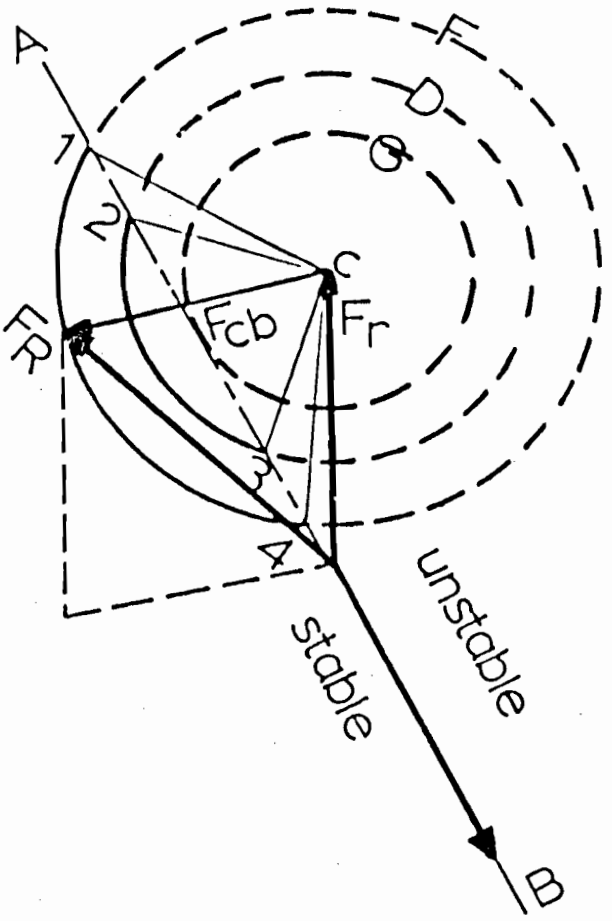

Figure 3.6. Controllable sectors as a function of the magnitude of F_{cb}.

(i) The reactive and active powers Q and P respectively contain a component at frequency $\omega_0 - \omega_n$. This results from the product of the steady state and the subsynchronous components of the line voltages and currents.

(ii) The field and amortisseur windings currents, since SSR induces a current component at the frequency of $\omega_0 - \omega_n$.

(iii) The shaft speed has a component of $\omega_0 - \omega_n$ produced by the pulsating torque.

3.5.2 F_{cb} Magnitude and Phase Requirement

Let us consider the line AB in Figure 3.6 as the theoretical stability line which separates the motoring and generating regimes. Thus, for stability F_R should be to the left of AB in the direction of motion. However, to be able to shift F_R to the left of AB, F_{cb} should have the proper magnitude and space angle.

The importance of F_{cb} magnitude on the system stability can be explained from Figure 3.6. Circles F, D and G in Figure 3.6 represent different F_{cb} magnitudes and F_r, F_s are the subsynchronous mmf phasors in the induction action. The line AB intersects circles

D and F at 2, 3 and 1, 4 respectively. For stability the arrow tip of F_R, which results from the vector sum of F_{cb} and F_r, should be on the solid arc 2-3 or 1-4. Thus, if F_{cb} has a magnitude equal to the radius of circle G, the system will be unstable irrespective of the phase of F_{cb}. This is because the vector sum of F_r and F_{cb} will result in a phasor F_R with the arrow tip on the dashed arc, that is the torque angle is obtuse and a generation action is obtained. Whereas if F_{cb} magnitude is equal to the radius of the circle D or the radius of the circle F, the system will be stable if F_{cb} falls in the angle $\hat{2c3}$ or $\hat{1c4}$ respectively.

The other requirement for shifting F_R into the motoring regime is the proper choice of the space angle of F_{cb}. From Figure 3.4 it is clear that F_{cb} should always lag F_r in the direction of motion. This can be achieved by controlling the angle of the control signal injected in the field winding. The possibility of controlling the space angle of F_{cb} will be explained in more detail in Section 3.6.2 .

3.6 Control Scheme

The feedback loop used for SSR suppression in this study is shown in Figure 3.7. It consists of a transducer to detect the presence of SSR oscillation and a filter which admits signals at subsynchronous frequency and gives the control signal the proper phase and magnitude.

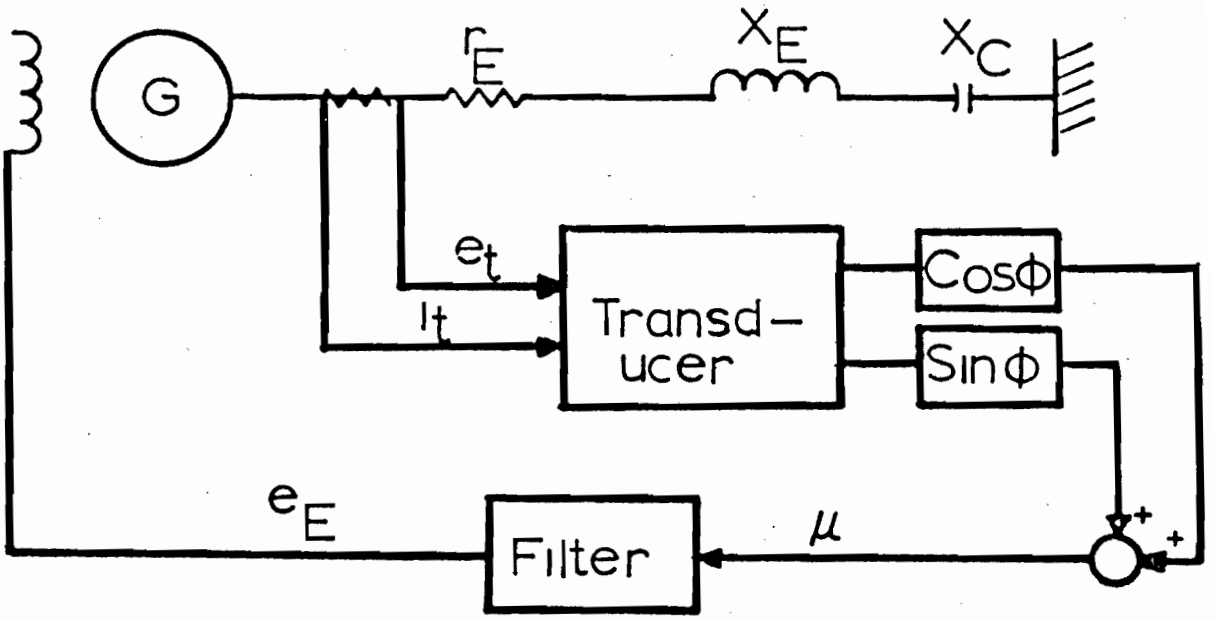

Figure 3.7. Feedback scheme for the suppression of SSR oscillations.

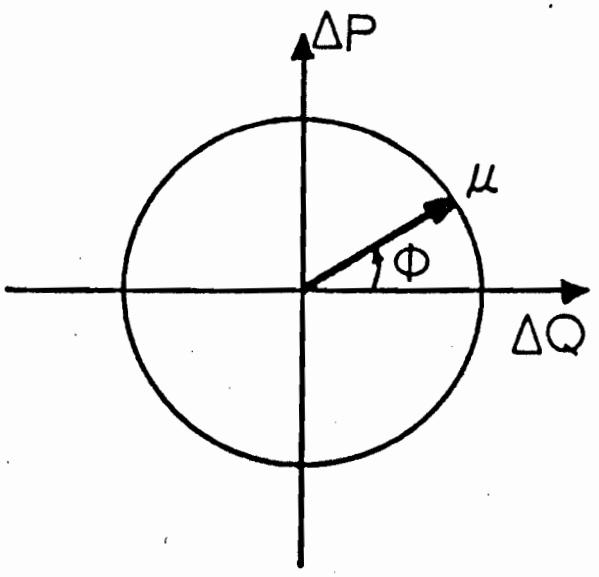

Figure 3.8. Δ P - Δ Q plane showing the rotation of the control signal μ .

3.6.1 Choice of Control Signal

From the different signals discussed previously a combination between the active and reactive powers P and Q respectively is used for the following reasons:

(i) The real (ΔP) and the reactive (ΔQ) powers contain the requisite feedback frequency $(\omega_0 - \omega_n)$. F_{cb} generated from these signals will always have the same speed as F_r.

(ii) The reactive power component at the frequency $(\omega_0 - \omega_n)$ lags the real power in time by 90°. Furthermore, their magnitudes are approximately the same. By combining these two signals, F_{cb} in Figure 3.6 can be varied in magnitude and space angle with respect to F_r. Their linear combination allows for maximum flexibility in design.

(iii) The virtue of using feedback signals based on detecting the SSR frequency is dependent on the degree of the series capacitor compensation. During faults and network topological changes, the SSR frequency is altered. However, the feedback system as conceived is adaptive in tracking the frequency changes.

3.6.2 Reactive and Active Power Transducer

The reactive power meter and the active power meter (wattmeter) which record the product of line current and voltage, give the steady state values of the active and reactive powers, P_0 and Q_0 respectively, and the transient powers at frequency of $\omega_0 - \omega_n$. Mathematically:

$$P = e_D i_D + e_Q i_Q \tag{3.6}$$

$$Q = e_Q i_D - e_D i_Q \tag{3.7}$$

From equations 3.6 and 3.7 the steady state reactive and active powers Q_0 and P_0 are :

$$P_0 = E_{d0} I_{d0} + E_{q0} I_{q0} \tag{3.8}$$

$$Q_0 = E_{q0} I_{d0} - E_{d0} I_{q0} \tag{3.9}$$

and the small perturbation power signals, ΔQ and ΔP, are:

$$\begin{bmatrix} \Delta Q \\ \Delta P \end{bmatrix} = \begin{bmatrix} -I_{q0} & I_{d0} \\ I_{d0} & I_{q0} \end{bmatrix} \begin{bmatrix} \Delta e_D \\ \Delta e_Q \end{bmatrix} + \begin{bmatrix} E_{q0} & -E_{d0} \\ E_{d0} & E_{q0} \end{bmatrix} \begin{bmatrix} \Delta i_D \\ \Delta i_Q \end{bmatrix} \tag{3.10}$$

The proposed control signal μ can be expressed as

$$\mu = K_1 \Delta Q + K_2 \Delta P \tag{3.11}$$

where K_1 and K_2 any arbitrary constants.

ΔP leads ΔQ by 90°, therefore, at subsynchronous frequency:

$$\mu = K_1 \cos (\omega_0 - \omega_n) t + K_2 \sin (\omega_0 - \omega_n) t$$

or

$$\mu = K_{12} \cos [(\omega_0 - \omega_n) t - \phi] \tag{3.12}$$

where

$$K_{12} = \sqrt{K_1^2 + K_2^2} \quad , \quad \phi = \tan^{-1} \frac{K_2}{K_1}$$

When μ is passed through the filter, the magnitude K_{12} is multiplied by the gain filter at $\omega_0-\omega_n$ and the angle ϕ is shifted by the filter angle at $\omega_0-\omega_n$. If the constant K_{12} is included in the filter gain, then equation 3.12 can be expressed as :

$$\mu = \sin \phi \ \Delta P + \cos \phi \ \Delta Q \tag{3.13}$$

From equation 3.13 the new combination between ΔQ and ΔP is to multiply the first by cos ϕ and the second by sin ϕ where ϕ is constant .

Equation 3.13 can be explained by the help of Figure 3.8, where the horizontal axis is assumed to be ΔQ and the vertical is ΔP,

since ΔP leads ΔQ by 90 electrical degrees. From Figure 3.7 the injected signal into the field winding (e_E) has the same frequency as μ which is the required frequency $\omega_0 - \omega_n$, and its phase angle is the algebraic sum of the filter angle calculated at $\omega_0 - \omega_n$ and the control angle ϕ. Therefore, the phase angle of e_E (and hence the space angle of F_{cb}) can be controlled by the angle ϕ, since the filter phase angle is constant. This indicates that by changing ϕ the space angle F_{cb} can be rotated over a complete cycle. Therefore, any required space angle of F_{cb} can be obtained by a proper choice of the control angle ϕ. Furthermore,without using the combination of ΔP and ΔQ the only variable parameter by which the feedback loop can be adjusted to achieve stability is the filter gain. By introducing the control angle ϕ, another variable parameter is added; that is, another degree of freedom can be used to achieve stability. The implementation of the angle ϕ is passing ΔP and ΔQ into ideal amplifiers with gains $\cos\phi$ and $\sin\phi$ as shown in Figure 3.7 .

3.6.3 Filter

The combined outputs of the ideal amplifiers are passed through a filter. This filter should discriminate between the dc and the required transient signals. In the steady state operation, the output signal from the filter should be zero. At subsynchronous frequency, the filter should amplify the control signal to the proper magnitude.

Finally, the feedback loop should inject F_{cb} with suitable magnitude and phase into the airgap of the synchronous generator whenever the subsynchronous resonance is detected. The filter gain and the control angle ϕ should be adjusted at the subsynchronous frequency to ensure that F_{cb} falls in the controllable sectors of Figure 3.6. The verification of this theory will be shown in Chapter IV by using eigenvalues to examine the stability of the system shown in Figure 2.2(a) with and without the feedback loop.

CHAPTER IV

SSR OSCILLATION IN UNREGULATED SYNCHRONOUS MACHINE - A SMALL PERTURBATION STUDY

4.1 Introduction

The purpose of this chapter is to demonstrate the validity of the theory introduced in Chapter III, using a numerical example of the system configuration shown in Figure 2.2(a). The concepts which have been explained in the previous chapter of how SSR can be suppressed by field excitation control, are confirmed one at a time.

For the sake of simplicity, the synchronous generator is assumed to be under constant excitation, i.e., the excitation system is neglected. Furthermore, the governor system is neglected as it will be the case throughout this thesis. However, the effects of the excitation system and any other supplementary loop will be considered in the next chapter.

The reason for this simplification is to give a deep understanding to the SSR suppression by field excitation control. In addition, this simplification is part of a step by step approach adopted in this thesis to fully explain the effect of the SSR phenomenon and its control, as it will be shown in the next chapter.

In the analysis, the system is assumed to be slightly perturbed from its steady state operation. Therefore, the linearized mathematical model described by equation 2.62 is used.

The eigenvalues and eigenvectors [53] technique is used in the analysis of the system stability. Instability is judged to be the case when the real part of any eigenvalue is positive. Eigenvectors are used to construct the SSR mmf phasor diagram (Figure 3.4) and to classify the different eigenvalues.

The effectiveness of the feedback loop under different operating points as well as the variation of the different modes with the filter gain and the control angle ϕ are shown.

4.2 Eigenvalues and Eigenvectors

The linearized model of the system of Figure 2.2(a) is described by equation 2.62 and it is written here as:

$$\frac{1}{\omega_0} [D] \frac{d}{dt} \underline{X} = [F] \underline{X} + \underline{U} \tag{4.1}$$

where $\underline{X}$ is the state variable vector which contains the perturbations in the currents, speed, angle and the series capacitor voltages. [F] and [D] are the constant matrices in equation 2.62, and for stability analysis the forcing function $\underline{U}$ is not perturbed. Therefore, equation 4.1 can be written in the general time-invariant state space form as:

$$\frac{d}{dt} \underline{X} = [A] \underline{X} \tag{4.2}$$

where $[A] = \omega_0 [D]^{-1} [F]$

Eigenvalues are defined by the singularity of the characteristic matrix $[\lambda I - A]$, i.e., the eigenvalues of matrix $[A]$ are those satisfying the following equation:

$$\det [\lambda I - A] = 0 \tag{4.3}$$

where λ denotes the unknown eigenvalues.

The technique used to calculate the eigenvalues of matrix $[A]$ is by similarity transformation which results in a diagonal matrix whose elements are the eigenvalues of $[A]$, mathematically:

$$[\lambda] = [P] [A] [R] \tag{4.4}$$

$[\lambda]$ is the eigenvalues matrix, and the columns of matrix $[P]$ are the eigenvectors. The transformation in equation 4.4 has the following property:

$$[R] = [P]^{-1} \tag{4.5}$$

Each eigenvector $\underline{v}_i$ is associated with each eigenvalue λ_i such that:

$$[A] \underline{v}_i = \lambda_i \underline{v}_i \tag{4.6}$$

matrix $[P]$ has the form:

$$[P] = [\underline{v}_1 \quad \underline{v}_2 \quad \underline{v}_3 \quad \cdots\cdots\cdots \quad \underline{v}_n] \tag{4.7}$$

where n is the dimension of the square matrix $[A]$.

In this thesis the eigenvalues are assumed to be distinct as in fact they are. Therefore, the eigenvectors associated with these eigenvalues are linearly independent.

From equation 4.6, it is clear that the components of the eigenvector $\underline{v}_i$ are the solutions to the system of n linear homogeneous algebraic equations, relating the n state variables defined by vector $\underline{X}$ for the eigenvalue λ_i . The determinant of the coefficient matrix of these equations is zero, thus, they have to be reduced by one. Therefore, the components of the eigenvector $\underline{v}_i$ are the state variables weighted in such a way as to reflect the content of the mode λ_i in each state variable . This property of the eigenvectors is useful in classifying the eigenvalues, as it is followed from [47] .

4.2.1 Eigenvalues and Eigenvectors Subroutine

Eigenvalues and eigenvectors of the matrix [A] are calculated numerically using a subroutine, called EIGRE, available at McGill University computer library. The subroutine is in the IMSL Library 1 Fortran IV IBM System / 370-360.

4.3 Numerical Example

The calculations carried out in this chapter are organized as follows:

(i) Eigenvalues are calculated for the case when the synchronous generator is connected to the infinite bus bar through an uncompensated transmission line, i.e., $X_C = 0.0$.

(ii) The eigenvalues and sometimes the eigenvectors are calculated for the case of a series capacitor compensated transmission line (Figure 2.2(a)) for two values of X_C . One, at which unstable SSR oscillation does not occur, i.e., the system is stable. The other, at which unstable SSR oscillation occurs, i.e., unstable system.

(iii) The feedback loop of SSR suppression is added to the system in a manner described in Figure 3.7, and the eigenvalues are calculated for different combinations of the control angle ϕ and the filter gain.

The system parameters, used in the calculations in this chapter, are those of the laboratory machine used by Saito et al [17]. This is used in this chapter to check the results with the experimental

data obtained by [17] . However, for a more realistic analysis, the parameters of the 10 GVA system of [17] will be used in the following chapters.

For the experimental system [17], the power delivered to the infinite bus bar is assumed to be 0.15 per-unit (0.15 p.u.), and the infinite bus bar voltage is assumed to be constant and equal to 1.0 p.u. In addition, the steady state voltages and currents are calculated from the steady state vector diagram shown in Figure 2.2(c) using the above values of the infinite bus bar voltage and power.

4.3.1 Open Loop System

The system without any feedback loop to suppress the unstable SSR oscillations is referred to as the open loop system. The laboratory machine parameters used in this chapter are listed in Appendix B-1 .

The seven eigenvalues for the case of an uncompensated transmission line ($X_C = 0.0$) is shown in Table 4.1(a). The eigenvalues are identified as follows [47] :

λ_{stator}	stator currents mode,
$\lambda_{mech.}$	mechanical mode,
$\lambda_{amort.}$	amortisseur mode,
λ_{field}	field winding mode.

TABLE 4.1

(a) Eigenvalues for the case of uncompensated transmission line. (Unregulated Machine).

	λ_{stator}	$\lambda_{mech.}$	$\lambda_{amort.}$	λ_{field}
Eigen-values	$-60.5 \pm j\ 376.$	$-1.72 \pm j\ 13.3$	$-27.7 \pm j\ 1.18$	-1.56

(b) Eigenvalues for the case of compensated transmission line, when $X_C = 0.092$ (Unregulated Machine).

	λ_{ssrn}	λ_{ssrp}	$\lambda_{mech.}$	$\lambda_{amort.}$	λ_{field}
Eigen-Values	$-32.8 \pm j\ 677.$	$-6.78 \pm j\ 73.1$	$-4.90 \pm j\ 17.6$	-42.7 -42.9	-2.32

For the case of a series capacitor compensated transmission line, the two values of the series capacitive reactance X_C are used. Table 4.1(b) shows the eigenvalues when the first value of X_C = 0.092 p.u. is used. The system is stable for this value and the stator currents mode is now resolved into two modes, defined here as:

λ_{ssrn} SSR negative sequence mode,

λ_{ssrp} SSR positive sequence mode.

The SSR negative sequence mode is identified by the large damping and it rotates at a supersynchronous speed of $\omega_0 + \omega_n$, where ω_0 is constant at 377 electrical r/s and ω_n can be calculated from equation 1.1 for X_C = 0.092 p.u. as:

$$\omega_n = \sqrt{\frac{0.092}{0.132 + 0.0112}} * 377 = 302.2 \text{ electrical r/s} \quad (4.8)$$

where 0.132 p.u. is the value of the negative sequence reactance X_2 and 0.0112 p.u. is the value of the line inductive reactance X_E, both values are taken from Appendix B-1 .

The SSR positive sequence mode rotates at a subsynchronous speed of $\omega_0 - \omega_n$ and has low damping. The system is stable because the net effective resistance in the path of the SSR positive sequence current is still positive.

Using the other value of the series capacitive reactance $X_C = 0.107$, which is higher than 0.092 p.u., the system is now unstable as is clear from the eigenvalues of Table 4.2. Instability is due to the positive real part of the SSR positive sequence mode λ_{ssrp} . This implies that at this new value of X_C the net effective resistance in the path of the SSR positive sequence current is now negative. This is known as the induction generation effect and this instability is due to unstable SSR oscillations as it was explained in Chapter I . Furthermore, the frequency of λ_{ssrp} , as shown in Table 4.2, is 54.83 r/s or 8.72 Hz which agrees with the experimental results obtained by [17] .

4.3.2 Closed Loop System

The closed loop system under study is shown in Figure 3.7. The feedback signal taken from real and reactive power transducers is fedback directly to the field winding.

The transfer function of the filter (NDS) used is the same as that given by Saito et al [17], where the values of its time constants are listed in Appendix B-1. The control signal μ , in our study,is taken as the combination of the reactive power ΔQ and the active power ΔP . In contrast, the control signal used by [17] is ΔQ only. Mathematically, μ can be written as:

$$\mu = \Delta Q \cos\phi + \Delta P \sin\phi \tag{4.9}$$

Substituting equation 3.10 into 4.9 we get:

$$\mu = \begin{bmatrix} E_{q0} \\ -E_{d0} \end{bmatrix}^T \begin{bmatrix} \Delta i'_D \\ \Delta i'_Q \end{bmatrix} + \begin{bmatrix} -I_{q0} \\ I_{d0} \end{bmatrix}^T \begin{bmatrix} \Delta e'_D \\ \Delta e'_Q \end{bmatrix} \tag{4.10}$$

where

$$\begin{bmatrix} \Delta i'_D \\ \Delta i'_Q \end{bmatrix} = \begin{bmatrix} \cos\phi & \sin\phi \\ -\sin\phi & \cos\phi \end{bmatrix} \begin{bmatrix} \Delta i_D \\ \Delta i_Q \end{bmatrix}, \quad \begin{bmatrix} \Delta e'_D \\ \Delta e'_Q \end{bmatrix} = \begin{bmatrix} \cos\phi & -\sin\phi \\ \sin\phi & \cos\phi \end{bmatrix} \begin{bmatrix} \Delta e_D \\ \Delta e_Q \end{bmatrix} \tag{4.11}$$

and E_{q0}, E_{d0}, I_{q0}, I_{d0} are defined in Section 2.7.5.

The closed loop system cannot be represented by the state space form similar to equation 4.2, unless the NDS is modelled by a set of first order differential equations. This can be done on the basis of equation B-2.4 given in Appendix B-2. Therefore, the state space model of the NDS is :

$$\frac{d}{dt} \begin{bmatrix} x_1 \\ x_2 \\ x_3 \end{bmatrix} = \begin{bmatrix} -a_1 & 1 & 0 \\ -a_2 & 0 & 1 \\ -a_3 & 0 & 0 \end{bmatrix} \begin{bmatrix} x_1 \\ x_2 \\ x_3 \end{bmatrix} + \begin{bmatrix} b_1 \\ 0 \\ 0 \end{bmatrix} \mu \tag{4.12}$$

where

$$a_1 = \frac{T_{ND1*}\ T_{ND2} + T_{ND3*}\ T_{ND2} + T_{ND1*}\ T_{ND3}}{T_{ND1}\ T_{ND2}\ T_{ND3}}$$

$$a_2 = \frac{T_{ND1} + T_{ND2} + T_{ND3}}{T_{ND1}\ T_{ND2}\ T_{ND3}}$$

$$a_3 = \frac{1}{T_{ND1}\ T_{ND2}\ T_{ND3}}$$

and

$$b_1 = K_{ND}\ T_{ND1}\ T_{ND2}$$

where the values of the time constants, T_{ND1}, T_{ND2}, T_{ND3} and the gain K_{ND} are given in Appendix B-1 .

The output voltage of the NDS Δe_E is:

$$\Delta e_E = a_3 x_1 \tag{4.13}$$

this voltage appears across the field winding under any disturbance. Therefore, the perturbation field voltage, Δe_{fd}, is now different from zero, which is not the case in the open loop system. However, Δe_{fd} is expressed in terms of the NDS state variables as:

$$\Delta e_{fd} = (r_{fd} / X_{ad})\ a_3 x_1 \tag{4.14}$$

where X_{ad}, r_{fd} are given in Appendix B-1 .

The state space model of the closed loop system can be obtained by combining equations 4.1, 4.12 and 4.14, which results in:

$$\begin{bmatrix} [D_{11}] & [D_{12}] \\ [D_{21}] & [D_{22}] \end{bmatrix} \frac{d}{dt} \begin{bmatrix} \underline{i} \\ \underline{x} \end{bmatrix} = \begin{bmatrix} [F_{11}] & [F_{12}] \\ [F_{21}] & [F_{22}] \end{bmatrix} \begin{bmatrix} \underline{i} \\ \underline{x} \end{bmatrix} + \begin{bmatrix} [B_1] \\ [B_2] \end{bmatrix} \mu \qquad (4.15)$$

where

$[D_{11}]$ is $\frac{1}{\omega_0}[D]$ from equation 4.1,

$[D_{12}]$ is a zero 9 * 3 matrix,

$[D_{22}]$ is a 3 * 3 identity matrix,

$[D_{21}]$ is a zero 3 * 9 matrix,

$[F_{11}]$ is matrix [F] in equation 4.1,

$[F_{12}]$ is a 9 * 3 matrix and equal to ,

$$\begin{bmatrix} 0 & 0 & d_1 & 0 & \dots & 0 \\ 0 & 0 & 0 & 0 & \dots & 0 \\ 0 & 0 & 0 & 0 & \dots & 0 \end{bmatrix}^T , \quad d_1 = a_3 \frac{r_{fd}}{x_{ad}}$$

$[F_{21}]$ is a zero 3 * 9 matrix,

$[F_{22}]$ is the 3 * 3 coefficient matrix on the right hand side of equation 4.12,

$[B_1]$ is a zero 9 * 1 matrix,

$[B_2]$ is a 3 * 1 matrix, equal to $[b_1 \quad 0 \quad 0]^T$,

$$\underline{i} = [\Delta i_D \; \Delta i_Q \; \Delta i_{fd} \; \Delta i_{kd} \; \Delta i_{kq} \; \Delta \bar{\omega} \; \Delta \delta \; \Delta e_{CD} \; \Delta e_{CQ}]^T,$$

$$\underline{x} = [x_1 \; x_2 \; x_3] . \qquad (4.16)$$

From equations 4.10 and 4.11, the control signal μ can be expressed in terms of the state variables Δi_D , Δi_Q, Δe_{CD} and Δe_{CQ}. Therefore, equation 4.15 can be written in a form similar to equation 4.1.

The closed loop system is of twelfth order, with two additional parameters, the gain of the NDS filter K_{ND}, and the control angle ϕ . To calibrate the results obtained from the present analysis with that obtained by [17], the control angle ϕ is assumed to be zero which means that the control signal μ is now the same as that used in [17] and equal to ΔQ only.

Table 4.3 shows the eigenvalues and eigenvectors of the closed loop system for the other value of the series capacitive reactance (X_C = 0.107 p.u.) at which the open loop system is unstable. The closed loop system is now stable and the three additional eigenvalues are defined as the NDS mode λ_{NDS} .

The eigenvalues in Table 4.2 and Table 4.3 are calculated for the same values of line resistance and series capacitive reactance r_E and X_C respectively, where the value of r_E is that given in Appendix B-1. However, these two parameters vary as the transmission lines are

TABLE 4.2.

EIGENVALUES AND EIGENVECTORS FOR X_C = 0.107 (UNREGULATED MACHINE).

	λ_{ssrn}		λ_{ssrp}		$\lambda_{mech.}$		$\lambda_{amort.}$		λ_{field}
Eigen-Values	-33.8 + j 701.	-33.8 - j 701.	+2.32 + j 54.8	+2.32 - j 54.8	-6.90 + j 18.1	-6.90 - j 18.1	-51.7 + j 4.11	-51.7 - j 4.11	-2.51
Eigenvectors Δi_D	0.834	0.834	2.37	2.37	0.39	0.390	3.80	3.80	7.90
	0.0420	-.0420	-33.2	33.2	-58.9	58.9	-75.1	75.1	180.
Δi_Q	0.834	0.834	2.55	2.55	1.75	1.75	5.25	5.25	0.138
	90.2	-90.2	64.1	-64.1	45.8	-45.8	173.	-173.	0.0
Δi_{fd}	0.257	0.257	0.901	0.901	0.244	0.244	0.288	0.288	7.73
	-2.06	2.06	-52.4	52.4	-85.5	85.5	-98.2	98.2	180.
Δi_{kd}	0.507	0.507	1.35	1.35	0.214	0.214	3.47	3.47	0.103
	1.43	-1.43	-16.3	16.3	-6.44	6.44	-72.5	72.5	0.0
Δi_{kq}	0.542	0.542	1.55	1.55	1.05	1.05	5.13	5.13	0.0148
	91.6	-91.6	81.6	-81.6	97.1	-97.1	175.	-175.	180.
$\Delta \bar{\omega}$	0.000126	0.000126	0.00490	0.00490	0.00955	0.00955	0.0106	0.0106	0.00127
	176.	-176.	156.	-156.	115.	-115.	178.	-178.	180.
$\Delta \delta$	0.000067	0.000067	0.0336	0.0336	0.185	0.185	0.0765	0.0765	0.191
	84.0	-84.0	68.2	-68.2	3.74	-3.74	3.05	-3.05	0.0

TABLE 4.2 (cont'd)

	λ_{ssrn}		λ_{ssrp}		$\lambda_{mech.}$		$\lambda_{amort.}$		λ_{field}
Eigen-	-33.8	-33.8	+2.32	+2.32	-6.90	-6.90	-51.7	-51.7	-2.51
Values	+	-	+	-	+	-	+	-	
	j 701.	j 701.	j 54.8	j 54.8	j 18.1	j 18.1	j 4.11	j 4.11	
Eigenvectors									
	0.103	0.103	0.316	0.316	0.190	0.190	0.570	0.570	0.0203
Δe_{CD}	-95.7	95.7	62.9	-62.9	45.9	-45.9	168.	-168.	0.0
	0.103	0.103	0.300	0.300	0.0500	0.0500	0.37	0.37	.845
Δe_{CQ}	-5.65	5.65	147.	-147.	128.	-128.	94.5	-94.5	0.0
	0.835	0.835	2.39	2.39	0.410	0.410	3.88	3.88	7.91
ΔQ	-2.00	2.00	-35.4	35.4	-67.3	67.3	-72.5	72.5	180.
	0.835	0.835	2.54	2.54	1.75	1.75	5.20	5.20	0.144
ΔP	88.2	-88.2	62.2	-62.2	45.3	-45.3	174.	-174.	180.

Note: For the eigenvectors, the first number is the magnitude and the second number is the angle in degrees.

TABLE 4.3.

EIGENVALUES AND EIGENVECTORS OF THE CLOSED LOOP SYSTEM FOR X_C = 0.107. K_{ND} = 13 , ϕ = 0.0 (UNREGULATED MACHINE).

	λ_{ssrn}		λ_{ssrp}		$\lambda_{mech.}$		$\lambda_{amort.}$		λ_{field}		λ_{NDS}	
Eigen-Values	-32.8 + j 701	-32.8 - j 701	-.223 + j 34.9	-.223 - j 34.9	-7.72 + j 18.5	-7.72 - j 18.5	-25.8 + j 55.5	-25.8 - j 55.5	-2.36	-139.	-51.9	-44.4
Eigenvectors Δi_D	0.431	0.431	1.26	1.26	0.595	0.595	0.649	0.649	6.37	0.166	0.302	0.188
	-176.	176.	-120.	120.	62.0	-62.0	-137.	137.	180.	180.	0.0	0.00
Δi_Q	0.432	0.432	0.863	0.863	1.41	1.41	0.651	0.651	0.114	0.134	5.28	0.0395
	-86.7	86.7	-18.0	18.0	132.	-132.	0.0	0.0	0.0	0.0	0.0	0.0
Δi_{fd}	0.130	0.130	0.881	0.881	0.368	0.368	0.586	0.586	6.24	0.280	2.27	3.29
	-178.	178.	-132.	132.	61.9	-61.9	178.	-178.	180.	180.	180.	0.00
Δi_{kd}	0.264	0.264	0.377	0.377	0.215	0.215	0.439	0.439	0.090	0.104	2.53	3.11
	-176.	176.	-88.2	88.2	77.9	-77.9	-71.8	71.8	0.0	0.0	0.0	180.
Δi_{kq}	0.281	0.281	0.502	0.502	0.875	0.875	0.461	0.461	0.012	0.100	5.19	0.0424
	-84.8	84.8	8.94	-8.94	-177	177.	15.8	-15.8	180.	0.0	0.0	0.00
$\Delta \omega$	.00007	.00007	0.0026	0.0026	.0075	.00750	0.0011	0.00110	0.001	0.0001	0.0110	0.0001
	-0.10	.10	70.5	-70.5	-160.	160.	64.2	-64.2	180.	0.0	0.0	0.0
$\Delta \delta$	0.00004	0.00004	0.0281	0.0281	0.141	0.141	.00680	.00680	0.155	0.0003	0.0780	0.0009
	-92.8	92.8	-20.0	20.0	87.1	-87.1	-51.1	51.1	0.0	180.	180.	180.

TABLE 4.3 (cont'd)

		λ_{ssrn}		λ_{ssrp}		$\lambda_{mech.}$		$\lambda_{amort.}$		λ_{field}		λ_{NDS}	
Eigen-		-32.8	-32.8	-.223	-.223	-7.72	-7.72	-25.8	-25.8	-2.36	-139.	-51.9	-44.4
Values		+	-	+	-	+	-	+	-				
		j 701	j 701	j 34.9	j 34.9	j 18.5	j 18.5	j 55.5	j 55.5				
Eigenvectors	Δe_{CD}	0.798	0.798	6.09	6.09	1.99	1.99	10.0	10.0	0.300	13.1	37.0	41.9
		104.	-104.	-41	41.0	-153.	153.	-91.1	91.1	180.	0.0	0.0	180.
	Δe_{CQ}	12.2	12.2	2060.	2060.	1090.	1090.	1610.	1610.	8220.	890.	5180.	6300.
		-170.	170.	22.6	-22.6	-134	134.0	-42.2	42.2	0.0	0.0	0.0	180.
	x_1	203.0	203.	31100.	31100.	17700.	17700.	29100.	29100.	22600.	16900.	127000.	168000.
		-170.	170.	48.3	-48.3	-85.5	85.5	-26.5	26.5	180.	0.0	0.0	180.
	x_2	0.0535	0.0535	0.105	0.105	0.154	0.154	0.0816	.0816	0.0164	0.0184	0.551	0.0018
		87.7	-87.7	-19.6	19.6	134.	-134.	-3.2	3.20	0.0	0.0	0	0.00
	x_3	0.0535	0.0535	0.145	0.145	.0719	.0719	0.0752	0.0752	0.681	0.0110	0.108	0.0200
		178.	-178.	60.7	-60.7	-118.	118.	52.7	-52.7	0.0	0.0	180.	180.

Note: For the eigenvectors, the first number is the magnitude and the second number is the angle in degrees.

switched to different topological configurations. Therefore, the mapping of the stability boundary in the $X_C - r_E$ plane is of practical advantage. Figure 4.1 shows the stability region in the $X_C - r_E$ plane with and without the NDS feedback. It is obvious that the closed loop system has a wider stability region.

4.4 Confirmation of Theory

In this section, the theory developed in Chapter III for SSR suppression will be confirmed using the results obtained in Table 4.2 and Table 4.3 for the open and closed loop systems respectively. The theory is said to be confirmed if the numerical results satisfy the following theoretical concepts, which have been explained in Chapter III:

(a) The speeds of the SSR negative and positive sequence currents are $\omega_0 + \omega_n$ and $\omega_0 - \omega_n$ respectively.

(b) In case of unstable SSR the torque angle is obtuse and for stable SSR the torque angle is reflex.

(c) For the closed loop operation, there exists a stability region in the $K_{ND} - \phi$ plane for which

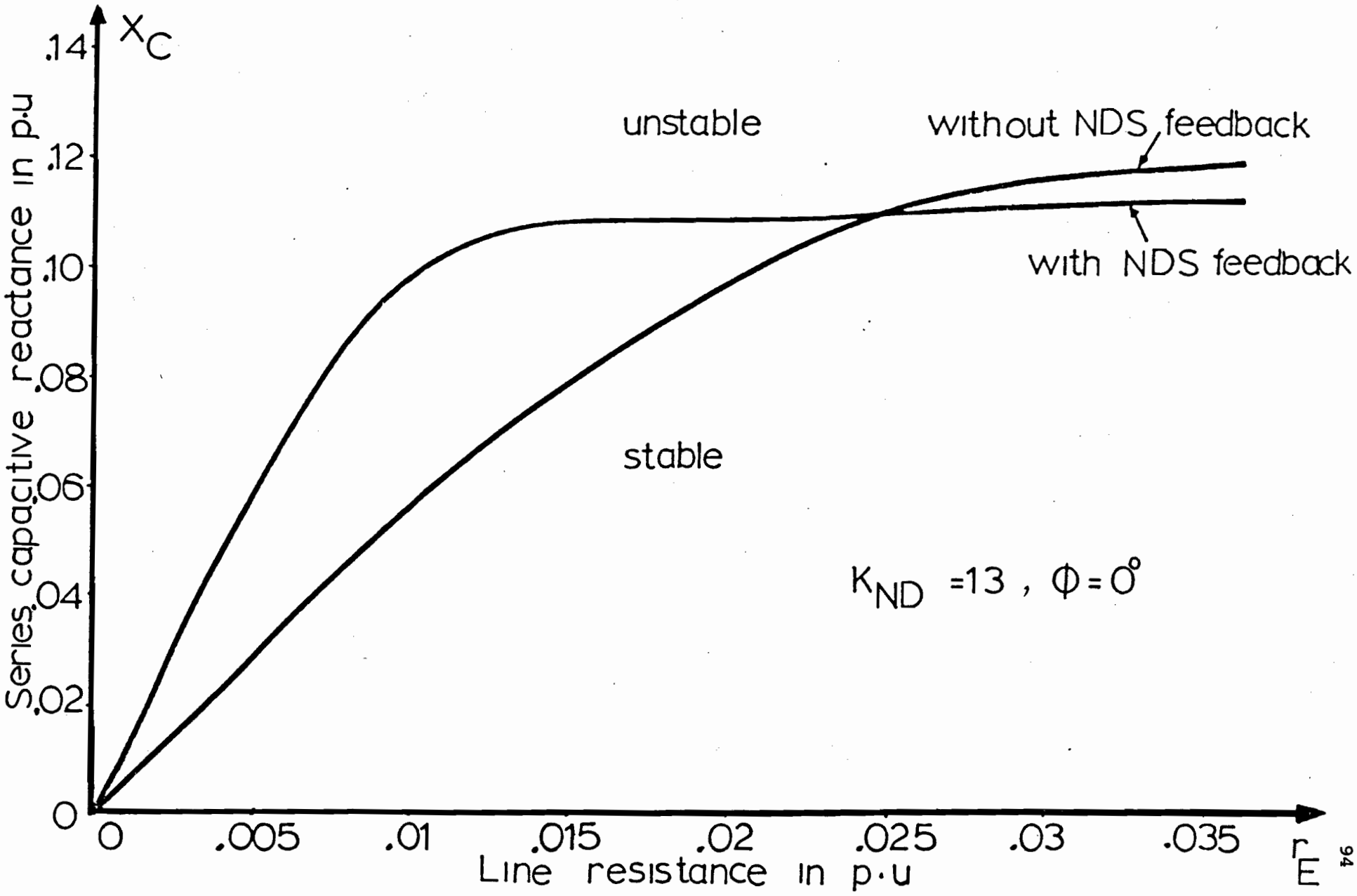

Figure 4.1. Stability boundary in the $X_C - r_E$ plane for the open and closed loop systems.

unstable SSR is stabilized by the feedback. Referring to the mmf phasor diagram of Figure 3.6, the feedback gain K_{ND} controls the magnitude of F_{cb}. The angle ϕ rotates F_{cb} about the pivot point c. The controllable sectors of Figure 3.6 corresponds to the stability region in the $K_{ND} - \phi$ plane.

4.4.1 Negative and Positive Sequence Concept

It was explained in Chapter III that the unbalanced SSR currents flowing into the stator are resolved into negative and positive sequence mmf phasors. The speeds of these mmf phasors with respect to the d - q axis, are $\omega_0 + \omega_n$ and $\omega_0 - \omega_n$ respectively.

From the results obtained in Tables 4.1(b), 4.2 and 4.3, the SSR negative sequence mode λ_{ssrn} has a speed of $\omega_0 + \omega_n$ and the SSR positive sequence mode λ_{ssrp} has a speed of $\omega_0 - \omega_n$. For instance, in Table 4.1(b) $\omega_n = 302$ electrical r/s ($X_C = 0.092$), λ_{ssrn} has a speed of $677 \simeq 377 + 302$ where $\omega_0 = 377$, and λ_{ssrp} has a speed of $73.1 \simeq 377 - 302$, whereas in Table 4.2 $\omega_n = 326$ electrical r/s and the speed of λ_{ssrn} is $701 \simeq 377 + 325$ and the speed of λ_{ssrp} is $54.8 \simeq 377 - 325$.

The damping of λ_{ssrn} is large (32.8 in all Tables) due to its positive slip, while that of λ_{ssrp} is small and very much influenced by changing X_C. This agrees with the first concept which was explained in Section 3.3.2.

4.4.2 The SSR mmf Phasor Diagram

The second concept of the theory of Chapter III is concerned with stable and unstable SSR oscillations, and both were explained on the basis of the torque angle between the SSR stator and rotor phasors at the subsynchronous frequency. In the mmf phasor diagram of Figure 3.3, the stable SSR is defined as the case when $180 < \delta < 360$, otherwise it is the case of unstable SSR.

The purpose of this section is to demonstrate the validity of this concept using the numerical results. The SSR mmf phasor diagram can be constructed for stable and unstable SSR from the eigenvectors shown in Tables 4.3 and 4.2 respectively.

The state variables of the positive sequence mode are sinusoidally varying with time at a frequency of ω_n electrical r/s. Their relative amplitudes and phase shifts are related to the eigenvector associated with λ_{ssrp} mode. Therefore, from Table 4.2, the free motion of the positive sequence SSR mode involves the following winding currents,

$$\begin{bmatrix} \Delta i_D(t) \\ \Delta i_Q(t) \\ \Delta i_{fd}(t) \\ \Delta i_{kd}(t) \\ \Delta i_{kq}(t) \end{bmatrix} = \exp(2.32\,t) \begin{bmatrix} 2.37 \cos(54.8\,t + 326.^{\circ}) \\ 2.55 \cos(54.8\,t + 64.1^{\circ}) \\ 0.901 \cos(54.8\,t + 307^{\circ}) \\ 1.35 \cos(54.8\,t + 343^{\circ}) \\ 1.55 \cos(54.8\,t + 81.6^{\circ}) \end{bmatrix} \qquad (4.17)$$

The contribution currents to the stator mmf component are Δi_D and Δi_Q. At an instant of time $t = 0$ the stator mmf phasor can be computed in the $d - q$ axis since the synchronously rotating frame and the $d - q$ rotating frame are the same at this instant of time. Therefore, the two d and q axes stator mmf phasors are:

$$F_{sd} = 2.37 \cos 326^{\circ},$$

$$F_{sq} = 2.55 \cos 64.1^{\circ},$$

$$F_s = \sqrt{F_{sd}^2 + F_{sq}^2} = 2.97,$$

$$\beta_{Fs} = \arctan\left(\frac{F_{sd}}{F_{sq}}\right) \quad \text{(stator mmf phase angle)}.$$

The rotor mmf phasor can be calculated from the rotor currents Δi_{fd}, Δi_{kd}, Δi_{kq} at the same instant of time. The d and q rotor mmf phasors are:

$$F_{rd} = 0.901 \cos 307 + 1.35 \cos 343 ,$$

$$F_{rq} = 1.55 \cos 81.6 ,$$

$$F_r = \sqrt{F_{rd}^2 + F_{rq}^2} = 1.85 ,$$

$$\beta_{Fr} = \arctan \left(\frac{F_{rd}}{F_{rq}}\right) \quad \text{(rotor mmf phase angle)} .$$

In the construction of the mmf phasor diagram, the stator mmf is reversed,according to the sign convention adopted in Chapter II, where the currents are flowing out of the stator. The resultant mmf diagram for the open loop system is shown in Figure 4.2(a). The torque angle in Figure 4.2(a) is an obtuse angle which indicates generation action and this is the condition for unstable SSR which is in fact the case.

In a similar way the eigenvectors given in Table 4.3 can be used to construct the SSR mmf phasor diagram for the closed loop system, which is stable as indicated by the eigenvalues in the same table. Figure 4.2(b) shows the mmf diagram of the closed loop system with the NDS gain $K_{ND} = 13$ and the control angle $\phi = 0$, from which the torque angle is now reflex which means motoring regime.

The mmf phasor diagrams in Figure 4.2 demonstrate the validity of the stable and unstable SSR concept. In addition, the principle of stabilizing the unstable SSR by reversing the power flow or by shifting from the generating regime to the motoring regime is possible.

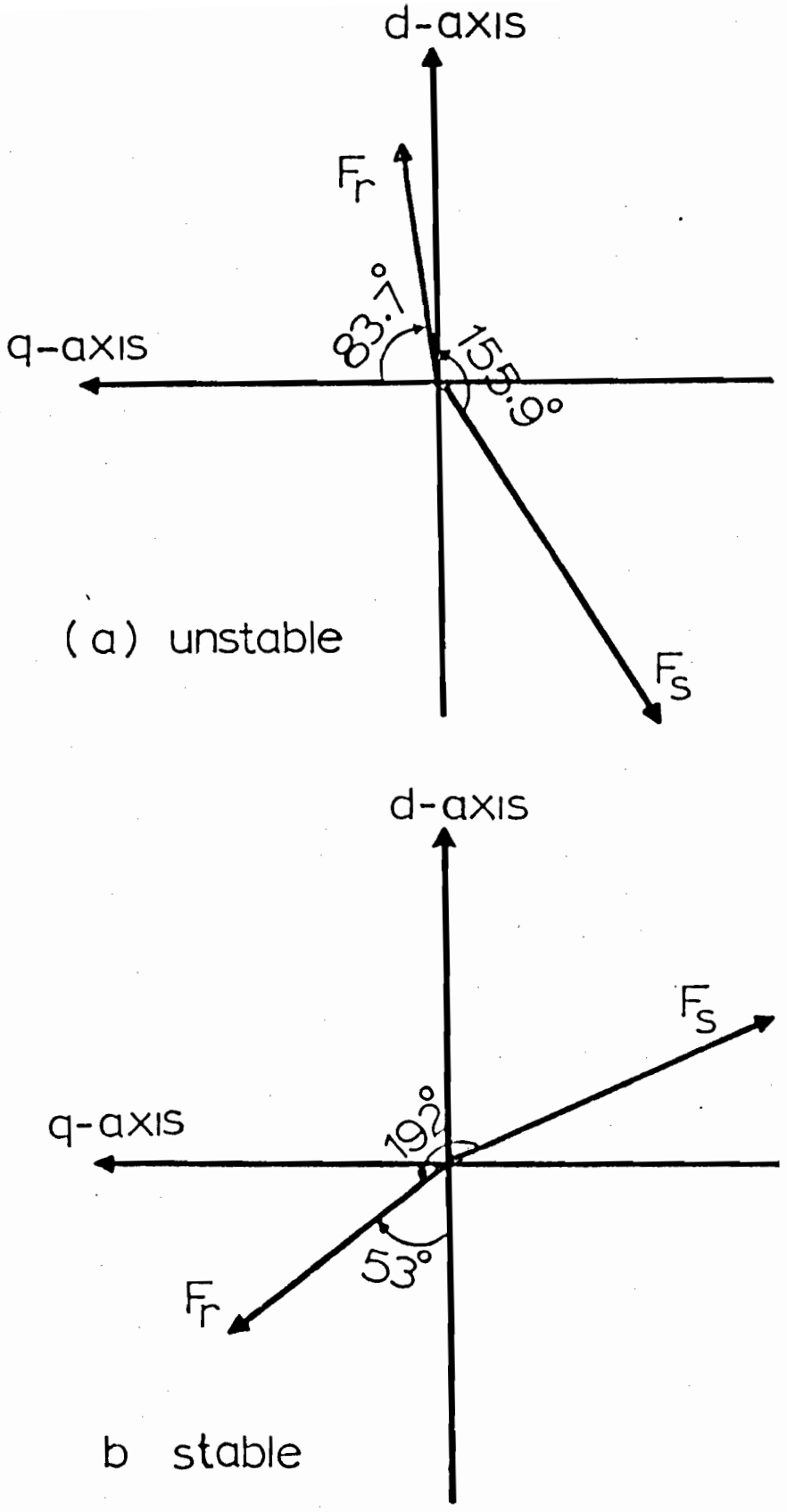

Figure 4.2. MMF phasor diagram for the SSR positive sequence mode constructed from the numerical results for:

(a) Open loop system

(b) Closed loop system

4.4.3 F_{cb} Phase and Magnitude

The phase and magnitude of the phasor F_{cb}, the mmf of the field winding produced by the feedback signal which is necessary for SSR suppression, are affected by the control angle ϕ and the NDS gain of the feedback loop K_{ND}. The input signal to the NDS filter is the combination of the transducer active and reactive power outputs, P and Q respectively, where:

$$P = P_0 + \Delta P \quad \text{and} \quad Q = Q_0 + \Delta Q \tag{4.18}$$

From the open loop eigenvectors shown in Table 4.2 ΔQ and ΔP can be related to Δi_{fd} as:

$$\Delta Q = 2.39 \angle 325.^\circ ,$$

$$\Delta P = 2.54 \angle 62.2^\circ ,$$

$$\Delta i_{fd} = 0.901 \angle 307.^\circ ,$$

these values are taken from the eigenvectors associated with λ_{ssrp} in Table 4.2 .

$$\begin{matrix} \Delta Q / \Delta i_{fd} \\ \Delta P / \Delta i_{fd} \end{matrix} = \begin{matrix} 2.65 \angle 17^\circ \\ 2.82 \angle 115^\circ \end{matrix} \tag{4.19}$$

From equation 4.19 it is clear that the outputs of the transducers are two signals of approximately equal magnitude and which are approximately 90° apart. This emphasizes the possibility of adding another degree of

freedom by combining the two outputs as it was explained in Section 3.6.2.

The output of the transducer passes through the NDS filter whose transfer function is given in Appendix B-1 and whose Bode plot is shown in Figure 4.3. The purpose of this transfer function is to filter out the dc component of the 60 Hz active and reactive powers P_0 and Q_0 respectively. The gain K_{ND} of the transfer function is chosen to give F_{cb} the required magnitude. The NDS filter gives an angle of 45^{o} and a magnitude of $0.493\ K_{ND}$ at the subsynchronous frequency of 54.8 r/s as can be seen from Figure 4.3 .

Therefore, the F_{cb} space angle is determined from the NDS and the control signal angles. The magnitude of F_{cb} is determined by the transducer gain, the filter magnitude and the NDS gain K_{ND}. Since the filter phase and magnitude and the transducer gain are fixed for a given subsynchronous frequency, then K_{ND} and ϕ are the two degrees of freedom by which F_{cb} can be injected to shift F_R from the generating regime to the motoring regime.

4.4.3.1 Stability Boundary

In the closed loop operation, we introduced two additional degrees of freedom; the NDS gain K_{ND} and the control angle ϕ .

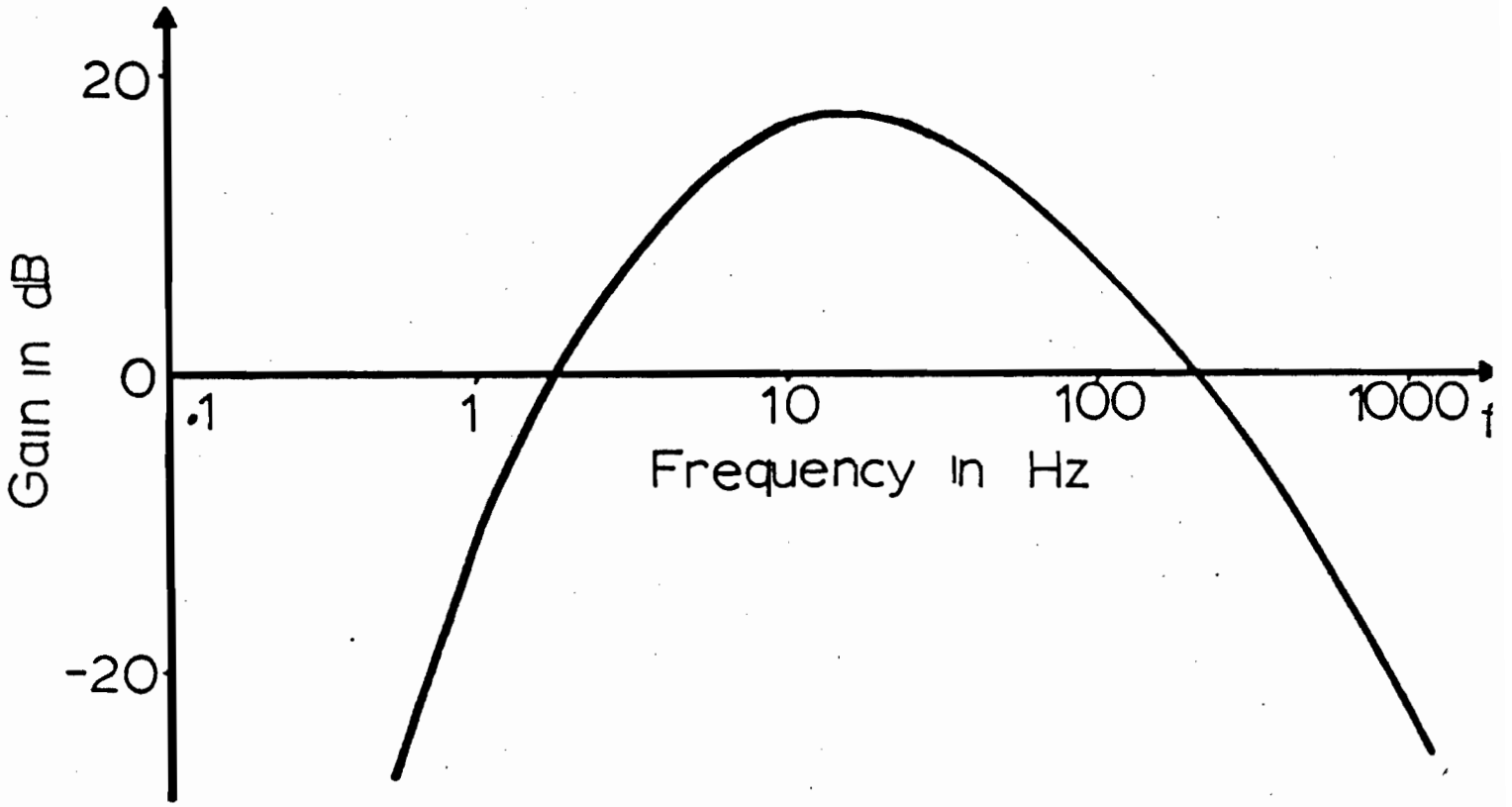

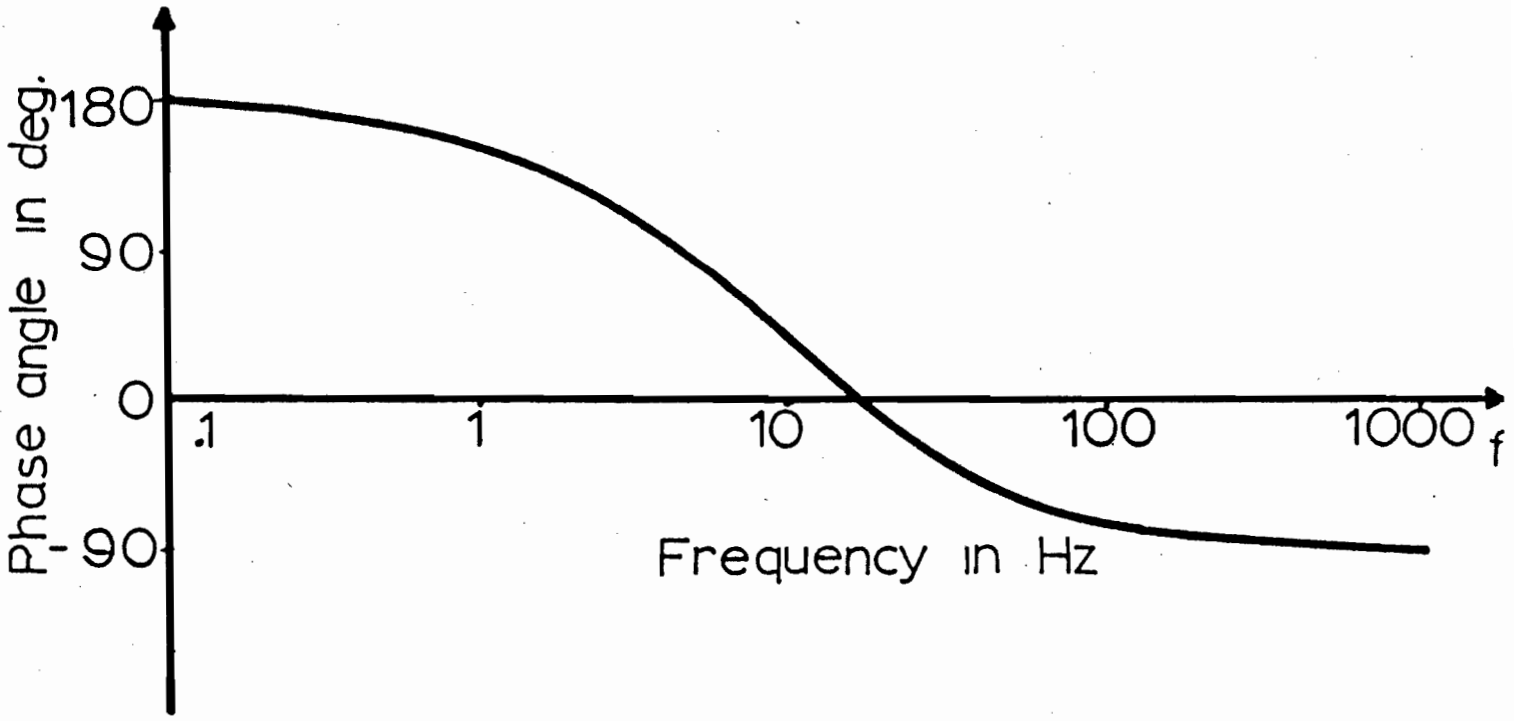

Figure 4.3. Bode plots for the NDS transfer function given in Appendix B-1 .

Suppression of SSR can be achieved if the right combination of K_{ND} and ϕ is used. This means that K_{ND} and ϕ should be chosen in a way to fulfill the phase and magnitude requirements of F_{cb} as was explained in the previous section. Therefore, the stability boundary in the K_{ND} - ϕ plane is necessary to verify the third concept dealing with F_{cb} phase and magnitude requirements.

In the SSR mmf phasor diagram shown in Figure 3.4, AB was considered as the theoretical stability boundary. For stable sub-synchronous resonance, the resultant mmf phasor F_R should lie on the left hand side of the line AB. A boundary line can be obtained from the current numerical analysis by changing K_{ND} and ϕ at the same time, while keeping X_C, r_E and P constants at 0.107 p.u., 0.0229 p.u. and 0.15 p.u. respectively.

The numerical stability boundary can be constructed using the mmf phasor diagram shown in Figure 4.2(a). In Figure 4.2(a) the angle between F_r and the q - axis is 83.7 degrees, and the q - axis represents the horizontal line with 90^o ahead of the d - axis in the direction of motion. The phasor diagram of Figure 4.2(a) can be transferred in a polar plane of different circles representing different values of K_{ND} with their centres at the point of intersection of different straight lines, which represent different values of the control angle ϕ as shown in Figure 4.4. The d and q axes in Figure 4.2(a) coincide with the straight lines representing ϕ = 90, 360 in Figure 4.4 respec-

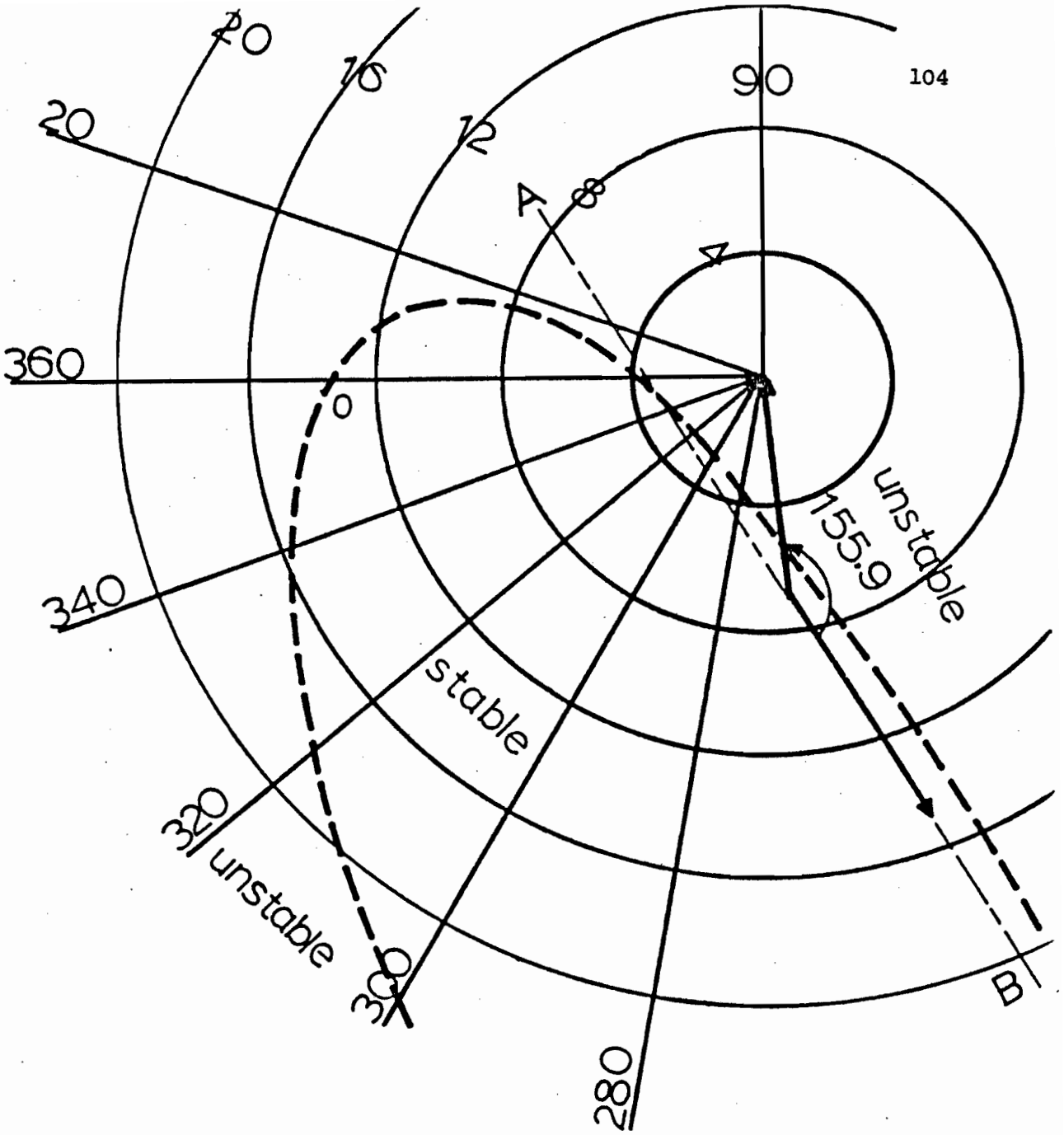

Figure 4.4. Stability boundary in the $K_{ND} - \phi$ plane showing the comparison between the theoretical stability boundary (AB) and the numerical stability boundary (broken line).

tively. Therefore, the stator and rotor mmf phasors of Figure 4.2(a) can be plotted on Figure 4.4, but with a slight change of the arrow tip of F_r fixed to the centre of the K_{ND} circles. Now, the line AB in Figure 4.4 represents the theoretical stability boundary and the broken line is the stability boundary obtained from the eigenvalue analysis. This stability boundary agrees with the line AB only approximately, because the closed loop system is a highly complex system of twelfth order.

Figure 4.4 gives a clear strategy of how ϕ and K_{ND} should be combined to ensure that the injected F_{cb} will have the required phase and magnitude to shift F_R into the stable region (motoring regime). For instance, if $K_{ND} = 2$ then for any value of the control angle ϕ, F_{cb} will not shift F_R into the stable region. Similarly, if $\phi = 90^{\circ}$, for any value of the NDS gain K_{ND}, F_{cb} will also not shift F_R into the stable region. Furthermore, for any fixed NDS gain, say $K_{ND} = 12$, the variation of ϕ from 20° to 0° in the counterclockwise direction will change the system from unstable to stable. This is because in changing ϕ, the phasor F_{cb} is rotated in a way such that when it is combined with F_r, the resultant phasor F_R will in the first case ($\phi = 20^{\circ}$) fall in the generation regime and in the second case, $\phi = 0^{\circ}$, fall in the motoring regime.

By this stability boundary, the concept of F_{cb} phase and magnitude requirement is now confirmed. Also, the possibility of rotating F_{cb} by changing the control angle ϕ is verified.

4.5 Study of Effect of Parameter Variation

In this section, the effect of the NDS gain K_{ND}, the control angle ϕ, and the effect of loading on the damping of different modes is studied. In the study, the line resistance r_E is kept constant at 0.0229 p.u. Only one parameter at a time is varied in these studies, i.e., the other parameters are kept constant.

4.5.1 Variation of K_{ND}

The effect of K_{ND} on the SSR positive sequence mode can be explained from Figure 4.5, where the damping coefficient of the SSR mode λ_{ssrp} is plotted against the variation of K_{ND} for two different values of ϕ. It is obvious that by changing ϕ from 360° to 300° the damping of the SSR positive sequence mode is improved. However, the mechanical mode damping is worst for $\phi = 300^{\circ}$ as is clear from Figure 4.6. In Figure 4.6 the loci of the amortisseur, the SSR, and the mechanical modes are plotted on the upper half of the s - plane. The loci are for the variations of the NDS gain, K_{ND}. Two cases are presented for control angles ϕ = 300 degrees and ϕ = 360 degrees. The values of X_C, r_E and P are fixed at 0.107 p.u., 0.0229 p.u. and 0.15 p.u. respectively. The negative sequence and the field winding modes do not change appreciably with K_{ND} and thus are not plotted in Figure 4.6.

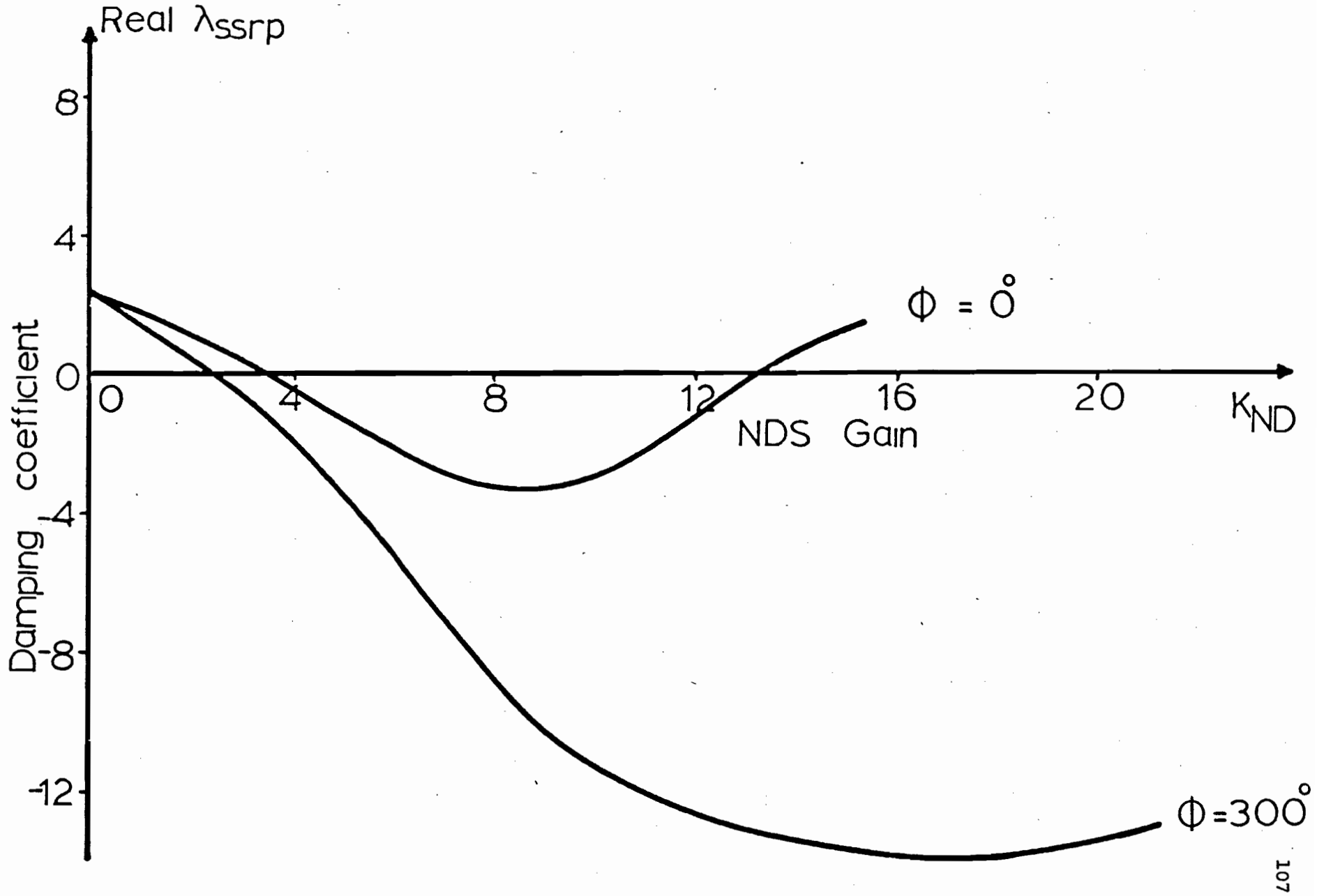

Figure 4.5. Variation of SSR positive sequence mode damping with the NDS gain K_{ND} for two values of ϕ .

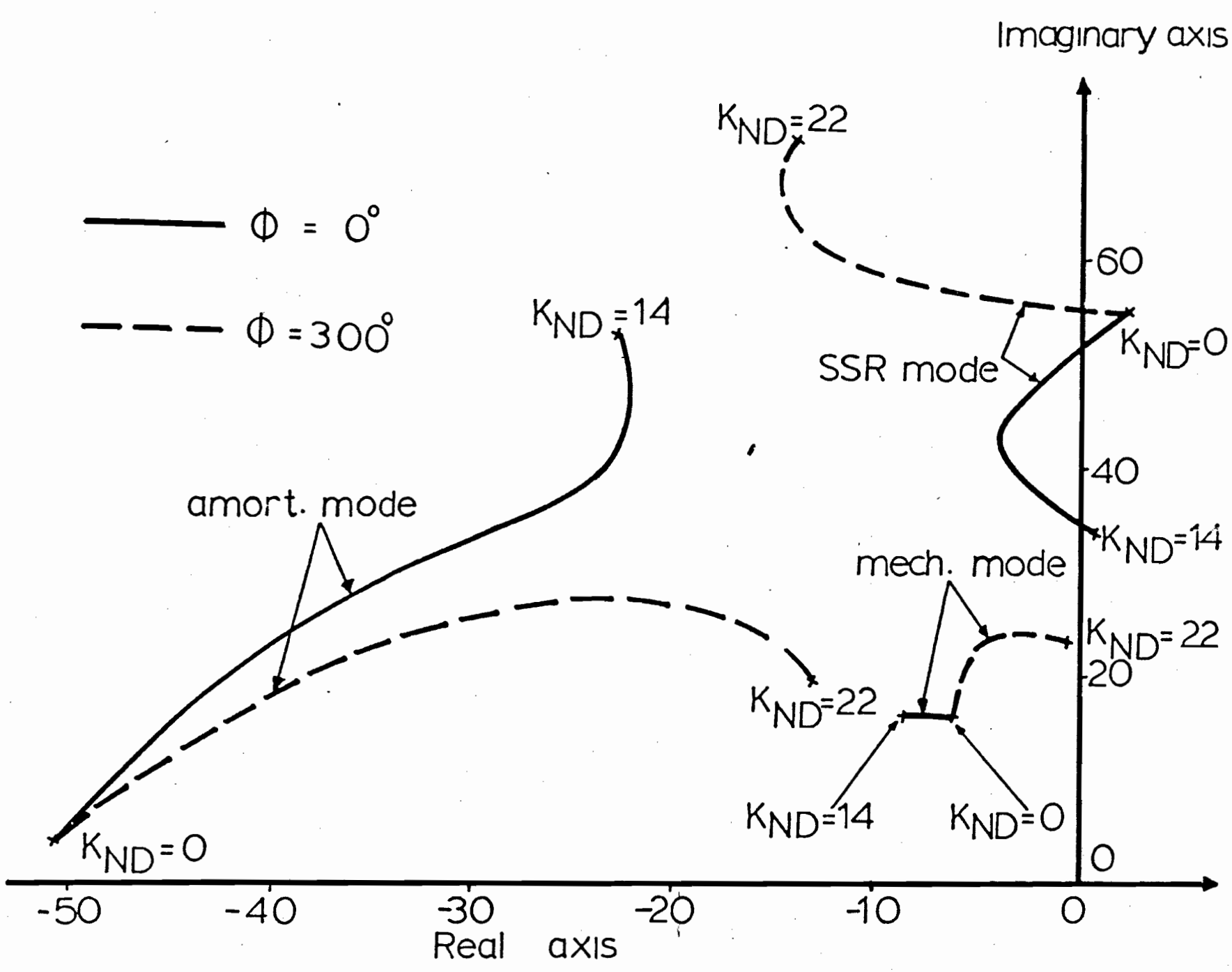

Figure 4.6. The loci of the amortisseur, the mechanical and the SSR positive sequence modes on the upper half of the s-plane for two values of ϕ. ϕ = 0.0, 300 .

4.5.2 Variation of ϕ

Keeping K_{ND} fixed at a value of 13 and changing ϕ over a complete cycle, the damping of the SSR positive sequence mode varies in the manner shown in Figure 4.7. It is clear that for the above value of the NDS gain K_{ND} ($K_{ND} = 13$), the system is unstable for $5^{o} < \phi < 235^{o}$ and it is stable for $235^{o} < \phi < 365^{o}$. Furthermore, the damping of λ_{ssrp} is the worst at an angle of about 120^{o} and it is the best at an angle of about 300^{o}.

The dampings of the other modes do not change appreciably with ϕ, except that the amortisseur mode changes from two negative real modes to a complex conjugate mode. The damping of these modes are not plotted in Figure 4.7.

4.5.3 Effect of Loading

The previous results for the open and closed loop systems were obtained when the power delivered to the infinite bus bar was kept constant at 0.15 p.u. When changing the power from 0.15 p.u. to 1.0 p.u., the damping of the SSR mode is improved, while the damping of the mechanical mode is deteriorated. Figure 4.8 shows the loci of the damping of the mechanical and the SSR modes as K_{ND} varies for two different values of loading. It is clear that for P = 1.0 p.u. the

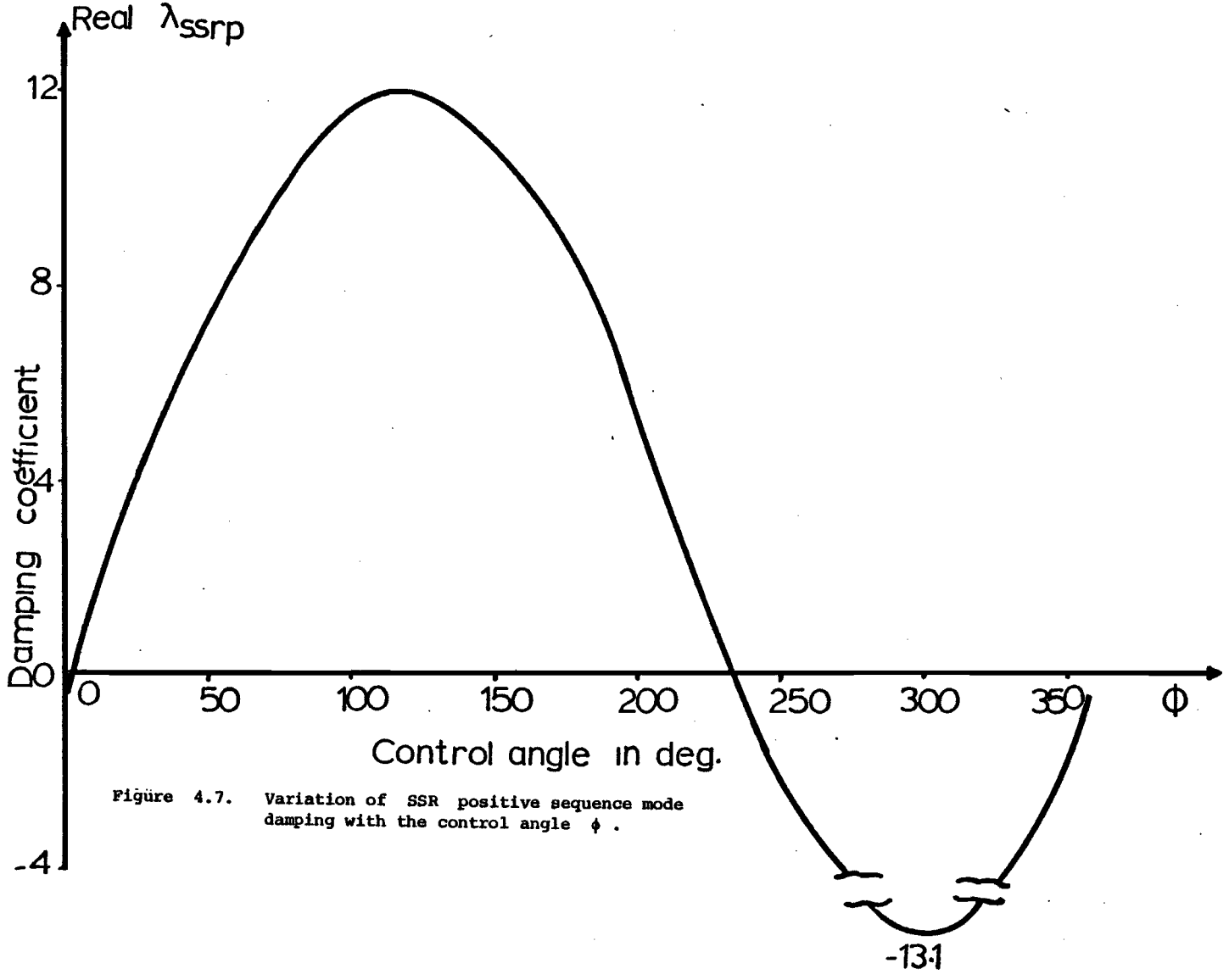

Figure 4.7. Variation of SSR positive sequence mode damping with the control angle ϕ .

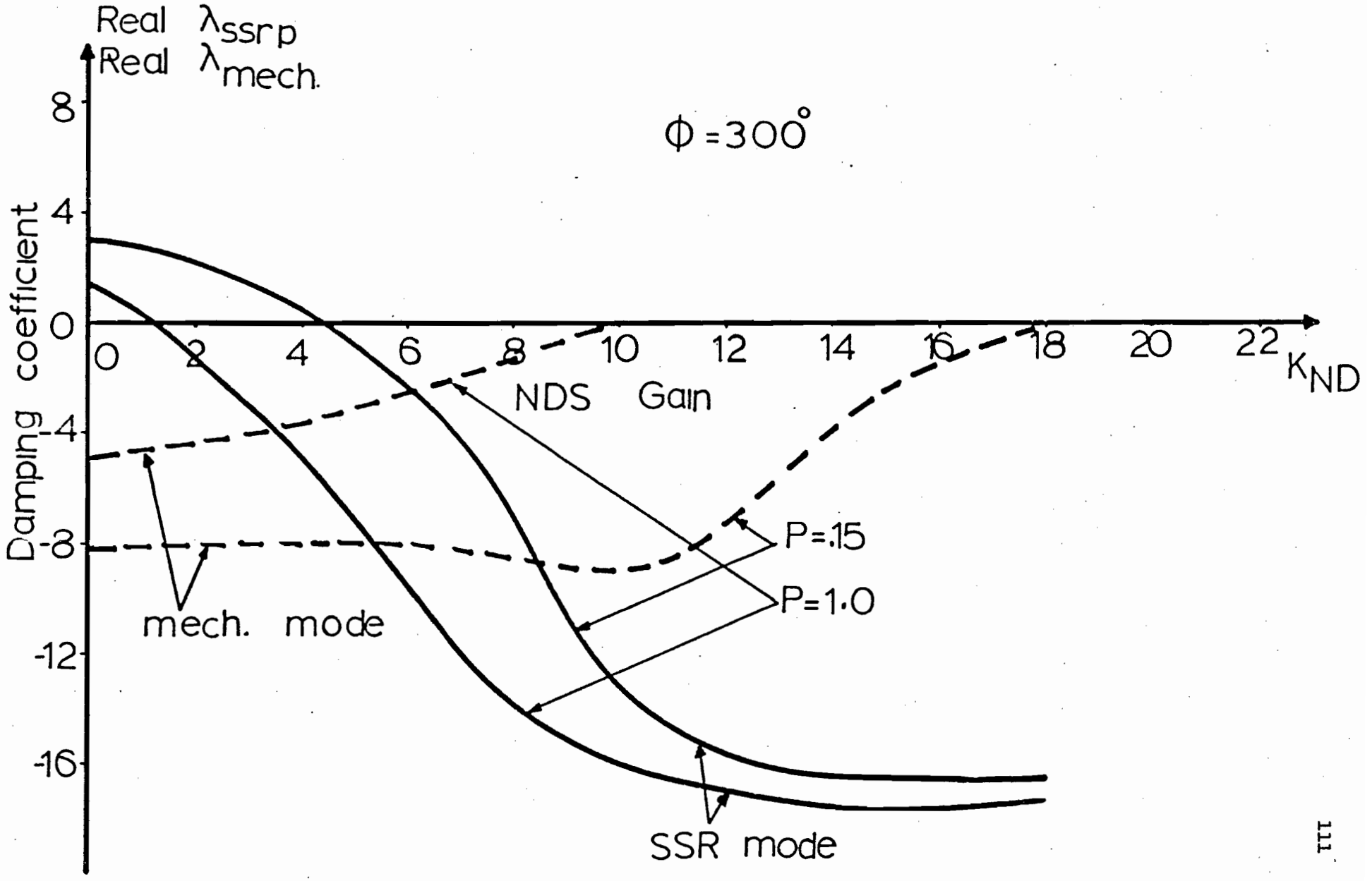

Figure 4.8. Variation of SSR positive sequence and mechanical mode dampings with K_{ND} for two values of loading P = 0.15 p.u., 1.0 p.u.

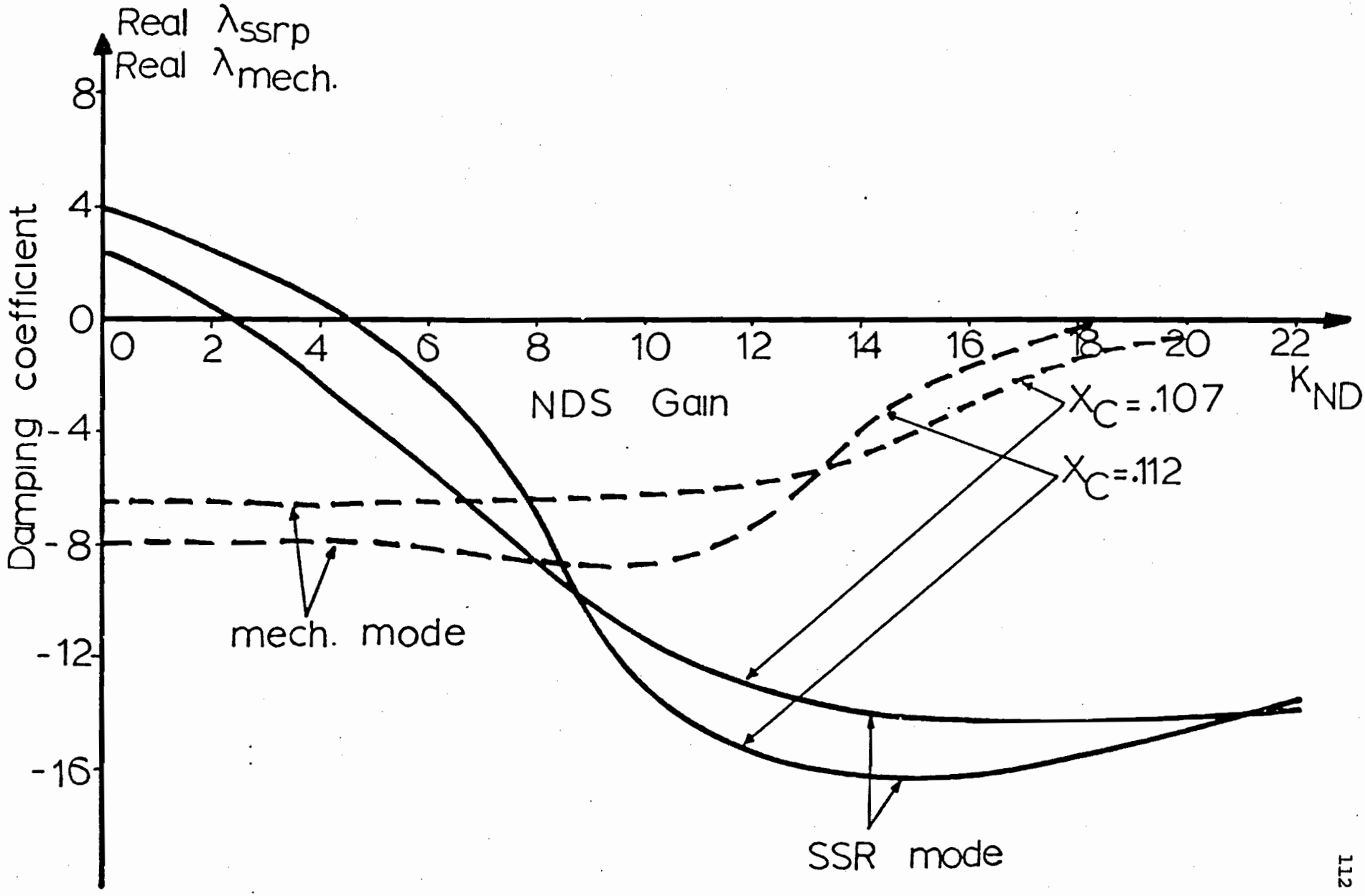

Figure 4.9. Variation of SSR positive sequence and mechanical mode dampings with K_{ND} for two values of X_C, X_C = .107 p.u., .112 p.u.

range of K_{ND} for which the system is stable lies between 1.5 to 10, whereas for P = 0.15 p.u., it lies between 2.5 and 18 .

In a similar way, the two mode dampings (the SSR and the mechanical modes) can be plotted against K_{ND} for constant P, ϕ , and using two values of the series capacitive reactance. Figure 4.9 shows the variation of the SSR and the mechanical mode dampings with K_{ND} for two values of X_C . It is clear that for a lower X_C the system is stable for a wider range of K_{ND} .

4.6 Discussion

The experimental results obtained by [17] and the numerical results obtained in this chapter support strongly the different aspects of the theory developed in Chapter III. Furthermore, the choice of the control signal as a combination between ΔP and ΔQ is superior to the use of ΔQ only.

The mechanical and the SSR modes are the only two which cause system instability. The damping of the two modes vary in opposite directions, i.e., when shifting one mode to the left of the imaginary axis on the s - plane, the other moves to the right. Therefore the practical choice is a compromise which gives both the necessary dampings.

The stability boundary is a guidance for the choice of K_{ND} and ϕ to achieve a robust system. Thus, the feedback loop used by [17], which has ΔQ only as an input signal, loses one degree of freedom in the choice of the operating point. In the context of Figure 4.4, the feedback loop of [17] corresponds to the 360^{o} line and $K_{ND} = 14.3$ and it is presented by point 0 in the diagram which is very sensitive to slight changes in the NDS gain K_{ND}.

CHAPTER V

SSR OSCILLATION IN REGULATED MACHINE - A SMALL PERTURBATION STUDY

5.1 Introduction

The feedback system considered for the suppression of unstable SSR discussed in Chapter IV is impracticable. This is because the feedback signals are applied directly to the field winding with no regard to the fact that the power levels required to energize the field winding can be quite substantial. In practice, the synchronous generator field winding current is obtained from an excitation system which is capable of amplifying signals of the power levels of transducers outputs to the power levels capable of perturbing the airgap magnetic fields significantly. The modern excitation system usually has already a voltage regulator feedback loop and a supplementary stabilizing loop such as the power system stabilizer loop (PSS). Conceivably, therefore, the signals from the SSR stabilizing feedback loop should be amplified through the excitation system in the same way as the signals of the voltage regulator and the PSS feedback.

This motivation of the study in this chapter is to show that the system of Chapter IV meets the stability performance requirements when the transfer function of the excitation system is included in the model and that there are no deleterious interactions with the other feedback loops so as to degrade the overall performance.

In this chapter, the synchronous machine is assumed to be equipped with Type 1 excitation system [55], and a power system stabilizer. Furthermore, the system under consideration is the 10 GVA system used by Saito et al [17] which is totally different from the one used in Chapter IV. However, the unregulated machine is first considered to help in clarifying the basic sub-systems functions.

The system stability analysis begins with the basic system, i.e., the system without the excitation feedback and without the power system stabilizer. Then, step-by-step, each complexity (sub-system) is added to glean an understanding of how each sub-system interacts with the rest.

A more practical feedback loop than the one used in [17] is proposed for the SSR oscillation control. Results are presented to show the stability regions and the loci of the eigenvalues for changes in system parameters.

5.2 Basic Sub-System Functions

The 10 GVA system is associated with two sub-systems: (i) the excitation system which consists of the voltage regulator and the exciter, (ii) the power system stabilizer PSS [56-61]. The excitation system is Type 1 of Reference [55]. The values of the gains and the time

constants are taken from [17]. Two kinds of systems are studied:

(a) The conventional excitation system (CE).

(b) The high response excitation system (HRE).

The parameters of the above two excitation systems are within the range recommended by [55] and their values are listed in Table 5.1.

In practice, the generator terminal voltage (e_t) is fedback to the input port of the excitation system through a low pass filter of the regulator which is neglected here. The output of this filter is amplified by the voltage regulator amplifier (in actual fact the regulator amplifier saturates and this is modelled by a voltage ceiling, however, this non-linearity cannot be treated by the small perturbation analysis used in this chapter and in consequence is neglected) and then fed to the exciter. Any changes in the generator terminal voltage is compensated by changes in the machine excitation voltage. The time response of the excitation system to any changes in e_t depends on the regulator and the exciter gains and time constants.

The recent practice of power industry required a higher response excitation system to ensure fast voltage regulation and transient stability. In using the high response excitation system, it is found that the electromechanical stiffness is improved but there is a poor electromechanical damping. To ensure dynamic stability by increasing the damping

when the high response excitation system is used, another feedback loop is necessary and this is the power system stabilizer (PSS).

The transient stabilizing signals of the PSS are usually obtained from the shaft speed (which is the one used in this chapter), the terminal frequency or the power transducers. The output of the PSS goes to the input port of the excitation system.

5.3 Mathematical Formulation

The state space form of the basic system (Figure 2.2(a)) is given by equation 4.1, where the only non-zero entry of the input vector $\underline{U}$ is Δe_{fd}. The mathematical model of each sub-system is added to equation 4.1 one at a time.

Figure 5.1(a) shows the basic system with the excitation feedback. The transfer function of the excitation system is shown in Figure 5.1(b) where the different gains and time constants are defined in [55]. The state space model of the excitation system can be written on the basis of equation B-2.4 given in Appendix B-2 as follows:

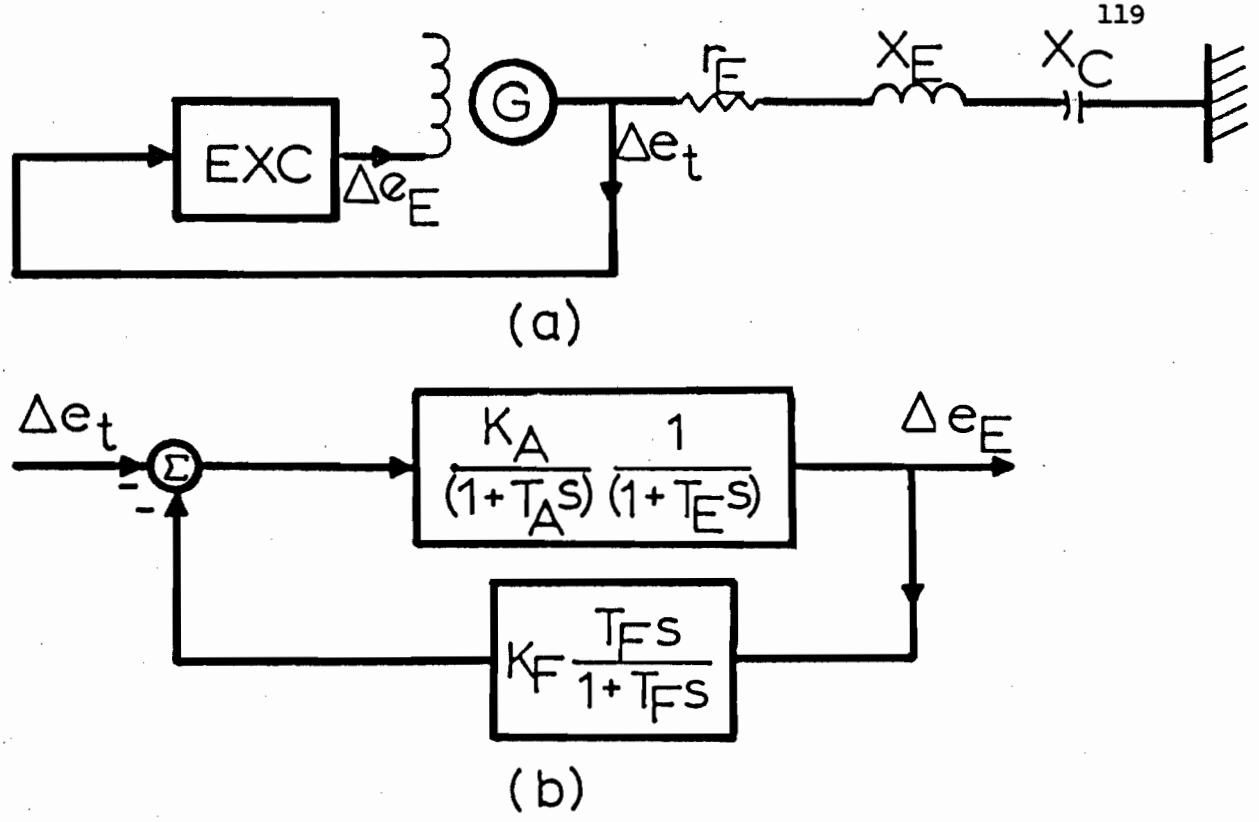

Figure 5.1. (a) The basic system with the excitation feedback.

(b) The transfer function of Type 1 excitation system.

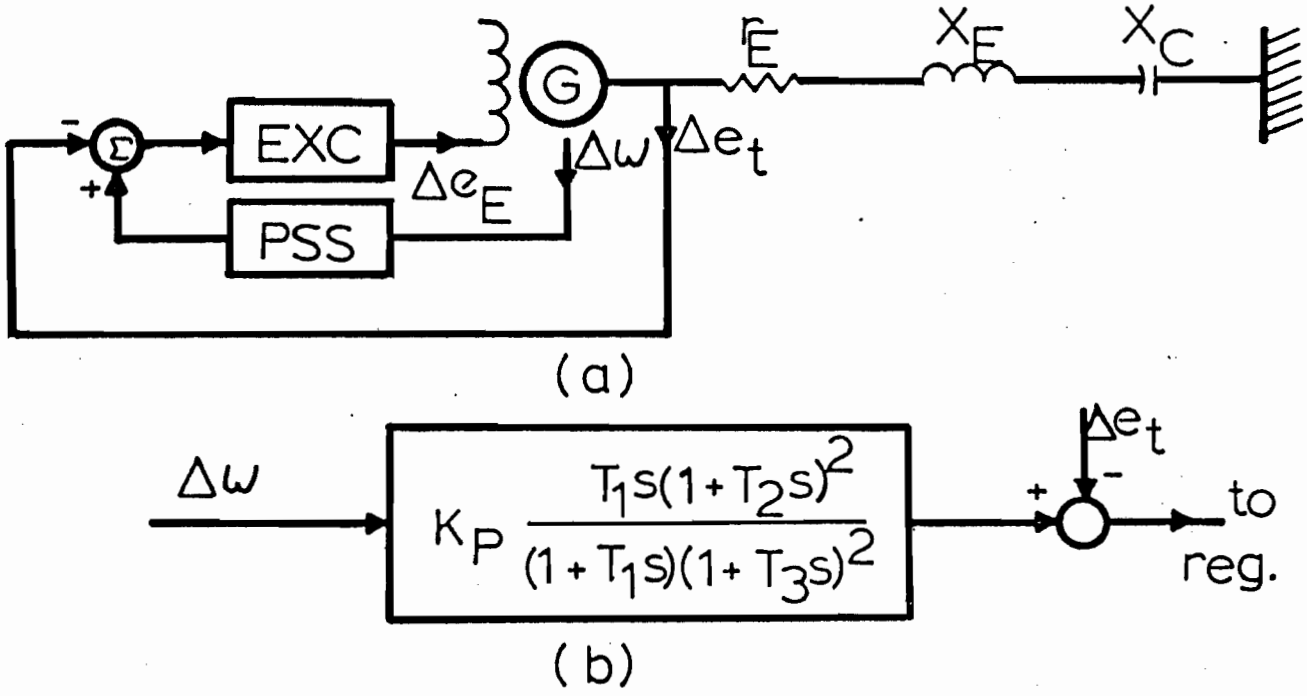

Figure 5.2. (a) The basic system with the high response excitation system (HRE) and the power system stabilizer (PSS).

(b) The transfer function of the PSS.

$$\frac{d}{dt}\begin{bmatrix} x_{E1} \\ x_{E2} \\ x_{E3} \end{bmatrix} = \begin{bmatrix} -a_{E1} & 1 & 0 \\ -a_{E2} & 0 & 1 \\ -a_{E3} & 0 & 0 \end{bmatrix} \begin{bmatrix} x_{E1} \\ x_{E2} \\ x_{E3} \end{bmatrix} + \begin{bmatrix} b_{E1} \\ b_{E2} \\ b_{E3} \end{bmatrix} (-\Delta e_t) \quad (5.1)$$

where

$$a_{E1} = \frac{T_F T_A + T_A T_E + T_E T_F}{T_F T_A T_E}$$

$$a_{E2} = \frac{T_A + T_F + T_E + K_F T_A T_F}{T_F T_A T_E}$$

$$a_{E3} = \frac{1}{T_F T_A T_E}$$

and

$$b_{E1} = 0$$

$$b_{E2} = K_A T_F$$

$$b_{E3} = K_A$$

The output of the excitation system Δe_E is:

$$\Delta e_E = a_{E3} x_{E1} \quad (5.2)$$

in a similar way to equation 4.14, Δe_{fd} can be obtained from equation 5.2 as :

$$\Delta e_{fd} = \frac{r_{fd}}{X_{ad}} a_{E3} x_{E1} \tag{5.3}$$

The state space equation of the basic system with the excitation feedback, Figure 5.1(a), can be obtained by combining equations 4.1, 5.1, and 5.3. The resulting equation is a homogeneous equation describing the above system which is of 12 state variables.

A final remark on equation 5.1 is that, it represents the mathematical model of the excitation system of Type 1 of Reference [55] for both the HRE and the CE systems. The input signal to the excitation system which is Δe_t in equation 5.1, is always associated with a negative sign since any increase in the generator terminal voltage will be compensated by decreasing its excitation voltage.

Figure 5.2(a) shows the basic system with both the excitation system and the power system stabilizer. It is worth reminding that the power system stabilizer is needed when the high response excitation system HRE is used. The transfer function of the PSS is shown in Figure 5.2(b). Once again, the state space model of the PSS can be written in a way similar to that of the excitation system which has the following form:

$$\frac{d}{dt}\begin{bmatrix} x_{P1} \\ x_{P2} \\ x_{P3} \end{bmatrix} = \begin{bmatrix} -a_{P1} & 1 & 0 \\ -a_{P2} & 0 & 1 \\ -a_{P3} & 0 & 0 \end{bmatrix} \begin{bmatrix} x_{P1} \\ x_{P2} \\ x_{P3} \end{bmatrix} + \begin{bmatrix} b_{P1} \\ b_{P2} \\ b_{P3} \end{bmatrix} \Delta \bar{\omega} \tag{5.4}$$

where

$$a_{P1} = \frac{2\,T_1\,T_3 + T_3\,T_3}{T_1\,T_3\,T_3}$$

$$a_{P2} = \frac{2\,T_3 + T_1}{T_1\,T_3\,T_3}$$

$$a_{P3} = \frac{1}{T_1\,T_3\,T_3}$$

and

$$b_{P1} = 2\,K_P\,T_1\,T_2 - K_P\,a_{P3}\,T_1\,T_2\,T_2\,(2\,T_1\,T_3 + T_3\,T_3)$$

$$b_{P2} = K_P\,T_1 - K_P\,a_{P3}\,T_1\,T_2\,T_2\,(2\,T_3 + T_1)$$

$$b_{P3} = K_P\,a_{P3}\,T_1\,T_2\,T_2$$

The output of the PSS e_P is :

$$e_P = a_{P3}\,x_{P1} + a_{P3}\,K_P\,T_1\,T_2\,T_2 \qquad (5.5)$$

The combination of equations 4.1, 5.1 (with the input Δe_t replaced by $\Delta e_t - e_P$) and equations 5.3, 5.4, 5.5 gives a homogeneous state space equation which describes the system of Figure 5.2(a). The constant coefficient matrices of this equation are of dimension 15 * 15 .

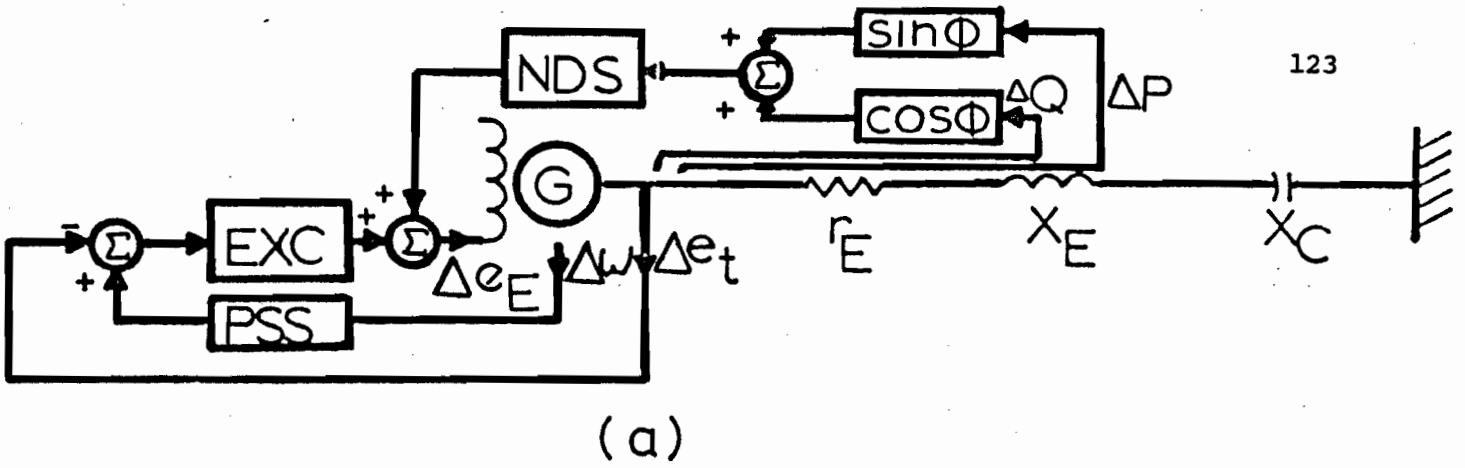

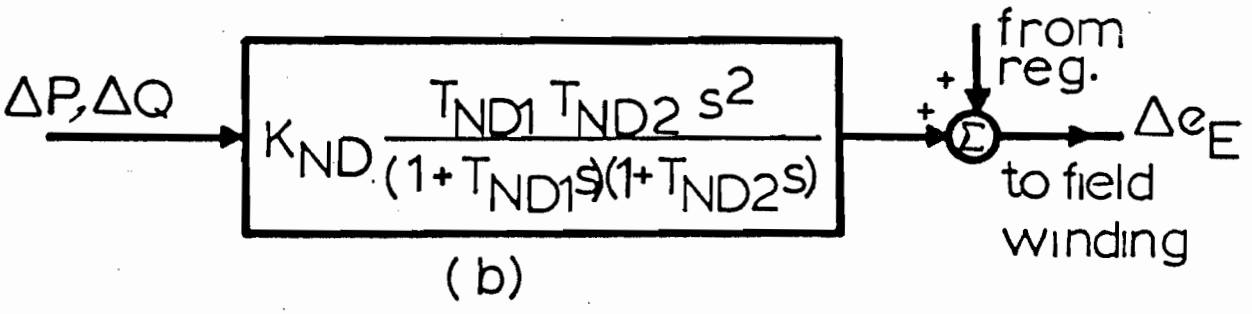

Figure 5.3. (a) The feedback scheme used by Saito et al [17].

(b) The transfer function of the NDS filter reported in [17] .

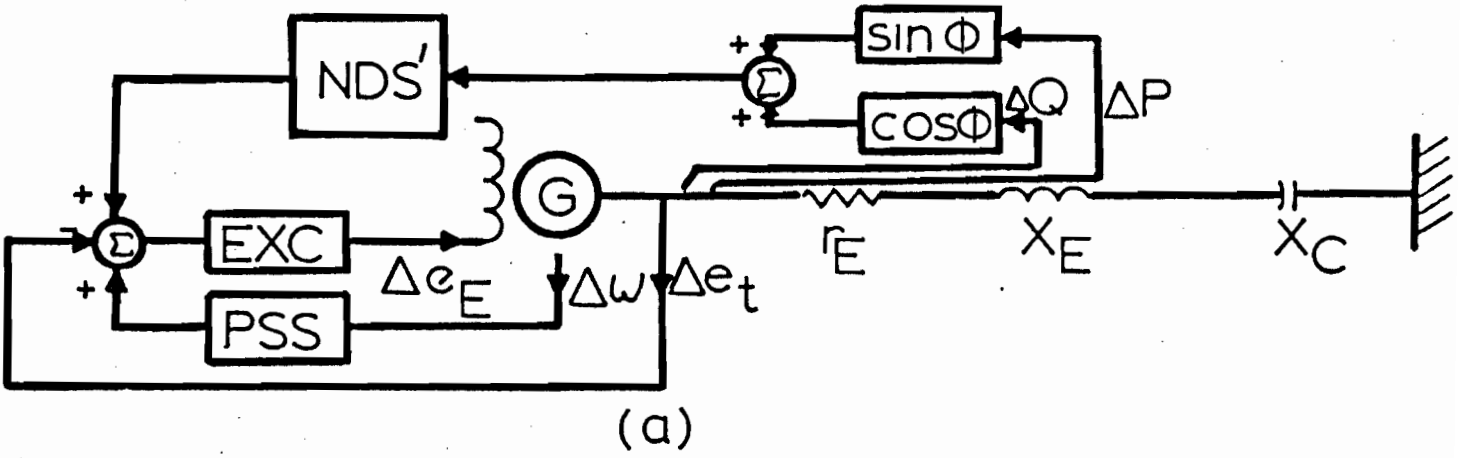

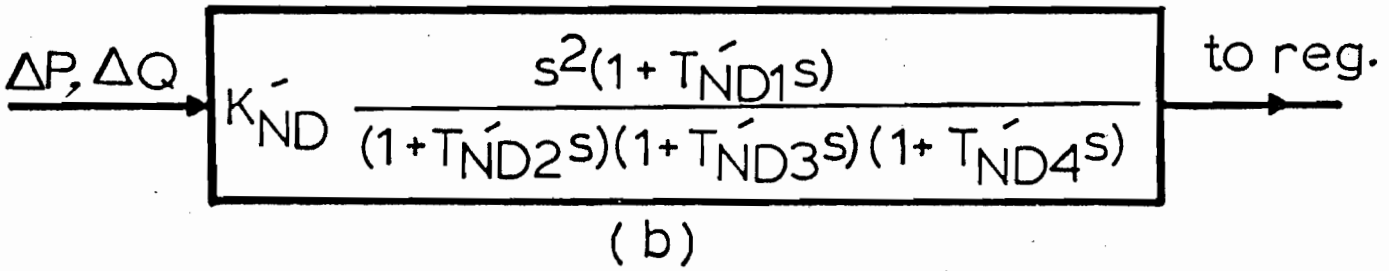

Figure 5.4. (a) The NDS' feedback scheme proposed in this thesis for the SSR suppression.

(b) The transfer function of the NDS' filter.

5.4 Feedback Scheme of the SSR Suppression

The feedback scheme proposed by Saito et al [17] for the field winding control of the SSR oscillation is shown in Figure 5.3(a). The transfer function of the filter used which was defined as the negative damping stabilizer (NDS), is shown in Figure 5.3(b). The output of this filter was added to the output of the excitation system.

In practice,it is necessary to power amplify the feedback signal to a level sufficient to derive the field current. Consequently, the output of the above NDS filter should be added to the input port of the excitation system. Therefore, the above feedback scheme is not realistic from the practical point of view. Nevertheless, this feedback loop is used in this thesis for the calibration of the proposed feedback loop. The mathematical derivation and the eigenvalues of the above scheme are shown in Appendix C.

In this chapter, a feedback loop which passes through the excitation system is proposed for the suppression of the unstable SSR oscillation. This scheme (see Figure 5.4(a)) will be referred to as the NDS' feedback scheme where its filter transfer function is shown in Figure 5.4(b). The state space model of the NDS' filter is obtained from Appendix B-2 as:

$$\frac{d}{dt}\begin{bmatrix} x_{N1} \\ x_{N2} \\ x_{N3} \end{bmatrix} = \begin{bmatrix} -a_{N1} & 1 & 0 \\ -a_{N2} & 0 & 1 \\ -a_{N3} & 0 & 0 \end{bmatrix} \begin{bmatrix} x_{N1} \\ x_{N2} \\ x_{N3} \end{bmatrix} + \begin{bmatrix} b_{N1} \\ b_{N2} \\ b_{N3} \end{bmatrix} \mu \qquad (5.6)$$

where

$$a_{N1} = \frac{T'_{ND2}\ T'_{ND3} + T'_{ND3}\ T'_{ND4} + T'_{ND2}\ T'_{ND4}}{T'_{ND2}\ T'_{ND3}\ T'_{ND4}}$$

$$a_{N2} = \frac{T'_{ND2} + T'_{ND3} + T'_{ND4}}{T'_{ND2}\ T'_{ND3}\ T'_{ND4}}$$

$$a_{N3} = \frac{1}{T'_{ND2}\ T'_{ND3}\ T'_{ND4}}$$

and

$$b_{N1} = K'_{ND} - K'_{ND}\ T'_{ND1}\ a_{N1}$$

$$b_{N2} = - K'_{ND}\ T'_{ND1}\ a_{N2}$$

$$b_{N3} = - K'_{ND}\ T'_{ND1}\ a_{N3}$$

The output from the NDS filter e_N is :

$$e_N = a_{N3}\ x_{N1} - b_{N3}\ \mu \qquad (5.7)$$

where μ is defined by equation 4.10.

The output of the NDS' feedback scheme is now added to the input port of the excitation system. This means, that when the closed loop system of Figure 5.4(a) is used in the analysis, the input signal of the excitation system which is Δe_E in equation 5.1, is now replaced by $\Delta e_t - e_N - e_P$. Furthermore, the system is now of eighteenth order. It has 18 eigenvalues: 9 corresponding to the basic system, 3 to the excitation system, 3 to the power system stabilizer PSS and 3 to the NDS' filter.

5.5 Sub-Systems Eigenvalues

In order to understand the interaction of the excitation, PSS and NDS' feedbacks, it is necessary to identify the eigenvalues associated with each sub-system. Because the system equations are augmented to a high order and because a numerical subroutine is involved to solve for the eigenvalues of matrix [A] , we quickly lose sight of the practical process involved. For this reason, the eigenvalues are calculated for the systems arranged as (1) system of Figure 5.1(a), (2) system of Figure 5.2(a), (3) system of Figure 5.4(a). The identification of the eigenvalues is accomplished by giving a physical interpretation to the weights in each element of each of the eigenvectors. The steps taken to identify the sub-system eigenvalues are:

(i) The basic system eigenvalues are calculated using equation 4.1. The nine eigenvalues obtained are identified in a way similar to that discussed in Chapter IV.

(ii) The eigenvalues are calculated for the basic system with the excitation system (Figure 5.1(a)). The state space equation used is that obtained from combining equations 4.1, 5.1 and 5.3. The additional three eigenvalues are related to the excitation system, and they will be called λ_{EXC}.

(iii) The basic system with the excitation system and the PSS (Figure 5.2(a)) is considered. The state space equation used is the combination of the one used in item (ii) and equations 5.4, 5.5. The additional three eigenvalues are related to the PSS and they will be called λ_{PSS}.

(iv) The system of Figure 5.4(a) is considered with the state space equation obtained by combining the one used in item (iii) and equations 5.6 and 5.7. The additional three eigenvalues are related to the NDS' filter and they will be called $\lambda_{NDS'}$.

Finally, all the sub-systems state space models derived in this chapter are in real time, and the basic system equation (equation 4.1) is also in real time. Therefore, all the eigenvalues are in real time which means that all the dampings and the natural frequencies associated with these eigenvalues are the physical dampings and frequencies of the system.

5.6 Numerical Example

The system under consideration has the following parameters:

TABLE 5.1

PARAMETERS OF THE 10 GVA [17] SYSTEM

Synchronous generator (reactances and resistances in p. u., when the base volt-ampere is 10 GVA and the base voltage is 500 KV).

H	=	2.83 sec.	X_{ad}	=	1.31	X_2	=	0.250	r_a	=	0.00150
X_d	=	1.50	X_{ffd}	=	1.42	X_{kkd}	=	1.40	r_{fd}	=	0.000630
X_q	=	1.49	X_{aq}	=	1.29	X_{kkq}	=	1.34	r_{kd}	=	0.0153
									r_{kq}	=	0.0207

Excitation System (Type 1 of Reference [55], Time Constants in Seconds).

	HRE	CE
K_A	500.	171.
T_A	0.0100	0.100
T_E	0.0250	3.00
K_F	0.00621	0.100
T_F	0.500	2.50

Power System Stabilizer, PSS (Time Constants in Seconds).

$K_P = 20.0$ $T_2 = 0.143$

$T_1 = 5.00$ $T_3 = 0.0670$

NDS' Filter (Time Constants in Seconds).

$K'_{ND} = 0.00100$ $T'_{ND1} = 0.0100$ $T'_{ND2} = 0.100$

$T'_{ND3} = 0.00600$ $T'_{ND4} = 0.0150$

Network (in p.u. values).

$r_E = 0.0295$ $X_E = 1.34$ X_C Variable

TABLE 5.2 (cont'd)

(b) - X_C = 0.1 , r_E = 0.0295 -

Eigenvalues

Row No.	System Configuration	λ_{ssrn}	λ_{ssrp}	$\lambda_{mech.}$	λ_{amort}	λ_{field}	λ_{EXC}		λ_{PSS}	
	Basic System	- 3.8	- 3.12	+ 2.21	- 32.8	- 3.3	- 70.8	- 3.30		
5	+	±	±	±	- 8.4	+	±	-		
	HRE	j 472	j 282	j 6.08		j 5.8	j 109	j 5.80		
	Basic System	- 3.8	- 3.1	- 10.6	- 37	- .26	- 70.8	-.260	- 2.5	
6	+	±	±	±	- 8.6	+	±	-	±	- 0.34
	HRE + PSS	j 472	j 282	j 3.2		j 4.1	j 109	j 4.10	j 13.0	

CE - Convention excitation system,

HRE - High response excitation system,

PSS - Power system stability.

5.6.3 Basic System and High Response Excitation System

Row No. 3 of Table 5.2 shows the eigenvalues of the same system (Figure 5.1(a)) but the CE excitation system is now replaced by the high response excitation system (HRE). A quick look on all the eigenvalues reveals that the mechanical mode is the only one which is largely affected by the use of the HRE system. The real part of this mode is now positive, indicating another kind of instability. This instability is known as the dynamic instability which is explained [56] as the building up oscillation of the rotor system of the synchronous generator against the infinite bus bar (Hunting). However, the field mode is complex with higher damping than in the case of CE and the response of the excitation system is now higher. This is indicated from the frequency and the damping associated with the excitation system eigenvalues ($-70.8 \pm j\ 109$). Therefore, the addition of the HRE system to the basic system gives fast voltage regulation and ensures the transient stability but results in dynamic instability. To ensure dynamic stability with the use of the HRE system, another supplementary signal is added to the input port of the excitation system through the power system stabilizer (PSS).

5.6.4 Basic System + HRE + PSS

Row No. 4 of Table 5.2 shows the eigenvalues of the system shown in Figure 5.2(a), where the PSS is now added to the system of

5.1(a). The addition of the PSS improves the mechanical mode by increasing its damping, but decreases the field mode damping to almost its value in the case of the system without the excitation feedback (Row No.1 in Table 5.2). Furthermore, the positive sequence SSR mode becomes more positive with a slight decrease in its natural frequency, and the amortisseur mode is improved. Physically, the introduction of the PSS produces damping torque which damps any mechanical oscillation, but interacts with the SSR positive sequence mode, since the input signal to the PSS is the shaft speed which contains a signal component at an angular frequency of $(\omega_0 - \omega_n)$. Remembering from Section 3.5.1 that the field excitation at this frequency affects the positive sequence SSR mode, it is not surprising that the PSS feedback will influence λ_{ssrp}. Using the phasor diagram Figure 3.6, it is evident that the phasor F_{cb}, which is introduced by the PSS signal,causes F_R to lie more in the unstable region.

The question which arises, is how does the level of series capacitor compensation influence the above conclusion ? This is answered in the fifth and sixth rows of Table 5.2 where the eigenvalues are calculated for a value of the series capacitive reactance X_C of 0.1 p.u. The exciter system is the HRE . The difference between the results in Rows Nos. 5 and 6 lies in the fact that the PSS feedback is absent and present respectively in the analysis. Comparing the results of Row No. 3 with Row No. 5 and Row No. 4 with Row No. 6, the SSR positive sequence mode has a higher frequency (see equation 1.1 and the concept of

the speed of the SSR positive sequence mmf phasor in the d-q rotating reference frame which was discussed in Section 3.3.2) and the frequency of the SSR negative sequence mode decreases. It is significant to note that the positive sequence SSR mode of λ_{ssrp}, which is unstable in Rows Nos. 3 and 4, becomes stable in Rows Nos. 5 and 6. This is because by decreasing X_C, the negative resistance, viewed by the SSR positive sequence current, decreases and at the value of X_C, where the net resistance in the path of the SSR positive sequence current is positive, stability is maintained and this is what happens at the low value of X_C. As is to be expected, the lower level of the series capacitor compensation implies that there is a lower frequency in the mechanical mode for $X_C = 0.1$ than $X_C = 1.2$, and this is apparent in the imaginary part of $\lambda_{mech.}$. Again, because the HRE system is used, the mechanical mode $\lambda_{mech.}$ is unstable without the PSS feedback as shown in Row No. 5. The need of the PSS feedback to stabilize the mechanical mode is demonstrated in Row No. 6.

5.6.5 The NDS' Feedback Loop

The proposed ΔP and ΔQ feedback scheme which is added to the system in the manner shown in Figure 5.4(a), is now considered in the analysis for evaluating its effectiveness in eliminating the unstable SSR oscillations. The transfer function of the NDS' filter is shown in

Figure 5.4(b) and the values of gain and time constants are given in Table 5.1. The transfer function of the NDS' filter is obtained from the following considerations:

(i) The NDS' filter is a band pass filter designed to provide the required magnitude and phase at the sub-synchronous frequency, as it was explained in Chapter III.

(ii) The NDS' feedback loop should not disturb the normal function of the PSS and the excitation system. This has been achieved by adjusting its gain and time constants.

However, the NDS' feedback scheme is calibrated against the scheme which was used in [17] as it is explained in Appendix C.

In Table 5.2, we noticed that the mode of λ_{ssrp} is unstable for $X_C = 1.2$. Our objective is to show that the NDS' feedback will stabilize this mode. Furthermore, our concern is that the fast voltage regulation and the transient stability of the HRE and the PSS systems are not deteriously affected by the new NDS' feedback loop.

Table 5.3 shows the eigenvalues of the closed loop system of Figure 5.4(a) for different values of the control angle ϕ . The eigenvalues in the first row of Table 5.3 demonstrate the dynamic

instability in the absence of the power system stabilizer when the HRE excitation system is used. Comparing these eigenvalues with those in the third row of Table 5.2, we notice that the SSR negative sequence mode λ_{ssrn} does not change. The SSR positive sequence mode is now stabilized as the real part of λ_{ssrp} is now negative. The real part of the mechanical mode is more positive and the field mode is a real negative eigenvalue with high damping. However, the excitation system is still characterized by high damping and high frequency of oscillation as it is clear from the real and the imaginary parts of its eigenvalues $(-81.0 \pm j\ 76.7)$. Therefore, the addition of the NDS' feedback loop does not disturb the normal function of the excitation system and it effectively suppresses the SSR mode. However, the mechanical mode becomes worse with the NDS' feedback loop which means that the NDS' feedback reduces the damping torques in the system, as it was noticed in Chapter IV. The second row of Table 5.3 shows the eigenvalues of the system of Figure 5.4(a), i.e., the PSS is now added to the system of the eigenvalues shown in the first row of the same table. A comparison between the eigenvalues in the first and second rows of Table 5.3 shows the interaction between the PSS and the SSR mode which reduces the damping of the SSR mode when the PSS is added.

The eigenvalues in the last three rows of Table 5.3 show the effect of changing the control angle ϕ from which it is clear that the damping of the SSR positive sequence mode λ_{ssrp} is improved for positive control angles $(\phi > 360)$ and it is worsened for negative control

TABLE 5.3

EIGENVALUES OF THE 10 GVA SYSTEM WITH THE NDS' FEEDBACK LOOP FOR $X_C = 1.2$, $r_E = 0.0295$, $K'_{ND} = .001$

Row No.	System Configu.	λ_{ssrn}	λ_{ssrp}	$\lambda_{mech.}$	$\lambda_{amort.}$	λ_{field}	λ_{EXC}		λ_{PSS}		$\lambda_{NDS'}$	
	Basic System	- 4.23	- 5.20	+ 2.00	- 23.1		- 81.0				- 118.1	
1 $\phi = 0^o$	+	±	±	±	±	- 2.27	±	- 4.20			±	- 9.23
	NDS'+HRE	j 705	j 55.9	j 11.1	j 17.7		j 76.7				j 45.7	
	System	- 4.22	- 3.38	- 7.02	- 27.1	- 1.54	-81.6	- 1.54	- 4.24		- 118.2	
2 $\phi = 0^o$	of	±	±	±	±	+	±	-	±	- .212	±	- 10.8
	Fig.5.4(a)	j 705	j 49.7	j 4.03	j 8.00	j 1.21	j 77.2	j 1.21	j 33.7		j 45.4	
	System	- 4.23	- 12.1	- 6.80	- 27.1	- 1.54	- 80.7	- 1.54	+ 5.22		- 120.	
3 $\phi = 30^o$	of	±	±	±	±	+	±	-	±	- .212	±	- 11.0
	Fig.5.4(a)	j 705	j 39.6	j 3.96	j 7.39	j 1.21	j 82.8	j 1.21	j 41.0		j 39.7	
	System	- 4.20	- 1.04	- 7.44	- 28.3	- 1.54	- 77.8	- 1.54	- 5.52		- 122.	
4 $\phi = 330^o$	of	±	±	±	±	+	±	-	±	- .212	±	- 10.5
	Fig.5.4(a)	j 705	j 55.6	j 3.86	j 7.67	j 1.21	j 85.0	j 1.21	j 27.5		j 33.8	
	System	- 4.18	+ .504	- 7.73	- 29.3	- 1.54	- 74.6	- 1.54	- 5.90		- 125.	
5 $\phi = 315^o$	of	±	±	±	±	+	±	-	±	- .212	±	- 10.2
	Fig.5.4(a)	j 705	j 56.8	j 3.67	j 7.11	j 1.22	j 91.1	j 1.22	j 25.2		j 22.3	

Eigenvalues

$\lambda_{NDS'}$ The eigenvalues related to the NDS' filter.

angles ($\phi < 360$) . In addition, the damping of the mechanical mode is improved for negative values of the control angle, ϕ ($\phi < 360$). However, for positive control angles the damping of the PSS mode λ_{PSS} decreases and for high positive value of ϕ (say, 30^{o} in Table 5.3), the PSS mode is unstable as it is shown in the third row of Table 5.3.

5.6.6 Eigenvectors and mmf Phasor Diagram of λ_{ssrp}

The system under consideration is unstable in the open loop operation when the value of the series capacitive reactance, X_C is 1.2 p.u. This is clear from the positive real part of the SSR mode in the eigenvalues of the fourth row of Table 5.2. As it was explained in Chapter III, this instability is due to the induction generation effect which occurs at the subsynchronous frequency. This can be explained on the basis of the SSR mmf phasor diagram constructed from the eigenvectors of the open loop system listed in Table 5.4 as shown in Figure 5.5(a). The torque angle is an obtuse angle which according to equation 3.1 indicates a generating regime.

The addition of the NDS' feedback loop stabilizes the system, as judged from the negative real parts of the eigenvalues of the second and fourth rows of Table 5.3. In the light of the concept of the field excitation control of the SSR oscillations which is introduced in Chapter III, the stabilization of the system under SSR oscillation is possible if the

NDS' feedback loop is capable of eliminating the induction generation action. This is demonstrated by the SSR mmf phasor diagram constructed from the closed loop eigenvectors of Table 5.5, as shown in Figure 5.5(b). The torque angle in Figure 5.5(b) is a reflex angle which indicates motoring regime.

5.7 The $X_C - r_E$ Stability Region

In the current analysis, three modes have been noticed to be the cause of system instability. The first mode is the positive sequence SSR mode λ_{ssrp} which causes building up oscillation at high level of series capacitor compensation, and this is stabilized by the NDS' feedback scheme. The second mode is the mechanical mode which causes the rotor system to oscillate against the electrical system and this is associated with the use of the HRE excitation system. This mode is stabilized by the introduction of the power system stabilizer with the shaft speed as the stabilizing signal. The third mode is the power system stabilizer mode and its instability occurs at high level of series capacitor compensation when the NDS' feedback scheme is used to suppress the SSR oscillation (see the third row of Table 5.3). This results from the interaction between the shaft speed signal feedback loop in the PSS and the ΔP and ΔQ feedback, since both of them have a frequency component. This is stabilized by the proper choice of the control angle ϕ. Furthermore, it was noticed from Table 5.2 that the use of the PSS and

TABLE 5.4

EIGENVALUES AND EIGENVECTORS FOR THE OPEN LOOP SYSTEM OF FIGURE 5.2(a) WHEN $X_C = 1.2$, $r_E = 0.0295$

Eigenvalues Classification	λ_{ssrn}		λ_{ssrp}		$\lambda_{mech.}$		$\lambda_{amort.}$		λ_{field}
Eigenvalues	- 4.174 + j 705	- 4.174 - j 705	+ 7.73 + j 43.8	+ 7.73 - j 43.8	- 7.52 + j 1.71	- 7.52 - j 1.71	- 36.2	- 26.3	- .745 + j 2.13
Eigenvectors Δi_D	125.E-5	125.E-5	88.E-6	88.E-6	122.E-6	122.E-6	36.E-5	67.E-5	214.E-5
	166.	-166.	-165.	165.	-92.7	92.7	0.0	0.0	-58.9
Δi_Q	124.E-5	124.E-5	80.E-5	80.E-5	134.E-6	134.E-6	43.E-5	140.E-5	38.E-4
	-104.	104.	-75.	75.	-135.	135.	180.	-180.	123.
Δi_{fd}	54.E-5	54.E-5	72.E-6	72.E-6	9.0E-5	9.0E-5	0.00260	0.00260	26.E-4
	163.	-163.	145.	-145.	-82.4	82.4	180.	-180.	-55.1
Δi_{kd}	66.E-5	66.E-5	52.E-6	52.E-6	70.0E-6	70.0E-6	0.00312	0.00312	24.E-5
	168.	-168.	145.	-145.	-105.	105.	0.0	0.0	-140.
Δi_{kq}	12.E-4	12.E-4	75.E-6	75.E-6	41.E-5	41.E-5	500.E-6	170.E-5	150.E-5
	-103.	103.	-67.5	67.5	-102.	102.	180.	-180.	-150.

TABLE 5.4 (cont'd)

Eigenvalues Classification		λ_{ssrn}		λ_{ssrp}		$\lambda_{mech.}$		$\lambda_{amort.}$		λ_{field}
Eigenvalues		- 4.174 + j 705	- 4.174 - j 705	+ 7.73 + j 43.8	+ 7.73 - j 43.8	- 7.52 + j 1.71	- 7.52 - j 1.71	- 36.2	- 26.3	- .745 + j 2.13
Eigenvectors	$\Delta\bar{\omega}$	3.E-7	3.E-7	40.E-8	40.E-8	388.E-8	388.E-8	380.E-9	840.E-9	20.E-6
		- 51.9	51.9	- 18.6	18.6	- 96.0	96.0	0.0	180.	- 145.
	$\Delta\delta$	184.E-9	184.E-9	34.E-7	34.E-7	19.E-5	19.E-5	390.E-8	120.E-7	34.E-4
		-142.	142.	- 98.6	98.6	97.1	- 97.1	180.0	0.0	106.
	Δe_{CD}	17.E-4	17.E-4	11.E-5	11.E-5	16.0E-5	16.0E-5	560.E-6	170.E-5	46.E-4
		75.4	- 75.4	- 76.2	76.2	- 135.	135.	180.	- 180.	123.
	Δe_{CQ}	17.E-4	17.E-4	12.E-5	12.E-5	15.0E-5	15.0E-5	400.E-6	400.E-6	26.E-4
		166.	-166.	13.4	- 13.4	86.3	- 86.3	180.	- 180.	122.
	x_{E1}	32.E-7	32.E-7	883.E-7	883.E-7	46.0E-5	46.0E-5	750.E-6	310.E-5	0.0662
		39.7	- 39.7	10.2	- 10.2	21.6	- 21.6	0.0	0.0	23.0
	x_{E2}	23.E-4	23.E-4	0.014	0.014	0.0620	0.0620	0.0796	0.356	9.35
		119.	- 119.	26.5	- 26.5	22.3	- 22.3	0.0	0.0	23.9

TABLE 5.4 (cont'd)

Eigenvalues Classification		λ_{ssrn}		λ_{ssrp}		$\lambda_{mech.}$		$\lambda_{amort.}$		λ_{field}
Eigenvalues		- 4.174 + j 705	- 4.174 - j 705	+ 7.73 + j 43.8	+ 7.73 - j 43.8	- 7.52 + j 1.71	- 7.52 - j 1.71	- 36.2	- 26.3	- .745 + j 2.13
Eigenvectors		1.57	1.57	1.55	1.55	7.29	7.29	9.84	42.7	1110.
	x_{E3}	- 152.	152.	33.3	- 33.3	22.4	- 22.4	0.0	0.0	24.0
		13.E-5	13.E-5	375.E-5	375.E-5	.00210	.00210	0.00970	.0310	0.055
	x_{P1}	140.	-140.	- 26.0	26.0	88.1	- 88.1	0.0	180.	- 158.
		0.0942	0.0942	. 693.	693.	0.339	0.339	1.32	4.50	9.48
	x_{P2}	- 143.	143.	- 12.2	12.2	88.7	- 88.7	0.0	180.	- 157.
		1.54	1.54	21.9	21.9	760.	760.	90.0	386.	2550.
	x_{P3}	- 142.	142.	51.8	- 51.8	84.5	- 84.5	0.0	180.	41.0

E represents Exponent, e.g., 125.E-5 = 125×10^{-5}

Note: The first row of the eigenvectors correspond to the magnitude of the state variable. The second row corresponds to the phase of the state variable.

TABLE 5.4 (cont'd)

Eigenvalues Classification		λ_{EXC}			λ_{PSS}	
Eigenvalues	- 7.45 - j 2.13	- 70.8 + j 109	- 70.8 - j 109	- .211	- 7.3 + j 27.2	- 7.3 - j 27.2
Eigenvectors Δi_D	214.E-5	.0370	.0370	35.E-7	124.E-5	124.E-5
	58.9	98.6	- 98.6	0.0	94.9	- 94.9
Δi_Q	38.E-4	0.0597	0.0597	55.E-7	58.E-5	58.E-5
	- 123.	- 64.0	64.	180.	-175.	175.
Δi_{fd}	26.E-4	98.E-11	98.E-11	42.E-7	222.E-5	222.E-5
	55.1	90.4	- 90.4	0.0	133.	- 133.
Δi_{kd}	24.E-5	90.E-11	90.E-11	36.E-9	14.E-4	14.E-4
	140.	- 88.4	88.4	0.0	- 7.26	7.26
Δi_{kq}	150.E-5	59.E-12	59.E-12	20.E-8	58.E-5	58.E-5
	150.	- 61.3	61.3	0.0	- 163.	163.
$\Delta \bar{\omega}$	20.E-6	48.E-15	48.E-15	27.E-10	70.E-7	70.E-7
	145.	75.2	- 75.2	0.0	- 163.	163.

TABLE 5.4 (cont'd)

Eigenvalues Classification		λ_{EXC}			λ_{PSS}	
Eigenvalues	- 7.45 - j 2.13	- 70.8 + j 109	- 70.8 - j 109	- .211	- 7.3 + j 27.2	- 7.3 - j 27.2
Eigenvectors $\Delta\delta$	34.E-4	14.E-14	14.E-14	49.E-7	934E-7	934E-7
	- 106.	- 47.8	47.8	180.	91.9	- 91.9
Δe_{CD}	46.E-4	80.E-12	80.E-12	67.E-7	81.E-5	81.E-5
	- 123	- 68.1	68.1	180.	- 173.	173.
Δe_{CQ}	26.E-4	31.E-12	31.E-12	42.E-7	154.E-5	154.E-5
	- 122.	- 43.3	43.3	180.	- 85.0	85.0
x_{E1}	0.0662	36.E-4	36.E-4	80.E-5	98.E-5	98.E-5
	- 23.0	81.8	- 81.8	180.	- 121.	121.
x_{E2}	9.35	0.467	0.467	0.115	0.134	0.134
	- 23.9	138.6	- 138.6	180.	- 110.	110.
x_{E3}	1110.0	0.221	0.221	13.7	15.2	15.2
	- 24.0	139.	- 139.	180.	- 109.	109.

TABLE 5.4 (cont'd)

Eigenvalues Classification		λ_{EXC}				λ_{PSS}	
Eigenvalues		- 7.45 - j 2.13	- 70.8 + j 109	- 70.8 - j 109	- .211	- 7.3 + j 27.2	- 7.3 - j 27.2
Eigenvectors		0.055	36.E-4	36.E-4	82.E-5	0.0763	0.0763
	x_{P1}	158.	- 98.2	98.2	0.0	- 146.	146.
		9.48	0.533	0.533	0.14	12.7	12.7
	x_{P2}	157.	- 51.2	51.2	0.0	- 137.	137.
		2550.	14.7	14.7	16.9	750.	750.
	x_{P3}	- 41.0	- 44.1	44.1	0.0	- 75.6	75.6

TABLE 5.5

EIGENVALUES AND EIGENVECTORS OF THE SYSTEM OF FIGURE 5.4(a)
(CLOSED LOOP SYSTEM) FOR $\phi = 0.0$, $K'_{ND} = 0.001$, $X_C = 1.2$, $r_E = .0295$

Eigenvalues Classification		λ_{ssrn}		λ_{ssrp}		$\lambda_{mech.}$		$\lambda_{amort.}$		λ_{field}
Eigenvalues		- 4.22 + j 705	- 4.22 - j 705	- 3.38 + j 49.7	- 3.38 - j 49.7	- 7.02 + j 4.03	- 7.02 - j 4.03	- 27.1 + j 7.95	- 27.1 - j 7.95	- 1.54 + j 1.21
Eigenvectors	Δi_D	0.0324	0.0324	0.0641	0.0641	.632	0.632	3.32	3.32	7.33
		158.	- 158.	- 102.	102.	- 123.	123.	88.2	- 88.2	- 112
	Δi_Q	0.0321	0.0321	0.0604	0.0604	.427	.427	3.57	3.57	11.4
		- 112.	112.	9.00	- 9.00	115.	- 115.	- 60.5	60.5	73.5
	Δi_{fd}	0.0141	0.0141	0.111	.111	.174	.174	10.6	10.6	6.70
		157.	- 157.	- 129.	129.	- 32.5	32.5	- 129.	129.	- 95
	Δi_{kd}	.0171	.0171	0.0573	0.0573	.818	.818	14.5	14.5	3.24
		159.	- 159.	26.3	- 26.3	- 135.	135.	62.1	- 62.1	- 150
	Δi_{kq}	0.0309	0.0309	0.0576	0.0576	.288	.288	4.18	4.18	1.16
		- 112.	112.	16.7	- 16.7	- 133.	133.	- 55.4	55.4	- 151

TABLE 5.5 (cont'd)

Eigenvalues Classification		λ_{ssrn}		λ_{ssrp}		$\lambda_{mech.}$		$\lambda_{amort.}$		λ_{field}
Eigenvalues		- 4.22 + j 705	- 4.22 - j 705	- 3.38 + j 49.7	- 3.38 - j 49.7	- 7.02 + j 4.03	- 7.02 - j 4.03	- 27.1 + j 7.95	- 27.1 - j 7.95	- 1.54 + j 1.21
Eigenvectors	$\Delta \bar{\omega}$	90.E-7	90.E-7	202.E-6	202.E-6	0.0100	0.0100	904.E-5	904.E-5	0.0533
		- 60.4	60.4	41.7	- 41.7	- 116.	116.	68.6	- 68.6	- 148
	$\Delta \delta$	48.E-7	48.E-7	153.E-5	153.E-5	.469	.469	0.121	0.121	10.2
		- 151.	151.	- 52.2	52.2	93.6	- 93.6	- 94.8	94.8	70.6
	Δe_{CD}	5.18	5.18	6.81	6.81	19.6	19.6	69.5	69.5	99.4
		55.8	- 55.8	- 135.	135.	57.5	- 57.5	- 37.0	37.0	30.4
	Δe_{CQ}	.329	.329	4.41	4.41	23.6	23.6	183.	183.	103.
		- 31.3	31.3	- 67.1	67.1	50.5	- 50.5	- 68.6	68.6	28.6
	x_{E1}	29.E-7	29.E-7	55.E-5	55.E-5	0.02280	0.0228	0.0432	0.0432	.497
		58.5	- 58.5	21.3	- 21.3	89.3	- 89.3	50.9	50.9	139.
	x_{E2}	0.0445	0.0445	0.0838	0.0838	.514	.514	4.47	4.47	13.7
		66.9	- 66.9	7.02	- 7.02	113.	- 113.	- 63.1	63.1	73.4

TABLE 5.5 (cont'd)

Eigenvalues Classification	λ_{ssrn}		λ_{ssrp}		$\lambda_{mech.}$		$\lambda_{amort.}$		λ_{field}
Eigenvalues	- 4.22 + j 705	- 4.22 - j 705	- 3.38 + j 49.7	- 3.38 - j 49.7	- 7.02 + j 4.03	- 7.02 - j 4.03	- 27.1 + j 7.95	- 27.1 - j 7.95	- 1.54 + j 1.21
Eigenvectors	0.0444	0.0444	0.0873	0.0873	.748	.748	3.66	3.66	8.73
x_{E3}	157.	- 157.	81.0	- 81.0	57.2	- 57.2	- 92.9	92.9	68.6
	42.E-8	42.E-8	129.E-6	129.E-6	.0235	.0235	0.0253	0.0253	.0900
x_{P1}	30.8	- 30.8	149.	- 149.	55.3	- 55.3	109.	- 109.	28.4
	47.E-7	47.E-7	143.E-5	143.E-5	.218	.218	.303	.303	.816
x_{P2}	30.9	- 30.9	151.	- 151.	67.5	- 67.5	111.	- 111.	27.1
	115.E-8	115.E-8	354.E-6	354.E-6	.0238	.0238	.0651	.0651	.464
x_{P3}	30.6	- 30.6	146.	- 146.	41.1	- 41.1	109.	- 109.	- 91.0
	155.E-9	155.E-9	121.E-8	121.E-8	111.E-7	111.E-7	100.E-6	100.E-6	205.E-6
x_{N1}	- 137.	137.	16.2	- 16.2	80.3	- 80.4	- 79.1	79.1	71.0

TABLE 5.5 (cont'd)

Eigenvalues Classification	λ_{ssrn}		λ_{ssrp}		$\lambda_{mech.}$		$\lambda_{amort.}$		λ_{field}
Eigenvalues	- 4.22 + j 705	- 4.22 - j 705	- 3.38 + j 49.7	- 3.38 - j 49.7	- 7.02 + j 4.03	- 7.02 - j 4.03	- 27.1 + j 7.95	- 27.1 - j 7.95	- 1.54 + j 1.21
Eigenvectors x_{N2}	142.E-7	142.E-7	957.E-7	957.E-7	732.E-6	732.E-6	697.E-5	697.E-5	.0134
	- 136.	136.	23.3	- 23.3	92.5	- 92.5	- 75.0	75.0	72.4
Eigenvectors x_{N3}	123.E-6	123.E-6	823.E-6	823.E-6	0.0118	0.0118	0.0843	0.0843	.0315
	-135.	135.	33.2	- 33.2	174.	- 174.	- 67.8	67.8	- 155.

E represents Exponent, e.g., .30.E-4 = 30×10^{-6}

Note: The first row of the eigenvectors represent the magnitude of the state variable and the second row is the phase of the vector in elec. degrees.

TABLE 5.5 (cont'd)

Eigenvalues Classification		λ_{EXC}			λ_{PSS}			$\lambda_{NDS'}$		
Eigenvalues	- 81.6 + j 77.2	- 81.6 - 77.2	- 1.54 - j 1.21	- 4.24 + j 33.7	- 4.24 - 33.7	- .212	- 118.0 + j 45.4	- 118.0 - j 45.4	- 10.8
Eigenvectors Δi_D	.201	.201	7.33	.712	.712	.946	0.0975	0.0975	7.35
	106.	- 106.	112.	- 199.	161.	180.	- 136.	136.	0.0
Δi_Q	.258	.258	11.4	.377	.377	1.50	0.0985	0.0985	.800
	- 67.1	67.1	- 73.5	- 52.0	52.0	0.0	50.1	- 50.1	180.
Δi_{fd}	4.68	4.68	6.70	1.34	1.34	1.10	2.72	2.72	1.47
	106.	- 106.	95.	- 140.	140.	180.	- 131.	131.	180.
Δi_{kd}	4.30	4.30	3.24	.661	.661	.0431	2.53	2.53	10.7
	- 71.6	71.6	150.	68.3	- 68.3	180.	49.9	- 49.9	0.0
Δi_{kq}	.257	.257	1.16	.367	.367	.0148	0.0988	0.0988	4.10
	- 65.0	65.0	151.	- 38.1	38.1	180.	51.1	- 51.1	0.0
$\Delta \tilde{\omega}$	162.E-6	162.E-6	0.0533	305.E-5	305.E-5	726.E-6	794.E-7	794.E-7	.0938
	87.2	- 87.2	148.	- 46.0	46.0	180.	- 139.	139.	0.0

TABLE 5.5 (cont'd)

Eigenvalues Classification		λ_{EXC}			λ_{PSS}			$\lambda_{NDS'}$	
Eigenvalues	- 81.6 + j 77.2	- 81.6 - 77.2	- 1.54 - j 1.21	- 4.24 + j 33.7	- 4.24 - 33.7	- .212	- 118.0 + j 45.4	- 118.0 - j 45.4	- 10.8
Eigenvectors $\Delta\ \delta$	544.E-6	544.E-6	10.3	0.0339	0.0339	1.29	236.E-6	236.E-6	3.27
	- 49.4	49.4	- 70.6	- 143.	143.	0.0	62.5	- 62.5	180.
Δe_{CD}	1020.	1020.	99.4	58.3	58.3	0.061	658.	658.	201.
	- 10.0	10.0	- 30.4	- 20.	20.	0.0	172.	- 172.	180.
Δe_{CQ}	467.	467.	103.	47.5	47.5	0.0613	291.	291.	275.
	- 128.	128.	- 28.6	- 63.0	63.0	0.0	22.3	- 22.3	180.
x_{E1}	262.E-4	262.E-4	.497	873.E-5	873.E-5	213.E-6	0.0145	0.0145	.194
	- 84.1	84.1	- 139.	23.5	- 23.5	180.	43.6	- 43.6	180.
x_{E2}	.357	.357	13.7	0.532	0.532	1.80	0.142	0.142	1.21
	- 70.8	70.8	- 73.4	- 53.0	53.0	0.0	47.3	- 47.3	180.
x_{E3}	.174	.174	8.73	0.898	0.898	1.13	0.0729	0.0729	8.79
	- 50.4	50.4	- 68.6	20.1	- 20.1	0.0	54.7	- 54.7	180

TABLE 5.5 (cont'd)

Eigenvalues Classification		λ_{EXC}			λ_{PSS}			$\lambda_{NDS'}$		
Eigenvalues	- 81.6 + j 77,2	- 81.6 - 77,2	- 1.54 - j 1.21	- 4.24 + j 33.7	- 4.24 - 33.7	- .212	- 118.0 + j 45.4	- 118.0 - j 45.4	- 10.8
Eigenvectors x_{P1}	535.E-7	535.E-7	.0900	.276E-2	.276E-2	388.E-5	238.E-7	238.E-7	.0228
	138.	- 138.	28.4	68.3	- 68.3	180.	- 114.	114.	180.
x_{P2}	605.E-6	605.E-6	.816	0.0307	0.0307	.140	270.E-6	270.E-6	2.65
	139.	- 139.	27.1	70.5	- 70.5	180.	- 114.	114.	0.0
x_{P3}	146.E-6	146.E-6	.464	0.00750	0.00750	1.13	648.E-7	648.E-7	.697
	137.	- 137.	91.0	63.5	- 63.5	180.	- 114.	114.	0.0
x_{N1}	145.E-7	145.E-7	205.E-6	109.E-7	109.E-7	266.E-7	143.E-7	143.E-7	155.E-6
	- 117.	117.	- 71.0	- 21.0	21.0	0.0	11.4	- 11.4	180.
x_{N2}	137.E-5	137.E-5	.0134	832.E-6	832.E-6	177.E-5	157.E-5	157.E-5	.0206
	- 105.	105.	- 72.4	- 14.	14.	0.0	22.0	- 22.0	180.
x_{N3}	0.0125	0.0125	.0315	717.E-5	717.E-5	385.E-6	0.0145	0.0145	.875
	- 102.	102.	155.	0.0	0.0	180.	23.5	- 23.5	180.

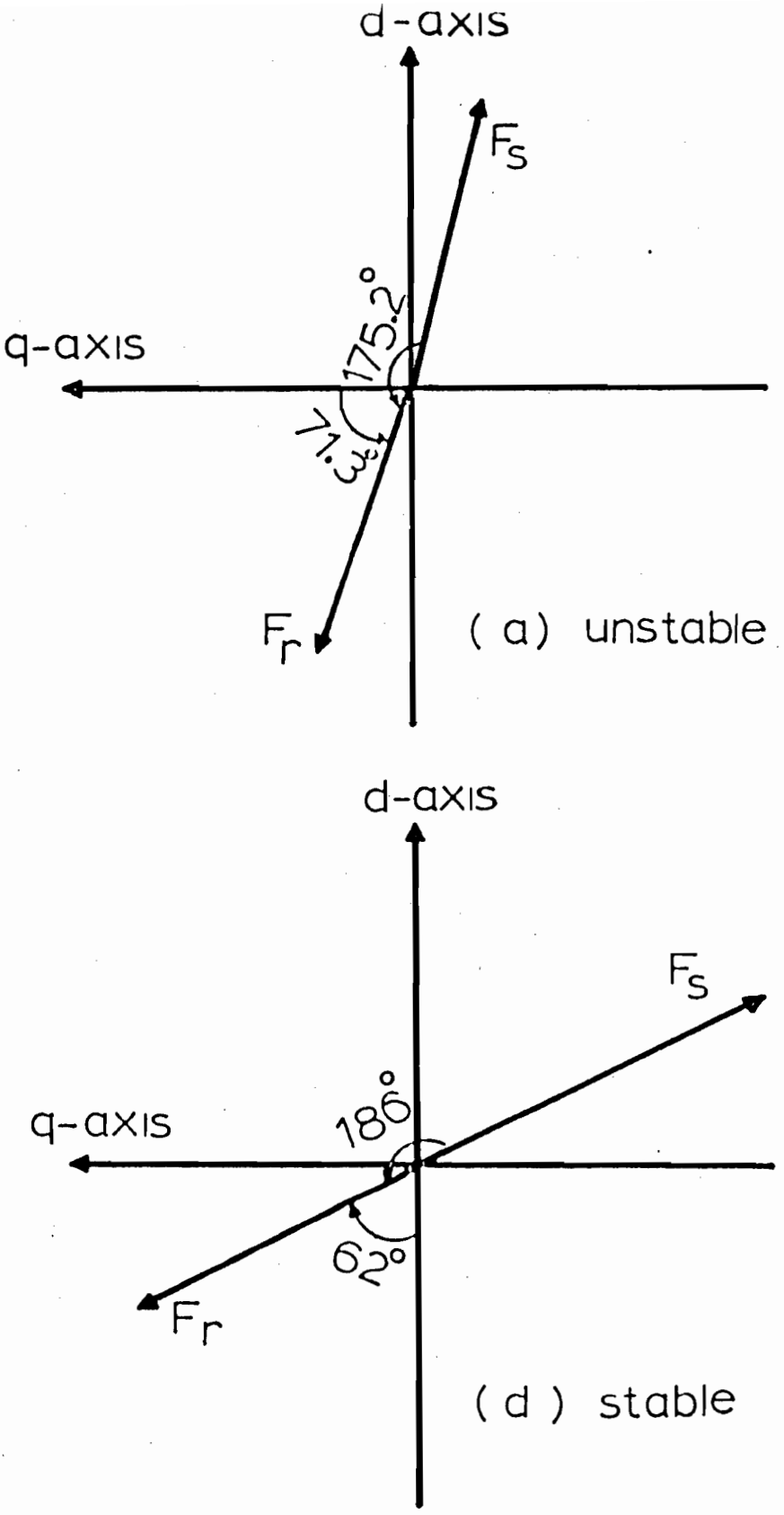

Figure 5.5. MMF phasor diagram for the SSR positive sequence mode constructed from the numerical results for:

(a) Open loop system (Figure 5.2(a))
(b) Closed loop system (Figure 5.4(a))

the HRE sub-systems makes the real part of the open loop positive sequence SSR mode λ_{ssrp} more positive. Thus, mapping the stability boundary on the $X_C - r_E$ plane will explain the effect of the system complexities on its stability. Practically, the values of the line resistance commonly used lie in the range of 0.01 - 0.06 p.u. Therefore, this range is going to be used in the $X_C - r_E$ plane for the stability boundary.

5.7.1 Effect of HRE and PSS

Figure 5.6 shows the stability boundary on the $X_C - r_E$ plane for the same operating condition given in Table 5.1. The solid line represents the case when the basic system or the basic system with the conventional excitation system (CE) are used. The broken line represents the case when the basic system, the high response excitation system HRE and the power system stabilizer PSS are used. It is clear that in the case of the HRE and the PSS systems, the stability region is now smaller.

5.7.2 Effect of NDS' Gain K'_{ND} and Angle ϕ

Figure 5.7 shows the stability boundary of the closed loop system of Figure 5.4(a) for different combinations of the NDS' gain K'_{ND} and the control angle ϕ. The stability boundaries in Figure 5.7

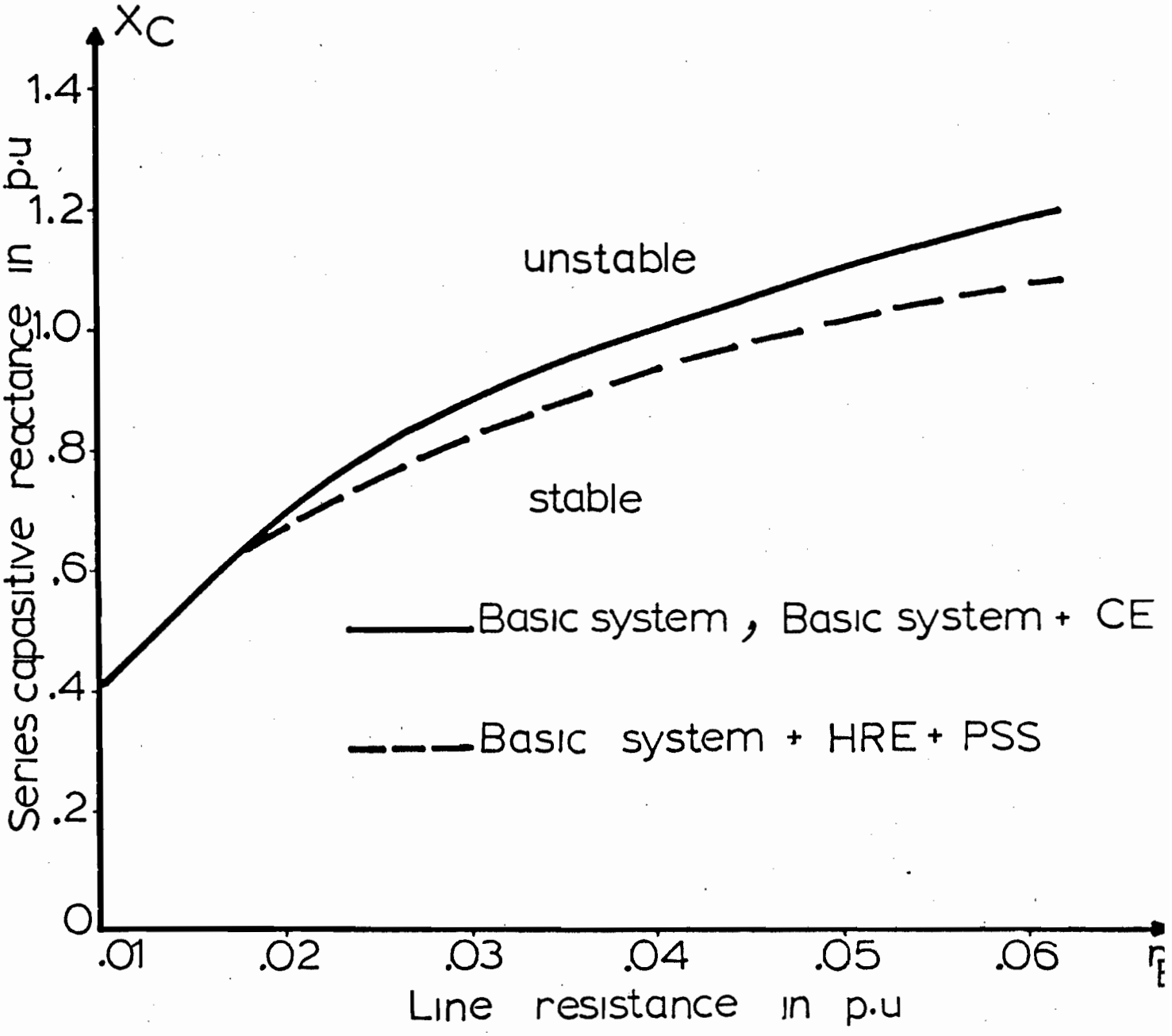

Figure 5.6. Stability boundary in the $X_C - r_E$ plane for the open loop system showing the effect of the HRE and PSS systems (broken line).

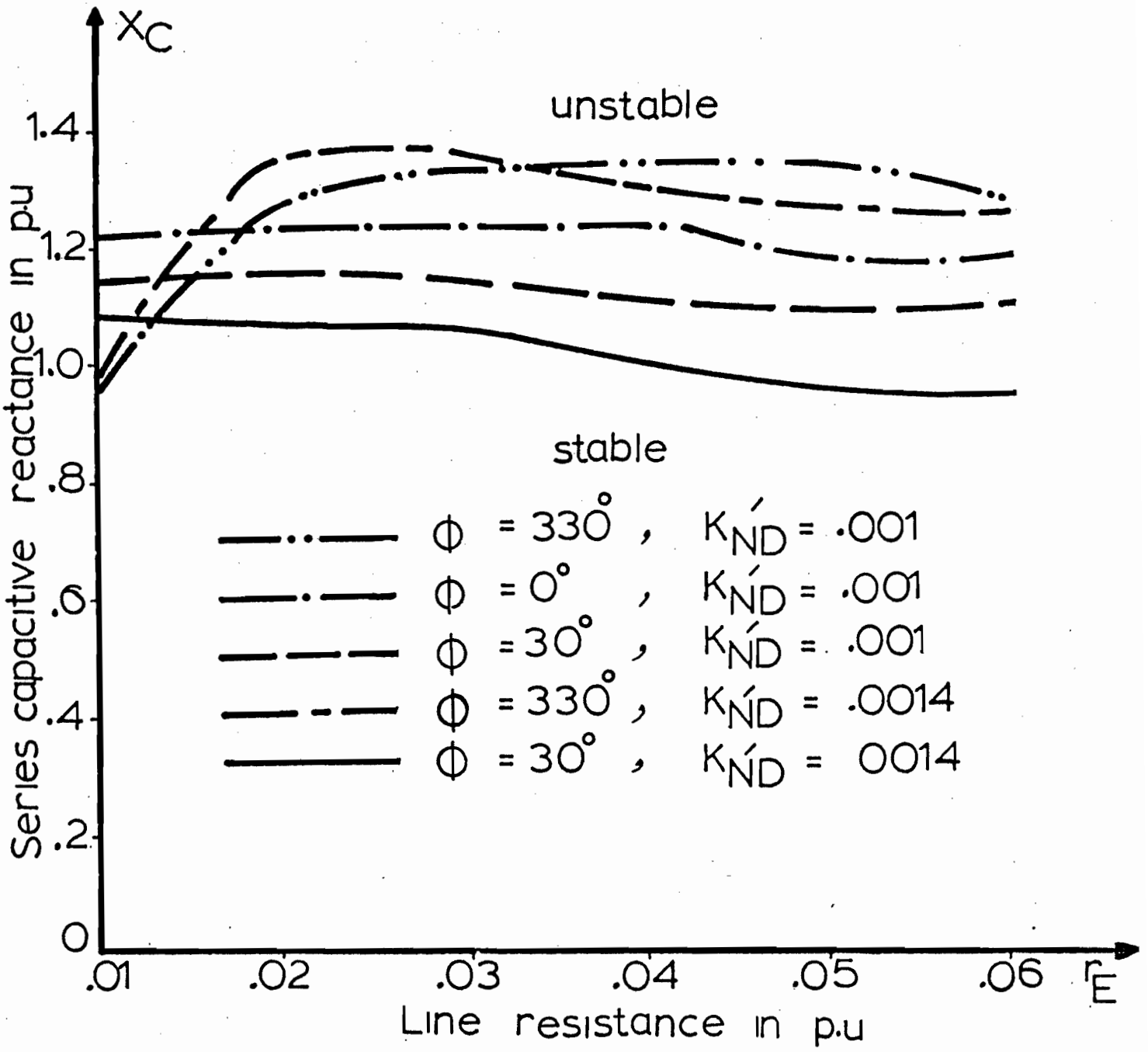

Figure 5.7. Stability boundary on the $X_C - r_E$ plane for the closed loop system (Figure 5.4(a)) for different combinations of the NDS' gain K_{ND}' and the control angle ϕ .

explore the possibility of improving the stability region of the closed loop system by a proper combination of the NDS' parameter (K'_{ND} and ϕ).

5.7.3 Effect of PSS gain K_P

It was explained previously that for high levels of series capacitor compensation and when the NDS' feedback loop is used to stabilize the system, the new unstable mode is that from the PSS . Therefore, a change in the PSS transfer function parameter may improve the stability regions. Figure 5.8 shows the case when the NDS' feedback scheme is used (see Figure 5.4(a)) for two different values of the PSS gain K_P . It shows that decreasing K_P the stability region becomes wider.

5.8 Effect of K'_{ND}

The 10 GVA system under consideration is unstable in the open loop operation at high levels of series capacitor compensation (see the broken line in Figure 5.6). This instability is because of building up SSR oscillations. However, in the closed loop operation and under high levels of series capacitor compensation, the closed loop is also unstable because of the shaft speed loop. This is clear from the positive

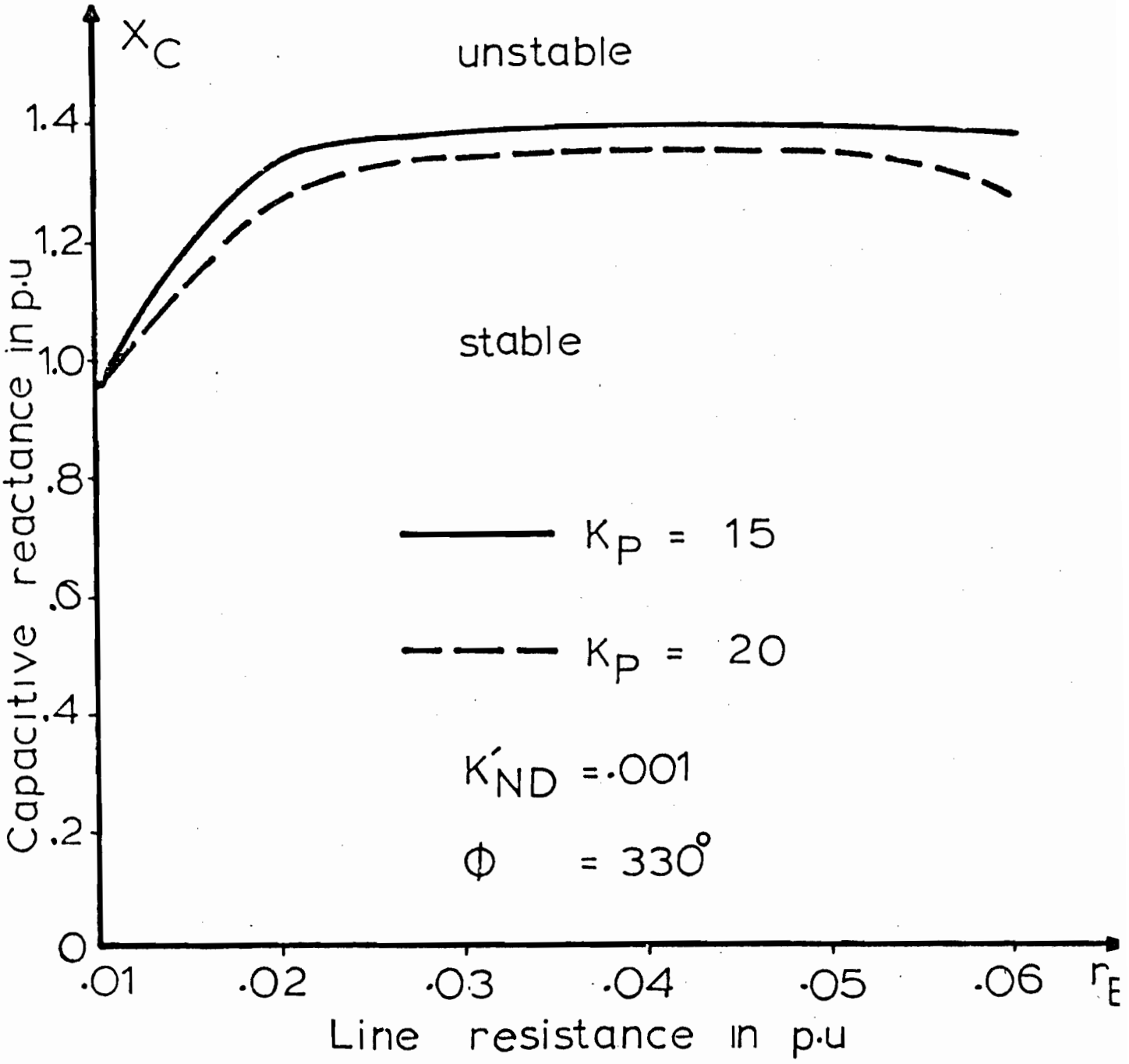

Figure 5.8. Stability boundary on the $X_C - r_E$ plane of the closed loop system (Figure 5.4(a)) for two values of PSS gain K_P, K_P = 20, 15 .

real part of the PSS mode λ_{PSS} shown in the third row of Table 5.3. The practical choice of the NDS' gain K'_{ND}, for a certain value of ϕ, is that which shifts the SSR mode λ_{ssrp} and the PSS mode λ_{PSS} in the left hand side of the s-plane.

The effect of K'_{ND} on the real parts of the above two modes can be examined by tracking the variations of these real parts as K'_{ND} varies. In Figure 5.9 these real parts are plotted against K'_{ND} for a fixed level of series capacitor compensation ($X_C = 1$) and fixed line resistance ($r_E = 0.0295$). The results are presented for two values of the control angle ϕ, which are $\phi = 30^\circ$ and $\phi = 330^\circ$.

From Figure 5.9, it is clear that for $\phi = 30^\circ$ (the solid curves) the value of K'_{ND} which ensures good damping for λ_{ssrp} and λ_{PSS} is around 0.0008. While for $\phi = 330$ (the broken curves in Figure 5.9) the value of K'_{ND} which ensures good damping for the same modes is around 0.0012.

5.9 Effect of the Control Angle ϕ

The variation of the real parts of the positive SSR sequence and the PSS modes with ϕ is shown in Figure 5.10. The value of K'_{ND} is kept constant at 0.001. It is clear from the variation of the SSR mode, that if the control signal is ΔP only, i.e., $\phi = 90^\circ$, then the system

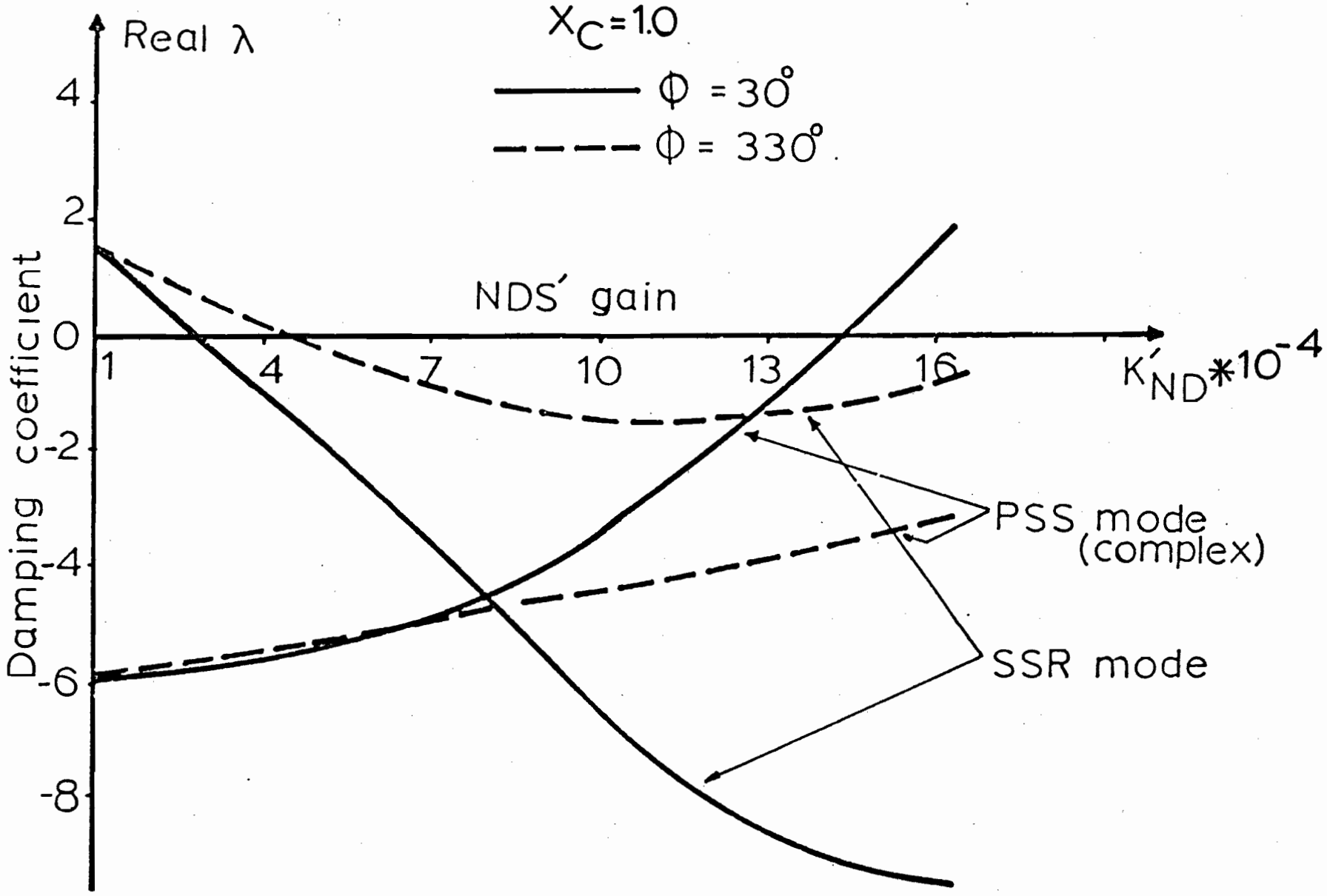

Figure 5.9. Variation of the PSS and the SSR mode dampings with K'_{ND}, for two values of the control angle ϕ, ϕ = 30, 330 .

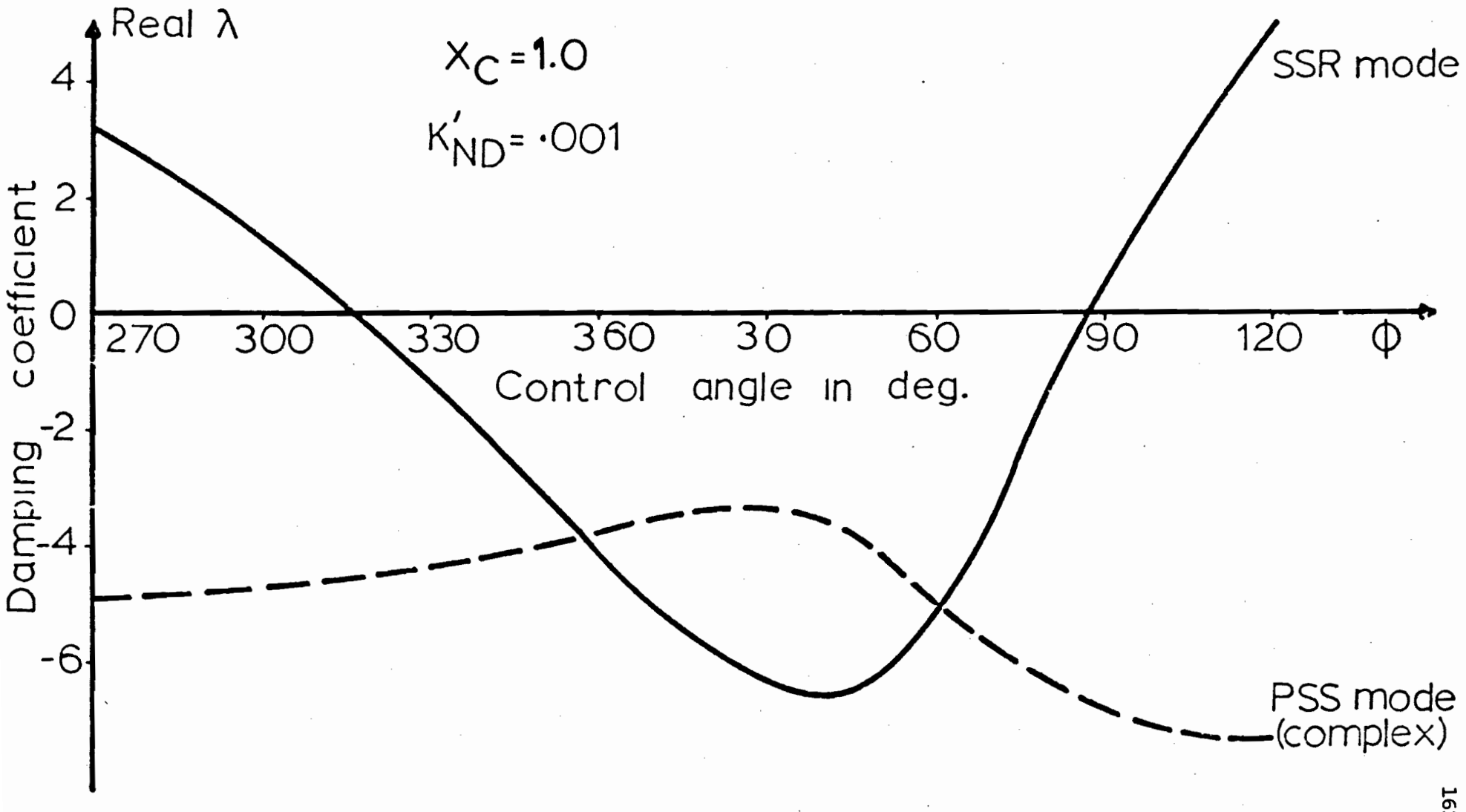

Figure 5.10. Variation of the SSR positive sequence and the PSS complex mode dampings with the control angle ϕ .

is unstable. From Figure 5.10, we can see that for $85^{\circ} < \phi < 315^{\circ}$ the λ_{ssrp} mode is unstable. Unlike Figure 5.9, the PSS mode does not become unstable as ϕ varies from $0^{\circ} < \phi < 360^{\circ}$. In the region $-3^{\circ} < \phi < 62^{\circ}$, the PSS mode is more lightly damped than the λ_{ssrp} mode and in fact, the maximum and the minimum of the two curves occur in this region.

5.10 Eigenvalues Loci on S-Plane

In Section 5.2, it was mentioned that the function of the PSS feedback is to ensure dynamic stability, i.e., to shift the mechanical mode $\lambda_{mech.}$ into the left hand side of the s-plane, and this is necessary when the high response excitation system (HRE) is used. It is to be reminded that the mechanical mode has been noticed (see Figure 4.6) to cause system instability as the filter gain K'_{ND} and the control angle ϕ vary. Furthermore, the NDS' feedback loop is added to the 10 GVA system to shift the λ_{ssrp} mode into the left hand side of the s-plane. Therefore, the objective of this section is to investigate the effect of the variations of K'_{ND} and ϕ on the λ_{ssrp} and the $\lambda_{mech.}$ modes.

On the upper half of the s-plane the loci of the SSR positive sequence and the mechanical modes for variations of K'_{ND} and ϕ are shown in Figures 5.11 and 5.12 respectively. In Figure 5.11, the

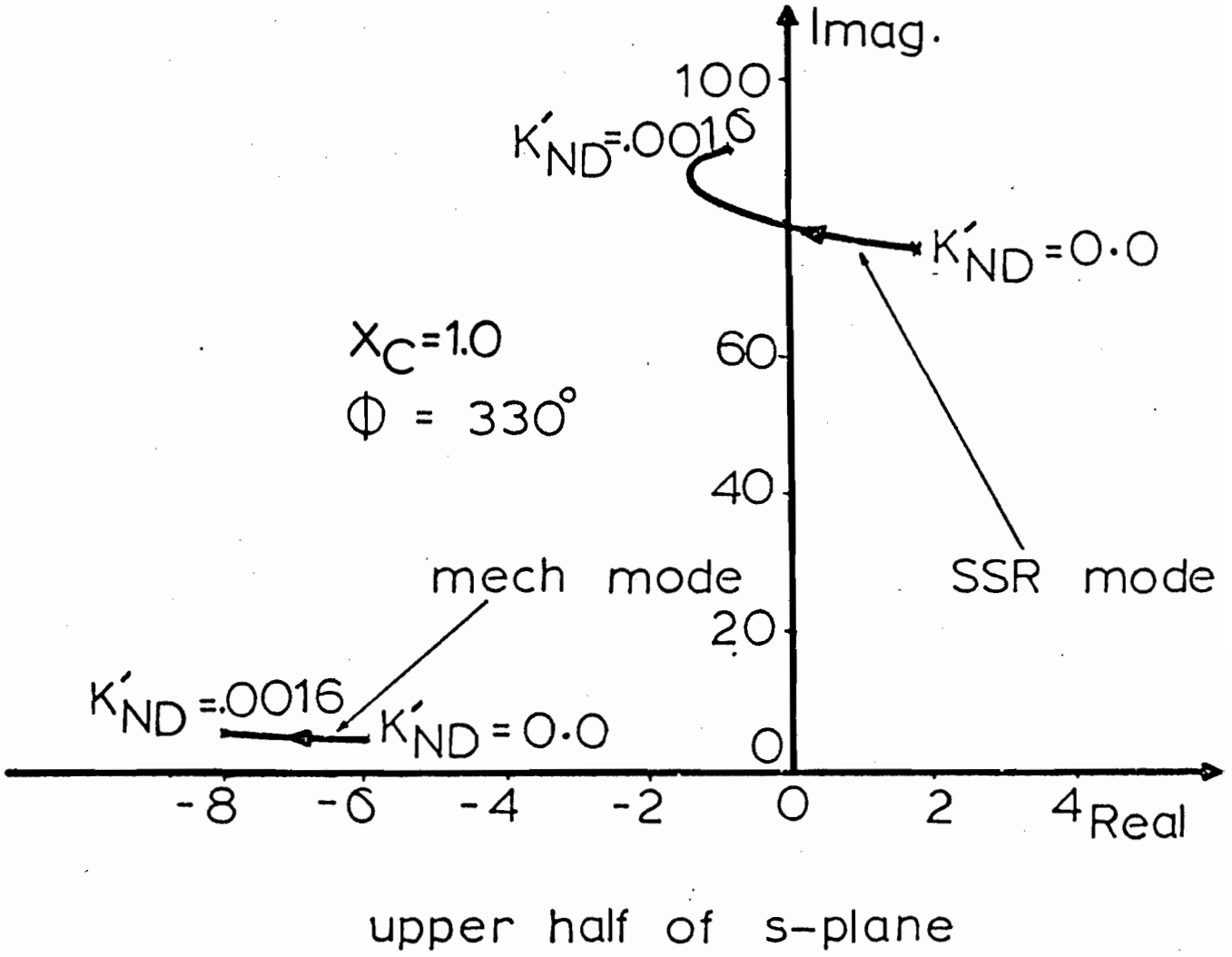

Figure 5.11. The loci of the SSR positive sequence and the mechanical modes as K'_{ND} varies on the upper half of the s-plane.

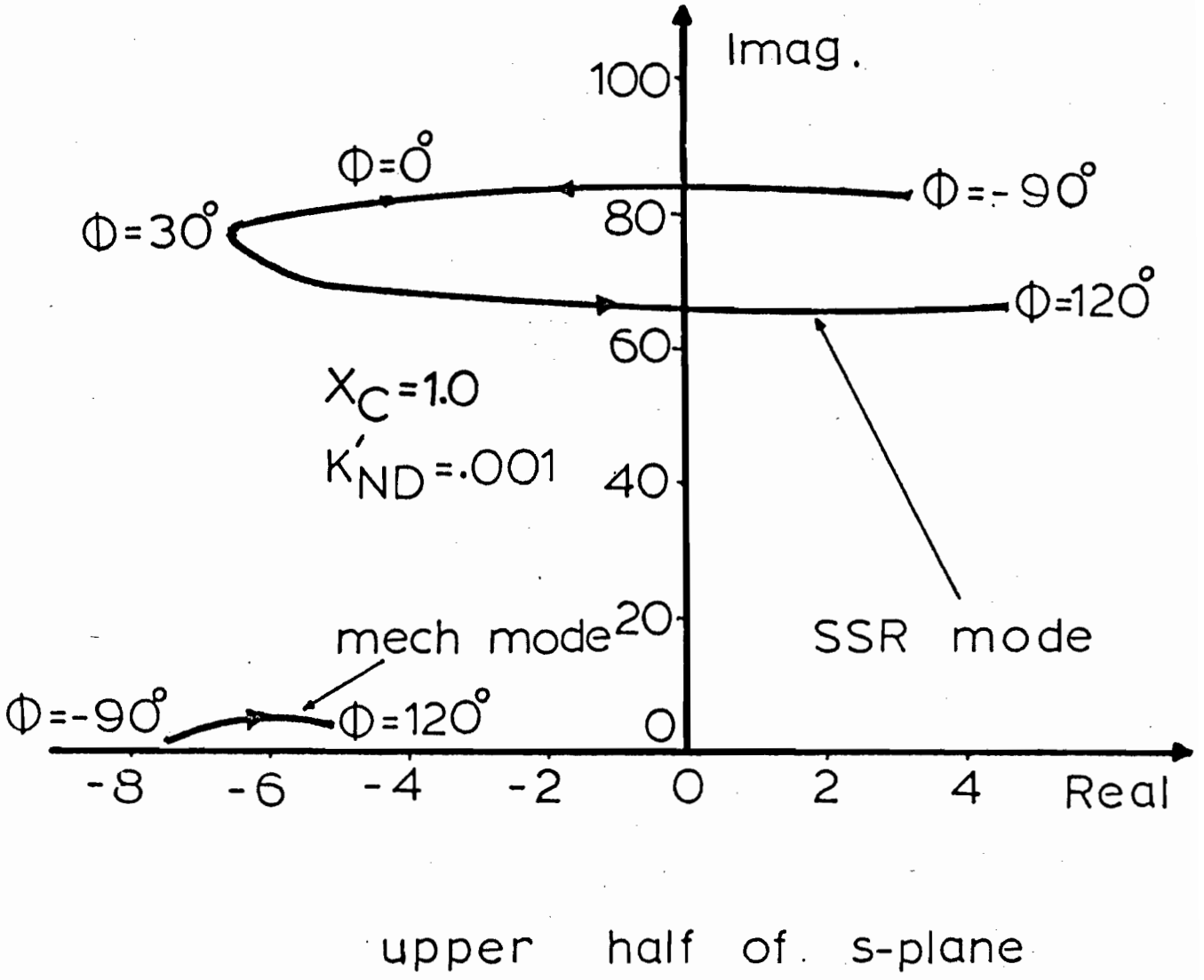

Figure 5.12. The loci of the SSR positive sequence and the mechanical modes as ϕ varies on the upper half of the s-plane.

value of ϕ is 330^{o} and K'_{ND} is varied. The SSR positive sequence mode moves from the right hand side to the left hand side of the s-plane and back again to the right hand side. However, the mechanical mode is always in the left hand side of the s-plane and moves in a small region. The variations of the above two modes with ϕ, which is shown in Figure 5.12, are similar to their variations with K'_{ND}.

Thus, we can conclude that the NDS' feedback does not affect the stability of the mechanical mode (hunting) significantly. This is to be contrasted by the results of Figures 5.9 and 5.10 where the mode of the PSS feedback filter is considered.

5.11 Effect of Loading

The last point to discuss is the effectiveness of the feedback scheme of Figure 5.4(a) under different loadings. All the results already discussed in this chapter are obtained for the operating conditions described in Table 5.1.

The two parameters which are always adjusted to stabilize the system operating in the closed loop of Figure 5.4(a) are ϕ and K'_{ND}. Our interest is to find a combination of K'_{ND} and ϕ in which stability is achieved under all considerable operating conditions.

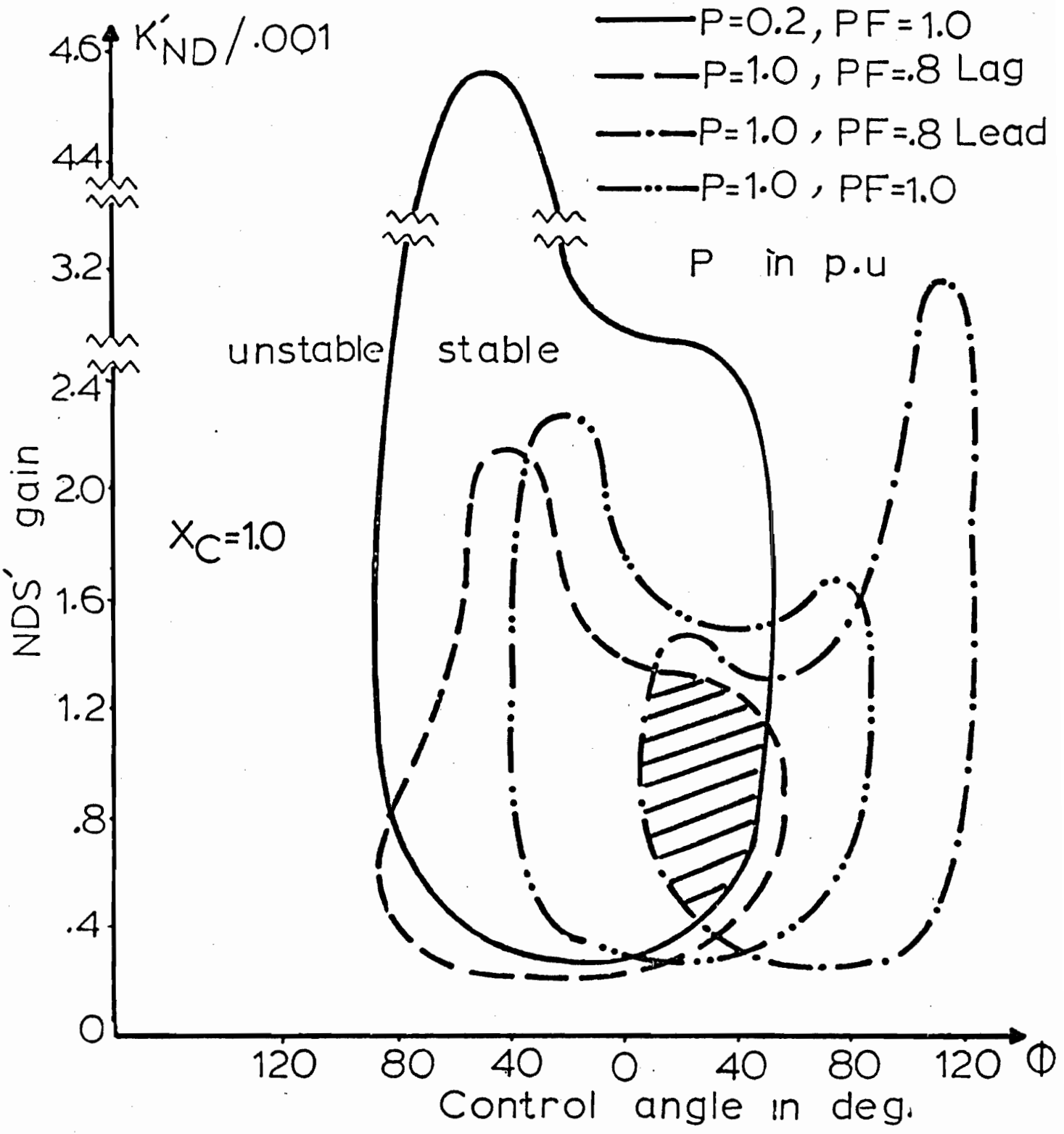

Figure 5.13. Stability boundary in the $K'_{ND} - \phi$ plane for different loadings.

Figure 5.13 maps the stability region on the $K'_{ND} - \phi$ plane for different values of loading. For light loading the stability region is wider than that for heavy loading. This is because the steady state stability is more secure under light loading (see Figure 1.1) than under heavy loading.

From Figure 5.13 it is apparent that the choice of (K'_{ND}, ϕ) to yield stability under a wide range of loading conditions is found in the region of intersection of all the stability regions. We may choose $K'_{ND} = 0.001$, $\phi = 30^{\circ}$ and from Figures 5.9, 5.10, 5.11 and 5.12 we find that the damping for the λ_{ssrp}, $\lambda_{mech.}$ and λ_{PSS} modes are acceptable.

5.12 Conclusion

The concluding remarks from this chapter can be summarized by the following points:

(i) The control signal formed from the combination of ΔP and ΔQ is emphatically superior to ΔQ alone in eliminating the unstable SSR oscillations.

(ii) The 10 GVA system which is equipped with high response excitation system (HRE) and power system stabilizer (PSS), is unstable under high levels of series capacitor compensation because of the following:

(a) SSR oscillations, when the NDS' feedback is disconnected, Figure 5.2(a).

(b) PSS feedback loop, when the NDS' feedback is added to the system, Figure 5.4(a).

(iii) The introduction of the NDS' feedback scheme through the excitation system to damp out the unstable SSR oscillations, does not interfere with the basic functions of the excitation system.

The application of the NDS' feedback scheme raises the problem of how large the disturbance this scheme can handle. In other words, if the regulator voltage ceilings which were neglected in the small perturbation study are considered and the system nonlinear model, derived in Section 2.7, is used, then to what extent the above scheme can suppress the unstable SSR oscillations. This problem will be discussed in the next chapter.

CHAPTER VI

FIELD EXCITATION CONTROL OF SSR OSCILLATION

A LARGE PERTURBATION STUDY

6.1 Introduction

The NDS' feedback scheme proposed in this thesis to suppress the unstable subsynchronous resonance (SSR) oscillations, has been tested against small disturbances. The analytical technique consists of small perturbation, linearization of the original nonlinear equations and finding the eigenvalues of the matrix [A] of the entire closed loop system. Stability is assured when all the eigenvalues lie on the left hand side of the s-plane. The numerical results obtained in Chapter V have demonstrated the capability of this scheme to suppress the unstable SSR oscillation without disturbing the normal function of the machine excitation system. Nevertheless, some approximations, such as the neglecting of the regulator voltage ceilings and the use of the linearized machine equations, were made in the previous analysis.

The small perturbation approximations are justified if the system is subjected only to a small disturbance from its steady state operation. However, under large disturbances such as instantaneous three-line-to-ground or synchronization-out-of-phase faults, the small perturbation approximations are no longer valid. This is because firstly, the quadratic product variables in the Taylor series expansion of the original nonlinear generator equations cannot be neglected. Secondly,

the voltage regulator becomes saturated for any corrective signal that goes beyond its ceilings. This means that the NDS' feedback output is subjected to a practical constraint (voltage ceilings) which limits its magnitude before it is injected in the field winding to suppress the SSR oscillations.

This chapter examines the capability of the NDS' feedback loop to suppress the SSR oscillations when the closed loop system of Figure 5.4(a) is assumed to be disturbed by a severe fault. The mathematical nonlinear model derived in Section 2.7.4 with both the excitation and the power system stabilizer models given by equations 5.1 and 5.4 respectively,are used in describing the above system.

In cases where the NDS' feedback scheme is unable to suppress the large unstable SSR oscillations, another external (outside the synchronous machine) scheme, which is a nonlinear resistor protection scheme, is added in parallel with the series capacitor to stabilize these oscillations. It is shown by digital simulations that this additional scheme plays a complementary role (working at the same time) with the NDS' feedback scheme in effectively suppressing the large unstable SSR oscillations.

6.2 Sources of Large Disturbance

The common sources of large disturbance considered in practice [62] are:

(i) Synchronization-out-of-phase fault.

(ii) Three-line-to-ground fault.

(iii) Line-to-line fault.

(iv) One-line-to-ground fault.

Among the above faults, the first two ((i), (ii)) are used in this chapter as sources of large disturbance.

6.2.1 Synchronization-out-of-phase Fault

This disturbance happens in faulty switching operations due to human, electrical or mechanical error. It also occurs in reclosure after system faults have caused the generators to swing apart electrically.

Synchronization-out-of-phase has been studied by Wood [63] and Hammons [64] for the case of transmission lines without series capacitor compensation. In these studies, the principal subject of interest is the maximum peak torque produced during the transients as a function of the switching angle Δ. These studies provide the essential

data for mechanical design where the maximum yield stress and the stress for fatigue failure must not be exceeded [29] . To the author's knowledge, this kind of investigation has not been extended to the case of series capacitor compensated transmission line and for this reason, it is felt important to enquire into this unknown territory.

6.2.2 Three-Line-to-Ground Fault

This fault originates from natural sources, like lightning strokes, storms, etc. It is assumed that the fault is located at the receiving end, that is, between the series capacitor and the infinite bus bar in Figure 2.2(a). The fault is assumed to last for 6 cycles ($\simeq$ 0.1 s) as is a reasonable period for power system transient stability studies.

The reason for using this fault is because it represents a very severe event from the standpoint of transient torques [13] . However, the peak torque in general is higher as the location of the fault is closer to the synchronous generator. Further, the longer the fault lasts the higher is the peak torque.

6.3 Mathematical Reformulation

6.3.1 Synchronous Generator

The nonlinear mathematical equations describing the synchronous generator in Figure 2.2(a), which are derived in Section 2.7, can be rewritten as:

$$-\frac{d}{dt}\begin{bmatrix}\psi_d\\ \psi_q\\ \psi_{fd}\\ \psi_{kd}\\ \psi_{kq}\end{bmatrix} = \omega_0\begin{bmatrix}-e_d\\ -e_q\\ -e_{fd}\\ 0\\ 0\end{bmatrix} + \omega_0\begin{bmatrix}-r_a & & & & \\ & -r_a & & & \\ & & r_{fd} & & \\ & & & r_{kd} & \\ & & & & r_{kq}\end{bmatrix}$$

$$\cdot\begin{bmatrix}i_d\\ i_q\\ i_{fd}\\ i_{kd}\\ i_{kq}\end{bmatrix} + \omega_0\,\bar{\omega}\begin{bmatrix}-\psi_q\\ \psi_d\\ 0\\ 0\\ 0\end{bmatrix} \qquad (6.1)$$

The mechanical equations are:

$$2H \frac{d\bar{\omega}}{dt} = T_m - T_e \tag{6.2}$$

$$\frac{d\delta}{dt} = \omega_0 (\bar{\omega} - 1) \tag{6.3}$$

$$T_e = i_q \psi_d - \psi_q i_d \tag{6.4}$$

Equations 6.1 - 6.4 can be put in a form suitable for numerical integration if the currents, i_d, i_q, i_{fd}, i_{kd} and i_{kq} are expressed in terms of the fluxes ψ_d, ψ_q, ψ_{fd}, ψ_{kd} and ψ_{kq}. This can be done by introducing the following definitions, which were reported in [51] :

$$\psi_{ad} = \frac{1}{A_1} \left[\frac{\psi_d}{X_{ld}} + \frac{\psi_{fd}}{X_{fd}} + \frac{\psi_{kd}}{X_{kd}} \right] \tag{6.5}$$

$$\psi_{aq} = \frac{1}{A_2} \left[\frac{\psi_q}{X_{lq}} + \frac{\psi_{kq}}{X_{kq}} \right] \tag{6.6}$$

where

$$\begin{aligned} X_{ld} &= X_d - X_{ad} \\ X_{lq} &= X_q - X_{aq} \\ X_{fd} &= X_{ffd} - X_{ad} \\ X_{kd} &= X_{kkd} - X_{ad} \\ X_{kq} &= X_{kkq} - X_{aq} \end{aligned} \tag{6.7}$$

and

$$A_1 = \frac{1}{X_{ad}} + \frac{1}{X_{fd}} + \frac{1}{X_{1d}} + \frac{1}{X_{kd}} \tag{6.8}$$

$$A_2 = \frac{1}{X_{aq}} + \frac{1}{X_{1q}} + \frac{1}{X_{kq}} \tag{6.9}$$

also

$$\begin{aligned} i_d &= \frac{1}{X_{1d}} (\psi_{ad} - \psi_d) \\ i_q &= \frac{1}{X_{1q}} (\psi_{aq} - \psi_q) \\ i_{fd} &= \frac{1}{X_{fd}} (\psi_{fd} - \psi_{ad}) \\ i_{kd} &= \frac{1}{X_{kd}} (\psi_{kd} - \psi_{ad}) \\ i_{kq} &= \frac{1}{X_{kq}} (\psi_{kq} - \psi_{aq}) \end{aligned} \tag{6.10}$$

6.3.2 Network

The network of Figure 2.2(a) was described by equations 2.47 and 2.48 which are written in real time as:

$$\omega_0 \begin{bmatrix} e_d \\ e_q \end{bmatrix} = \omega_0 \begin{bmatrix} r_E & \\ & r_E \end{bmatrix} \begin{bmatrix} i_d \\ i_q \end{bmatrix} + \begin{bmatrix} X_E & \\ & X_E \end{bmatrix} \frac{d}{dt} \begin{bmatrix} i_d \\ i_q \end{bmatrix}$$

$$+ \omega_0 \bar{\omega} \begin{bmatrix} 0 & -X_E \\ X_E & 0 \end{bmatrix} \begin{bmatrix} i_d \\ i_q \end{bmatrix} + \omega_0 \begin{bmatrix} e_{Cd} + e_{0d} \\ e_{Cq} + e_{0q} \end{bmatrix} \tag{6.11}$$

and

$$\frac{d}{dt} \begin{bmatrix} e_{Cd} \\ e_{Cq} \end{bmatrix} = \omega_0 \begin{bmatrix} X_C & 0 \\ 0 & X_C \end{bmatrix} \begin{bmatrix} i_d \\ i_q \end{bmatrix} + \omega_0 \bar{\omega} \begin{bmatrix} 0 & 1 \\ -1 & 0 \end{bmatrix} \begin{bmatrix} e_{Cd} \\ e_{Cq} \end{bmatrix} \tag{6.12}$$

A complete model describing the system of Figure 2.2(a) in the d-q rotating reference frame when the excitation system of the synchronous generator is neglected, can be obtained by substituting equation 6.10 into equations 6.1, 6.4, 6.11 and 6.12 to eliminate the currents and by combining the resulting equations. This results in a set of first order nonlinear differential equations which are written in the state space form as:

$$\frac{d}{dt} \underline{X} = f(\underline{X}) + \underline{U} \tag{6.13}$$

$$\underline{X}(0) = \underline{X}_0 \qquad \text{the steady state values}$$

where

$$\underline{X} = [\ \psi_d \quad \psi_q \quad \psi_{fd} \quad \psi_{kd} \quad \psi_{kq} \quad \bar{\omega} \quad \delta \quad e_{Cd} \quad e_{Cq}\ ]^T$$

and

$$\underline{U} = [\ e_{0d} \quad e_{0q} \quad e_{fd} \quad 0 \quad 0 \quad T_m \quad -\omega_0 \quad 0 \quad 0\ ]^T$$

6.3.3 The Excitation System Mathematical Model

The state space equation describing the excitation system of the transfer function shown in Figure 5.1(b) is given by equation 5.1. However, the regulator voltage ceilings were not described in this equation. Therefore, a new set of first order differential equations will be derived to describe the excitation system with the voltage ceilings nonlinearity as shown in Figure 6.1. Figure 6.1 shows the same excitation system used in Chapter V, which is Type 1 of Reference [55], but with the voltage ceilings. The differential equations describing this system are:

$$\frac{d}{dt} x_2 = -\frac{1}{T_A} x_2 + \frac{K_A}{T_A} (E_{ref} - e_t - v_f) \tag{6.14}$$

$$x_1 = \begin{cases} x_2 & \text{if } V_{min} < x_2 < V_{max} \\ V_{max} & \text{if } x_2 > V_{max} \\ V_{min} & \text{if } x_2 < V_{min} \end{cases} \tag{6.15a}$$

$$\frac{d}{dt} e_E = - \frac{1}{T_E} e_E + \frac{K_E}{T_E} x_1 \qquad (6.15b)$$

$$\frac{d}{dt} v_f = - \frac{1}{T_F} v_f + K_F \left(- \frac{1}{T_E} e_E + \frac{K_E}{T_E} x_1 \right) \qquad (6.16)$$

The values of the gains and time constants of the excitation, which will be used in this chapter, are those listed in Table 5.1 for the HRE system. The voltage ceiling limits V_{max}, V_{min} are used as + 8 p.u., - 8 p.u. respectively according to the standard values described in [55] .

6.3.4 The Power System Stabilizer (PSS) Mathematical Model

Since the PSS which has the transfer function shown in Figure 5.2(b) is a linear system, then its mathematical model used in the small perturbation study, which is given by equation 5.4, will be used in this chapter for the large perturbation study. This is rewritten here as:

$$\frac{d}{dt} \begin{bmatrix} x_{P1} \\ x_{P2} \\ x_{P3} \end{bmatrix} = \begin{bmatrix} - a_{P1} & 1 & 0 \\ - a_{P2} & 0 & 1 \\ - a_{P3} & 0 & 0 \end{bmatrix} \begin{bmatrix} x_{P1} \\ x_{P2} \\ x_{P3} \end{bmatrix} + \begin{bmatrix} b_{P1} \\ b_{P2} \\ b_{P3} \end{bmatrix} \bar{\omega} \qquad (6.17)$$

where a_{P1} , a_{P2} , a_{P3} , b_{P1} , b_{P2} and b_{P3} are the same as defined in Chapter V .

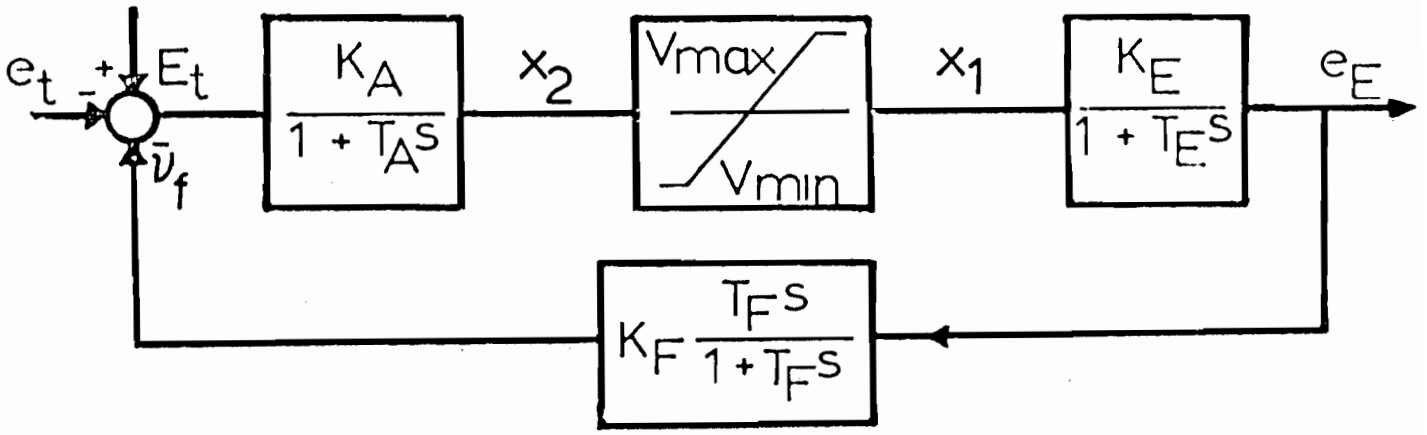

$$V_{max} = +8 \quad p.u$$

$$V_{min} = -8 \quad p.u$$

Figure 6.1. Transfer function of the excitation system including the voltage ceilings.

6.3.5 The NDS' Filter Mathematical Model

In a similar way to the PSS, the NDS' filter which has the transfer function shown in Figure 5.4(b), is also a linear system. Therefore, equation 5.6 will be used in the large perturbation study and it is rewritten here as:

$$\frac{d}{dt}\begin{bmatrix} x_{N1} \\ x_{N2} \\ x_{N3} \end{bmatrix} = \begin{bmatrix} -a_{N1} & 1 & 0 \\ -a_{N2} & 0 & 1 \\ -a_{N3} & 0 & 0 \end{bmatrix} \begin{bmatrix} x_{N1} \\ x_{N2} \\ x_{N3} \end{bmatrix} + \begin{bmatrix} b_{N1} \\ b_{N2} \\ b_{N3} \end{bmatrix} \mu \qquad (6.18)$$

where a_{N1}, a_{N2}, a_{N3}, b_{N1}, b_{N2}, b_{N3} and μ are the same as defined in Chapter V.

In summary, the nonlinear mathematical models which are going to be used in the forthcoming analysis to describe different system configurations, are listed in Table 6.1.

6.3.6 System Nonlinearities

The nonlinearities included in the mathematical models are:

(i) The product terms appearing in the synchronous generator equations, such as the rotor shaft speed $\bar{\omega}$ with the

TABLE 6.1

MATHEMATICAL MODELS OF DIFFERENT SYSTEM CONFIGURATIONS

	SYSTEM CONFIGURATION	NONLINEAR MATHEMATICAL MODEL
1.	Basic system (Figure 2.2(a))	Equation 6.13.
2.	Basic system + Excitation system, or Open loop system, (Figure 5.2(a), and Figure 6.1 for the HRE system).	Combination of equations 6.13, 6.14, 6.15(a), 6.15(b), 6.16 and 6.17.
3.	Basic system + Excitation system + NDS' feedback loop, or Closed loop system, (Figure 5.4(a) and Figure 6.1 for the HRE system).	Combination of equations 6.13, 6.14, 6.15(a), 6.15(b), 6.16, 6.17 and 6.18.
4.	Closed loop system without voltage ceilings, (Figure 5.4(a)) .	The combination of the same equations in (3), except equation 6.15(a), becomes $x_1 = x_2$.

stator fluxes ψ_d and ψ_q in equation 6.1 and the stator currents i_d, i_q with the stator fluxes in equation 6.4.

(ii) The regulator voltage ceilings nonlinearity as shown in Figure 6.1 and is described by equation 6.15(a).

The ferromagnetic saturation of the iron core of the synchronous generator is neglected as it was assumed in Chapter II.

6.4 Numerical Integration

The solution to the nonlinear first order differential equations described in Section 6.3 is analytically intractable. The two methods generally used for their solutions are by simulation using an analogue computer or by numerical integration using a digital computer. In this study, the numerical integration will be pursued.

Many excellent books [65 -66] cover the various methods of numerical integration. One of these methods, which is used here, is based on the fourth order Runge Kutta method with the modification due to Gill [65]. A computer subroutine using this method to solve the nonlinear first order differential equations, called RKGS [67], was used in the digital computer calculation of the numerical solutions.

The implementation of this method requires a considerable amount of computation time. However, to achieve economy of computer time, two things can be done:

(i) Since the central idea of numerical integrations is based on knowing the states of the system at time t, one could evaluate the gradient and use the gradient information to extrapolate to later time t + h, where h is the step size, in order to arrive at the solution. In the 4th order RKGS subroutine, the processing of this information consists of evaluating f ($\underline{X}$ (t+h)) four times at each step. Therefore it is important to ensure that f ($\underline{X}$) is presented to the computer to minimize the computer time. The form of f ($\underline{X}$) described in equation 6.13 is very economical in computation time [51].

(ii) The computer time can be reduced by choosing as large a step size h as it is permitted by the required accuracy. Many workers, including the author, have found h = 1 ms to be adequate in power system studies.

6.4.1 Computer Program Checking Procedure

The difficulty in using computer programs is the task of proving the correctness of the results. This is solved by calibrating

the digital outputs with experimental or analytical results obtained by other workers. In addition, the computer program has been spot checked against programming mistakes or wrong formulation by the following tests:

(i) Synchronization-in-phase of the generator should not produce any transients. This means that if the generator is switched to the infinite bus bar when its terminal voltage has the same magnitude and phase as the infinite bus bar voltage, then no transients should occur.

(ii) The program must be able to simulate the steady state solutions, which in the d-q axis frame are constant time invariant quantities. In other words, if the initial values of the states, which are fed to the computer, are the same as the system steady state values, then the computer output plot should be straight lines representing the states steady state values.

6.5 Results

6.5.1 Synchronization-Out-Of-Phase

Figure 6.2 shows the maximum peak torque of the transients of the generator plotted as a function of Δ, the switching angle, at

which the generator is synchronized to the infinite bus. The curves are for different values of X_C , the series capacitive reactance, and their shapes take the same form of Reference [63] for the uncompensated transmission line.

The maxima of the curves of Figure 6.2 occur for the switching angle $\Delta = 120^{\circ}$. The results are for the basic system whose parameters are listed in Table 5.1 . There is no excitation feedback for these results, since previous work by Hammons [64] showed that the excitation system has no effect on the peak torque.

The similarity between the curves of Figure 6.2 with that of the uncompensated transmission line of Reference [63], invites the conjecture that one can treat the effect of the compensating capacitance on the peak torque transients as simply as that of a reduced inductive reactance whose value is $X'_E = X_E - X_C$.

6.5.1.1 Torque Peaks for Compensated and Uncompensated Lines

Figure 6.3 plots the maximum peaks of the torque transients following switching angle $\Delta = 120$ electrical degrees. The solid line is for the case of a fixed inductive reactance $X_E = 1.34$ p.u. but for different values of X_C . The abscissa of the solid line is $X'_E = X_E - X_C$. The broken line is for the case of uncompensated transmission line and the

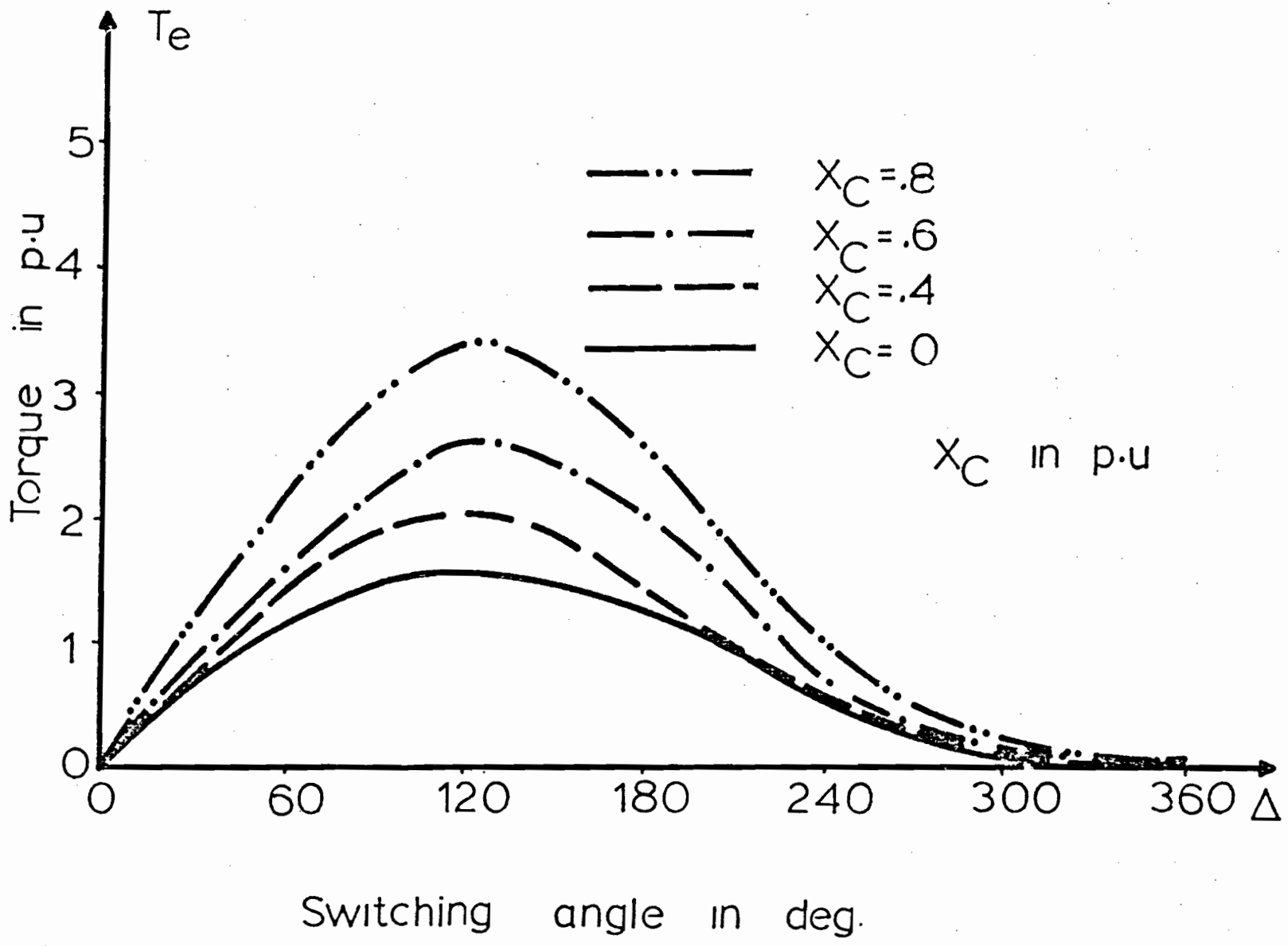

Figure 6.2. Maximum peak torque characteristic as a function of synchronization-out-of-phase angle for different values of X_C .

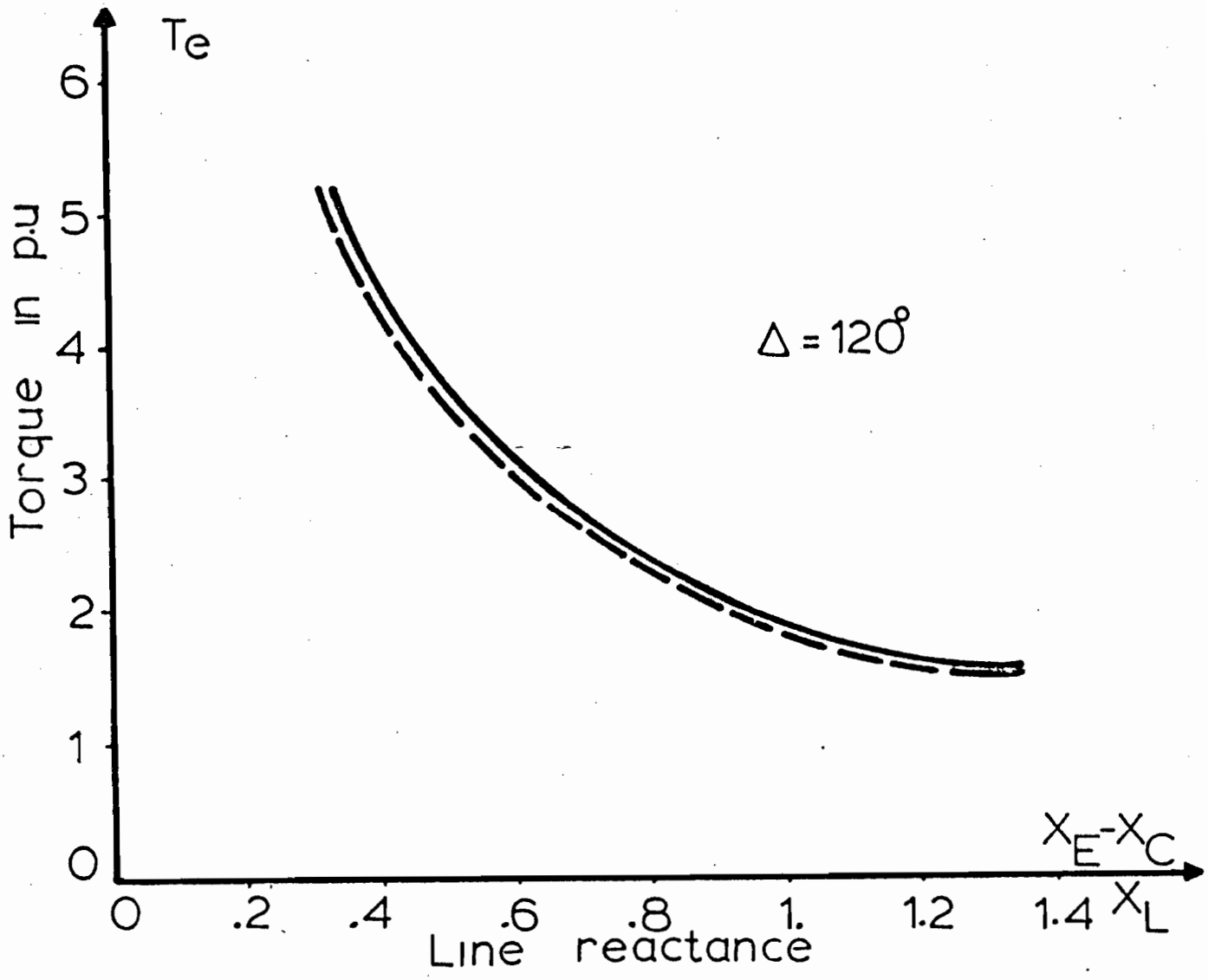

Figure 6.3. Maximum peak torque for synchronization-out-of-phase angle of 120° as a function of $X_E - X_C$ (solid line) in series capacitor compensated line and as a function of the line inductive reactance X_L (broken line) in uncompensated line.

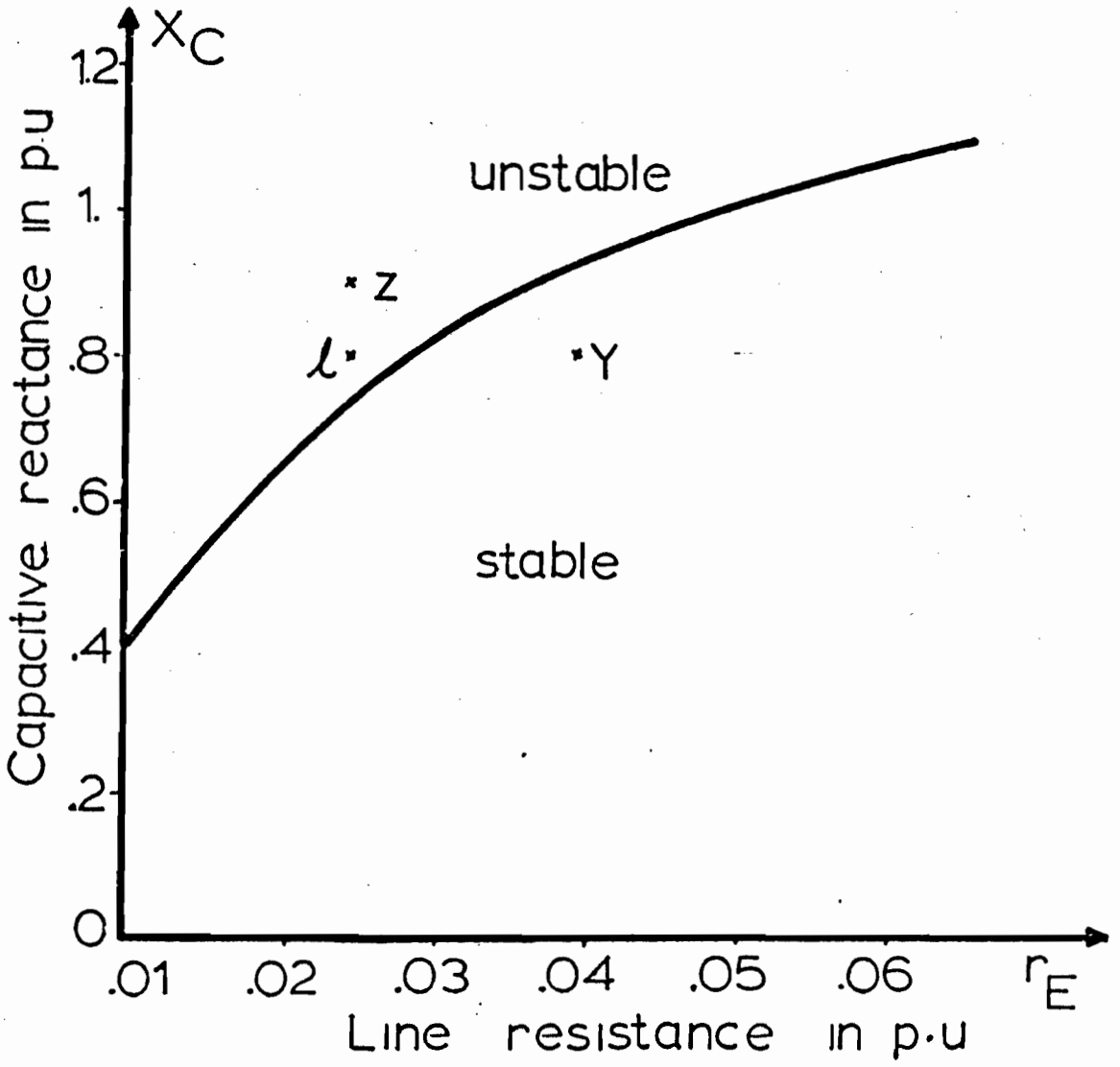

Figure 6.4. Stability boundary in the X_C - r_E plane of the 10 GVA system, without the NDS' feedback, showing the three points which are taken as the steady state operating points in the digital simulations.

abscissa is the inductive reactance X_L . The very close agreement between the two curves validates the conjecture and shows that the case of the series capacitor compensated lines can be unified with the results of Reference [63] .

6.5.1.2 The NDS' Feedback Capability

In this section the capability of the NDS' feedback scheme to suppress the large unstable SSR oscillations is examined by graphical display of the 10 GVA system time response to the synchronization-out-of-phase fault which is obtained from the numerical integration. Table 6.2 lists the feedback connections, the switching angles, and the operating impedances for Figures 6.5, 6.6 and 6.7.

Figure 6.5 shows the torque, line current and capacitor voltage time responses for the system of Figure 5.4(a) and the excitation system is represented by Figure 6.1. The steady state operating point used is point ℓ on Figure 6.4 which has the line parameter values X_C = 0.8 p.u., r_E = .025 p.u. At this point, the open loop system is originally unstable, and it was stabilized against small perturbations by the NDS' feedback scheme as it was shown in Chapter V . The synchronization-out-of-phase angle Δ is assumed to be 15 electrical degrees. The time responses in Figure 6.5 indicate that the system is unstable and the NDS' feedback scheme is not capable of stabilizing the system after a severe disturbance.

TABLE 6.2.

THE 10 GVA SYSTEM TIME RESPONSES TO THE SYNCHRONIZATION-OUT-OF-PHASE FAULT

Figure Number	HRE	PSS	NDS' Scheme	Voltage Ceilings	Operating Point in Fig. 6.4	X_C	r_E	Synchronization Phase Δ	System Configuration
Fig. 6.5	X	X	X	X	ℓ	0.8	0.025	15^o	Fig. 5.4(a) with Fig. 6.1 for HRE .
Fig. 6.6	X	X	X		ℓ	0.8	0.025	15^o	Fig. 5.4(a) with Fig. 5.1(b) for HRE.
Fig. 6.7	X	X	X	X	ℓ	0.8	0.25	5^o	Fig. 5.4(a) with Fig. 6.1 for HRE .

However, the question is whether the NDS' feedback scheme can suppress the large unstable SSR oscillations if the voltage ceilings are neglected. Figure 6.6 shows the torque, the line current and the capacitor voltage time responses when the simulation of Figure 6.5 is repeated but the regulator voltage ceilings are now neglected. It is clear from Figure 6.6 that the closed loop system is stable under the absence of the voltage ceilings. This will be explained in detail in Section 6.6.

Figures 6.5 and 6.6 show that when the system is stable, the electrical torque, the line current and the capacitor voltage time responses are damped out, and they are building up with time when the system is unstable. In addition, their responses have the same frequency and shape in spite of their differences in peaks and steady state values (for stable system). Therefore, because of space economy, only the torque response will hereafter be displayed for the results.

The other question to settle is to what degree of fault severity the NDS' feedback scheme is capable of damping out the large unstable SSR oscillations. Figure 6.7 shows the torque time response of the 10 GVA system when the synchronization angle Δ is reduced to 5 electrical degrees. Point ℓ on Figure 6.4 is still considered as the system steady state operating point. In the results shown in Figure 6.7, the closed loop system is considered with Figure 6.1 to represent the HRE system. Figure 6.7 indicates that the system is stable and the

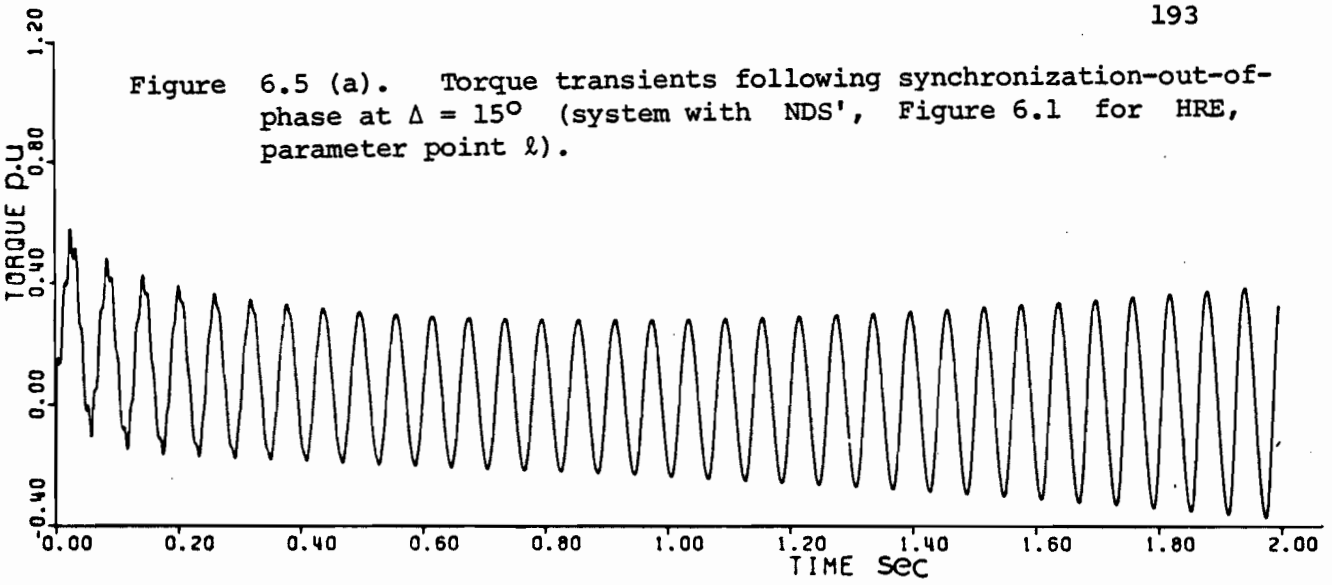

Figure 6.5 (a). Torque transients following synchronization-out-of-phase at $\Delta = 15^{o}$ (system with NDS', Figure 6.1 for HRE, parameter point ℓ).

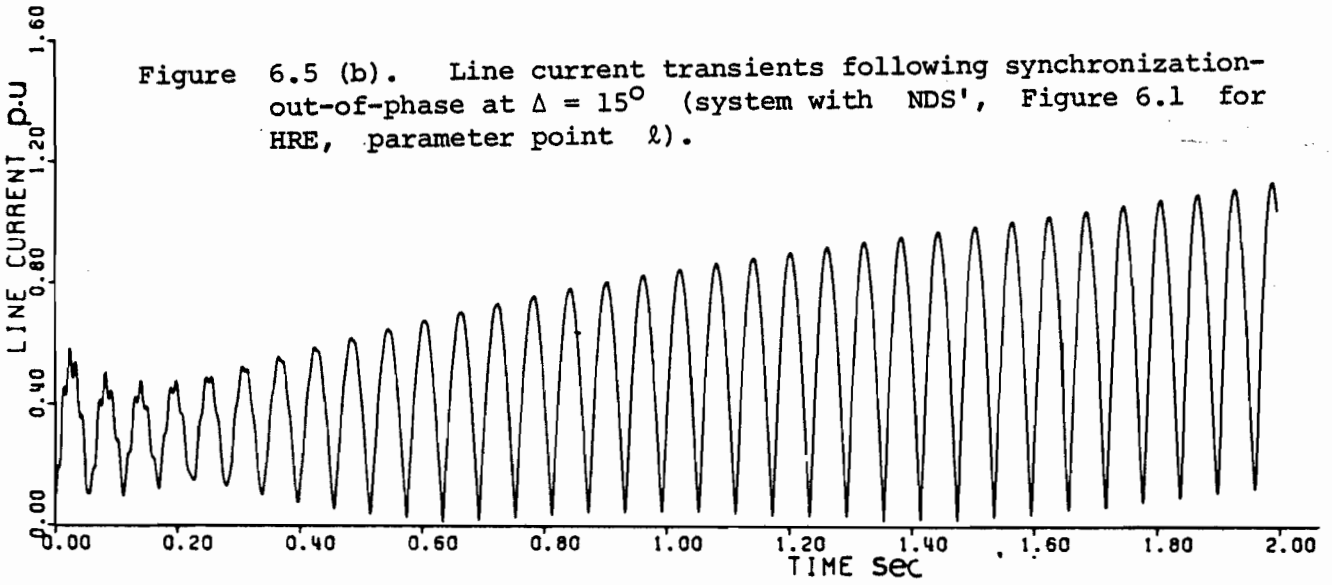

Figure 6.5 (b). Line current transients following synchronization-out-of-phase at $\Delta = 15^{o}$ (system with NDS', Figure 6.1 for HRE, parameter point ℓ).

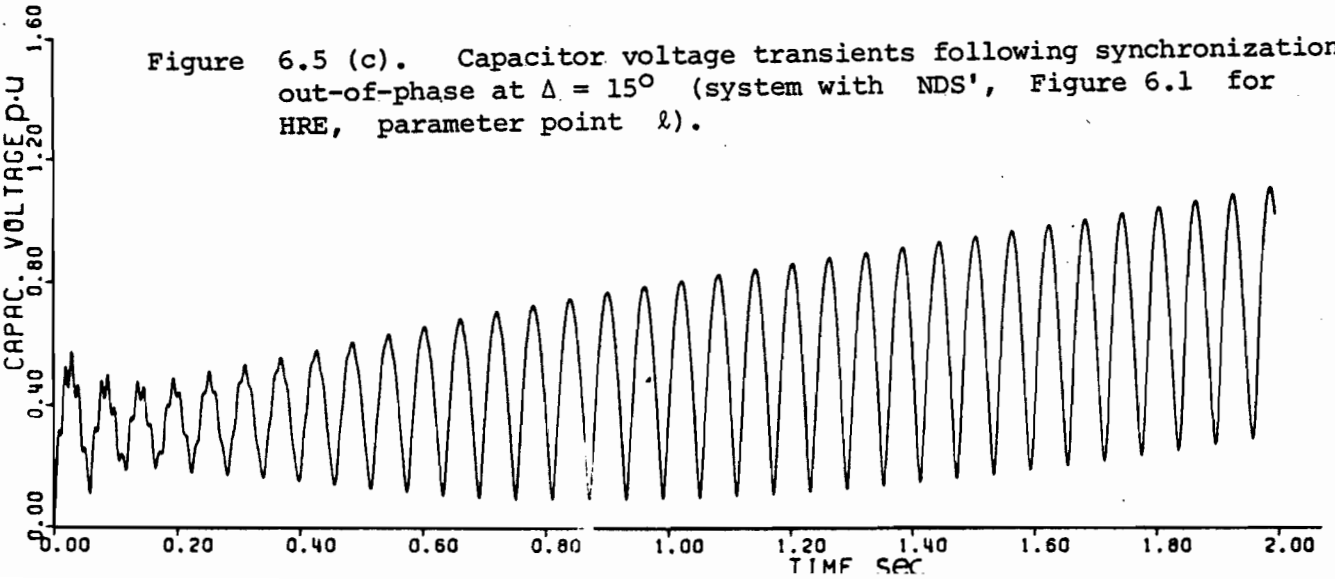

Figure 6.5 (c). Capacitor voltage transients following synchronization-out-of-phase at $\Delta = 15^{o}$ (system with NDS', Figure 6.1 for HRE, parameter point ℓ).

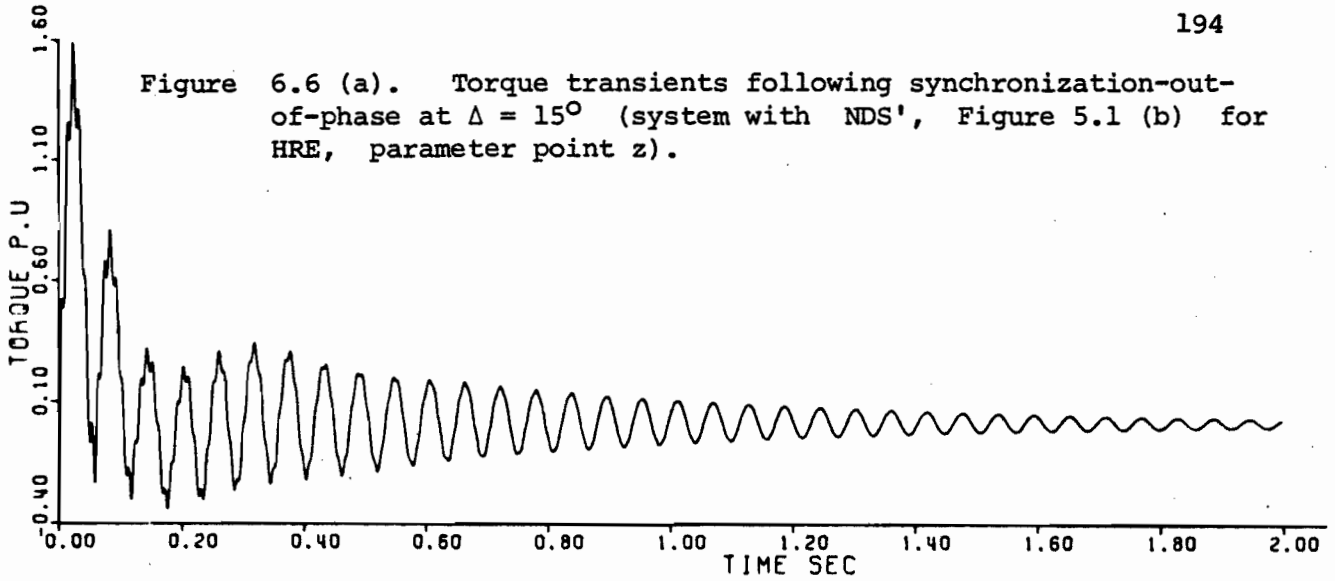

Figure 6.6 (a). Torque transients following synchronization-out-of-phase at $\Delta = 15^{o}$ (system with NDS', Figure 5.1 (b) for HRE, parameter point z).

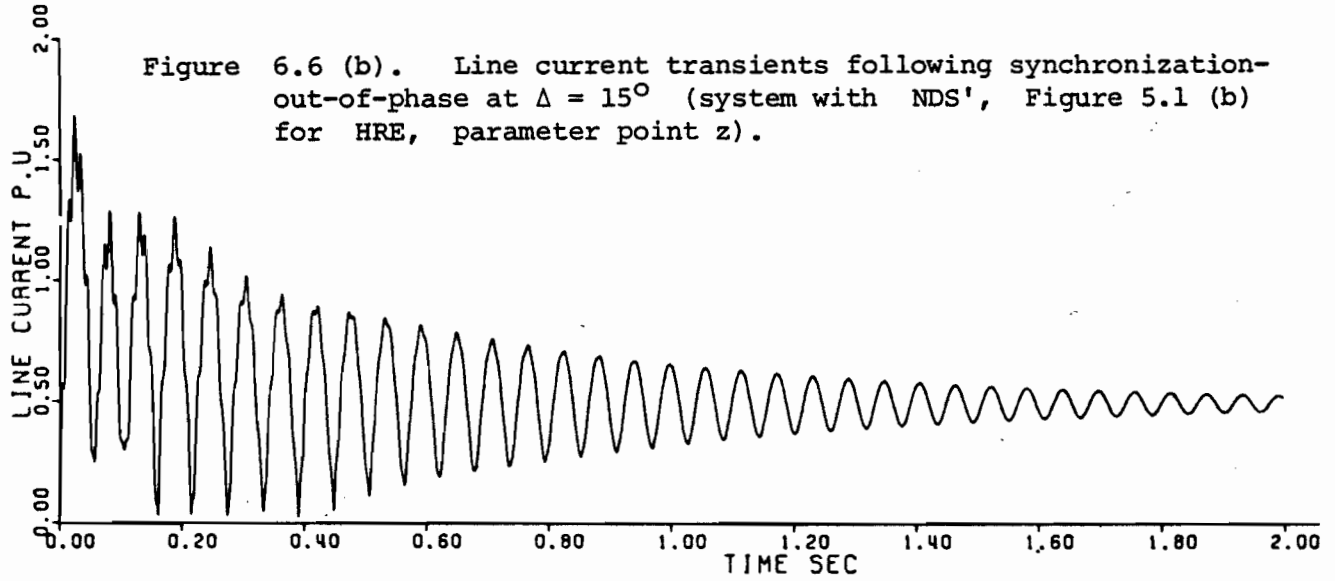

Figure 6.6 (b). Line current transients following synchronization-out-of-phase at $\Delta = 15^{o}$ (system with NDS', Figure 5.1 (b) for HRE, parameter point z).

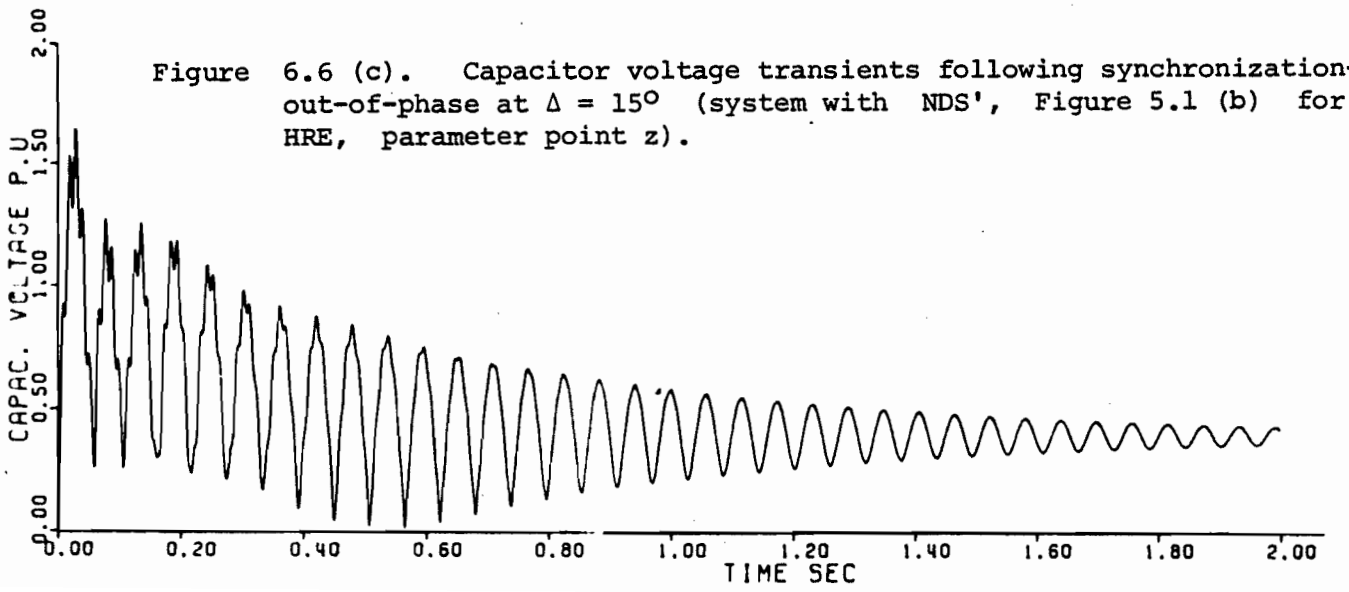

Figure 6.6 (c). Capacitor voltage transients following synchronization-out-of-phase at $\Delta = 15^{o}$ (system with NDS', Figure 5.1 (b) for HRE, parameter point z).

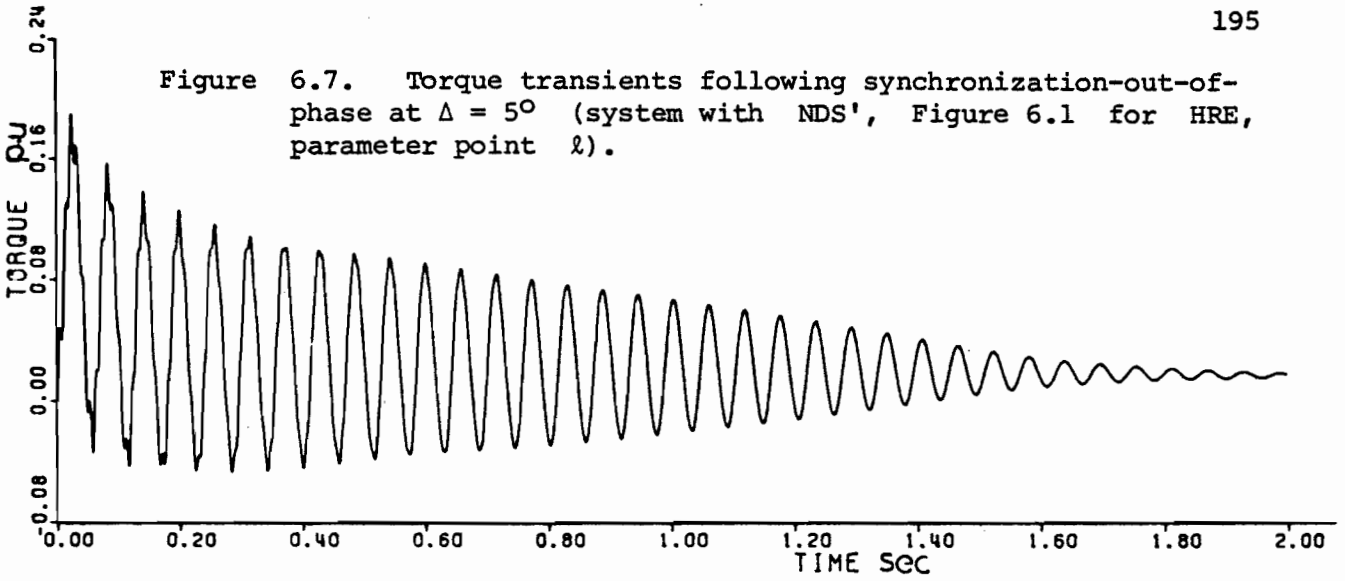

Figure 6.7. Torque transients following synchronization-out-of-phase at $\Delta = 5^{o}$ (system with NDS', Figure 6.1 for HRE, parameter point ℓ).

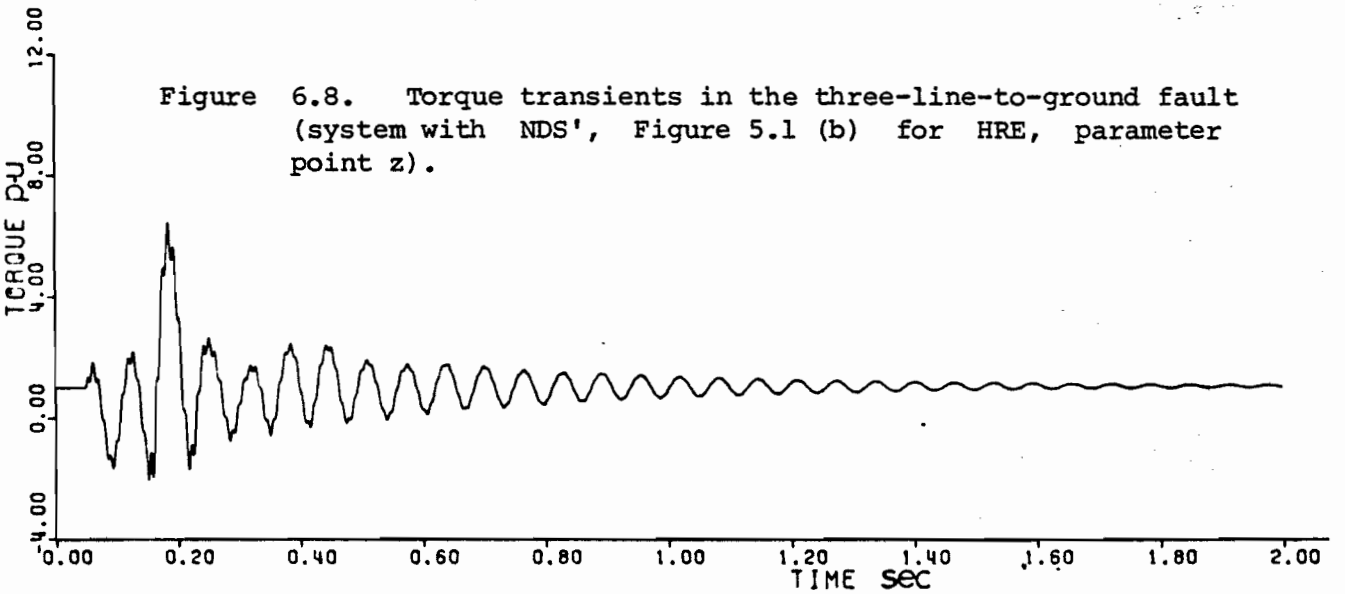

Figure 6.8. Torque transients in the three-line-to-ground fault (system with NDS', Figure 5.1 (b) for HRE, parameter point z).

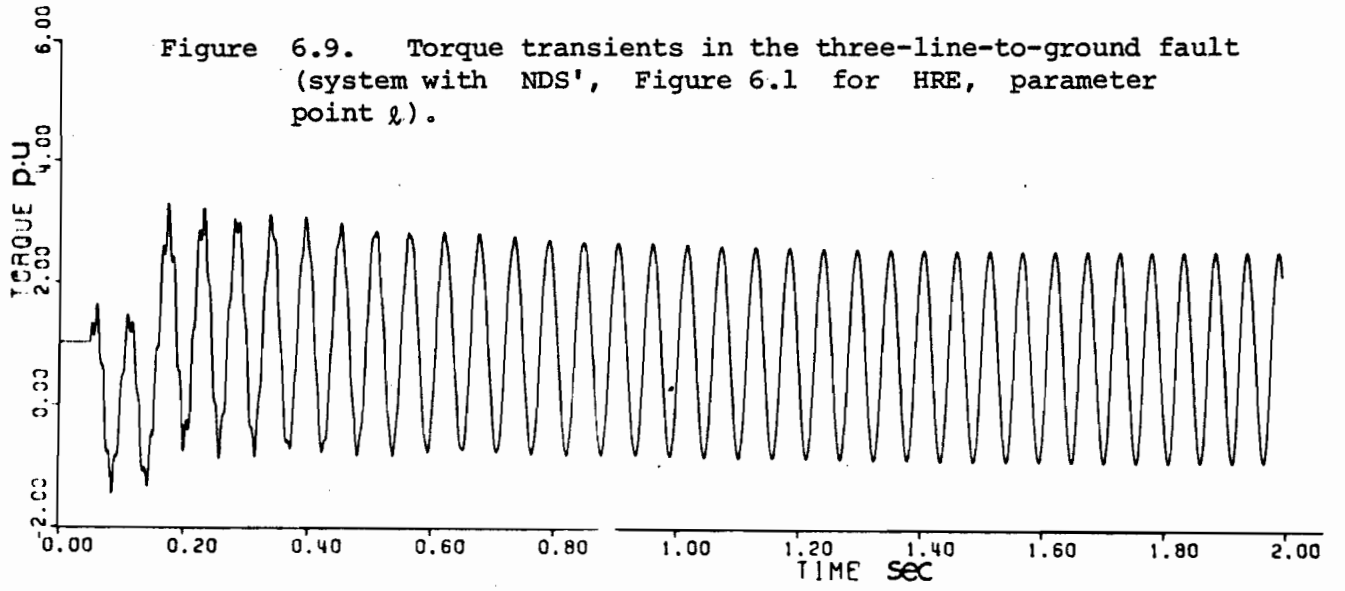

Figure 6.9. Torque transients in the three-line-to-ground fault (system with NDS', Figure 6.1 for HRE, parameter point ℓ).

NDS' feedback scheme is capable of stabilizing the system when the excitation system is incorporated with the regulator voltage ceilings.

6.5.1.3 Time Response Frequency of Oscillation

It is worth mentioning that the frequency of the time responses in Figures 6.5, 6.6 and 6.7 is approximately 110 electrical r/s. This frequency (110 r/s) is approximately equal to $\omega_0 - \omega_n$, where ω_0 is 377 r/s and ω_n is 267.4 r/s for $X_C = 0.8$ (see equation 1.1). This agreement can be explained as follows:

(a) It was explained in Section 1.2.2, at subsynchronous frequency, a pulsating torque at a frequency of $\omega_0 - \omega_n$ is produced on the rotor shaft by the SSR positive sequence current. Therefore, in displaying the torque response, its frequency of oscillation should be $\omega_0 - \omega_n$ as is in fact the case.

(b) Under any disturbance, the L - C circuit derives a line current component at a frequency of ω_n (see Section 1.2.2) The frequency of this current, when viewed by the d-q axis, is $\omega_0 - \omega_n$ (see Section 3.3.2. Therefore, when displaying the line current, its frequency of oscillation is $\omega_0 - \omega_n$ as it is the case in the present analysis.

(c) Since the voltage drop across the series capacitor is the integral of the line current, there exists a capacitor voltage component at a frequency of ω_n and/or at a frequency of $\omega_0 - \omega_n$ in the d-q axis representation. This frequency is the frequency of oscillation of the graphical display in Figures 6.5 and 6.6 .

6.5.2 Instantaneous Three-Line-To-Ground Fault

The other source of disturbance used in this study is the three-line-to-ground fault located at the receiving end. The period of fault is assumed to last 6 cycles of the supply frequency. In the graphical displays of the results, the fault occurs at 0.05s from the time origin. In the period $0 < t < 0.05s$ the graphs show the steady state solutions prior to the occurrence of the fault transients. The 10 GVA system of parameters and operating conditions described in Table 5.1 is used in the digital simulations.

6.5.2.1 Effect of Voltage Ceilings

It was mentioned in Section 6.5.1.2 that the NDS' feedback scheme is capable of suppressing the large unstable SSR oscillations

in the absence of the regulator voltage ceilings. In this section, this is emphasized by simulating the 10 GVA system subjected to the three-line-to-ground fault when the voltage ceilings are neglected as shown in Figure 6.8 and when they are included in the excitation system as shown in Figure 6.9.

Figure 6.8 shows the torque response of the closed loop system when the HRE excitation system is represented by Figure 5.1(b) (without the voltage ceilings). The steady state operating point is considered to be point z (X_C = .9 p.u., r_E = .025 p.u.) in Figure 6.4 which is further inside the unstable region than the point ℓ . The time response shown in Figure 6.8 demonstrates the elimination of the large unstable SSR oscillations. The peak torque is more than 6.0 p.u. which is much higher than that in Figures 6.5 - 6.7.

Figure 6.9 repeats the simulation of Figure 6.8 but the excitation system is now represented by Figure 6.1 (with the voltage ceilings) and the steady state operating point is considered as point ℓ in Figure 6.4. Figure 6.9 indicates that the closed loop system is now unstable and the NDS' is not capable of suppressing the large unstable SSR oscillations under the limitation of the regulator voltage ceilings.

6.6 Uncontrollability of Large SSR Oscillations

The failure of the NDS' feedback loop to control the large unstable SSR oscillations is explained in the light of the mmf phasor diagram developed in Section 3.3.2. The basic idea of controlling the SSR oscillations by field excitation is to inject current in the field winding which produces a phasor F_{cb} in the air gap rotating at the same speed as F_r. Damping of SSR oscillations is achieved if the torque angle is a reflex angle. For the sake of clarity, the mmf phasor diagram of Figure 3.3 is replotted in Figure 6.10.

The effect of the voltage ceilings on the output signal of the NDS' feedback loop can be explained as a circle with fixed radius representing the voltage ceiling limitations. Any corrective signal of magnitude inside this circle will see a linear excitation system, whereas any corrective signal of magnitude exceeding this circle will be circumscribed as shown in Figure 6.10.

Under large disturbances the mmf phasor magnitudes F_s, F_r increase. Consequently, the magnitude of F_{cb} required to shift F_R into the motoring regime should also increase. In more detail, let us assume that two different faults occur on the system, one is severer than the other. In the context of Figure 6.10 the phasors F_{r1} and F_{s1} represent the mmf phasors of the less severe fault. F_{r2} and F_{s2} are the mmf phasors of the severe fault. The magnitude of F_{cb} has a maximum value equal to the radius of the circle imposed by the voltage

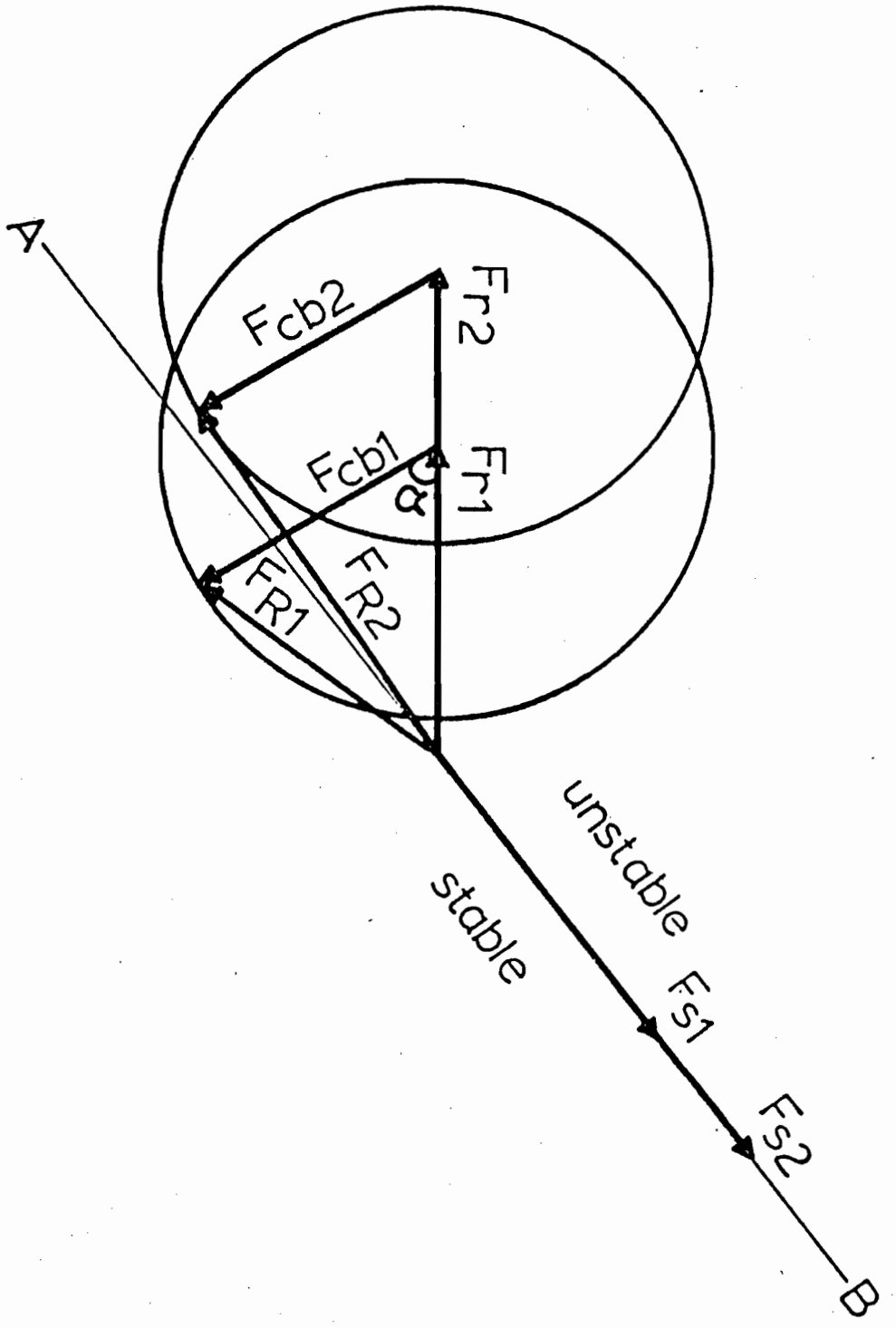

Figure 6.10. MMF phasor diagram of the positive sequence SSR mode showing the principle of stabilization through the excitation phasor F_{cb}. The magnitude of F_{cb} is limited by the voltage ceilings and this limit is illustrated by circles.

ceilings. Figure 6.10 shows that for the case of the less severe fault, the magnitude of F_{cb1} is sufficient to shift F_{R1} into the motoring regime if its phase is within the angle α. But for the severer fault the magnitude of F_{cb2} cannot go beyond the circle limit, which means that the system cannot be stabilized irrespective of the phase of F_{cb2}.

6.7 Suppression of the Large Perturbation SSR by a Nonlinear Resistor Protection Scheme

Due to the inherent limitation of the field excitation feedback to stabilize the large unstable SSR oscillations, one looks into the capacitor protection schemes, now in use to limit capacitor over voltage [8, 42] as a means of suppressing the large unstable SSR oscillations also. Typically, the schemes consist of a spark gap connected in parallel with the series compensating capacitor.

The idea of these protection schemes is to remove the series capacitor from the line when a fault is detected and reinsert it after a few cycles from clearing the fault. The most common scheme now in use is the one with the line diagram shown in Figure 6.11(a). This accomplishes the shunting of the series capacitor bank with a parallel spark gap set to spark-over when the short-time over-voltage rating of the capacitor is exceeded. A low reactance is usually included in series with the spark gap

to limit the capacitor discharge current at gap spark-over. A switch is connected in parallel with the spark gap to protect it from heavy currents and to de-ionize it before reinserting the series capacitor as shown in Figure 6.11(a).

The series capacitor is usually reinserted in the circuit after a few cycles (usually 5 to 8 cycles [8]) from clearing the fault. This is done by extinguishing the spark gap (when the switch is not used for this purpose) to transfer the line current back to the capacitor. Different methods are employed to interrupt the bypass current. One of these methods uses a blast at high pressure air to extinguish the spark gap current.

The interruption of the spark current leads to a transient capacitor voltage. The act of reinsertion will stimulate the unstable SSR oscillations unless they are properly time phased. The capacitor voltage will grow again and cause re-ignition of the spark gap, especially if the line current is high and no insertion resistor is used. To limit the reinsertion transient voltage across the capacitor to a value less than the maximum gap setting, Hartley et al [8] suggested the use of the non-linear resistor in series with the spark gap. Reference [8] showed that a value of the nonlinear resistance, at reinsertion, between 3 and 4 times the capacitive reactance,limits the transient reinsertion voltage to 90 % of the maximum gap spark-over voltage.

Reference [42] explored the idea of using the nonlinear resistor by implementing a new protection scheme that consists of a spark gap in series with the nonlinear resistor and both connected in parallel with the series capacitor bank as shown in Figure 6.11(b). The nonlinear resistor saturation level was designed to the flash over level of the spark gap. The nonlinear resistor conducts high current by the time the spark gap flashes over and gradually diverts some of its current through the capacitor while the fault is clearing. The reinsertion of the series capacitor occurs gradually and by the time the spark gap is extinguished, the line current passing through the nonlinear resistor is very small. Therefore, the transient reinsertion voltage is reduced to a great extent.

All the above protection schemes reported in the literature were associated with a system which is stable in the open loop operation, i.e., the system with the steady state operating points lying in the stable region of Figure 6.4, e.g., point Y . Therefore, after controlling the reinsertion transients by the nonlinear resistor, it is unlikely that these transients will build up in time, since the system is originally stable.

In this chapter the nonlinear resistor protection scheme shown in Figure 6.11(b) is not only used to reduce the capacitor transient voltage which results from severe faults, but also to bring down the large unstable SSR oscillations to a level where the NDS' feedback loop can effectively suppress these oscillations. Without the NDS' feedback the unstable SSR would grow again as the nonlinear protection scheme is not in

operation below the flash over voltage. In other words, the schemes complement each other in eliminating the large unstable SSR oscillations. This can be achieved by a proper design of the nonlinear resistor to limit the reinsertion transients to a level determined by the capability of the NDS' feedback loop. Therefore, the protection scheme of Figure 6.11(b) will be used with a different nonlinear resistor from that used in [42] and it is proposed in this thesis to reduce the transients and to stabilize the unstable SSR oscillations.

6.7.1 Volt-Ampere Characteristic of the Nonlinear Resistor

The volt-ampere characteristic of the proposed nonlinear resistor is shown in Figure 6.12 where for programming, the curve is approximated by piece-wise continuous straight lines. The spark-over voltage of the spark gap is set to three times the steady state capacitor voltage. On spark-over, the nonlinear resistor effectively shunts out the capacitor and on reinsertion the nonlinear resistor is disconnected by opening the switch s-1.

6.7.2 Results

The function of the nonlinear resistor protection scheme is demonstrated by the digital simulations of the 10 GVA system when it is

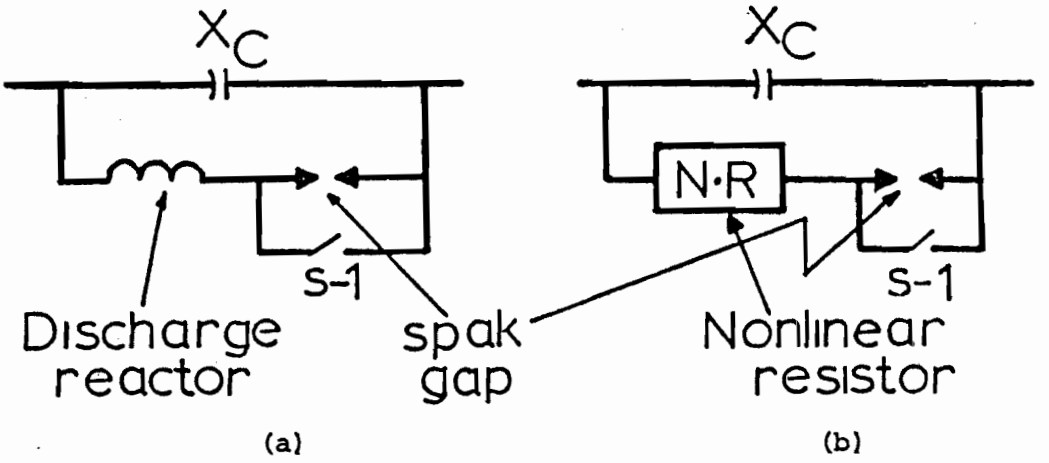

Figure 6.11. (a) The conventional protection scheme.

(b) The nonlinear resistor protection scheme.

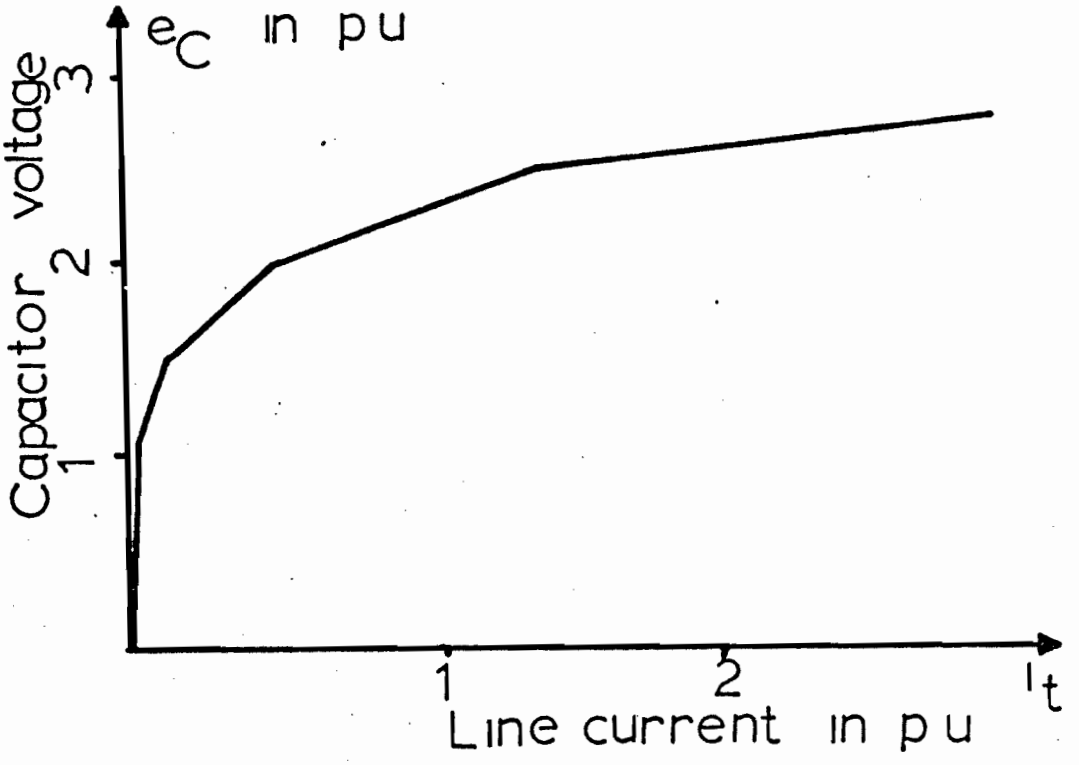

Figure 6.12. Volt-ampere characteristic of the nonlinear resistor for digital simulation.

disturbed by the three-line-to-ground fault. The operating condition used in the simulation are those described in Table 5.1. The simulations are done for both the open loop system, i.e., the 10 GVA system without the NDS' feedback scheme as shown in Figure 5.2(a), and for the closed loop system shown in Figure 5.4(a). The synchronous generator is always assumed to have the HRE excitation system represented by Figure 6.1 and the power system stabilizer PSS with a transfer function shown in Figure 5.2(b). Table 6.3 summarizes all the time responses obtained to evaluate the performance of the nonlinear resistor protection scheme shown in Figure 6.11(b) in two cases: (a) when the SSR oscillations are originally stable without the NDS' feedback scheme, (b) when the SSR oscillations are originally unstable.

6.7.2.1 Effect of the Nonlinear Resistor on Large Stable SSR

Figure 6.13 shows the torque, the line current and the capacitor voltage time responses when the open loop system is subjected to the three-line-to-ground fault. The system is operating without the NDS' feedback and without the nonlinear resistor protection schemes. The steady state operating point is considered as point Y in Figure 6.4 at which the open loop system was stable when tested against the small perturbation. The time responses of Figure 6.13 indicate that the open loop system is stable with a peak torque of 3.3 p.u.

TABLE 6.3.

TIME RESPONSES OF THE 10 GVA SYSTEM FOR THE THREE-LINE-TO-GROUND FAULT

Figure Number	HRE of Fig. 6.1	PSS	NDS'	Operating Point in Fig. 6.4	X_C	r_E	Nonlinear Resistor	System Configuration
Fig. 6.13	X	X		Y	0.8	0.04		Fig. 5.2(a).
Fig. 6.14	X	X		Y	0.8	0.04	X	Fig. 5.2(a) with Fig. 6.11(b).
Fig. 6.15	X	X	X	Y	0.8	0.04	X	Fig. 5.4(a) with Fig. 6.11(b).
Fig. 6.16	X	X	X	ℓ	0.8	0.025	X	Fig. 5.4(a) with Fig. 6.11(b).
Fig. 6.17	X	X		ℓ	0.8	0.025	X	Fig. 5.2(a) with Fig. 6.11(b).
Fig. 6.18	X	X	X	z	0.9	0.025	X	Fig. 5.4(a) with Fig. 6.11(b).

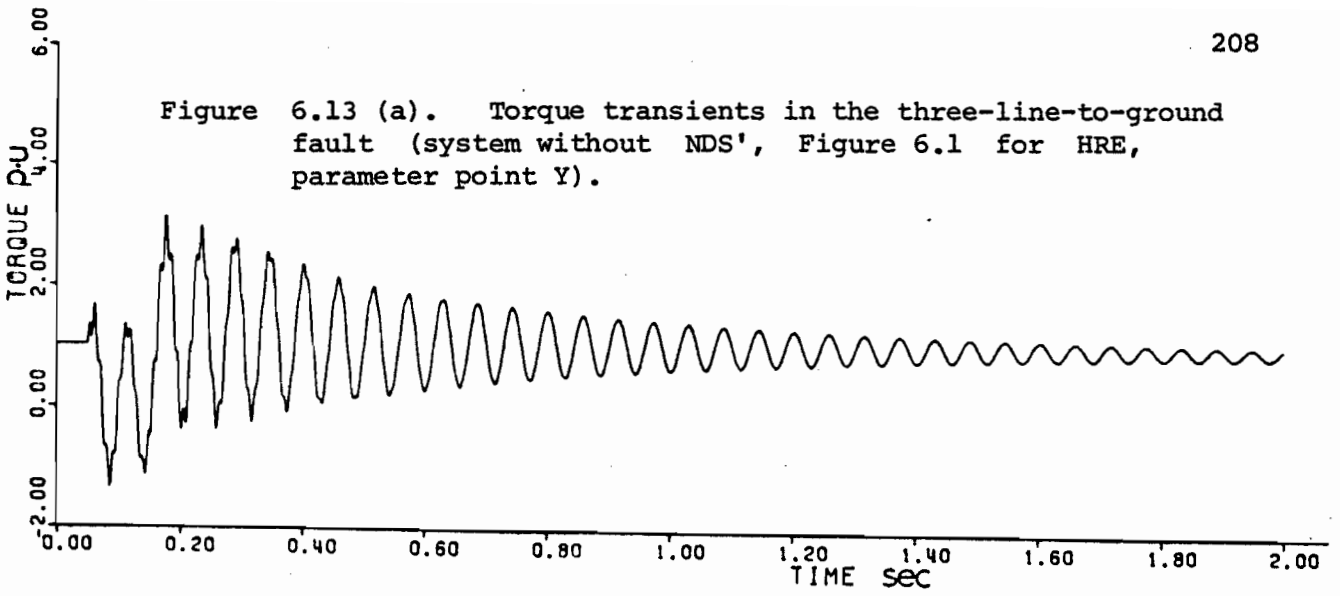

Figure 6.13 (a). Torque transients in the three-line-to-ground fault (system without NDS', Figure 6.1 for HRE, parameter point Y).

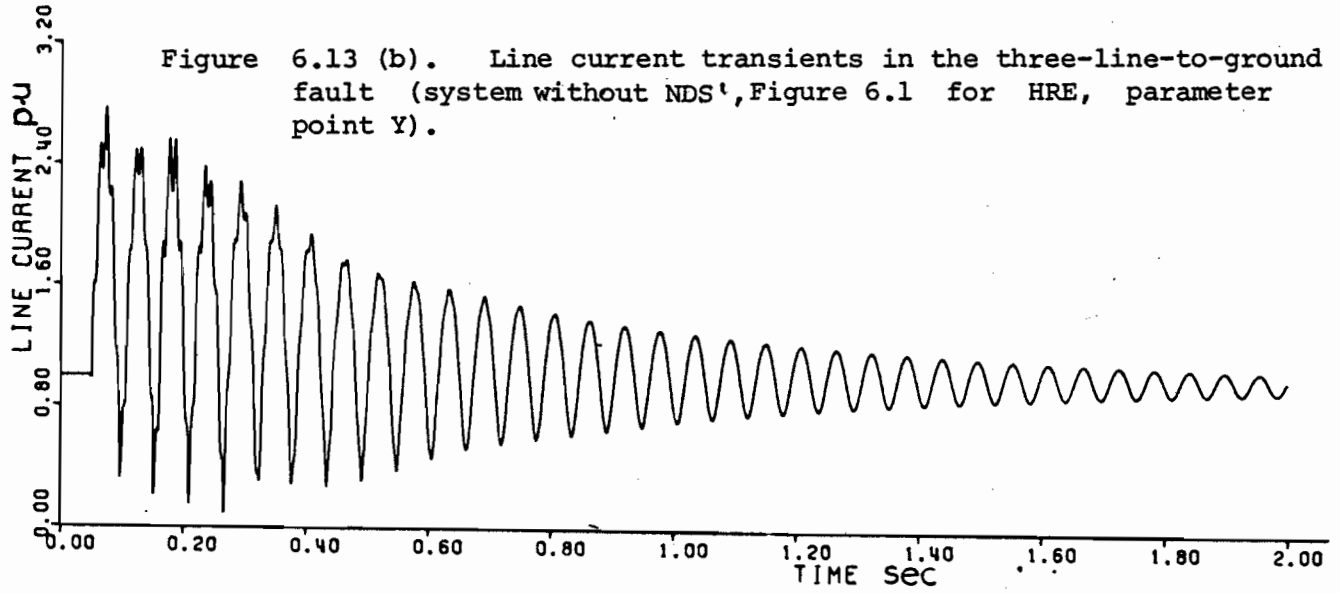

Figure 6.13 (b). Line current transients in the three-line-to-ground fault (system without NDS',Figure 6.1 for HRE, parameter point Y).

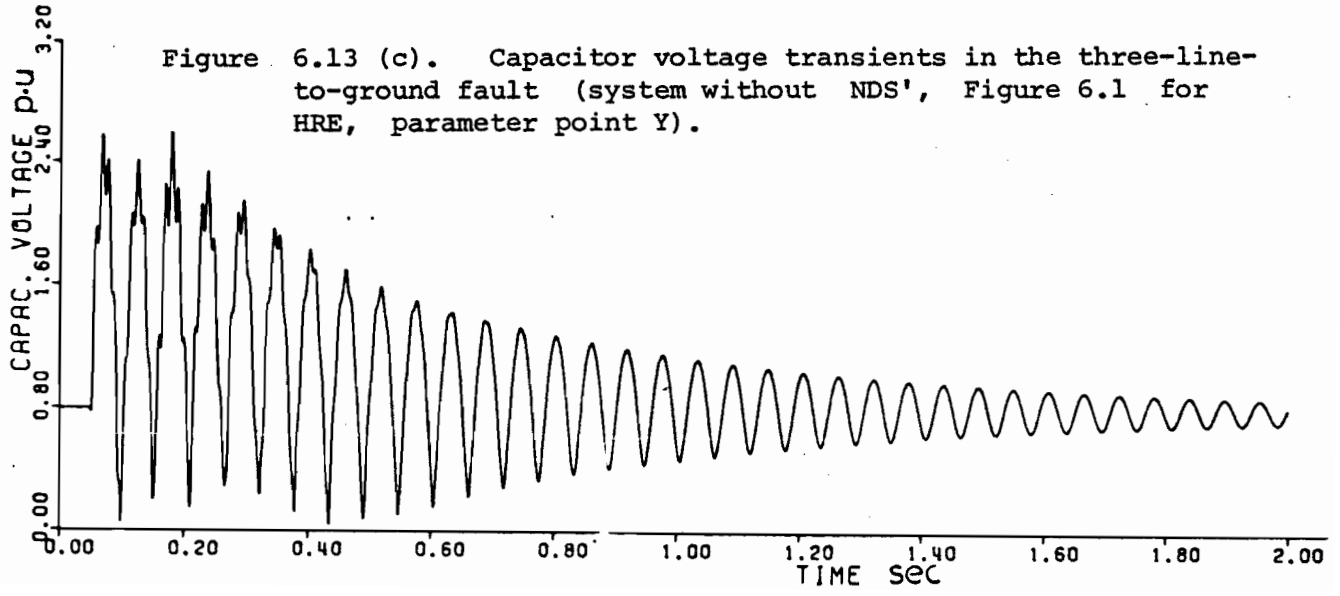

Figure 6.13 (c). Capacitor voltage transients in the three-line-to-ground fault (system without NDS', Figure 6.1 for HRE, parameter point Y).

Figure 6.14 shows the torque, the line current and the capacitor voltage time responses of the above system working under the protection of the nonlinear resistor scheme. The system is still working without the NDS' feedback scheme and with point Y as the steady state operating point. The nonlinear resistor is disconnected after 0.2s from the commencement of the fault. A comparison between Figure 6.13 and Figure 6.14 shows that the nonlinear resistor reduces the peaks of the torque, the line current and the capacitor voltage from 3.3 p.u., 2.8 p.u. and 2.6 p.u., in Figure 6.13 to 1.63 p.u., 2.6 p.u. and 2.3 p.u. in Figure 6.14 respectively. Furthermore, the reinsertion transients are very small and damp out quickly.

The inclusion of the line current and the capacitor voltage responses in Figures 6.13 and 6.14 is to show the similarity between their behaviour and the torque behaviour in both figures. Therefore,only the torque time response will be used in the next presentation of simulation results.

The above simulations establish the role of the nonlinear resistor in reducing the peak oscillations in the absence of the NDS' feedback loop. However, it is worth investigating how the NDS' feedback scheme can effect the large stable SSR oscillations in the presence of the nonlinear resistor protection scheme. Figure 6.15 shows the torque time response when the same system of time responses shown in Figure 6.14 is simulated with the NDS' feedback scheme in operation. The torque

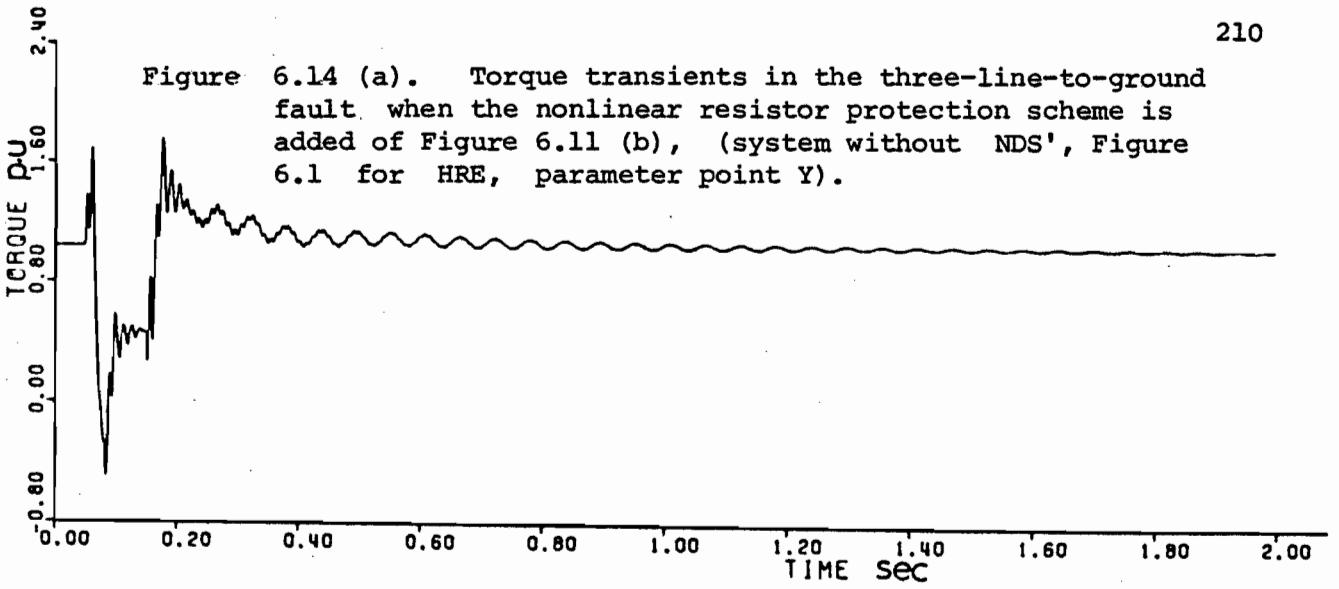

Figure 6.14 (a). Torque transients in the three-line-to-ground fault when the nonlinear resistor protection scheme is added of Figure 6.11 (b), (system without NDS', Figure 6.1 for HRE, parameter point Y).

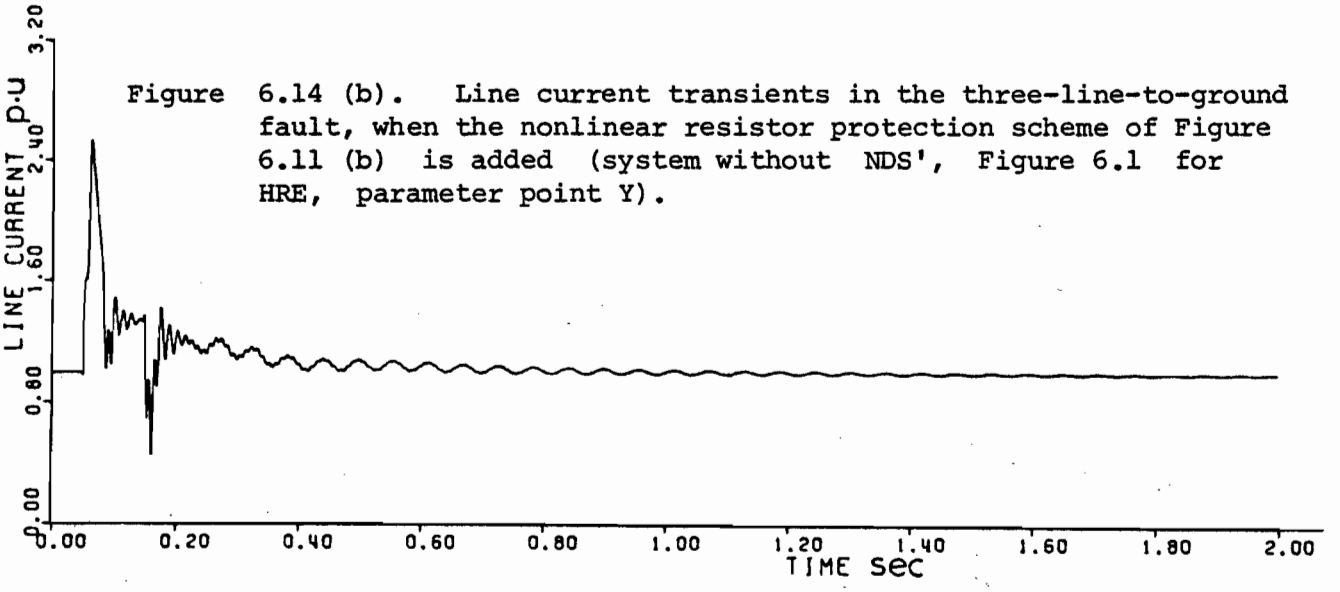

Figure 6.14 (b). Line current transients in the three-line-to-ground fault, when the nonlinear resistor protection scheme of Figure 6.11 (b) is added (system without NDS', Figure 6.1 for HRE, parameter point Y).

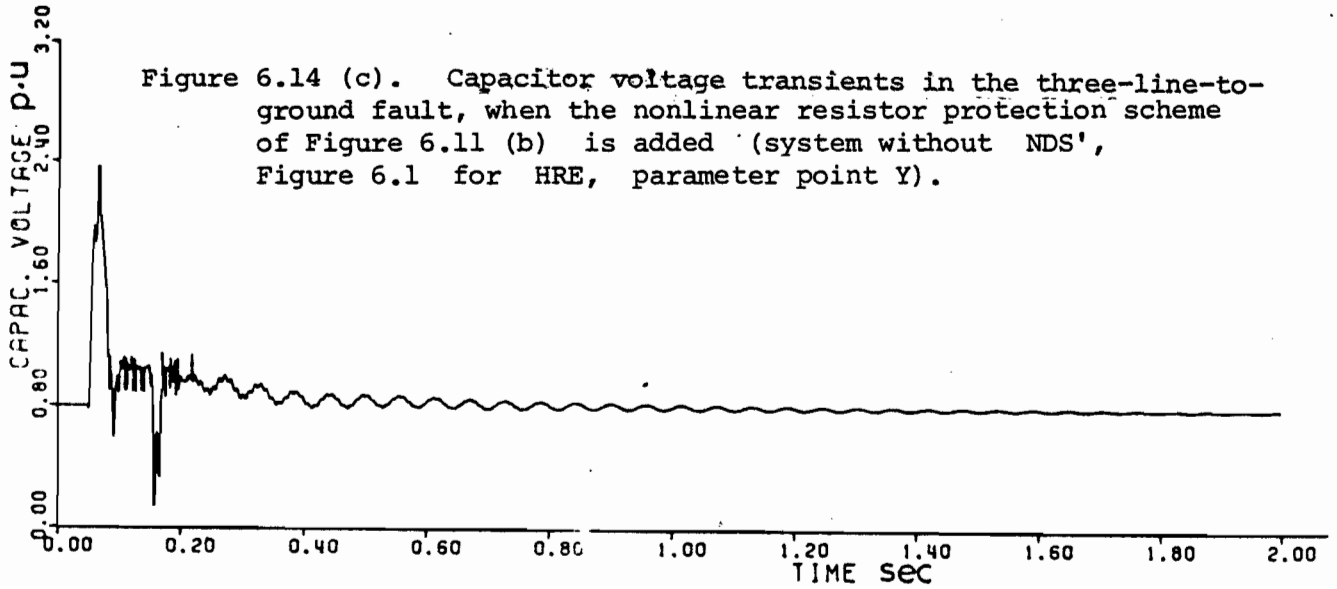

Figure 6.14 (c). Capacitor voltage transients in the three-line-to-ground fault, when the nonlinear resistor protection scheme of Figure 6.11 (b) is added (system without NDS', Figure 6.1 for HRE, parameter point Y).

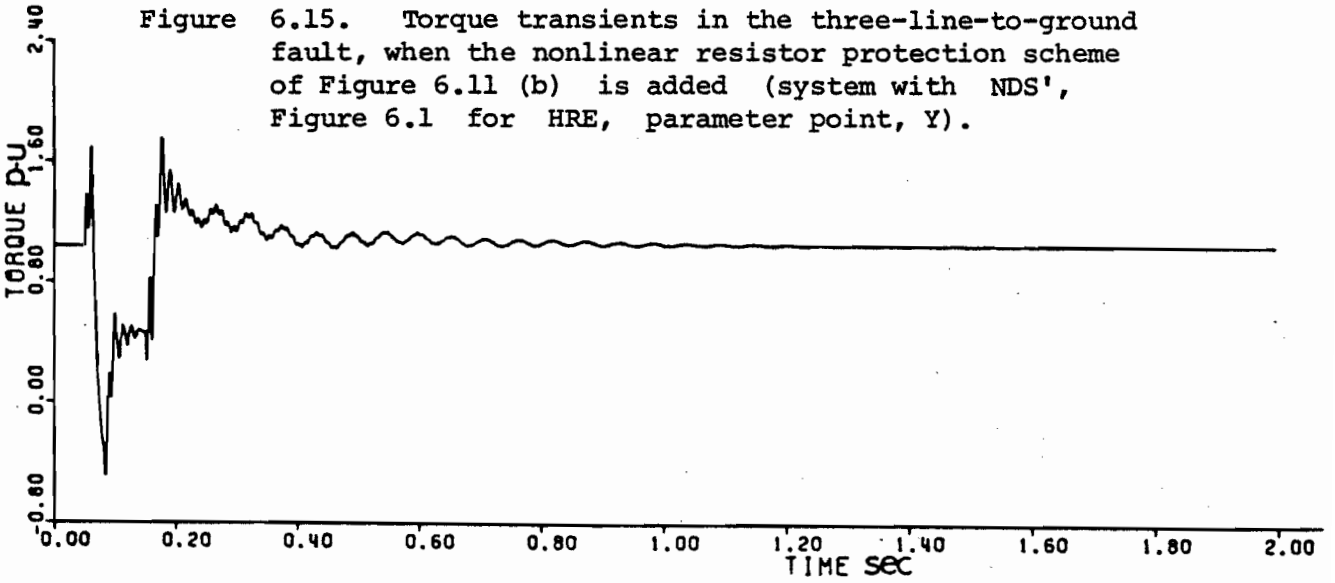

Figure 6.15. Torque transients in the three-line-to-ground fault, when the nonlinear resistor protection scheme of Figure 6.11 (b) is added (system with NDS', Figure 6.1 for HRE, parameter point, Y).

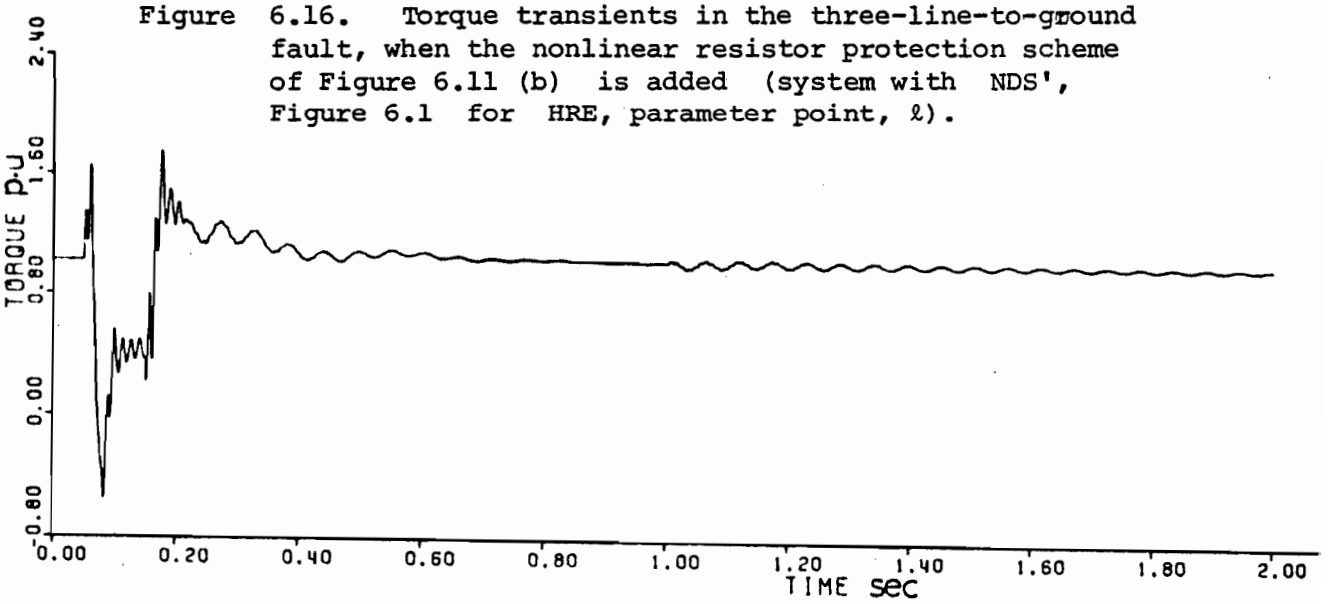

Figure 6.16. Torque transients in the three-line-to-ground fault, when the nonlinear resistor protection scheme of Figure 6.11 (b) is added (system with NDS', Figure 6.1 for HRE, parameter point, ℓ).

response in Figure 6.15 shows that the NDS' feedback loop does not effect the peak torque but damps out quickly the reinsertion transients as it is clear from the comparison of Figure 6.15 with Figure 6.14.

6.7.2.2 Effect of the Nonlinear Resistor on Large Unstable SSR

In Section 6.7.2.1 the system has been considered as a stable system in the open loop operation. In this section the system under consideration is unstable under the open loop operation that is its steady state opeating point falls in the unstable region of Figure 6.4 such as points ℓ and z .

Figure 6.16 shows the torque time response of the closed loop system (with the NDS' feedback loop) working under the nonlinear resistor protection scheme when it is subjected to the three-line-to-ground fault. Its steady state operating point is assumed to be point ℓ in Figure 6.4 at which the open loop system is unstable under small disturbances (see Chapter V) and it was stabilized by the NDS' feedback loop. However, the closed loop system is also unstable at this point when it is subjected to the three-line-to-ground fault as it was shown in Figure 6.9. It is to be reminded that the excitation system (HRE) of the synchronous generator includes the voltage ceilings and the operating conditions are the same as those described in Table 5.1. The nonlinear resistor is disconnected after 0.95s from the beginning of the fault. The torque response in

Figure 6.16 indicates the elimination of any building up oscillations after disconnecting the nonlinear resistor. Therefore, the system is stable and the NDS' feedback loop damps the reinsertion oscillations.

To demonstrate the complementary role of both the nonlinear protection and the NDS' feedback schemes in effectively suppressing the large unstable SSR oscillations, the simulation of Figure 6.16 is repeated but without the NDS' feedback loop as shown in Figure 6.17. Figure 6.17 shows the torque response of the open loop system with point ℓ as its steady state operating point and the nonlinear resistor is disconnected after 0.95s from the beginning of the fault. Figure 6.17 shows that after disconnecting the nonlinear resistor, the reinsertion transients build up in time which eventually reach the level at which the spark gap sparks-over. Then the nonlinear resistor is reinserted to reduce the unstable oscillations and when it is disconnected these oscillations will build up again and the same process is repeated. This is because the steady state operating point (point ℓ) of the open loop system is originally an unstable point.

The simulation results in Figures 6.16 and 6.17 emphasizes the necessity of using both the nonlinear resistor and the NDS' feedback loop to damp out the large unstable SSR oscillations. Their effectiveness in eliminating these oscillations is assessed by simulating the closed loop system associated with the nonlinear resistor protection scheme when it is subjected to the three-line-to-ground fault. The steady state operating point considered in Figure 6.4 is point z which is deep in

the unstable region as shown in Figure 6.18. The torque response in Figure 6.18 clearly demonstrates a stable system.

6.7.3 Time Response Frequency of Oscillation

The other point to discuss is the frequency of the torque oscillation (since the oscillations of the other quantities are similar) in the absence of the nonlinear resistor protection scheme and when it is engaged with the system during fault conditions. For instance, in the torque time response in Figure 6.14, the frequency of oscillation in the period of $0.05s < t < 0.2s$, i.e., when the nonlinear resistor is in operation, is different from that in the period of $t > 0.2s$ or when the nonlinear resistor is disconnected. This is because the effective series capacitive reactance X_C, in both periods is different that is, when the spark gap flashes over (the nonlinear resistor is connected) X_C is almost zero. Therefore, the subsynchronous resonance frequency ω_n is very small (see equation 1.1). Hence, the speed of the SSR positive sequence current which is $\omega_0 - \omega_n$ in the d-q axis rotating frame, is approximately equal to ω_0, or the frequency of oscillation in the beginning of the period $0.05 < t < 0.2$ in Figure 6.14 is about 60 Hz. Gradually, the series capacitor is inserted in the circuit during the same period $(0.05 < t < 0.2)$, which means that ω_n increases and the frequency of the torque oscillation decreases until switch s-1 is opened (the nonlinear resistor is dis-

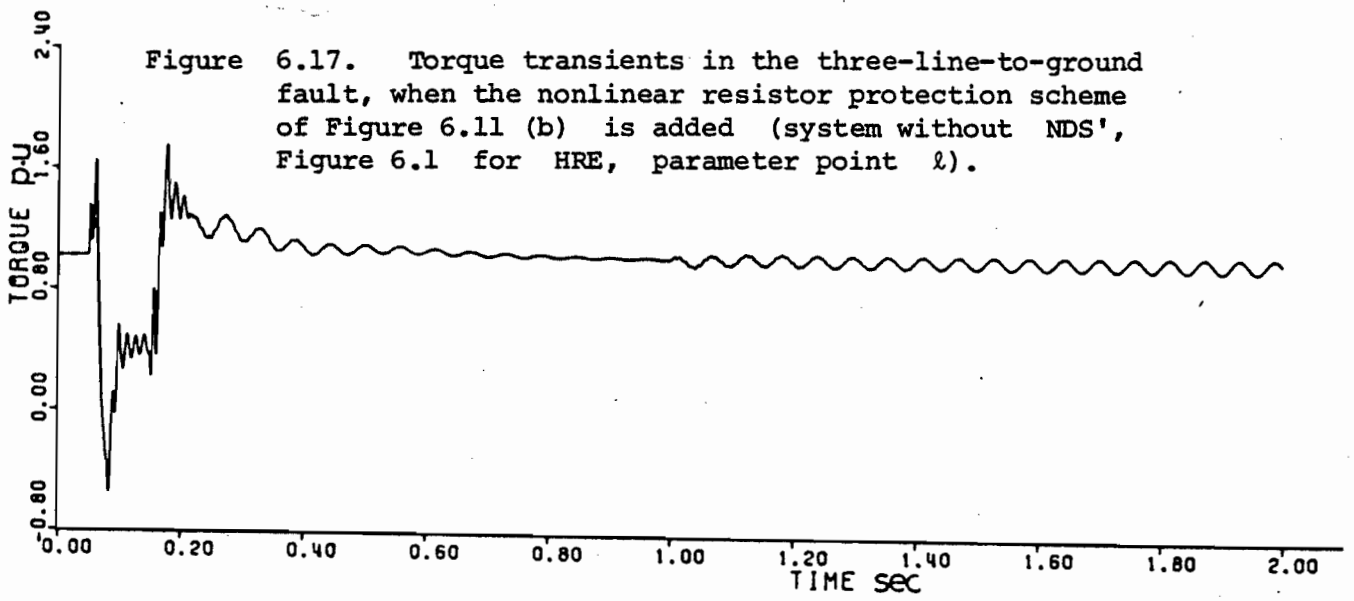

Figure 6.17. Torque transients in the three-line-to-ground fault, when the nonlinear resistor protection scheme of Figure 6.11 (b) is added (system without NDS', Figure 6.1 for HRE, parameter point ℓ).

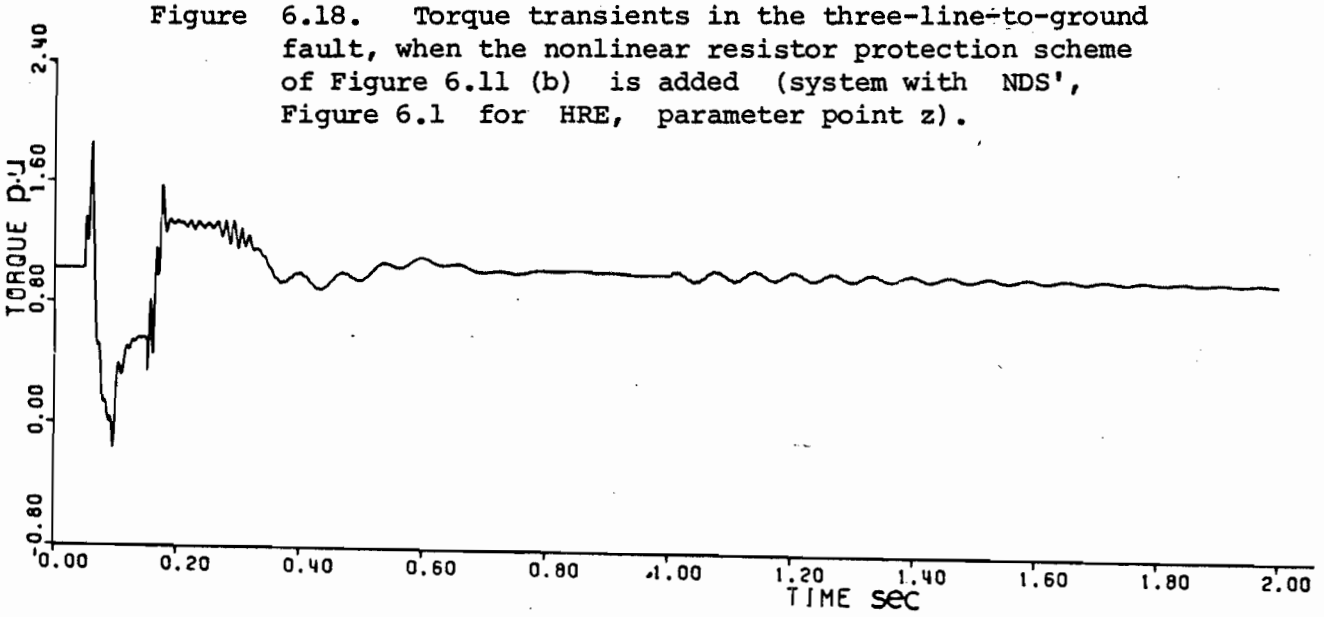

Figure 6.18. Torque transients in the three-line-to-ground fault, when the nonlinear resistor protection scheme of Figure 6.11 (b) is added (system with NDS', Figure 6.1 for HRE, parameter point z).

connected). Then the frequency of the torque oscillation is $\omega_0 - \omega_n$ as shown in Figure 6.14 for the period $t > 0.2s$. Therefore, the frequency of this oscillation lies in the range between $\omega_0 - \omega_n$ and ω_0.

6.8 Discussion

The suppression of the large unstable SSR oscillations by the nonlinear resistor protection scheme and the NDS' feedback loop can be explained in the light of Figure 6.19. In Figure 6.19 the high order system is represented for simplicity by a two dimensional system with the origin as its steady state operating point. In the context of Figure 6.4, this origin is a stable point if it lies in the stable region of Figure 6.4, e.g., point Y, otherwise, it is unstable, e.g., points ℓ and z. Let us assume that the open loop system has a steady state operating point which is unstable under any kind of disturbance, therefore the origin in Figure 6.19(a) is an unstable point and under disturbance, the oscillations divert away from this point.

Consider the system of the same steady state operating point, but working in the closed loop manner (system of configuration shown in Figure 5.4(a)) and with the presence of the voltage ceilings. The NDS' feedback loop is capable of suppressing the SSR oscillations if its size is within the circle imposed by the voltage ceilings as shown in Figure 6.19(b). Therefore, any oscillation inside the circle will converge to the

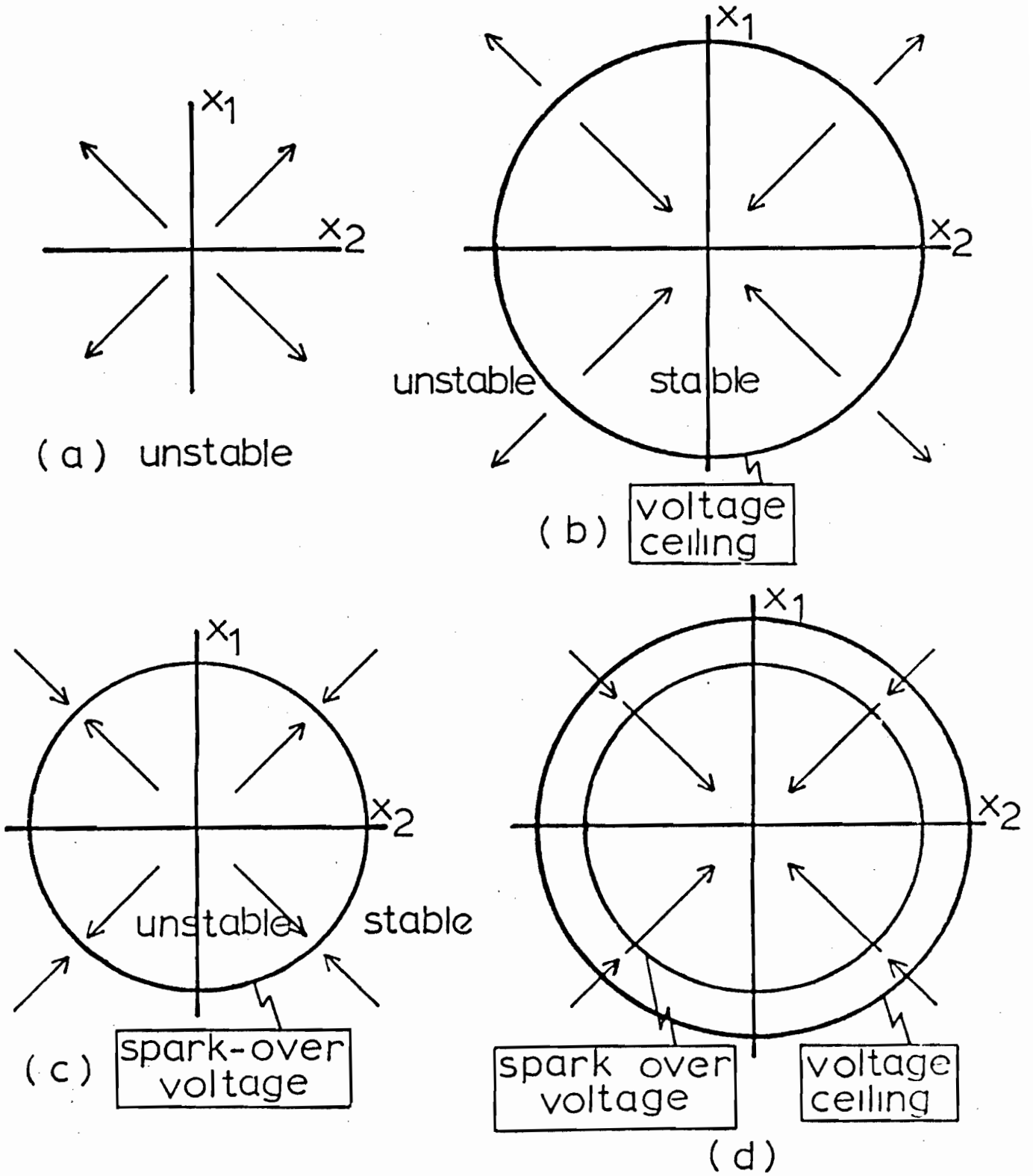

Figure 6.19. Two dimensional representation of x_1, x_2 space showing:

(a) SSR instability (any point in the unstable region of Figure 6.4)

(b) The stability limit of the system with the NDS' (Figure 5.4 (a)) under voltage ceilings.

(c) Conditions of limit cycle arising from the spark-over voltage dead-zone of the nonlinear resistor protection.

(d) Overall stability from a combination of NDS' feedback and the nonlinear resistor protection.

origin by the NDS' feedback action, and any oscillation outside the circle will divert away from the origin.

Similarly, consider the open loop system shown in Figure 5.2(a) which is incorporated with the nonlinear protection scheme and its steady state operating point lies in the unstable region of Figure 6.4. Under severe disturbance, the nonlinear resistor brings down the oscillation to a low level. This means that at the time the spark gap flashes over, the nonlinear resistor clamps the peak oscillation by providing another passage to current rather than flowing in the series capacitor. Since the system is unstable in the open loop, therefore, the small oscillations resulting from disconnecting the nonlinear resistor will build up in time. In the context of Figure 6.19, the effect of the nonlinear resistor can be represented by a circle, where any oscillation outside this circle is brought down by the nonlinear resistor. But any oscillation inside this circle is not influenced by the nonlinear resistor, and it diverts away from the origin, since the origin is an unstable point as shown in Figure 6.19(c).

To stabilize the large SSR oscillations, the two schemes should be incorporated with the system in such a way that the nonlinear resistor protection scheme limit should fall within the voltage ceilings limit. In the context of Figure 6.19, the circle of Figure 6.19(c) should fall inside the circle of Figure 6.19(b) as shown in Figure 6.19(d).

The conclusion of this chapter is that unstable SSR oscillation that occurred in the synchronous machine connected to a series capacitor compensated transmission line is eliminated during severe faults by the complementary action of both the NDS' feedback and the nonlinear resistor protection schemes. This is very clear from Figures 6.16 and 6.17.

The other conclusion concerns the peak torque characteristics of the synchronous generator in case of compensated transmission line during synchronization-out-of-phase in Figure 6.2. The results obtained in Figure 6.2 take the same shape as those obtained in [63] for the case of uncompensated transmission lines.

CHAPTER VII

TORSIONAL RESONANCE INTERACTION

7.1 Introduction

Chapters V and VI have discussed the phenomenon of sub-synchronous resonance in series capacitor compensated transmission lines without considering the interaction of torsional resonance of the turbine-generator shaft inertia systems. The torque amplifications in the shaft can be disastrously large when the SSR resonance frequency ω_n is nearly equal to $\omega_0 - \omega_m$ where ω_m is any one of the mechanical resonant frequencies.

The torsional resonance of the turbine-generator shaft inertias is considered in this chapter, and its effect on the system stability is demonstrated by mapping the stability boundary on the $X_C - r_E$ plane. Furthermore, the protection of the system from the torsional resonance interaction damaging effect is removed by installing a power blocking filter on the terminal of the generator.

7.2 Mathematical Formulation

In this chapter the analysis and the mathematical formulation are restricted to the multi-inertia system of the hydro-turbine power station, since the principle of the analysis and formulation of the multi-inertia systems of other power stations (e.g., steam-turbine power station) is the same. The

stability of the hydro-turbine system under torsional resonance interaction is investigated by the same methodologies used in Chapters V and VI, which are:

(i) The small perturbation study.

(ii) The large perturbation study.

(i) In the small perturbation study that is, when the system of Figure 7.1 is slightly disturbed from its steady state operation, the system stability is studied by calculating its eigenvalues. The linearized differential equations describing the generator, the network, the machine excitation system, the PSS and the NDS' feedback loop are those derived in Chapters II and V. These equations are: equations 2.52 and 2.53 for the synchronous generator, equations 2.57 and 2.58 for the network, equation 5.1 for the excitation system, equation 5.4 for the PSS and equation 5.6 for the NDS' feedback loop.

The mechanical equations which are described by equations 2.54 and 2.55 are replaced here by a new set of mechanical equations. This new set includes the mechanical dynamics of the hydro-turbine system necessary for studying the torsional resonance interaction effect. The new mechanical equations are derived in Appendix D. The rotor system of the hydro-turbine system is modelled by two moments of inertia connected by a torsional spring. One moment of inertia ($2 H_G$) represents the generator and the other ($2 H_T$) represents the water turbine. These equations

are written in linearized form as:

$$\begin{bmatrix} 2H_G & & & \\ & 2H_T & & \\ & & 1 & \\ & & & 1 \end{bmatrix} \frac{d}{dt} \begin{bmatrix} \Delta\bar{\omega}_G \\ \Delta\bar{\omega}_T \\ \Delta\delta_G \\ \Delta\delta_T \end{bmatrix} = \begin{bmatrix} -D_G-D_{GT} & D_{GT} & -K_{GT} & K_{GT} \\ D_{GT} & -D_T-D_{GT} & K_{GT} & -K_{GT} \\ 1 & 0 & 0 & 0 \\ 0 & 1 & 0 & 0 \end{bmatrix}$$

$$\cdot \begin{bmatrix} \Delta\bar{\omega}_G \\ \Delta\bar{\omega}_T \\ \Delta\delta_G \\ \Delta\delta_T \end{bmatrix} + \begin{bmatrix} -\Delta T_e \\ 0 \\ 0 \\ 0 \end{bmatrix} \qquad (7.1)$$

where ΔT_e is described in equation 2.56.

H_G and H_T are the generator and the water turbine inertia constants.

D_G, D_T and D_{GT} are the generator, the water turbine and the shaft damping coefficients.

K_{GT} is the torsional spring stiffness coefficient.

$\Delta\bar{\omega}_G$ and $\Delta\delta_G$ are the perturbations in the generator inertia angular speed and position.

$\Delta\bar{\omega}_T$ and $\Delta\delta_T$ are the perturbations in the water turbine inertia angular speed and position.

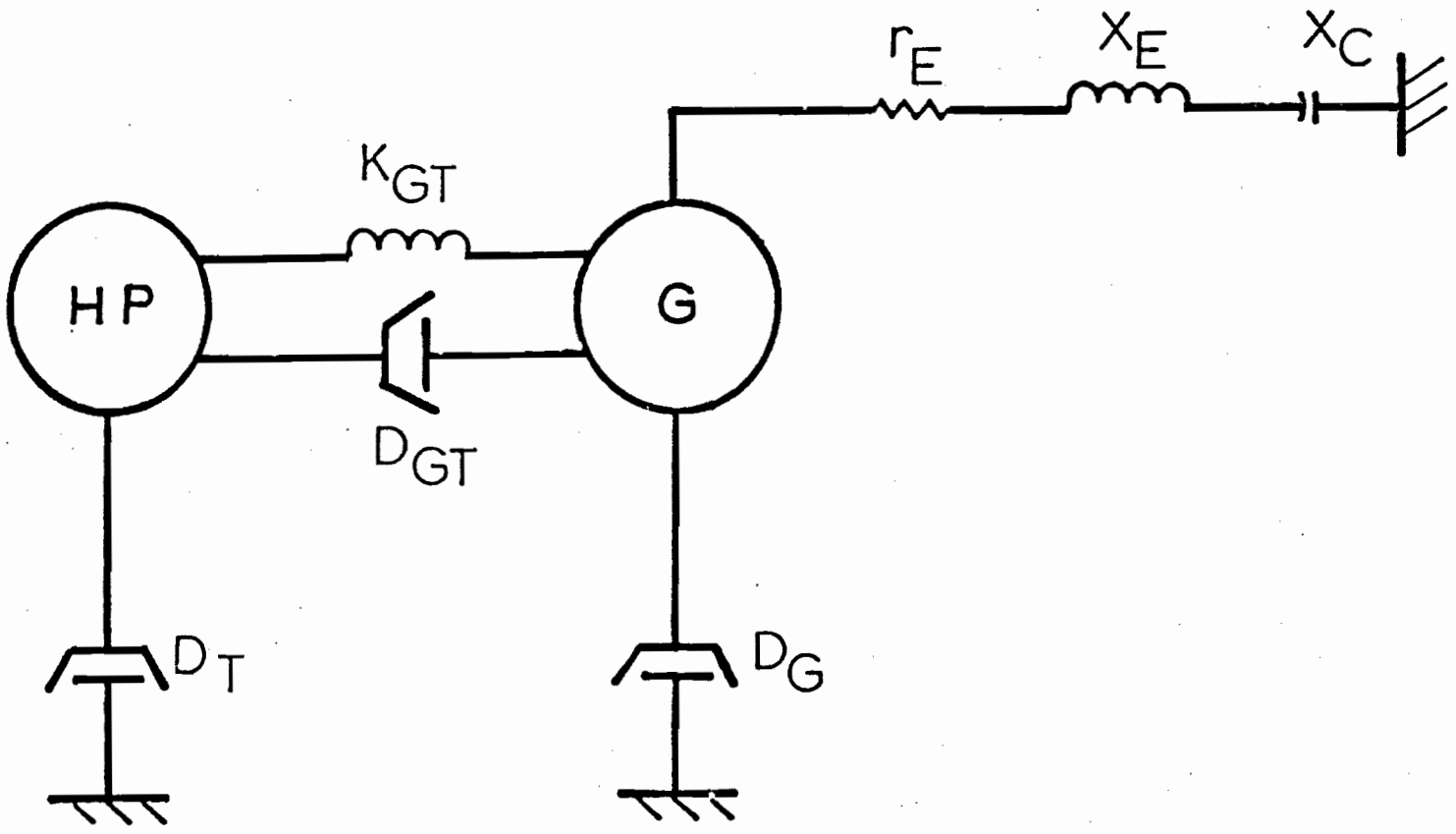

Figure 7.1. Hydro-system connected to a series capacitor compensated transmission line.

The linearized model of the system shown in Figure 7.1 is obtained by combining equations 2.52, 2.53, 2.57 and 2.58 (after transforming them to the D-Q synchronously rotating reference frame) with equation 7.1. The resultant model does not include the machine excitation system. To obtain the linearized model for the regulated open loop system, the above model should be combined with equations 5.1 and 5.4 for the HRE and the PSS systems respectively. The final linearized model is required for the closed loop system. This can be obtained from the linearized model of the regulated open loop system with equation 5.6, which describes the NDS' filter state space model.

(ii) In the large perturbation study that is, when the system of Figure 7.1 is disturbed by the three-line-to-ground fault discussed in Chapter VI, the system stability is studied by the numerical integration of its nonlinear differential equations. For this purpose, two nonlinear models are required. The first one is to describe the regulated open loop system and this is obtained by combining equations 6.1, 6.4, D.2 (from Appendix D), 6.5, 6.6, 6.7, 6.8, 6.9, 6.10, 6.17 (for the PSS) and equations 6.14 - 6.16 for the HRE excitation system. The second one is to describe the regulated closed loop system and this is obtained by combining the first model with equation 6.18 for the NDS' filter.

7.3 Simplified View

As it was mentioned in Section 1.3, torsional resonance interaction occurs when the frequency of the pulsating torque, which is produced by the interaction between the subsynchronous stator magnetic field component with the steady state airgap magnetic field, is approximately equal to one of the rotor system resonance frequencies. The physics of this interaction is that under any disturbance, the rotor oscillation at a frequency of f_m Hz will produce a velocity component [23]. This velocity component will produce in the stator of the generator a positive sequence voltage component at a frequency of $f_0 - f_m$ Hz. If this frequency is approximately equal to the L - C resonance frequency f_n, then a large positive sequence current at a frequency of f_n will flow in the external circuit. This current, when it flows in the generator stator windings, will produce a magnetic field component rotating in the airgap at a frequency of f_n. The interaction between the f_0 Hz airgap field and this magnetic field component will produce a pulsating torque at a frequency of $f_0 - f_n$ or at a frequency of f_m approximately. This pulsating torque will produce a positive sequence current in the stator windings of the generator in phase with the oscillating current at a frequency of f_n [23]. This amplifies the stator current at the frequency of f_n and hence the pulsating torque at the frequency of f_m. This process results in a positive feedback on the rotor shaft. Ultimately the torque level is sufficiently high so as to cause the mechanical damage.

In other words, this torsional resonance interaction is due to a negative damping. The rotor oscillation at a frequency of f_n is limited only by the mechanical damping (D). Since the oscillating current produces a pulsating torque in phase with the rotor oscillation, then the generator stator with the network behaves as a negative damping as viewed by the rotor. If this negative damping is greater than D then the pulsating torque will be amplified to cause shaft damage.

The hydro-system, which is described by all the parameters in Table 5.1, except those for the damping (D) and the inertia constant (H), has one mechanical resonance frequency, ω_m, which is approximately calculated from the following equation :

$$f_m \simeq \sqrt{\frac{K_{GD}}{4 \pi f_0 H_R}} \qquad f_0 \quad \text{Hz} \tag{7.2}$$

where $f_0 = 60$ Hz the synchronous frequency

$$H_R = \frac{H_G \; H_T}{H_G + H_T} \tag{7.3}$$

The values of the mechanical parameters are [39] :

$$K_{GT} = 22.5 \quad ,$$

$$D_T = D_G = 0.5 \quad ,$$

$$D_{GT} = 0.6 \quad ,$$

$$H_G = 2.22 \text{ s} ,$$

$$H_T = 0.633 \text{ s} .$$

The system of Figure 7.1 has its L-C circuit resonating at the subsynchronous frequency f_n Hz (ω_n r/s) corresponding to a fixed value of the series capacitive reactance X_C . Torsional resonance interaction occurs if the following condition is satisfied :

$$f_m \simeq f_0 - f_n \tag{7.4}$$

In the current analysis, one expects that there is one value of X_C around which torsional resonance interaction occurs, since the rotor system has one resonance frequency.

7.4 Torsional Interaction - The Small Perturbation Study

7.4.1 Torsional Resonance Mode

The mechanical system, which was described by two equations in Section 2.6, is now described by four first order differential equations (see equation 7.1). Therefore, the eigenvalues of the unregulated system are now 11 instead of 9 previously, and of the regulated system without the NDS' feedback is 17 instead of 15 in Chapter V . Finally, the eigenvalues of the regulated system with the NDS' feedback are now 20.

The torsional inertia system of the rotor system adds on two differential equations. The question raised is whether the eigenvalues associated with them will ever go unstable.

In answer to this question, it is found that the additional eigenvalues exist in complex conjugate pairs which will hereafter be identified as λ_{tor}. It is also found that the stability boundary in the $X_C - r_E$ plane takes the form,as shown in Figure 7.2, where the indentation around $X_C = 0.89$; $r_E = 0.1$ is caused by the torsional interaction mode λ_{tor} going unstable.

Table 7.1 lists the eigenvalues of the unregulated system for a number of sample operating parameter points in X_C and r_E. As can be seen, the instability in column 1 and 4 are due to positive real parts in λ_{tor}. Instability in columns 2, 3 and 6 are due to the SSR mode whose eigenvalues, λ_{ssrp}, have positive real parts.

Based on equations 1.1, 7.2 and 7.4, the value of X_C whose L-C resonance frequency interacts with the torsional resonant frequency is $X_C \simeq 0.89$ p.u. Not surprisingly, λ_{tor} is unstable in columns 1 and 4 because the values of X_C are 0.89 and 0.90 p.u., respectively.

The sample X_C in columns 2, 3, 5 and 6 are deliberately chosen to avoid torsional interactions. In the cases where the system is unstable as in columns 2, 3 and 6, the instability is due to λ_{ssrp}. Column 5, however, is stable.

TABLE 7.1

EIGENVALUES OF THE UNREGULATED MACHINE WITH THE ROTOR DYNAMICS

Col. No.	1	2	3	4	5	6
Instability	Torsional Resonance Interaction	SSR Oscillation	SSR Oscillation	Torsional Resonance Interaction		SSR Oscillation
Parameters	r_E=0.035, X_C=.89	r_E=.035, X_C=.93	r_E=.035, X_C=.97	r_E=.05, X_C=.9	r_E=0.05, X_C=.97	r_E=.05, X_C=1.1
λ_{ssrn}	- 4.95 ± j 660.	- 4.95 ± j 666.	- 4.96 ± j 672.	- 6.73 ± j 661.	- 6.75 ± j 672.	- 6.77 ± j 691.
λ_{ssrp}	- 2.28 ± j 96.2	+ .142 ± j 88.8	+ .523 ± j 82.4	- 2.71 ± j 94.0	- 1.30 ± j 82.3	+ .415 ± j 63.2
λ_{amort}	- 33.1 - 15.4	- 33.2 - 16.0	- 33.2 - 16.6	- 33.1 - 15.5	- 33.3 - 16.6	- 33.6 - 19.2

TABLE 7.1 (cont'd)

Col. No	1	2	3	4	5	6
Instability	Torsional Reso-nance Interaction	SSR Oscillation	SSR Oscillation	Torsional Reso-nance Interaction		SSR Oscillation
Parameters	r_E=0.035, X_C=.89	r_E=.035, X_C=.93	r_E=.035, X_C=.97	r_E=.05, X_C=.9	r_E=0.05, X_C=.97	r_E=.05, X_C=1.1
λ_{mech}	- .605 ± j 9.36	- .649 ± j 9.60	- .698 ± j 9.86	- .613 ± j 9.54	- 0.693 ± j 10.0	- .910 ± j 11.1
λ_{tor}	+ 1.52 ± j 96.0	- .527 ± j 97.1	- .502 ± j 97.4	+ .262 ± j 96.5	- 0.457 ± j 97.4	- .480 ± j 97.7
λ_{field}	- .187	- .189	- .191	- .188	- .191	- .198

7.4.2 Identification of λ_{tor}

In Table 7.1, the instability has been classified as due to either λ_{ssrp} or λ_{tor}. In this section, it will be shown how the distinctions are made, based on the expected frequency and also on the eigenvectors.

In part, the eigenvalue can be related to the mode from the imaginary part, which gives angular frequency of oscillations. Using the approximate formula of equation 7.2 and referring it to the d-q reference frame, one can recognize the numerical value for the torsional mode. Likewise, using the approximate formula in equation 1.1 for the SSR angular frequency, and again referring it to the d-q reference frame, the two modes λ_{ssrp} and λ_{ssrn} can be easily recognized.

However, when the imaginary values of λ_{ssrp} and λ_{tor} are approximately equal, it is necessary to examine their eigenvectors to tell the difference. The eigenvectors, for the cases when λ_{ssrp} and λ_{tor} are exclusively unstable, are shown in Tables 7.2 and 7.3 respectively. As the elements of the eigenvectors of λ_{ssrp} and λ_{tor} are compared, the significant information is that the magnitudes of $\Delta \bar{\omega}_G$, $\Delta \delta_G$, $\Delta \bar{\omega}_T$ and $\Delta \delta_T$ are substantially larger in the columns of λ_{tor} than those of λ_{ssrp}. The entries in the current and voltage state variables are of comparable magnitudes.

The eigenvectors in Table 7.2 are calculated for the case where SSR instability occurs ($X_C = 0.93$, $r_E = 0.035$). The SSR mode λ_{ssrp} is identified by the unstable mode, since at this point there is no torsional resonance interaction. The torsional mode λ_{tor} is identified from its frequency (see equation 7.2). Basically λ_{tor} and λ_{ssrp} modes in Table 7.3 are not identified, since in this case there is torsional resonance interaction only ($X_C = 0.9$, $r_E = 0.05$) and the two modes have the same frequency which is not the case in Table 7.2. However, by comparing the eigenvectors in Table 7.3 with those in Table 7.2, the two modes can be identified. This is achieved as follows:

In the third and fifth columns of Table 7.2, the angle between Δe_{CD} and Δe_{CQ} is about 90^o in both columns, and their magnitudes are almost equal. However, the rotor state variables, $\Delta\bar{\omega}_G$, $\Delta\bar{\omega}_T$, $\Delta\delta_G$ and $\Delta\delta_T$, magnitudes in the third column are much less than their magnitudes in the fifth column. This is expected since the fifth column is associated with the λ_{tor} mode. Following the same procedure and comparing the third and fifth columns of Table 7.3, one can see that the appreciable changes between the eigenvectors in the third and the fifth columns occur in the magnitudes of $\Delta\bar{\omega}_G$, $\Delta\delta_G$, $\Delta\bar{\omega}_T$ and $\Delta\delta_T$ which implies that the fifth column is associated with λ_{tor}.

In conclusion, we must exercise some care in distinguishing the causes of instability because the unstable mode can be due to torsional resonance interaction or due to SSR. At present, the physical mechanism

TABLE 7.2

EIGENVECTORS FOR UNREGULATED MACHINE WITH ROTOR DYNAMICS FOR $X_C = 0.93$, $r_E = 0.035$

	λ_{ssrn}		λ_{ssrp}		λ_{tor}		$\lambda_{amort.}$		$\lambda_{mech.}$		λ_{field}
Eigenvalues	- 4.95 + j 666.	- 4.95 - j 666.	+ .143 + j 88.8	+ .143 - j 88.8	- .527 + j 97.1	- .527 - j 97.1	- 33.2	- 16.0	- .649 + j 9.60	- .649 - j 9.60	- .189
Δi_D	.545	.545	.553	.553	.455	.455	.0943	.0789	1.37	1.37	1.36
	178.	- 178	- 59.1	59.1	114.	- 114	180.	0.0	- 151	151.	0.0
Δi_Q	.541	.541	.544	.544	.400	.400	.0364	2.45	2.19	2.19	2.49
	- 91.6	91.6	34.9	- 34.9	- 143	143.	0.0	180.	- 137	137.	180.
Δi_{fd}	.237	.237	.279	.279	.220	.220	.634	.300	1.90	1.90	1.84
	175.	- 175	- 75.5	75.5	94.1	- 94.1	0.0	0.0	- 158	158.	0.0
Δi_{kd}	.289	.289	.276	.276	.225	.225	.777	.105	.351	.351	.0692
	- 179	179.	- 41.1	41.1	126.	- 126	180.	180.	- 86.0	86.0	0.0

TABLE 7.2 (cont'd)

	λ_{ssrn}		λ_{ssrp}		λ_{tor}		$\lambda_{amort.}$		$\lambda_{mech.}$		λ_{field}
Eigenvalues	- 4.95 + j 666.	- 4.95 - j 666.	+ .143 + j 88.8	+ .143 - j 88.8	- .527 + j 97.1	- .527 - j 97.1	- 33.2	- 16.0	- .649 + j 9.60	- .649 - j 9.60	- .189
Δi_{kq}	.521	.521	.523	.523	.432	.432	.0386	4.10	.675	.675	.0175
	- 91.1	91.1	38.5	- 38.5	- 144	144.	0.0	180.	- 81.5	81.5	0.0
$\Delta\omega_G$	.227E-3	.227E-3	.46E-3	.46E-3	.0178	.0178	.33E-3	.0122	.044	.044	.00111
	- 31.8	31.8	- 105	105.	93.4	- 93.4	180.	- 180	- 55	55.0	0.0
$\Delta\delta_G$	.13E-3	.13E-3	.00195	.00195	.0691	.0691	.00379	.288	1.70	1.70	2.22
	- 122	122.	165.	- 165	3.04	- 3.04	0.0	0.0	- 149	149.	180.
Δe_{CD}	.660	.660	.663	.663	.511	.511	.0412	2.28	2.05	2.05	2.32
	87.2	- 87.2	34.1	- 34.1	- 146	146.	0.0	180.	- 136	136.	180.

TABLE 7.2 (cont'd)

	λ_{ssrn}		λ_{ssrp}		λ_{tor}		$\lambda_{amort.}$		$\lambda_{mech.}$		λ_{field}
Eigenvalues	- 4.95 + j 666.	- 4.95 - j 666.	+ .143 + j 88.8	+ .143 - j 88.8	- .527 + j 97.1	- .527 - j 97.1	- 33.2	- 16.0	- .649 + j 9.60	- .649 - j 9.60	- .189
Δe_{CQ}	.658	.658	.670	.670	.553	.553	.0841	.0233	1.29	1.29	1.26
	177.	- 177	122.	- 122	- 63.8	63.8	0.0	0.0	26.5	- 26.5	180.
$\Delta\omega_T$	.4E-5	.4E-5	.0076	.0076	.0667	.0667	.29E-3	.0118	.044	.044	.00111
	150.	- 150	88.7	- 88.7	- 86.8	86.8	180.	- 180	- 55	55.	0.0
$\Delta\delta_T$	.22E-5	.22E-5	.0322	.0322	.260	.260	.00331	.279	1.73	1.73	2.22
	59.4	- 59.4	- 1.2	1.2	- 177	177.	0.0	0.0	- 149	149.	180.

1.0 E-3 = 1.0×10^{-3}.

Note: The first line in the eigenvectors indicate the magnitude of the state.

The second line in the eigenvectors indicate the phase of the state.

TABLE 7.3

EIGENVECTORS FOR UNREGULATED MACHINE WITH ROTOR DYNAMICS FOR $X_C = 0.9$, $r_E = 0.05$

(TORSIONAL RESONANCE INTERACTION)

	λ_{ssrn}		λ_{ssrp}		λ_{tor}		$\lambda_{amort.}$		$\lambda_{mech.}$		λ_{field}
Eigenvalues	- 6.73 + j 661.	- 6.73 - j 661.	- 2.71 + j 94.0	- 2.71 - j 94.0	+ .262 + j 96.5	+ .262 - j 96.5	- 33.1	- 15.5	- .613 + j 9.54	- .613 - j 9.54	- .188
	.549	.549	.570	.570	.552	.552	.0925	.141	.451	.451	1.36
Δi_D	- 179.	179.	- 93.4	93.4	- 134.	134.	180.	0.0	- 111.	111.	0.0
	.545	.545	.548	.548	.543	.543	.0300	2.36	.790	.790	2.49
Δi_Q	- 88.3	88.3	.300	- .300	- 35	35.0	0.0	180.	- 96.2	96.2	180.
	.239	.239	.283	.283	.265	.265	.636	.378	.646	.646	1.835
Δi_{fd}	179.	- 179.	- 110.	110.	- 151.	151.	0.0	0.0	- 117.	117.	0.0
	.291	.291	.290	.290	.270	.270	.777	.127	.119	.119	.0692
Δi_{kd}	- 176.	176.	- 76.7	76.7	- 118.	118.	180.	- 180	- 45.1	45.1	0.0

TABLE 7.3 (cont'd)

	λ_{ssrn}		λ_{ssrp}		λ_{tor}		$\lambda_{amort.}$		$\lambda_{mech.}$		λ_{field}
Eigenvalues	- 6.73 + j 661.	- 6.73 - j 661.	- 2.71 + j 94.0	- 2.71 - j 94.0	+ .262 + j 96.5	+ .262 - j 96.5	- 33.1	- 15.5	- .613 + j 9.54	- .613 - j 9.54	- .188
Δi_{kq}	.525	.525	.537	.537	.535	.535	.0310	4.01	.242	.242	.0172
	- 87.8	87.8	4.10	- 4.10	- 35	35.	0.0	180.	- 42	42.0	0.0
$\Delta\bar{\omega}_G$	.24E-3	.24E-3	.00287	.00287	.0104	.0104	.35E-3	.0118.	.0155	.0155	.00112
	- 27.9	27.9	- 76.6	76.6	167.	- 167	180.	- 180.	- 13.9	13.9	0.0
$\Delta\delta_G$	.134E-3	.134E-3	.0115	.0115	.0406	.0406	.00402	.286	.611	.611	2.23
	- 118.	118.	- 168.	168.	77.3	- 77.3	0.0	0.0	- 108.	108.	180.
Δe_{CD}	.654	.654	.662	.662	.657	.657	.0341	2.12	.714	.714	2.24
	90.1	- 90.1	.100	- .100	- 37.0	37.0	0.0	180.	- 95.4	95.4	180.
Δe_{CQ}	.653	.653	.678	.678	.664	.664	.0803	.0393	.412	.412	1.22
	180.	- 180.	87.9	- 87.9	47.8	- 47.8	0.0	180.	66.8	- 66.8	180.

TABLE 7.3 (cont'd)

	λ_{ssrn}		λ_{ssrp}		λ_{tor}		$\lambda_{amort.}$		$\lambda_{mech.}$		λ_{field}
Eigenvalues	- 6.73 + j 661.	- 6.73 - j 661.	- 2.71 + j 94.0	- 2.71 - j 94.0	+ .262 + j 96.5	+ .262 - j 96.5	-33.1	- 15.5	- .613 + j 9.54	- .613 - j 9.54	- .188
$\Delta\bar{\omega}_T$	.41E-5	.41E-5	.0147	.0147	.0413	.0413	.31E-3	.0114	.0157	.0157	.00112
	154.	- 154.	86.5	- 86.5	- 8.4	8.4	180.	- 180.	- 13.9	13.9	0.0
$\Delta\delta_T$	.23E-5	.23E-5	.0592	.0592	.1612	.1612	.00351	.277	.618	.618	2.23
	62.9	- 62.9	- 5.15	5.15	- 98.2	98.2	0.0	0.0	- 108.	108.	180.

1.0E-3 = 1×10^{-3} .

Note: The first line in the eigenvectors indicate the magnitude of the state.

The second line in the eigenvectors indicate the phase of the state.

of torsional resonance interaction is not altogether clear. It is believed that the instability is due to negative electromechanical damping from the synchronous generator associated with the currents induced in the generator windings by the rotor oscillations. As these currents are at a frequency near the L-C resonance of the series capacitor compensated transmission line, these currents have a propensity to be large. Furthermore, as the angular frequency is below the synchronous speed at which the rotor is turning, induction generator action takes place. Whether the induction generator action is self-sustaining depends on the value of r_E in the armature circuit. As Section 7.4.2 shows that λ_{tor} is unstable for values of r_E at which λ_{ssrp} is still stable, it appears that the negative electromechanical damping contributes to the instability. The origins of the negative electromechanical damping has not been unravelled. It is conjectured here as being due to the positive slope of the torque - speed curve associated with the induction generator action.

7.4.3 Stability Boundary of Unregulated System

Figure 7.2 maps the stability boundary in the $X_C - r_E$ diagram for the system of Figure 7.1. The excitation system is not included in the synchronous generator. The operating conditions are the same as described in Table 5.1. The significant addition to the system model is the elaboration of the mechanical system as two moments of in-

ertias H_G and H_T are connected by an elastic shaft of torsional spring constant K_{GT}, as described in equation 7.1. The inclusion of the shaft torsional resonance results in the indentation of the unstable region as shown in Figure 7.2. This is already well known in the literature [32]. For completeness, we shall list here the three aspects of instability which affect the stability boundary of Figure 7.2.

1. SSR Instability (λ_{ssrp}). This occurs at low line resistance r_E and high capacitive reactance X_C.

2. Mechanical Instability or Hunting ($\lambda_{mech.}$). This is associated with the combined inertias $(H_G + H_T)$ as they swing together with respect to the electromechanical stiffness of the generator. The mechanical damping of this mode is directly proportional to the ratio of line reactance to line resistance [32, 33]. In consequence, the portion of the stability boundary associated with this mode is where r_E takes large values.

3. Torsional Resonance Interaction (λ_{tor}). The instability associated with this mode is around $X_C \simeq 0.9$ in Figure 7.2 where the unstable region engulfs into the stable region. This is the mode which is the subject of this chapter and Section 7.4.1 has already devoted description and identification of this mode.

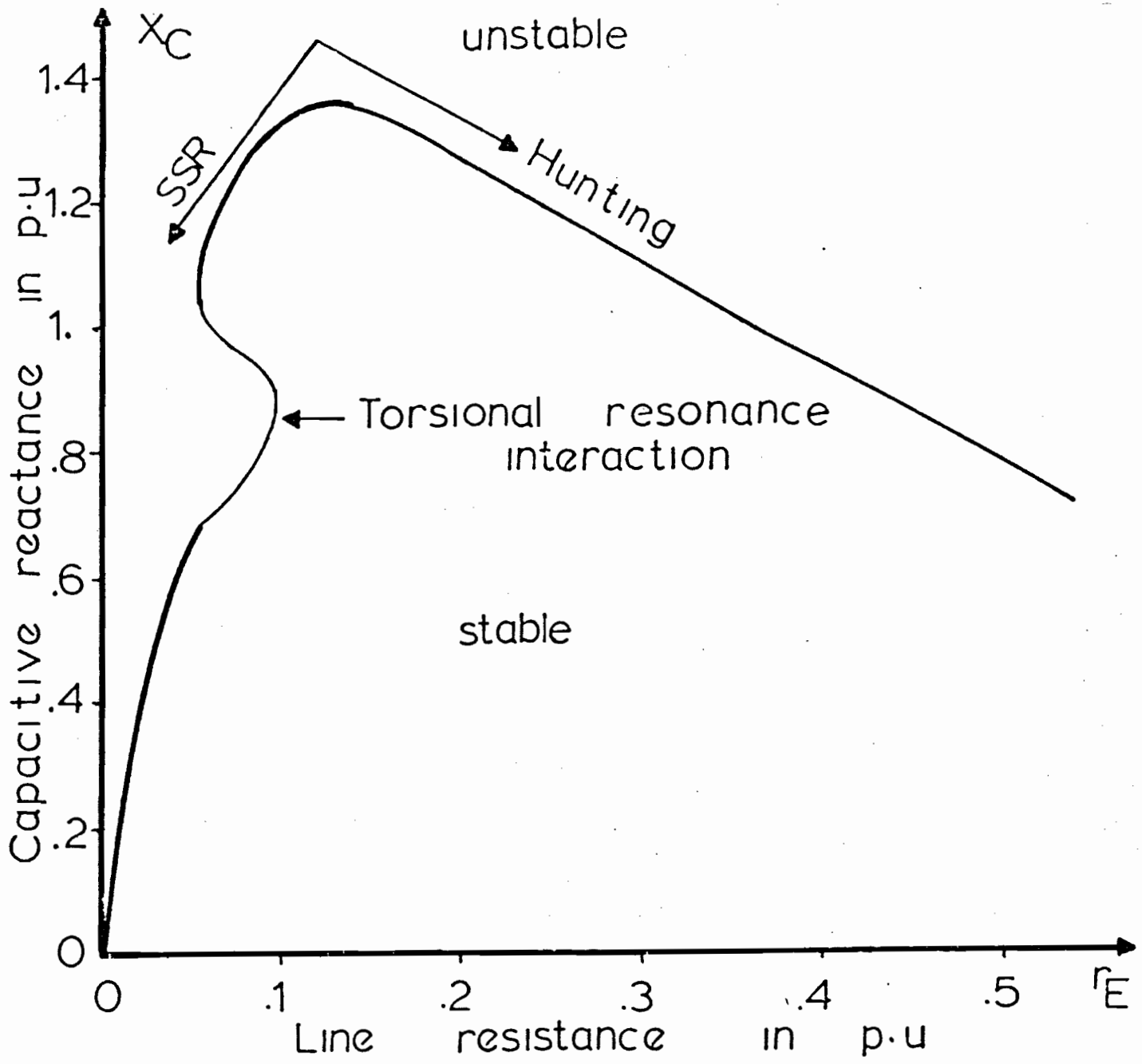

Figure 7.2. Stability boundary in the X_C - r_E plane of unregulated system showing the SSR, Hunting and the torsional resonance interaction instabilities.

7.4.3.1 Effect of Generator Inertia on Torsional Resonance Interaction

Figure 7.3 shows the stability boundary of the same system used in Section 7.4.2 but with the inertia constants switched around, i.e., H_G is now equal to 0.633s and H_T = 2.22s . The unstable region caused by the torsional resonance interaction is now larger than that in Figure 7.2. This was also noticed by [39]. The question is why this happens, and why for large range of X_C , still there is torsional resonance interaction.

The enlargement of the unstable region in Figure 7.3 can be explained as follows:

As the torsional resonance interactions have their origins from mechanical vibrations, it is useful to firstly consider the amplitudes of the torsional vibrations. For the case of Figure 7.2 in which H_G / H_T = 2.22 / 0.633, we know from Table 7.3 that $| \Delta \bar{\omega}_G |$ / $| \Delta \bar{\omega}_T |$ = 0.0104 / 0.0413 and $| \Delta \delta_G |$ / $| \Delta \delta_T |$ = 0.0406 / 0.1612 for the torsional mode λ_{tor} . We know also from Table 7.3, that the phase angles between the angular velocity and the angular displacement are approximately 180° apart showing that the two inertias are twisting the torsional shaft at either ends. However, as we reverse the inertia ratio so that H_G / H_T = 0.633 / 2.22 as is the case for Figure 7.3, we expect that $| \Delta \bar{\omega}_G |$ / $| \Delta \bar{\omega}_T |$ ≃ 0.0413 / 0.0104 and $| \Delta \delta_G |$ / $| \Delta \delta_T |$ ≃ 0.1612 / 0.0406 . Physically, this means that both the amplitude and the velocity of the generator shaft oscillations would have increased.

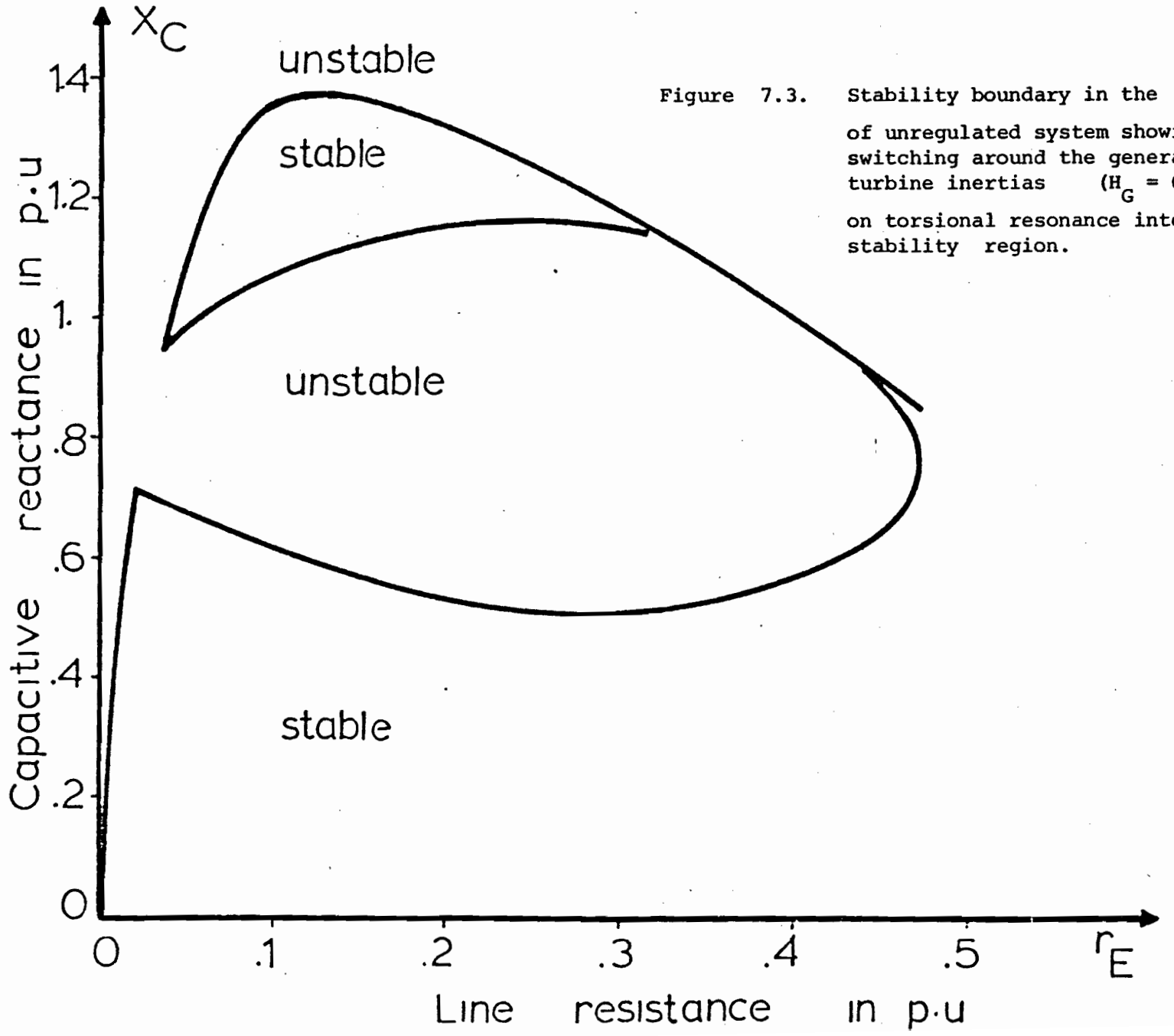

Figure 7.3. Stability boundary in the $X_C - r_E$ plane of unregulated system showing the effect of switching around the generator and the water turbine inertias ($H_G = 0.633$, $H_T = 2.22$) on torsional resonance interaction instability region.

Since the frequency of torsional resonance and the electrical system parameters remain the same, the induced electrical voltages and currents would likely to be so much the larger for the case in Figure 7.3 than for Figure 7.2 for each point in the $X_C - r_E$ plane. In consequence, the unstable indent enlarges in the r_E direction because the equivalent negative resistance associated with the induced voltage of the larger torsional oscillations would take a larger value of r_E to stabilize it.

The unstable indent also enlarges in the X_C direction. As we have indicated before, $X_C = 0.9$ p.u. represents the value in which the electrical circuit is tuned to resonate with the torsional resonance. As we move in the direction of X_C away from $X_C = 0.9$, we move away from the resonant frequency and effectively the electrical gain is diminished. But because the oscillation of the generator inertia is very large now, then,the degree of electrical detuning can be worse before the system passes from instability to stability.

7.4.4 Stability Boundary of Regulated System

In mapping out the stability boundary in the $X_C - r_E$ diagram, Reference [32] has disregarded the effects of the excitation system and the feedback loops in the synchronous generator. However, Reference [33] showed that the excitation system is not effective in improving the system stability boundary. It is of importance to study the

way the high response excitation system (HRE) and the power system stabilizer feedback alter the stability boundary. Will the indentation due to torsional resonance enlarge? This is a subject which (to the author's knowledge) has not been studied before.

Figure 7.4 shows the stability boundaries of the system of Figure 7.1 when the synchronous generator is unregulated and when it is equipped with the HRE excitation system and the PSS feedback loop. The abscissa is plotted with an expanded scale with the ordinate intersecting at r_E = 0.01 p.u. The stability boundary for the case of unregulated machine is plotted for the sake of comparison with the case of unregulated machine. The important point to note is the enlargement of the unstable indentation caused by the inclusion of the excitation system and the feedbacks. It was noticed that the terminal voltage feedback loop through the excitation system has little effect on the unstable region caused by the torsional resonance interaction while the PSS feedback loop does effect this unstable region.

7.4.4.1 Effect of PSS

Curves 2 and 3 in Figure 7.4 show the reduction of the unstable region caused by the torsional resonance interaction when the PSS gain K_p is reduced from 20 to 5. It is to be reminded that the input signal to the PSS is the generator rotor speed. The enlargement of the

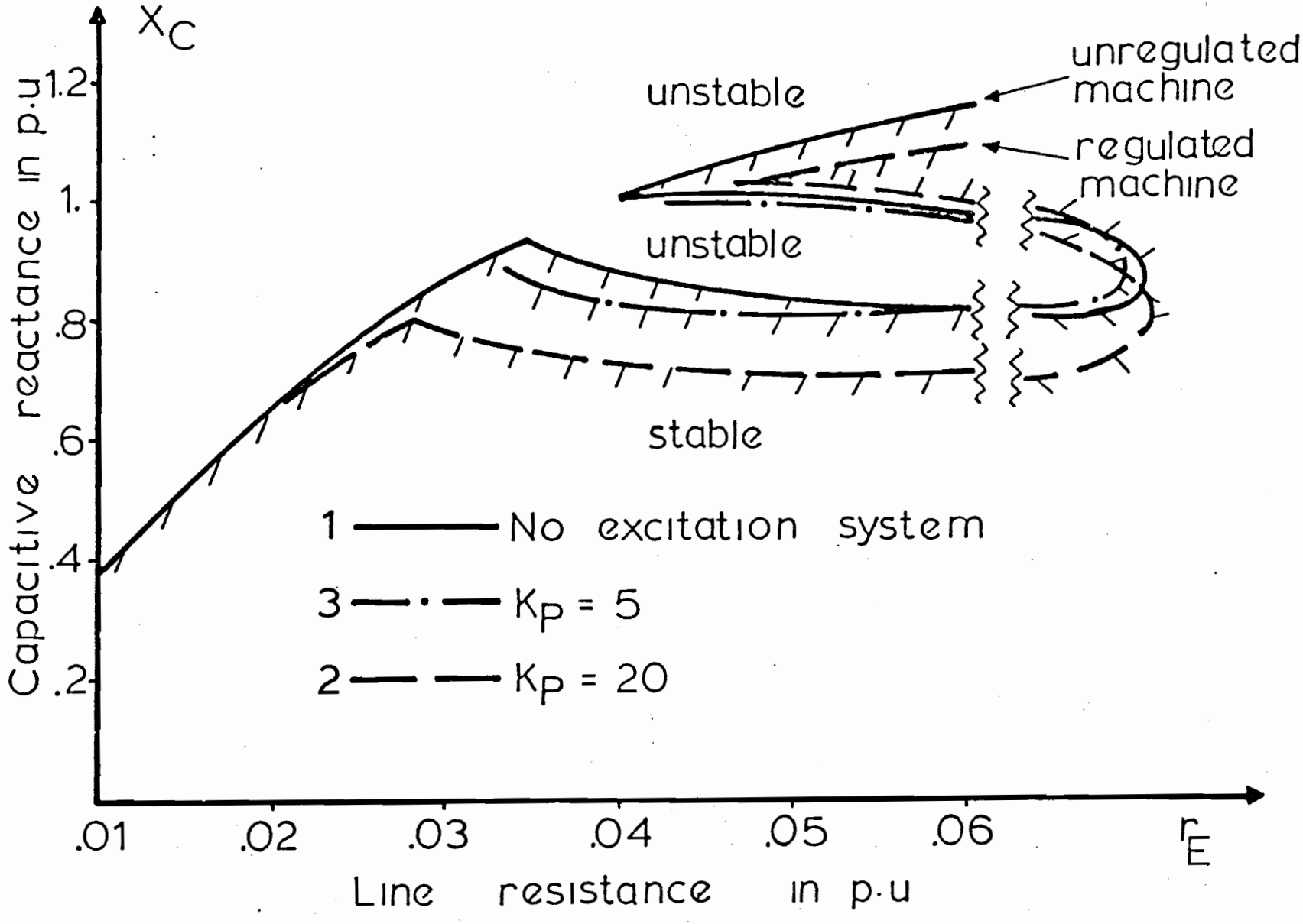

Figure 7.4. Stability boundary in the X_C - r_E plane of regulated and unregulated systems and showing the effect of the PSS gain K_P on the torsional resonance interaction in case of regulated system.

indentation caused by the torsional resonance interaction when $K_p = 20$ is explained as follows:

As the generator rotor oscillates at a resonant frequency f_m, the PSS input picks up this signal and transmits it through the excitation system to produce a rotor field current at that frequency. The field winding is physically rotating at synchronous speed, and the stator currents induced by this alternating field current component coming from the PSS loop, will have positive and negative sequence components at frequencies of $(60 - f_m)$ Hz and $(60 + f_m)$ Hz respectively.

Note that in Section 7.3, we have already argued that stator currents at these frequencies are already being produced by the dc currents of the field winding as the generator rotor oscillates about the synchronous speed at the torsional resonant frequency f_m. The interaction of the positive sequence components of the stator currents at $(60 - f_m)$ Hz are believed to produce the negative electromechanical damping which gives rise to instability of λ_{tor}.

It seems highly probable that the $(60 - f_m)$ Hz produced by the PSS feedback will contribute to aggravate the unstable region if they are phased so as to reinforce the torsional vibration effects. The solution consists of redesigning the PSS filter so that the $(60 - f_m)$ Hz stator current, which is produced by the PSS signal, cancels the stator current at the same frequency that is produced by the dc rotor field in

torsional vibration. However, the PSS has already the function of ensuring dynamic stability. A redesign of the PSS transfer function to satisfy dynamic stability and to suppress torsional resonance interaction is an interesting and challenging problem.

7.4.4.2 Effect of the NDS' Feedback Loop

Figure 7.5 shows the stability boundary for the system of Figure 7.1 where the NDS' feedback is included in the excitation system in addition to the voltage regulator feedback and the PSS feedback. Both the gain K'_{ND} and the control angle ϕ of the NDS' feedback turned out to have negligible influence on the size of the unstable indentation. However, the control angle ϕ does shift the position of the unstable region due to the torsional resonance interaction up and down along the X_C axis as is shown in Figure 7.5.

At this point, we abandon further attempts of controlling the λ_{tor} instability by the ΔP and ΔQ feedback through the NDS' filter. Two courses are open to us:

(a) redesigning of the PSS feedback,

(b) adopting the Power Blocking Filter ,

Figure 7.5. Stability boundary in the $X_C - r_E$ plane of the system with NDS' feedback showing the effect of the control angle ϕ on the torsional resonance interaction instability region.

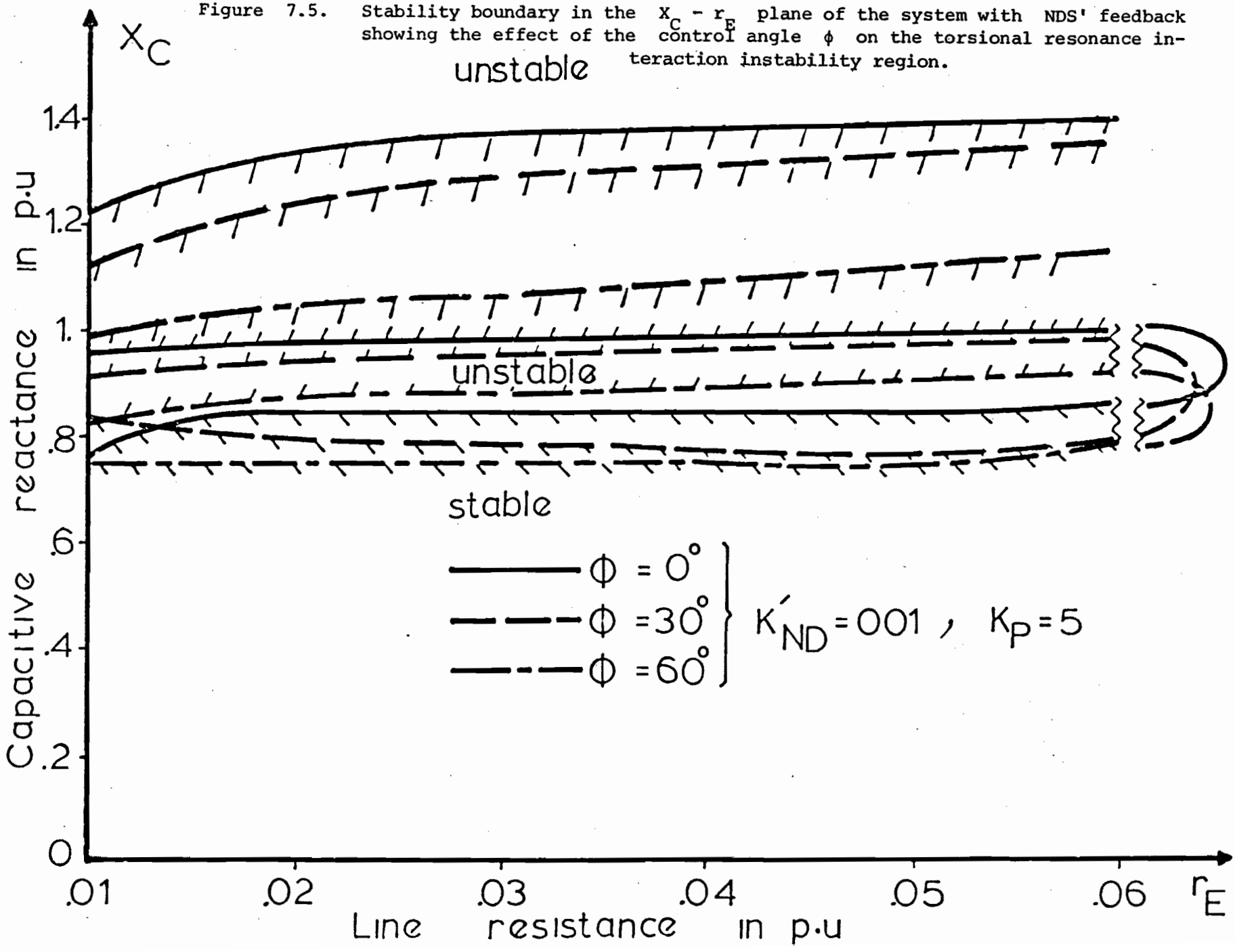

7.5 Power Blocking Filter

One of the proposed solutions [18, 36, 37, 38, 39] for the torsional resonance interaction instability is to install an L-C tank circuit in series with the generator as shown in Figure 7.6. The tank circuit of the filter is tuned to filter out the positive sequence current associated with the torsional resonance frequency $(60 - f_m)$. Reference [36] has used such filters for Navajo power station, but unfortunately there are no quantitative results reported to show its effectiveness in eliminating torsional resonance interaction under small and large disturbances. Therefore, the rest of this chapter is devoted to the evaluation of this filter for the hydro-system under small and large disturbances. To do this, the filter mathematical model and the parameter values should be derived.

7.5.1 Filter Parameter Values

The power blocking filter shown in Figure 7.6 has its resonant frequency f_r related to its inductance, capacitance and resistance, L_f, C_f and R_f respectively as follows:

$$f_r = \frac{1}{2\pi}\sqrt{\frac{1}{L_f C_f} - \frac{R_f^2}{L_f^2}} \text{ Hz} \qquad (7.5)$$

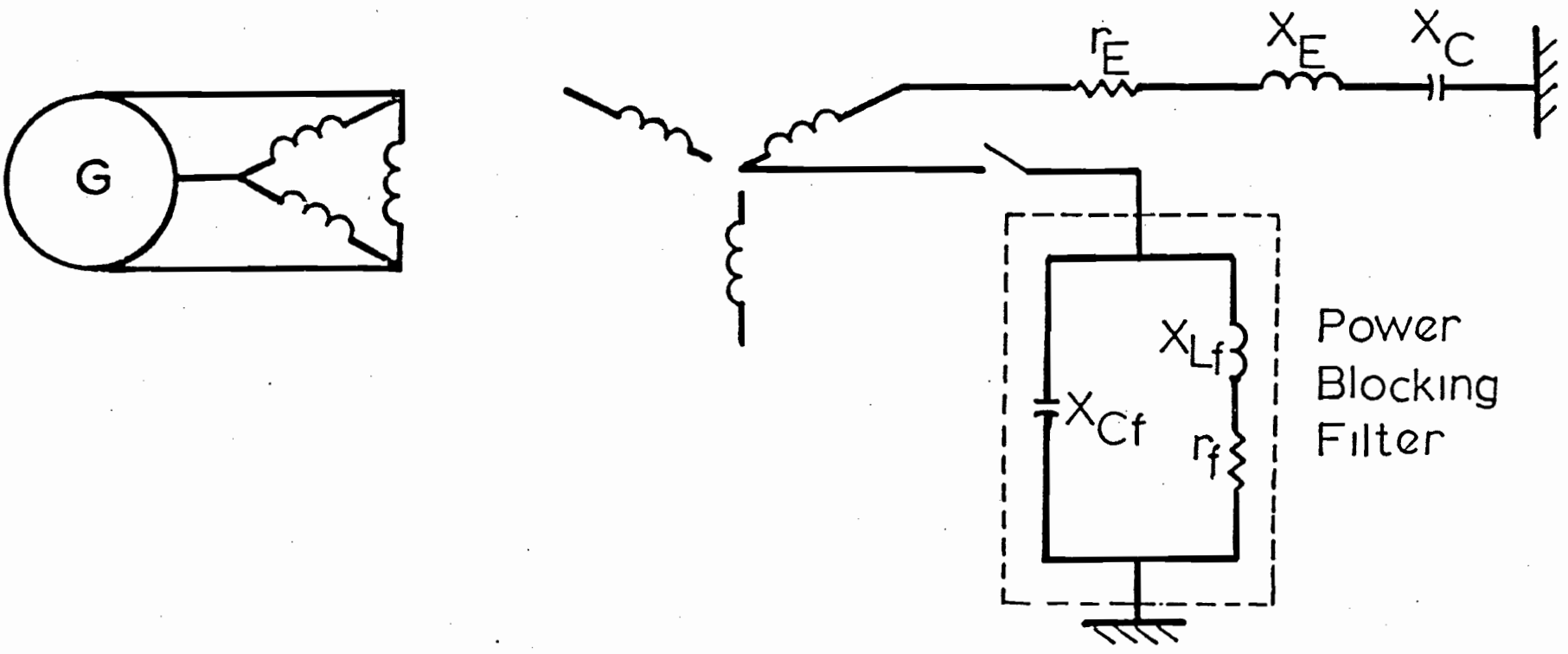

Figure 7.6. The connection of the power blocking filter required to remove the torsional resonance interaction.

where L_f in Henry, C_f in Farad and R_f in ohm,

or

$$\omega_r^2 = \frac{1}{L_f C_f} - \frac{R_f}{L_f^2} \tag{7.6}$$

in using p. u. values, $L_f = X_{Lf}$, $C_f = \frac{1}{X_{Cf}}$ and $R_f = r_f$

therefore :

$$\omega_r^{-2} = \frac{X_{Cf}}{X_{Lf}} - \frac{r_f}{X_{Lf}^2} \tag{7.7}$$

usually $X_{Lf}^2 >> r_f$ therefore:

$$\omega_r^{-2} \simeq \frac{X_{Cf}}{X_{Lf}} \tag{7.8}$$

This resonance frequency should be equal to the frequency of the oscillating current (f_n) produced by the rotor oscillation at a frequency of f_m:

$$\omega_r^{-2} = \omega_n^{-2} = (1 - f_m / 60)^2 \tag{7.9}$$

at this resonance frequency the filter impedance Z_r is:

$$Z_r \text{ (at } f_m) = \frac{X_{Lf} \cdot X_{Cf}}{r_f} \text{ in p.u.} \tag{7.10}$$

In the steady state operation, the filter impedance should not effect the

operating conditions specified before inserting the filter. At steady state, the filter per-unit impedance Z_f is:

$$Z_f \text{ (at 60 Hz)} = \frac{\frac{1}{j\,X_{Cf}}\,(r_f + j\,X_{Lf})}{r_f + j\,(X_{Lf} - X_{Cf})} \tag{7.11}$$

therefore,

$$Z_f << r_E + j\,(X_E - X_C) \tag{7.12}$$

For the hydro-system under consideration, the filter resonance frequency $\bar{\omega}_r$ is a 0.74 p.u. Substituting this value in equation 7.8, we obtain:

$$\sqrt{\frac{X_{Cf}}{X_{Lf}}} = 0.74 \tag{7.13}$$

By considering equations 7.13, 7.12, and 7.10 the filter parameters are chosen as follows:

$$X_{Cf} = 0.055 \text{ p.u.},$$

$$X_{Lf} = 0.1 \text{ p.u.},$$

$$r_f = 0.00033 \text{ p.u.}$$

The above design values have been adopted in the study.

The quality factor of the filter is 300 which is conservative and therefore, attainable by the manufacturer. Further, it adds a resistance of

416 Ω to the line resistance at the frequency of $f_0 - f_m$ which is in the range reported in [18] . The economic design depends on the cost trade-offs of their relative values. As no design values have been reported in the literature, this study will accept these values tentatively. In any case, the objective is to demonstrate the effectiveness of the power blocking filter in elimination of torsional resonance.

7.5.2 Filter Mathematical Model

The differential equations describing the blocking filter can be derived on the basis of the voltage drop across the line resistance, the inductance and the series capacitor which are defined in Section 2.7.2 in the D-Q synchronously rotating reference frame. Let us define the currents passing through the filter inductance i_{DLf} and i_{QLf} in the D and Q axes respectively as shown in Figure 7.7. Therefore, the currents passing through the filter capacitance i_{DCf} , i_{QCf} are:

$$i_{DCf} = i_D - i_{DLf} \tag{7.14}$$

$$i_{QCf} = i_Q - i_{QLf} \tag{7.15}$$

where i_D and i_Q are the line currents in the D-Q synchronously rotating reference frame. The voltage drops across the blocking filter capacitance e_{DCf} , e_{QCf} can be written in a similar way to that given in Section 2.7.2 as:

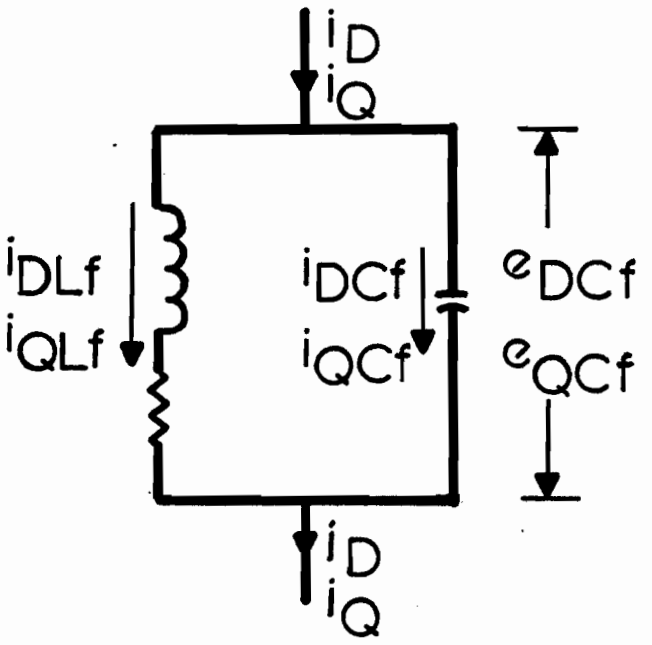

Figure 7.7. Circuit diagram of the power blocking filter.

$$e_{DCf} = -\frac{1}{\omega_0}\frac{d}{dt}e_{QCf} + X_{Cf}(i_Q - i_{QLf}) \tag{7.16}$$

$$e_{QCf} = \frac{1}{\omega_0}\frac{d}{dt}e_{DCf} - X_{Cf}(i_D - i_{DLf}) \tag{7.17}$$

The voltage drops across the blocking filter inductance and resistance e_{DLf}, e_{QLf}, e_{Drf}, e_{Qrf} respectively, can be related to e_{DCf} and e_{QCf} as:

$$e_{DCf} = e_{DLf} + e_{Drf} \tag{7.18}$$

$$e_{QCf} = e_{QLf} + e_{Qrf} \tag{7.19}$$

On the basis of Section 2.7.2 the expressions of e_{DLf}, e_{QLf}, e_{Drf}, e_{Qrf} are:

$$e_{DLf} = X_{Lf} \frac{1}{\omega_0} \frac{d}{dt} i_{DLf} - X_{Lf} i_{QLf} \tag{7.20}$$

$$e_{QLf} = X_{Lf} \frac{1}{\omega_0} \frac{d}{dt} i_{QLf} + X_{Lf} i_{DLf} \tag{7.21}$$

$$e_{Drf} = r_f i_{DLf} \tag{7.22}$$

$$e_{Qrf} = r_f i_{QLf} \tag{7.23}$$

The mathematical model of the power blocking filter suitable for numerical integration can be obtained from the combinations of equations 7.16 - 7.23 and it is written as:

$$\frac{d}{dt} \begin{bmatrix} e_{DCf} \\ e_{QCf} \\ i_{DLf} \\ i_{QLf} \end{bmatrix} = \omega_0 \begin{bmatrix} 0 & 1 & -X_{Cf} & 0 \\ -1 & 0 & 0 & -X_{Cf} \\ 1/X_{Lf} & 0 & -r_f/X_{Lf} & 1 \\ 0 & 1/X_{Lf} & -1 & -r_f/X_{Lf} \end{bmatrix} \begin{bmatrix} e_{DCf} \\ e_{QCf} \\ i_{DLf} \\ i_{QCf} \end{bmatrix}$$

$$+ \omega_0 \begin{bmatrix} X_{Cf} & 0 \\ 0 & X_{Cf} \\ 0 & 0 \\ 0 & 0 \end{bmatrix} \begin{bmatrix} i_D \\ i_Q \end{bmatrix} \tag{7.24}$$

Equation 7.24 will be used in the large perturbation study. However, the linearized model of equation 7.24 which will be used in the small perturbation study is:

$$\frac{d}{dt}\begin{bmatrix}\Delta e_{DCf}\\ \Delta e_{QCf}\\ \Delta i_{DLf}\\ \Delta i_{QLf}\end{bmatrix} = \omega_0 \begin{bmatrix}0 & 1 & -X_{Cf} & 0\\ -1 & 0 & 0 & -X_{Cf}\\ 1/X_{Lf} & 0 & -r_f/X_{Lf} & 1\\ 0 & 1/X_{Lf} & -1 & -r_f/X_{Lf}\end{bmatrix}\begin{bmatrix}\Delta e_{DCf}\\ \Delta e_{QCf}\\ \Delta i_{DLf}\\ \Delta i_{QLf}\end{bmatrix} + \omega_0 \begin{bmatrix}X_{Cf} & 0\\ 0 & X_{Cf}\\ 0 & 0\\ 0 & 0\end{bmatrix}\begin{bmatrix}\Delta i_D\\ \Delta i_Q\end{bmatrix} \qquad (7.25)$$

7.5.3 Results of Small Perturbation Study

Figure 7.8 shows the stability boundaries for the following systems:

Curve 1 the basic system with HRE and PSS systems.

Curve 2 the system of curve 1 with the blocking filter.

Curve 3 the system of curve 2 with the NDS' for $\phi = 0.0$.

Curve 4 the same system of curve 3, but $\phi = 30^{\circ}$.

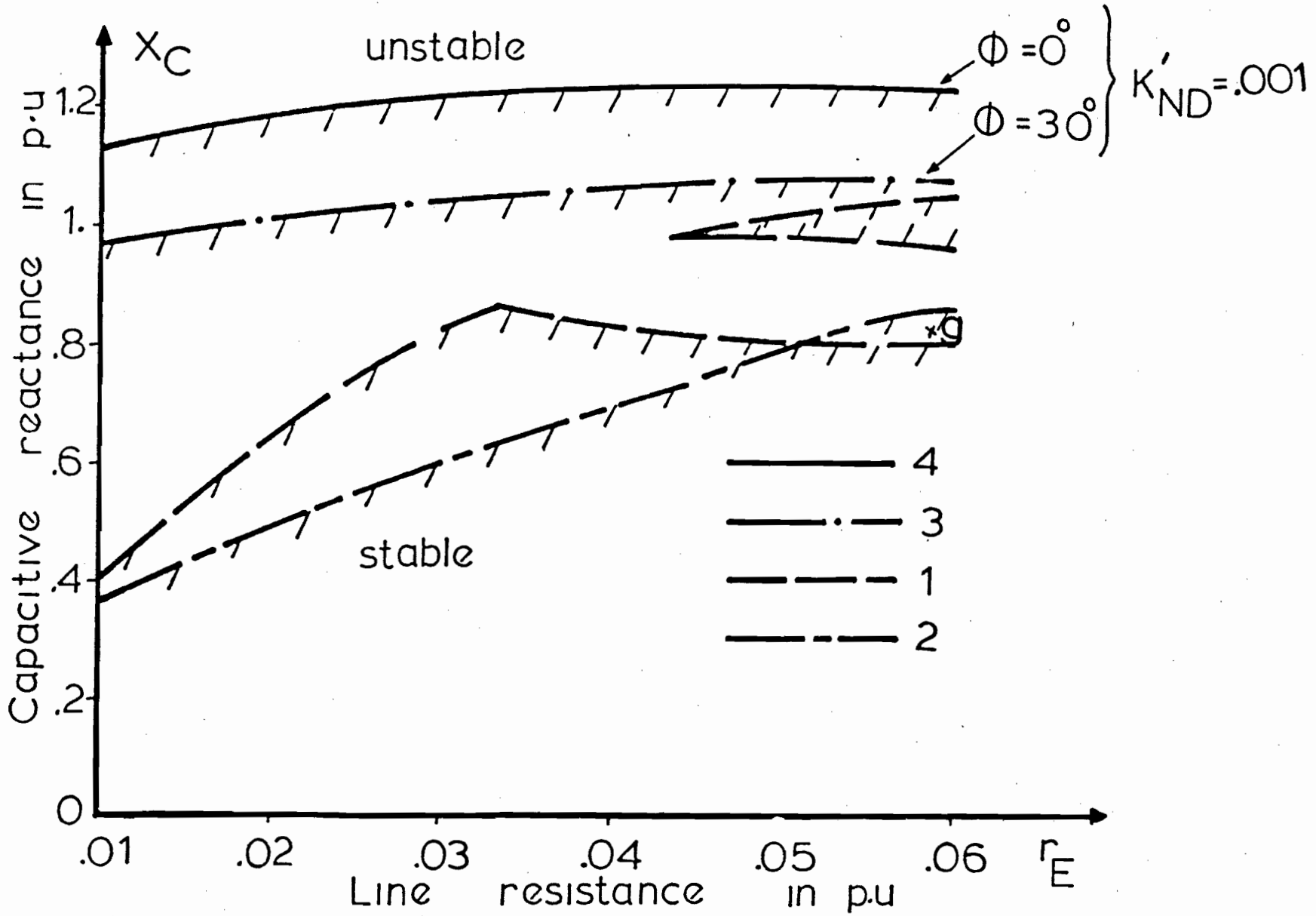

Figure 7.8. Stability boundary in the X_C - r_E plane of the system under torsional resonance (curve 1) and the effect of the power blocking filter in eliminating the torsional resonance interaction when added to the system as in Figure 7.6 (curve 2) and the effect of the NDS' in improving the stability region in the presence of the blocking filter (curves 3 and 4).

The blocking filter removes the torsional resonance interaction but lowers the stability boundary as it is clear from the comparison between curve 1 and curve 2. In addition, the blocking filter shifts the subsynchronous frequency, since at the steady state it adds to the series capacitive reactance X_C an amount of:

$$\Delta X_C = r_f^2 * X_{Cf} + (X_{Lf} * X_{Cf} * (X_{Lf} - X_{Cf})) / r_f^2 + (X_{Lf} - X_{Cf}^2)) \quad (7.26)$$

and to r_E an amount of:

$$\Delta r_E = r_f^2 * X_{Cf} / (r_f^2 + (X_{Lf} - X_{Cf})^2) \quad (7.27)$$

Curves 3 and 4 of Figure 7.8 show the effect of the NDS' feedback loop on the stability of the system associated with the power blocking filter. It is clear that the NDS' feedback and the blocking filter give a wide stability region in which the instability region due to the torsional resonance interaction is completely removed.

7.5.3.1 Effect of Filter Parameters

Figure 7.9 shows the stability boundary of the system with the blocking filter (curves b and c), but the blocking filter parameters are assumed to be:

Figure 7.9. Stability boundary in the $X_C - r_E$ plane for:
(a) The system under torsional resonance interaction.

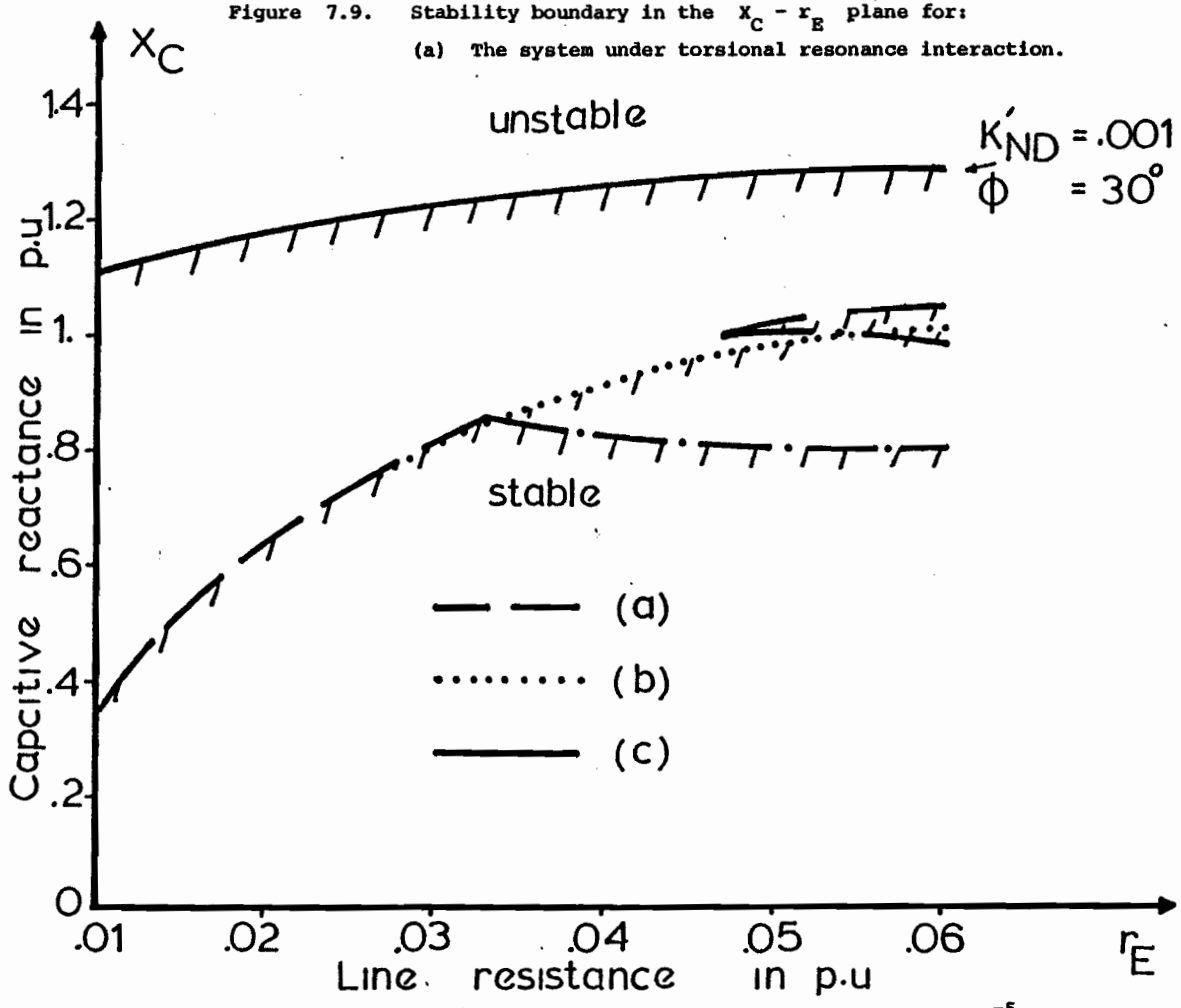

Figure 7.9. (b) When the blocking filter with parameters $r_f = 1 \times 10^{-5}$, $X_{Cf} = 0.0055$ p.u., $X_{Lf} = 0.01$ p.u., is added to the system.
(c) The effect of the NDS' in the presence of this filter.

r_f = 0.000001 p.u.,

X_{Cf} = 0.0055 p.u.,

X_{Lf} = 0.01 p.u.,

for these parameters the filter quality factor is high and the resistance, which the blocking filter adds to the circuit at its resonance frequency ω_n (see equation 7.10) is also high. Curve b in Figure 7.9 shows the stability boundary when the system of curve a (basic system + HRE + PSS) is incorporated with the blocking filter. This filter is effective in removing the indentation due to the torsional resonance with little change of the system stability boundary. The addition of the NDS' feedback loop to the system of curve b improves the stability region in which the system is protected against torsional resonance instability.

7.5.4 Results of Large Perturbation Study

In the previous section, the capability of the blocking filter was evaluated under small disturbances. Figure 7.8 shows the elimination of the torsional resonance interaction by this filter, and the improvement of the stability region by the NDS' feedback loop. For completeness, the blocking filter should be tested against large disturbances as well as the improvement by the NDS' feedback loop.

Figures 7.10 and 7.11 show the torque, the line current and the capacitor voltage time responses of the 10 GVA system incorporated with the blocking filter and the closed loop system with the blocking filter respectively. The source of disturbance is assumed to be the three-line-to-ground fault located at the receiving end for a period of 6 cycles. The steady state operating point is assumed to be point g on Figure 7.8 which has the coordinates of $X_C = .8$ and $r_E = .06$. It is to be reminded that at this point the system is unstable due to the torsional resonance interaction without the blocking filter and it is stabilized by the introduction of the blocking filter.

Figure 7.10 demonstrates the capability of the blocking filter of the design parameters derived in Section 7.5.1 in damping out the unstable oscillations resulting from the torsional resonance interaction. Figure 7.11 shows the additional damping produced by the NDS' feedback loop, which is apparent in the tail end of the oscillations. However, the effect of the NDS' feedback loop is small because of the regulator voltage ceiling limits which are considered in the above simulations.

7.6 Discussion of Results

From the analysis of the torsional resonance interaction, the following points are concluded:

(i) Torsional resonance interaction causes an indentation in the stable region in the $X_C - r_E$ plane.

(ii) At torsional resonance interaction, the torsional mode λ_{tor} goes unstable.

(iii) The NDS' feedback loop shifts the unstable region caused by the torsional resonance interaction but it does not remove this instability.

(iv) The Power Blocking filter is effective in eliminating the torsional resonance interaction instability as is demonstrated by the small and the large perturbation studies. Furthermore, the NDS' feedback gives an additional damping to the system during the torsional resonance interaction.

Figure 7.10. Torque (a), line current (b) and capacitor voltage (c) transients in the three-line-to-ground fault, when the power blocking filter (Figure 7.6) is added (system without NDS', Figure 6.1 for HRE, parameters $X_C = 0.8$, $r_E = 0.06$).

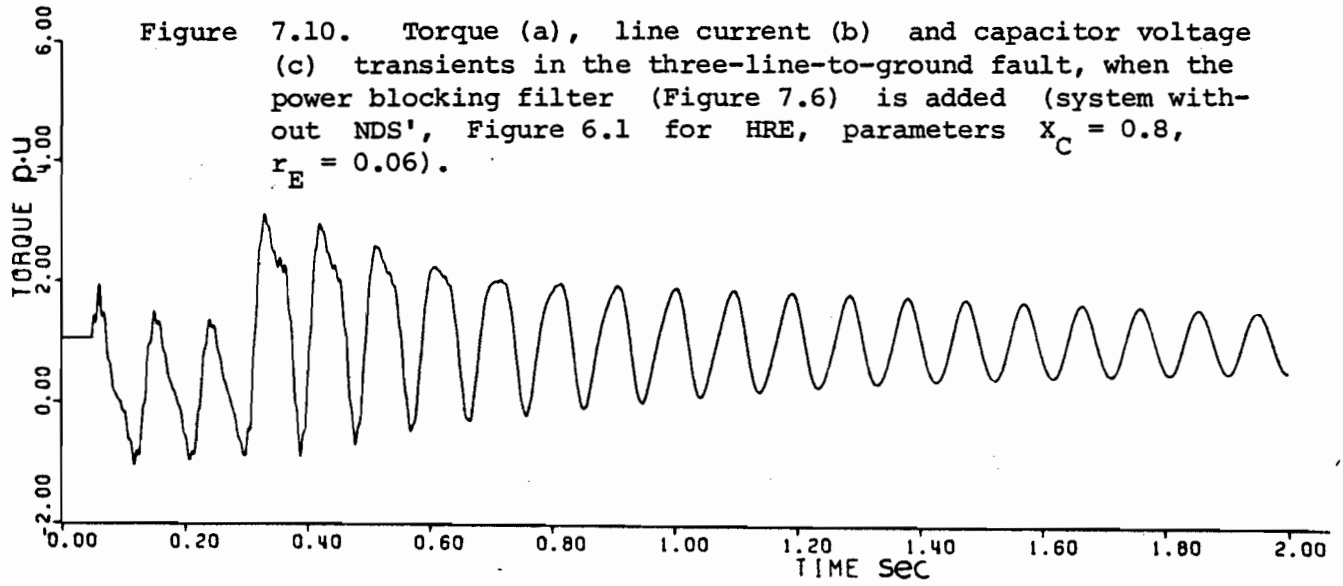

(a)

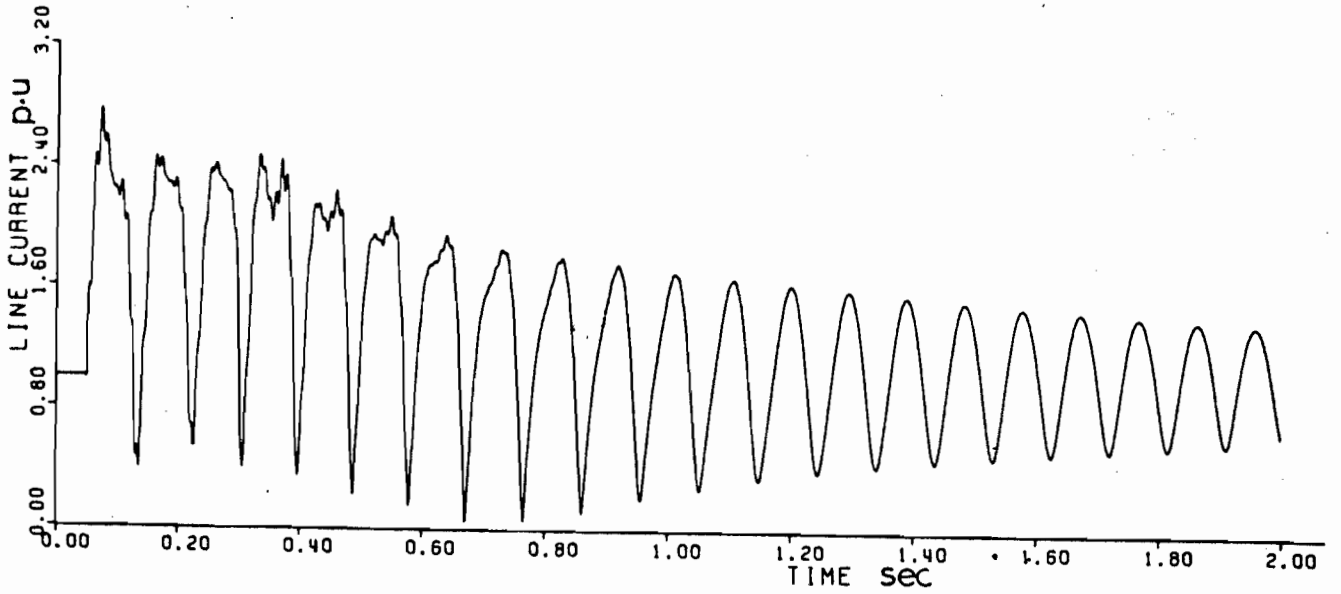

(b)

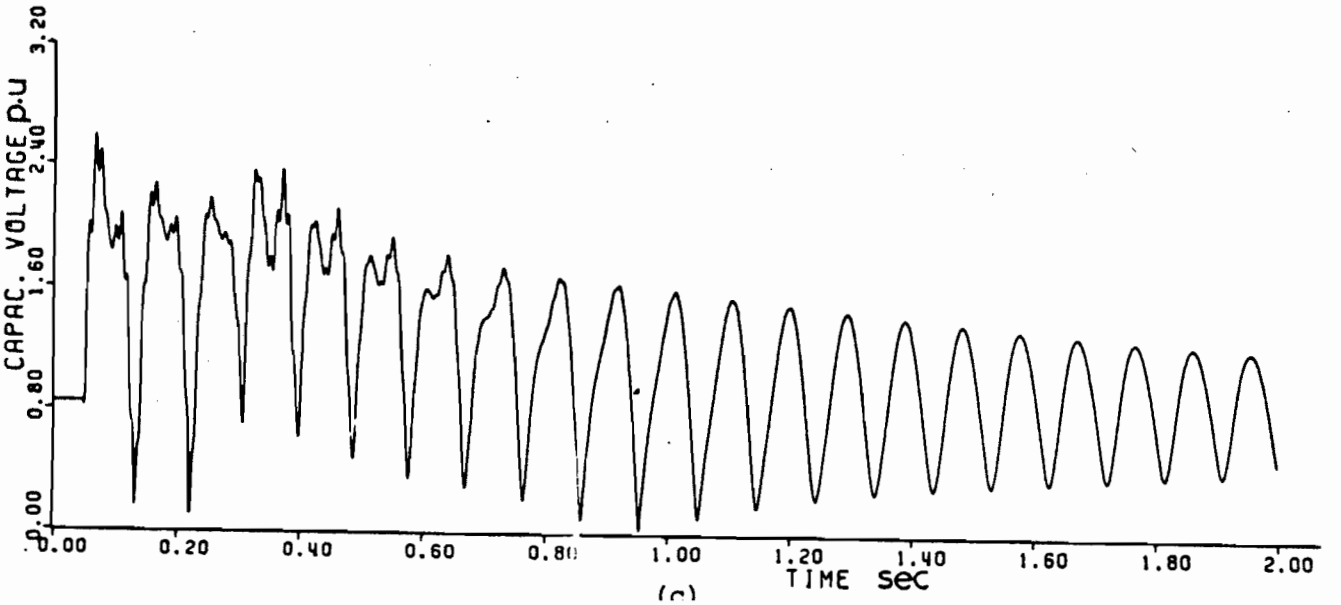

(c)

Figure 7.11. Torque (a), line current (b) and capacitor voltage (c) transients in the three-line-to-ground fault, when the power blocking filter (Figure 7.6) is added (system with NDS', parameters $X_C = 0.8$, $r_E = 0.06$).

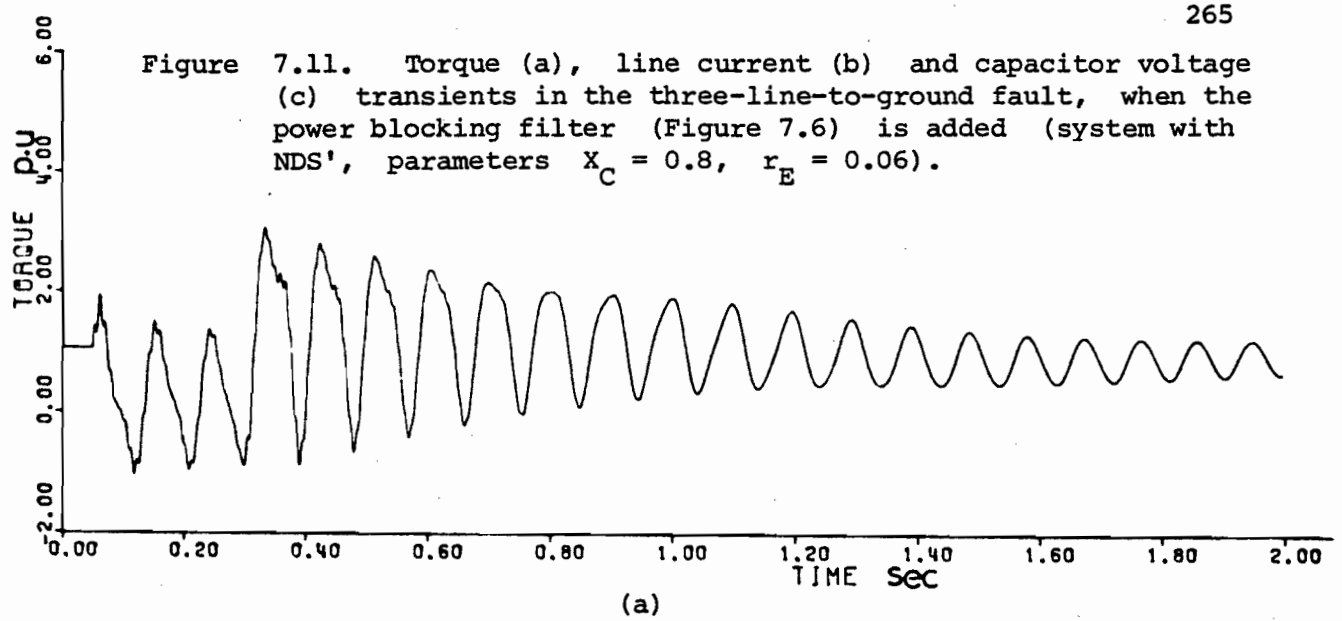

(a)

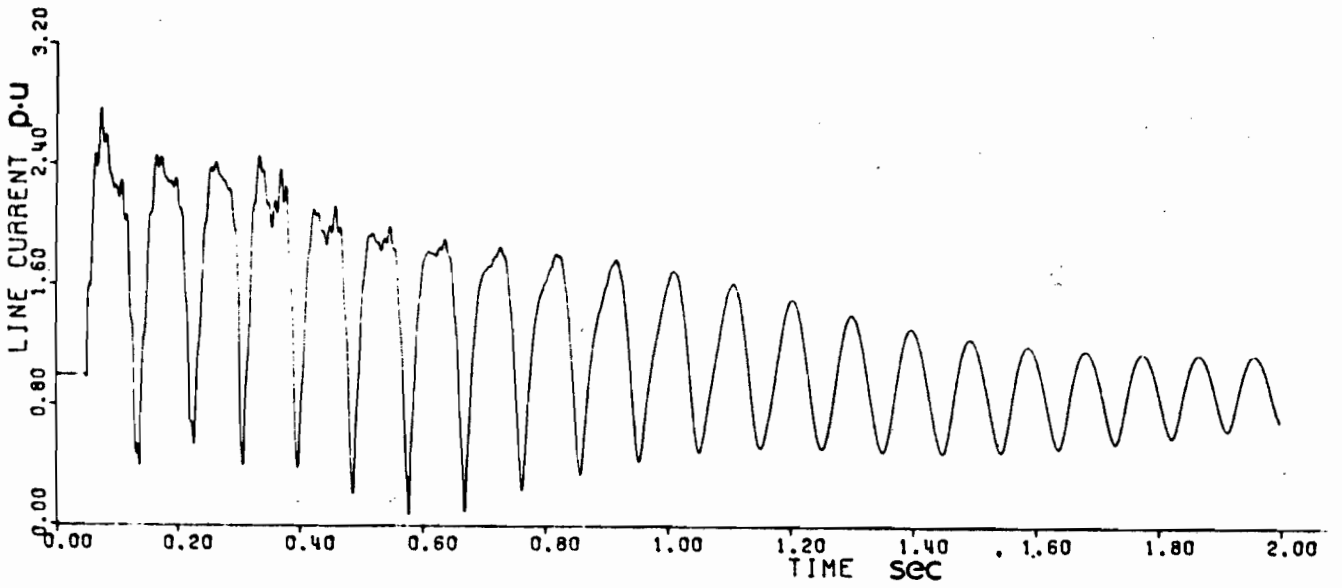

(b)

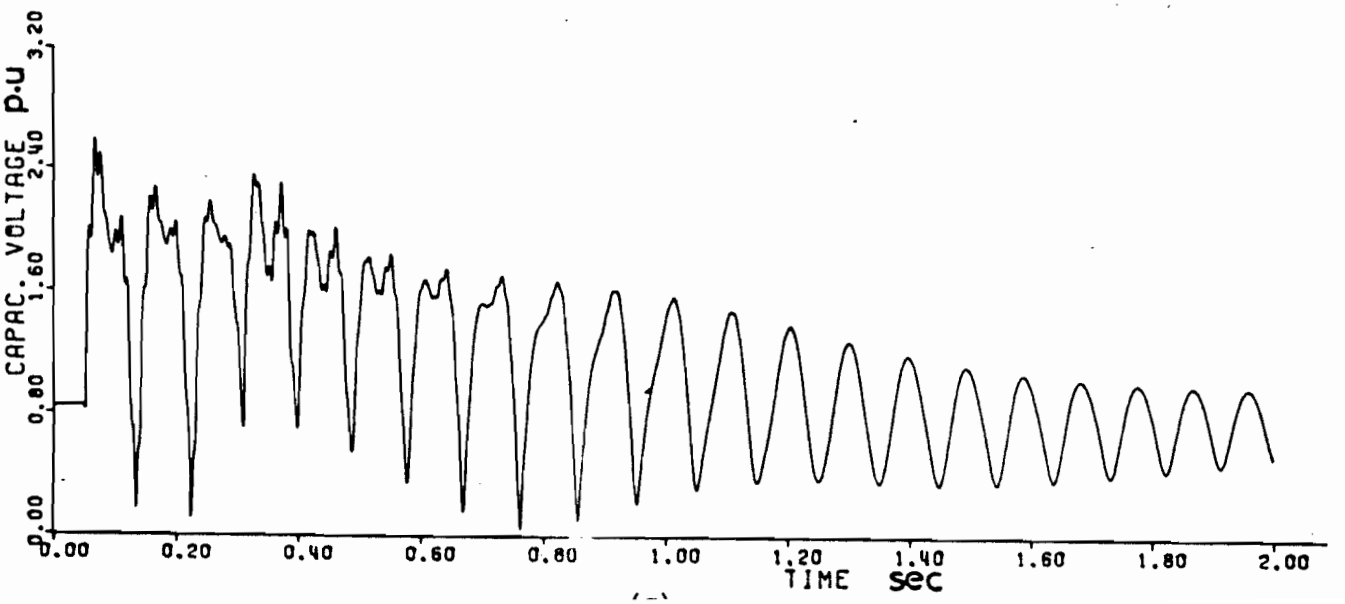

CHAPTER VIII

AVOIDANCE OF SSR PHENOMENON BY SHUNT COMPENSATION

8.1 Introduction

In the previous chapters, the main concern was the analysis and the determination of the power system stability as affected by the series capacitor compensation. It was mentioned before, that the series capacitor compensation is required in long transmission lines to increase the power transfer capability and to improve the transient stability. However, series capacitor compensation is not the only means to ensure the transient stability in the UHV transmission system when long transmission lines are used.

In this chapter, the possibility of avoiding subsynchronous resonance phenomenon is achieved by using shunt compensation [1] instead of series capacitor compensation. A synchronous capacitor connected to the middle of the transmission line is considered here as a means of shunt compensation.

The improvement of the steady state stability by shunt compensation is demonstrated by a numerical example. Since our objective in this chapter is to show that a system which is unstable in the steady state when connected to a long transmission line, can be stabilized by shunt compensation, then the eigenvalues are calculated only for two cases:

(a) A synchronous generator connected to an infinite bus through a long transmission line. In this case, such a system is unstable for high value of the line reactance.

(b) The above system with a synchronous capacitor connected to the middle of the transmission line. This system is stable for the same line reactance at which the system in item (a) is unstable.

As this is the penultimate chapter of this thesis, the purpose here is not to open up a new extensive area of investigation. Rather the objective is to close the subject of subsynchronous resonance by pointing out that the patchwork solutions of field excitation control, nonlinear resistor protection, power blocking filter would not be necessary if the transmission system does not give rise to the SSR problems in the first place. Shunt compensation is believed to avoid this SSR [1].

8.2 Basic Idea of Shunt Compensation

It is well known that if the machine rotor angle δ at which the electrical power is transmitted is approximately more than 90 electrical degrees (assuming all resistances are neglected and constant excitation system), then the system is unstable (see Figure 1.1). In the case where the system is shunt compensated, the above condition (when

$\delta > 90^{o}$) for system instability is not valid any more [1]. To explain this, Figure 8.1 (a) shows the voltage diagram where $|\tilde{E}_0| \angle 0$ and $|\tilde{E}_t| \angle \beta$ represent the voltage of the generator and the bus end of the transmission line whose impedance is z_E. The circumscribing circle shows that the voltages at the two terminals are kept at equal magnitudes. The closing side of the phasor triangle represents the voltage drop due to the current $\tilde{I}_t$ across the line reactance X_E (assuming $X_E >> r_E$). Clearly if β exceeds 90^{o} (constant terminal and infinite bus voltages) the system is unstable [68].

However, if we add a voltage support half way between the line, then the situation is shown by the vector diagram as shown in Figure 8.1 (b). Assuming the voltage support provided by a synchronous capacitor or a static compensation regulator, the voltage half way between is at a fixed magnitude $|\tilde{E}_{t1}| = |\tilde{E}_t| = |\tilde{E}_0|$, then the three bus voltages $|\tilde{E}_{t1}|$, $|\tilde{E}_t|$ and $|\tilde{E}_0|$ lie on the circumference of the same circle. The voltage drops across each half of the transmission line are now $(j \tilde{I}_1 X_E / 2)$, $(j \tilde{I}_2 X_E / 2)$. Note that during mechanical disturbances, the generator bus voltage $\tilde{E}_t$ swings against the voltage support bus $\tilde{E}_{t1}$ so that $(\beta - \beta_1)$ (the infinite bus is taken as a reference) between the generator and the voltage support is less than 90^{o} which means a stable system. In other words, the condition of instability of the system shown in Figure 8.3 is when the angle between two adjacent constant voltages exceeds 90 electrical degrees [69]

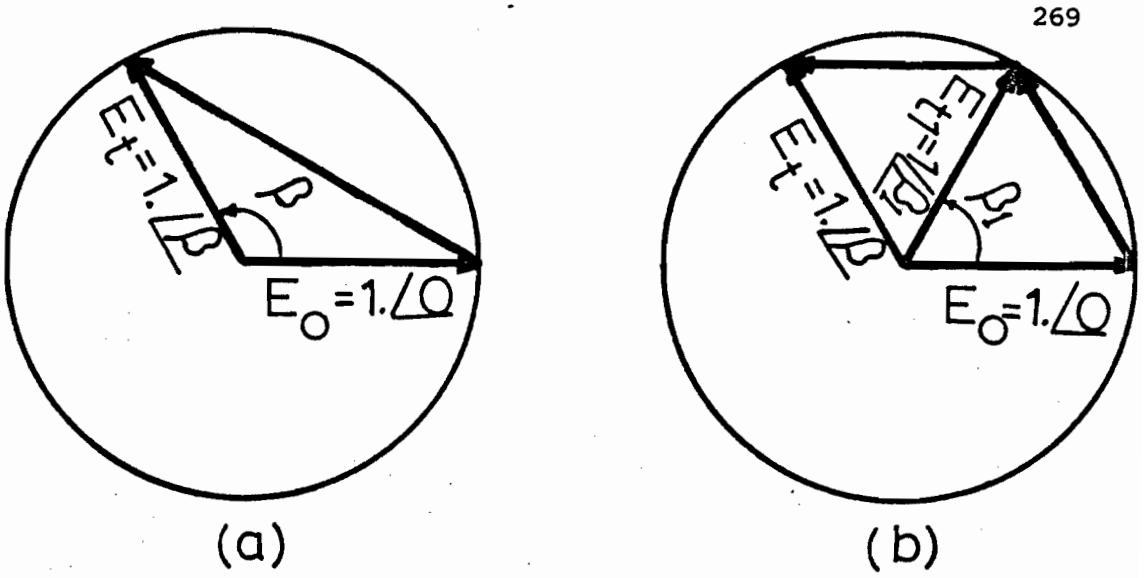

Figure 8.1. Effect of shunt compensation device on system stability.

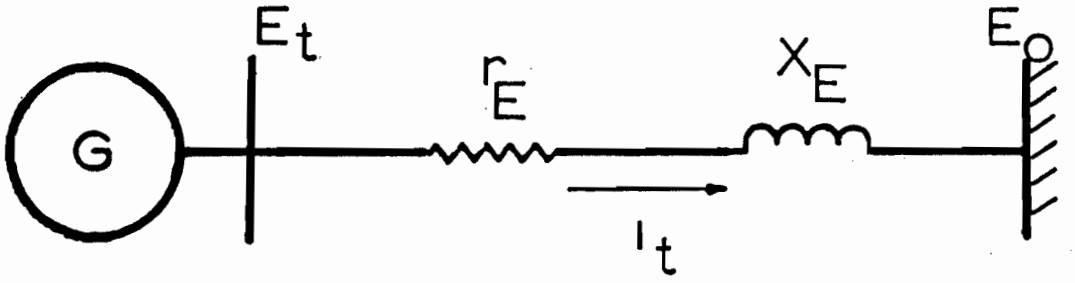

Figure 8.2. Single machine connected to an infinite bus through an uncompensated transmission line.

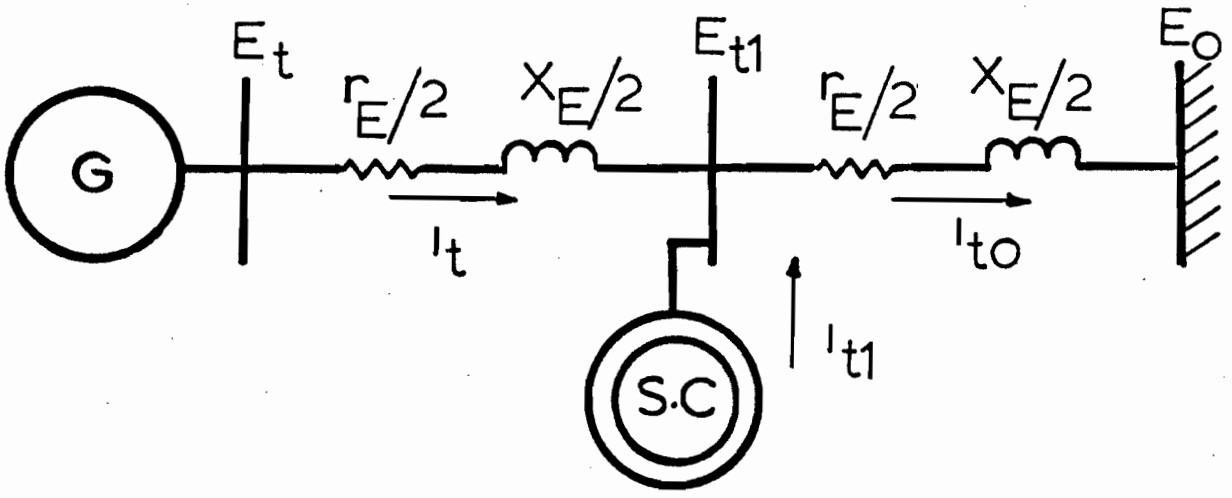

Figure 8.3. Synchronous capacitor connected to the middle of the transmission line.

As is evident in Figure 8.1 (b), the power angle between the transmitting voltage $\tilde{E}_t$ and the receiving end voltage $\tilde{E}_0$ is $\beta = 2\beta_1$ which can now exceed 90°. In this chapter, only one synchronous capacitor will provide voltage support at the midpoint of the transmission line. However, in principle any number of synchronous capacitors can be strung along at intermediate points of a very long line.

The question is whether there are any problems associated with the shunt compensation which might affect the system behaviour. In fact these are problems which differ from one voltage support equipment to another as it will be mentioned in the next section.

8.3 Methods of Shunt Compensation

The methods reported in the literature for controlling the voltage along the transmission line are [70]:

(i) linear reactors and linear capacitors [71],

(ii) synchronous capacitor [69, 72, 73, 74],

(iii) d.c. controller reactors [75],

(iv) thyristor controlled reactors [76, 77, 78],

(v) saturated reactors [79].

Linear reactors (inductors) are switched to the line, especially under light load to reduce the over voltages and to compensate for the line shunt reactive power [71]. The line inductors are either connected permanently to the line or switched in and out depending upon load conditions. Linear capacitors are connected to the line to supply reactive power when the line voltage is reduced. They are also used for power factor correction. The other four devices, which are now in use, support the voltage along the transmission line by absorbing or supplying reactive power since they have variable reactances.

The problems associated with the variable reactance devices (the last three devices) are the generation of time harmonics [79, 80]. The problem of a synchronous capacitor is believed to be the slow voltage response. However, the recent advancement in the excitation system technology which can produce faster response excitation system, has renewed the prospects of using the synchronous capacitor in shunt compensation.

8.4 Steady State Stability of Uncompensated System

It is well known in the literature [68] that the system which consists of a cylindrical synchronous generator connected to an infinite bus, is unstable if the generator terminal angle (β) with respect to the infinite bus exceeds 90 electrical degrees (assuming all resistances are neglected and constant terminal voltage).

Table 8.1 shows the eigenvalues of the system of Figure 8.2 for different values of the transmission line reactance X_E. The system under consideration is completely different from the one used in the previous chapters. The data of this system (Figures 8.2 and 8.3) are taken from a collaborating group of investigators [81] working on the analogue simulation of this system when it is shunt compensated by a synchronous capacitor. Therefore, the machine parameter and its regulating system are given in Appendices E-1 and E-2 respectively.

The calculation of the eigenvalues in Table 8.1 are for the regulated machine and the generator terminal steady state voltage $|\tilde{E}_t|$ is always unity. The infinite bus bar steady state voltage is always kept constant at $1.0 \angle 0.0$. In addition, the power delivered to the infinite bus bar is always unity.

The eigenvalues of Table 8.1 show that the system is stable when $X_E = 0.586$ p.u. and the steady state generator terminal angle $\beta = 36.3$. The more X_E is increased, the more β is increased until the system is unstable as shown from the eigenvalues of the mechanical mode in the third column of Table 8.1. The identification of the eigenvalues is followed from [47].

TABLE 8.1

EIGENVALUES OF THE SYSTEM SHOWN IN FIGURE 8.2 FOR DIFFERENT VALUES OF X_E.

(THE MAGNITUDES OF THE GENERATOR TERMINAL AND THE INFINITE BUS VOLTAGES ARE KEPT CONSTANT AT 1 p.u.)

	$X_E = 0.586$	$X_E = 0.85$	$X_E = 0.98$
Eigenvalues			
λ_{stator}	$-9.64 \pm j\,377.$	$-7.38 \pm j\,377.$	$-6.49 \pm j\,377.$
$\lambda_{amort.}$	-15.8 -10.6	-15.1 -6.53	-14.5 -5.13
$\lambda_{mech.}$	$-2.15 \pm j\,3.30$	$-0.0340 \pm j\,1.77$	$-2.30 + 4.70$
λ_{EXC}	-61.2 $-3.01 \pm j\,9.66$	-60.9 $-6.93 \pm j\,9.77$	-60.7 $-8.84 \pm j\,10.9$
λ_{field}	-0.685	-0.634	-0.735
Load PF (Leading)	0.94	0.840	0.700
β	36.3°	60.1°	89.0°

λ_{stator}: stator mode.

$\lambda_{amort.}$: amortisseur mode.

$\lambda_{mech.}$: mechanical mode.

λ_{EXC} : excitation mode.

λ_{field} : field mode.

P.F. : The infinite bus bar power factor. Leading pf means that the current flowing into the infinite bus is leading its voltage.

β : The steady state phase angle between the generator terminal voltage and the infinite bus voltage.

8.5 Effect of the Synchronous Capacitor

The results obtained in Table 8.1 demonstrate the difficulty in maintaining stability at large line inductive reactance or in long transmission lines when the power transmitted is kept constant at 1.0 p.u. However, by shunt compensation the system stability can be improved without decreasing the power transmitted.

Figure 8.3 shows the system of Figure 8.2 when it is shunt compensated by a synchronous capacitor. The synchronous capacitor is connected to the middle of the transmission line. The parameters and the excitation system of the synchronous capacitor are given in Appendices E-3 and E-4 respectively. The infinite bus bar steady state voltage and the power delivered are always assumed to be $1 \angle 0$ and 1.0 p.u. respectively. The magnitudes of the synchronous capacitor steady state terminal voltage and the generator steady state terminal voltage are always assumed to be unity.

8.5.1 Mathematical Formulation

The system under consideration is a multi-machine system as shown in Figure 8.3. The small perturbation study of this system requires a linearized mathematical model which describes the system behaviour when it is subjected to a small disturbance from its steady state operating

point. Undrill [82] has discussed the problem of multi-machine system in which he derived a mathematical model for two machines system. The idea behind the derivation [82] is to assume a common (D - Q) synchronously rotating reference frame for the bus system and the transmission network. The equations of each of the two synchronous machines are written for their respective local $d_1 - q_1$, $d_2 - q_2$ reference frames. The point to stress is that as each synchronous machine hunts during the electromechanical transients, each of the $d_1 - q_1$, $d_2 - q_2$ axes rock with respect to the synchronously rotating (D - Q) frame. This is because the $d_1 - q_1$, $d_2 - q_2$ axes are conceptually fixed to the rotors of the machine. The formal procedure to relate the electrical equations of the synchronous machines to the equations of the transmission system is through reference frame transformation.

For the system of Figure 8.3 the D - Q synchronously rotating reference frame will be used as the common frame, and the D axis of this frame coincides with the infinite bus bar voltage as shown in Figure 8.4. The transformation matrix which relates the quantities in the synchronous machine $d_1 - q_1$ and the synchronous capacitor $d_2 - q_2$ reference frames to the D - Q reference frame is:

$$\begin{bmatrix} e_{D1} \\ e_{Q1} \\ e_{D2} \\ e_{Q2} \end{bmatrix} = \begin{bmatrix} \cos\sigma_1 & -\sin\sigma_1 & 0 & 0 \\ \sin\sigma_1 & \cos\sigma_1 & 0 & 0 \\ 0 & 0 & \cos\sigma_2 & -\sin\sigma_2 \\ 0 & 0 & \sin\sigma_2 & \cos\sigma_2 \end{bmatrix} \begin{bmatrix} e_{d1} \\ e_{q1} \\ e_{d2} \\ e_{q2} \end{bmatrix} \tag{8.1}$$

and

$$\frac{d\,\sigma_1}{dt} = \omega_1 - \omega_0 \tag{8.2}$$

$$\frac{d\,\sigma_2}{dt} = \omega_2 - \omega_0 \tag{8.3}$$

where ω_1 and ω_2 are the synchronous generator rotor speed and the synchronous capacitor rotor speed in electrical r / s respectively.

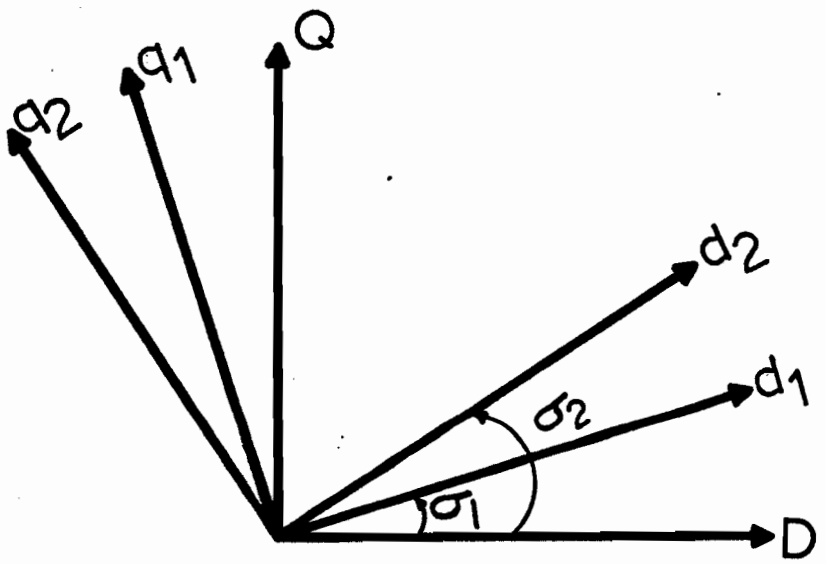

Figure 8.4. Relation between the $d_1 - q_1$, the $d_2 - q_2$ and the D - Q reference frames.

e_{D1} and e_{Q1} are the voltages in the D - Q axis at bus 1 .

e_{D2} and e_{Q2} are the voltages in the D - Q axis at bus 2 .

e_{d1} and e_{q1} are the synchronous generator terminal voltage in the $d_1 - q_1$ reference frame.

e_{d2} and e_{q2} are the synchronous capacitor terminal voltage in the $d_2 - q_2$ reference frame.

The linearized differential equations describing each machine are the same as equations 2.52, 2.53, 2.54 and 2.55 with the quantities in each of these equations written with suffix d_1, q_1 for the synchronous generator and d_2, q_2 for the synchronous capacitor, e.g., Δe_{d1} , Δe_{q1} instead of Δe_d , Δe_q for the synchronous generator. The differential equations describing the network of Figure 8.3 are usually written in the D - Q axis frame . These are derived in a similar way to that used in Section 2.7.2, and result in:

$$\begin{bmatrix} 1 & 0 & -1 & 0 \\ 0 & 1 & 0 & -1 \\ 0 & 0 & 1 & 0 \\ 0 & 0 & 0 & 1 \end{bmatrix} \begin{bmatrix} \Delta e_{D1} \\ \Delta e_{Q1} \\ \Delta e_{D2} \\ \Delta e_{Q2} \end{bmatrix} = \frac{1}{2\omega_o} \begin{bmatrix} X_E & 0 & 0 & 0 \\ 0 & X_E & 0 & 0 \\ X_E & 0 & X_E & 0 \\ 0 & X_E & 0 & X_E \end{bmatrix} \frac{d}{dt} \begin{bmatrix} \Delta i_{D1} \\ \Delta i_{Q1} \\ \Delta i_{D2} \\ \Delta i_{Q2} \end{bmatrix}$$

$$+ \frac{1}{2} \begin{bmatrix} r_E & -X_E & 0 & 0 \\ X_E & r_E & 0 & 0 \\ r_E & -X_E & r_E & -X_E \\ X_E & r_E & X_E & r_E \end{bmatrix} \begin{bmatrix} \Delta i_{D1} \\ \Delta i_{Q1} \\ \Delta i_{D2} \\ \Delta i_{Q2} \end{bmatrix} \qquad (8.4)$$

where i_{D1} , i_{Q1} are the D and Q axes currents injected from the generator into Bus 1 ,

i_{D2} , i_{Q2} are the D and Q axes currents injected from the synchronous capacitor into Bus 2 .

The linearized mathematical model describing the system of Figure 8.3 can be obtained by transforming the machine equations (equations 2.52, 2.53, 2.54, 2.55) to the D - Q axis frame using the linearized form of equation 8.2 which can be derived in a similar way to that used in deriving equation 2.59. The resultant model will consist of 14 first order differential equations describing the system of Figure 8.3 with unregulated machines.

When the machines are incorporated with excitation systems where the excitation system of the synchronous machine is shown in Appendix E-2 and that of the synchronous capacitor is shown in Appendix E-4, the system has 19 state variables and the differential equations describing each excitation system can be obtained on the basis of equation B-2.4 in Appendix B-2. However, it is to be reminded that the governor system of the synchronous generator is neglected and there is no governor system for the synchronous capacitor since it has no mechanical input.

8.5.2 Results

Table 8.2(a) shows the eigenvalues of the system of Figure 8.3 for different values of the transmission line reactance X_E and when the synchronous machines are regulated. The calculations are carried out under the assumption that the infinite bus bar has a unity voltage, i.e., $1 \angle 0$ and the power delivered is 1 p.u. In addition, the magnitudes of the voltages of the synchronous capacitor and the generator terminals are fixed to unity with unknown phase angles relative to the infinite bus. The other constraint on the system is that there is no power delivered to the synchronous capacitor.

The eigenvalues in the first three columns of Table 8.2(a) are calculated for the same line reactances which are used in Table 8.1. By comparing the results obtained in Table 8.2(a) with those in Table 8.1, the following points are concluded:

(i) In case of shunt compensation (Figure 8.3) the system is stable at high values of the line reactance X_E. In contrast, the system of Figure 8.2 is unstable at $X_E = 0.98$ p.u.

(ii) With shunt compensation, the synchronous generator synchronizing torque is improved and this is apparent from the imaginary part of the mechanical mode λ_{mech} in Table 8.2(a). This is because the line reactance X_E viewed by the generator is half, in case of shunt compensation (Figure 8.3), of that in case of Figure 8.2 (without shunt compensation).

(iii) The system of Figure 8.3 is stable, although the phase angle between the generator terminal and the infinite bus β is more than 90° as shown in the last column of Table 8.2(b).

(iv) The synchronous capacitor divides the phase angle between the generator and the infinite bus into approximately half. This is clear from the comparison of the angle β in Table 8.1 and β , β_1 in Table 8.2(b).

(v) The synchronous capacitor improves the power factor for the same line reactance and power transmitted. This is demonstrated from the load power factors in Tables 8.1 and 8.2(b).

8.6 Conclusion

The numerical results obtained in Tables 8.1 and 8.2 show that it is possible to improve the system steady state stability by shunt compensation. In addition, it is clear from Table 8.2 that the shunt compensated system is stable at high values of line reactance (X_E = 1.6 p.u.).

From this chapter, one can see that the system stability can be maintained in long-line transmission without risking the SSR problem. This is possible by substituting the series compensation by shunt compensation.

As the subject of shunt compensation is still in its infancy, it is still too early to judge whether shunt compensation will supercede series capacitor compensation. Further, experience in the field may reveal unsuspected pitfalls arising from shunt compensation. However, a detail study which takes into consideration the economical aspects over the series capacitor compensation, is required.

TABLE 8.2(a)

EIGENVALUES OF THE SYSTEM OF FIGURE 8.3 FOR DIFFERENT VALUES OF X_E .

(THE MAGNITUDES OF THE GENERATOR TERMINAL, THE SYNCHRONOUS CAPACITOR TERMINAL AND THE INFINITE BUS VOLTAGES ARE KEPT CONSTANTS AT 1.0 p.u.)

		$X_E = 0.586$	$X_E = 0.850$	$X_E = 0.980$	$X_E = 1.60$	
Synchronous Generator Eigenvalues	λ_{stator}	$-10.3 \pm j\,377.$	$-7.63 \pm j\,377.$	$-6.78 \pm j\,377.$	$-4.33 \pm j\,377.$	λ_{stator} : stator mode
	$\lambda_{amort.}$	$-16.3 \pm j\,2.4$	$-14.3 \pm j\,1.85$	$-13.5 \pm j\,1.18$	$-14.9 \quad -7.2$	λ_{amort} : amortisseur mode
	λ_{EXC}	$-61.4 \quad -1.72 \pm j\,2.43$	$-61.0 \quad -1.96 \pm j\,2.81$	$-60.6 \quad -1.97 \pm j\,3.15$	$-55.5 \quad -5.23 \pm j\,8.1$	λ_{EXC} : excitation mode
	λ_{field}	$-.672$	$-.679$	$-.680$	$-.672$	λ_{field} : field mode
Synchronous Capacitor Eigenvalues	λ_{stator}	$-6.94 \pm j\,377.$	$-6.04 \pm j\,377.$	$-5.68 \pm j\,377.$	$-4.51 \pm j\,377.$	
	$\lambda_{amort.}$	$-126. \quad -73.1$	$-126. \quad -66.8$	$-126. \quad -64.7$	$-126. \quad -61.7$	
	λ_{EXC}	$-28.7 \pm j\,54.9$	$-27.6 \pm j\,59.6$	$-27.0 \pm j\,61.3$	$-24.6 \pm j\,66.9$	

TABLE 8.2(a) (cont'd)

	X_E = 0.586	X_E = 0.850	X_E = 0.980	X_E = 1.60
λ_{field}	- 3.30	- 3.37	- 3.38	- 3.43
$\lambda_{mech.}$	- .900 ± j 8.44	- 1.40 ± j 7.6	- 1.79 ± j 7.21	- .463 ± j 3.0
	- 1.29 ± j 11.96	- 1.5 ± j 11.4	- 1.52 ± j 11.0	- .94 ± j 9.43

TABLE 8.2 (b)

STEADY STATE VALUES OF THE SYSTEM OF FIGURE 8.3

	X_E = .586	X_E = 0.85	X_E = 0.98	X_E = 1.6
Load PF (Leading)	.984	.97	.962	.887
β	34.4	47.5	55.0	107
β_1	17.2	25.0	29.	54.

β : Generator steady state terminal voltage angle relative to the infinite bus.

β_1 : Synchronous capacitor steady state terminal voltage angle relative to the infinite bus.

PF : Load power factor (at the infinite bus) and when it is leading means that $\tilde{I}_{t0}$ is leading $\tilde{E}_0$.

CHAPTER IX

SUMMARY AND CONCLUSIONS

9.1 Summary

This study has dealt with the problem of SSR suppression in series capacitor compensated lines. This thesis has been organized as a systematic attack based on first understanding the principle of field current control of the SSR phenomenon in the basic system consisting of a synchronous generator supplying a load through a series capacitor compensated transmission line. After this understanding, a feedback strategy has been proposed. The feedback scheme uses a combination of ΔP and ΔQ signals which pass through an NDS' filter before being inputted to the excitation system. The basic system is increased in complexity by adding mathematical models of the voltage regulator and the power system stabilizer (PSS) feedback. The study is oriented towards ensuring that the excitation system can take on the additional duty of SSR suppression without impairing its normal voltage regulation and fast stabilization functions. Numerical analyses show that the SSR mode can be stabilized against small perturbation, but because of the voltage ceilings in the excitation system, large SSR instabilities which follow line-to-ground faults or synchronization-out-of-phase cannot be suppressed by the field excitation feedback. In order to suppress large perturbation SSR instabilities, a nonlinear resistor protection scheme connected across the compensating capacitors has been tested and has been shown to

be successful. However, because all voltages below the spark-over limit in the nonlinear resistor system lie in the dead-band, it has been shown that the system would limit cycle unless the field excitation feedback is also present to suppress the small perturbation instability. Next, the system complexity is augmented one step further by modelling the generator shaft system as distributed inertias connected by torsional springs. It has been shown that in addition to the SSR mode, the torsional resonant interactional mode is added. It is found that the ΔP and ΔQ feedback cannot suppress the torsional mode instability. In consequence, the power blocking filter is added to the system and this has been found to be effective.

Finally, in the philosophy that prevention is better than cure, a complete different approach based on avoidance of SSR rather than suppression has been touched on. This has been demonstrated by a modest study based on shunt compensation using a single synchronous capacitor to provide voltage support at an intermediate point of a long transmission line.

9.2 Conclusion

The conclusions listed below include the outcome of this study which are felt to be of particular significance and are believed to be extensions to the knowledge of the subsynchronous resonance.

(i) A definitive theory of field excitation control of SSR has been presented. Field excitation control of unstable SSR oscillation is achieved by making an electromechanical motoring process dominate over the induction generation process (see Section 3.4). The properties of the control signal necessary for this matter are given (Section 3.5.1) [84].

A combination of ΔP and ΔQ as the control signal is found to be superior to the other control signals. The numerical results obtained in Chapter IV and the experimental results reported in [17] give strong support to this theory.

(ii) The study showed that the machine excitation system can take on an additional function of suppressing the unstable SSR oscillations. The NDS' feedback with ΔP and ΔQ as the control signal is effective in stabilizing the SSR mode without impairing the basic functions of the machine excitation system.

The power system stabilizer loop which takes the shaft speed as its input signal, does interact with ΔP and ΔQ loop. This interaction can cause the PSS mode to go unstable (see Section 5.7). The PSS interaction has been found to put an upper limit to the improvement of the SSR damping mode [85].

(iii) It is found that the voltage ceiling limits in the excitation system prevents the NDS' feedback scheme from suppressing the large unstable SSR oscillation (see Section 6.5.1.2) [86]. Because of the voltage ceiling limitations, it was shown that the nonlinear resistor protection and the NDS' feedback schemes are both necessary for damping the large unstable SSR oscillations (see Section 6.7) [86]. Since the nonlinear resistor protection scheme is good for large perturbations and the NDS' scheme damps out the small perturbations, then their combination will ensure stable operation under any disturbance.

(iv) When testing the NDS' scheme against the torsional resonance interaction instability, it is found that this scheme is not effective. However, the NDS' scheme shifts the unstable region caused by the torsional resonance interaction (see Section 7.4.4.2) [87].

However, the shaft speed loop through the PSS is shown to effect the torsional resonance interaction. Therefore, a proper design of the PSS may help in eliminating torsional resonance instability (see Section 7.4.4.1).

The above instability is effectively removed under small and large disturbances by installing a power blocking filter in series

with the generator. This filter should be tuned to the frequency of oscillation of the SSR currents produced by this interaction (see Sections 7.5.3 and 7.5.4) [87].

(v) Steady state stability and power transmission capability of a system where long transmission lines are used, are improved by shunt compensation. The preliminary study presented in Chapter VIII which considered only one shunt compensation device, promises the possibility of having better improvement of system stability by connecting more than one shunt compensation device along the transmission line.

As a by-product of this study, it was shown [86] that the synchronization-out-of-phase torque characteristic of the series capacitor compensated system takes the same shape as for an uncompensated system when its line inductive reactance is reduced.

9.3 Suggestions for Future Work

(1) A theoretical basis for the design of the NDS' feedback loop based on knowing the system modes.

(2) A redesign of the PSS to reduce the interaction with the SSR mode and to eliminate the instability region caused by the torsional resonance interaction.

(3) Since the system topological network changes under load and fault conditions, it is very interesting to study the possibility of stabilizing the system over a wide range of subsynchronous frequencies.

(4) Shunt compensation is a new area of investigation. The economical aspects of it and its theoretical analysis are new topics of research.

APPENDIX A-1

abc TO odq TRANSFORMATION

In general, the transformation from the abc stationary reference frame to the odq reference frame can be written in terms of the transformation matrix $[C_{odq}^{abc}]$ as follows:

$$\underline{i}_{odq} = [C_{odq}^{abc}]\, \underline{i}_{abc} \tag{A-1.1}$$

The voltage and flux relations between the two frames can be obtained from (A-1.1) by using e, ψ instead of i, and since $[C_{odq}^{abc}]$ is the only transformation matrix used in the current derivations, it will be used as [C] .

Park used the following transformation:

$$\begin{bmatrix} i_o \\ i_d \\ i_q \end{bmatrix} = \frac{2}{3} \begin{bmatrix} 1/2 & 1/2 & 1/2 \\ \cos\theta & \cos(\theta - 120) & \cos(\theta + 120) \\ -\sin\theta & -\sin(\theta - 120) & -\sin(\theta + 120) \end{bmatrix} \begin{bmatrix} i_a \\ i_b \\ i_c \end{bmatrix} \tag{A-1.2}$$

The above transformation is not power invariant, i.e., the transformation matrix in equation (A-1.2) does not satisfy the following equation,

$$[C]^{-1} = [C]^{T} \tag{A-1.3}$$

Note, power invariant is the same as orthogonal. Modern theories on transformation from the abc frame to the odq frame have used the orthogonal form given by,

$$\begin{bmatrix} i_o \\ i_d \\ i_q \end{bmatrix} = \sqrt{\frac{2}{3}} \begin{bmatrix} 1/\sqrt{2} & 1/\sqrt{2} & 1/\sqrt{2} \\ \cos\theta & \cos(\theta - 120) & \cos(\theta + 120) \\ -\sin\theta & -\sin(\theta - 120) & -\sin(\theta + 120) \end{bmatrix} \begin{bmatrix} i_a \\ i_b \\ i_c \end{bmatrix} \quad \text{(A-1.4)}$$

The two forms of transformation given in equations (A-1.3) and (A-1.4) can be written in a general form necessary for further analysis as,

$$\underline{i}_{odq} = K_3 \begin{bmatrix} K_4 & K_4 & K_4 \\ \cos\theta & \cos(\theta - 120) & \cos(\theta + 120) \\ -\sin\theta & -\sin(\theta - 120) & -\sin(\theta + 120) \end{bmatrix} \underline{i}_{abc} \quad \text{(A-1.5)}$$

The transformation matrix [C] is defined as,

$$[C] = K_3 [W] = K_3 \begin{bmatrix} K_4 & K_4 & K_4 \\ \cos\theta & \cos(\theta - 120) & \cos(\theta + 120) \\ -\sin\theta & -\sin(\theta - 120) & -\sin(\theta + 120) \end{bmatrix} \tag{A-1.6}$$

and

$$[C]^{-1} = \frac{2}{3K_3} \begin{bmatrix} 1/2\ K_4 & \cos\theta & -\sin(\theta) \\ 1/2\ K_4 & \cos(\theta - 120) & -\sin(\theta - 120) \\ 1/2\ K_4 & \cos(\theta + 120) & -\sin(\theta + 120) \end{bmatrix} = \frac{2}{3K_3} [G] \tag{A-1.7}$$

The condition for orthogonal transformation (see equation (A-1.3)) is fulfilled if $K_3 = \sqrt{2/3}$ and $K_4 = \sqrt{1/2}$ where Park used $K_3 = 2/3$ and $K_4 = 1/2$.

The constant inductance matrix that appeared in equation (2.14) , can be obtained by substituting equation (A-1.5) for currents . and fluxes in equation (2.6) as follows,

$$\begin{bmatrix} [C] & 0 \\ 0 & [I] \end{bmatrix} \begin{bmatrix} \underline{\psi}_s \\ \underline{\psi}_r \end{bmatrix} = \begin{bmatrix} [C] & 0 \\ 0 & [I] \end{bmatrix} \begin{bmatrix} -[L_{ss}] & [L_{sr}] \\ -[L_{rs}] & [L_{rr}] \end{bmatrix} \begin{bmatrix} [C]^{-1} & 0 \\ 0 & [I] \end{bmatrix} \begin{bmatrix} [C] & 0 \\ 0 & [I] \end{bmatrix} \begin{bmatrix} \underline{i}_s \\ \underline{i}_r \end{bmatrix} \tag{A-1.8}$$

or

$$\underline{\psi}_{odq} = \begin{bmatrix} -[C]\ [L_{ss}]\ [C]^{-1} & [C]\ [L_{sr}] \\ -[C]^{-1}\ [L_{rs}] & [L_{rr}] \end{bmatrix} \underline{i}_{odq} \qquad \text{(A-1.9)}$$

substituting equations (A-1.6) and (A-1.7) into (A-1.9) we get;

$$\underline{\psi}_{odq} = \left[\begin{array}{c|c} -K_3\ [W]\ [L_{ss}]\ \frac{2}{3K_3}\ [G] & K_3\ [W]\ [L_{sr}] \\ \hline -\frac{2}{3K_3}\ [G]\ [L_{rs}] & [L_{rr}] \end{array}\right] \underline{i}_{odq} \qquad \text{(A-1.10)}$$

Irrespective of the value of K_4 in equation (A-1.5), when one substitutes the expressions of $[L_{ss}]$, $[L_{sr}]$, $[L_{rs}]$ and $[L_{rr}]$ given in equations (2.7), (2.8), (2.9), (2.10) and (2.11) in equation (A-1.10), the resultant equation after neglecting the zero sequence will be,

$$\begin{bmatrix} \psi_d \\ \psi_q \\ \psi_{fd} \\ \psi_{kd} \\ \psi_{kq} \end{bmatrix} = \begin{bmatrix} -L_d & 0 & \frac{3}{2}K_3L_{afd} & \frac{3}{2}K_3L_{akd} & 0 \\ 0 & -L_q & 0 & 0 & \frac{3}{2}K_3L_{akq} \\ \frac{2}{3K_3}(-\frac{3}{2}L_{afd}) & 0 & L_{ffd} & L_{fkd} & 0 \\ \frac{2}{3K_3}(-\frac{3}{2}L_{akd}) & 0 & L_{kfd} & L_{kkd} & 0 \\ 0 & \frac{2}{3K_3}(-\frac{3}{2}L_{akq}) & 0 & 0 & L_{kkq} \end{bmatrix} \begin{bmatrix} i_d \\ i_q \\ i_{fd} \\ i_{kd} \\ i_{kq} \end{bmatrix}$$

(A-1.11)

where L_d and L_q are given in equations (2.15) and (2.16) respectively.

For $K_3 = 2/3$, which is the value used by Park, equation (A-1.11) is the same as equation (2.14). For $K_3 = \sqrt{2}/3$, which is used for orthogonal transformation, the resultant inductance matrix in equation (A-1.11) will have a coefficient of $\sqrt{3}/2$ in the off diagonal submatrices. Because of the widespread use of Park's transformation which has been used quite generally in industry, the nonsymmetry in equation (2.14), ignoring the negative sign, is removed usually by the per-unitization procedure.

APPENDIX A-2

PER-UNIT SYSTEM [47]

In this Appendix the per-unitized equations in the d - q rotating reference frame are derived using the X_{ad} - base as the per-unit system. The base quantities selected for the stator of the synchronous machine are:

(i) The rms line current, which is the same as the rms phase current, defined as $\underline{I}_{SB}$.

(ii) The line to neutral rms voltage defined as $\underline{E}_{SB}$.

(iii) The rated synchronous speed ω_0 .

From the above defined base values the following base quantities are also defined.

$$\underline{I}_{SB} = \begin{bmatrix} I_{dB} \\ I_{qB} \end{bmatrix} \quad , \quad \underline{E}_{SB} = \begin{bmatrix} E_{dB} \\ E_{qB} \end{bmatrix} \tag{A-2.1}$$

The following notation $\underline{Y} \,/\, \underline{Y}_B$ is defined in the following way:

$$\underline{\bar{Y}} = \frac{\underline{Y}}{\underline{Y}_B} = \begin{bmatrix} Y_1 \\ Y_2 \\ \vdots \\ Y_n \end{bmatrix} \Big/ \begin{bmatrix} Y_{1B} \\ Y_{2B} \\ \vdots \\ Y_{nB} \end{bmatrix} = \begin{bmatrix} Y_1 \,/\, Y_{1B} \\ Y_2 \,/\, Y_{2B} \\ \vdots \\ Y_n \,/\, Y_{nB} \end{bmatrix} = \begin{bmatrix} \bar{Y}_1 \\ \bar{Y}_2 \\ \vdots \\ \bar{Y}_n \end{bmatrix} \tag{A-2.2}$$

From equation (A-2.1)

$$[Z_{SB}] = \begin{bmatrix} Z_{dB} & \\ & Z_{qB} \end{bmatrix} = \begin{bmatrix} E_{dB} / I_{dB} & \\ & E_{qB} / I_{qB} \end{bmatrix} \qquad \text{(A-2.3)}$$

and

$$\psi_{SB} = \begin{bmatrix} \psi_{dB} \\ \psi_{qB} \end{bmatrix} = \frac{1}{\omega_0} \begin{bmatrix} E_{dB} \\ E_{qB} \end{bmatrix} = [-L_{SB}] \underline{I}_{SB} = \begin{bmatrix} -L_{dB} & \\ & -L_{qB} \end{bmatrix} \begin{bmatrix} I_{dB} \\ I_{qB} \end{bmatrix} \qquad \text{(A-2.4)}$$

Stator Voltage Equations (See Equation (2.13))

$$\underline{e}_s = -[R_s]\, i_s + \frac{d}{dt}\, \underline{\psi}_s + \omega \begin{bmatrix} 0 & -1 \\ 1 & 0 \end{bmatrix} \underline{\psi}_s \qquad \text{(A-2.5)}$$

$$\frac{\underline{e}_s}{E_{SB}} = -[Z_{SB}]^{-1} [R_s] \frac{\underline{i}_s}{I_{SB}} + \frac{d}{dt} \frac{\underline{\psi}_s}{\omega_0 \underline{\psi}_{SB}} + \frac{\omega}{\omega_0} \begin{bmatrix} 0 & -1 \\ 1 & 0 \end{bmatrix} \frac{\underline{\psi}_s}{\psi_{SB}} \qquad \text{(A-2.6)}$$

where $\underline{E}_{SB} = [Z_{SB}]\ \underline{I}_{SB} = \omega_0\, \underline{\psi}_{SB}$

From equation (A-2.6) the per-unitized stator voltage equation is :

$$\underline{\bar{e}}_s = - [\bar{R}_s]\, \underline{\bar{i}}_s + \frac{1}{\omega_0} \frac{d}{dt}\, \underline{\bar{\psi}}_s + \bar{\omega} \begin{bmatrix} 0 & -1 \\ 1 & 0 \end{bmatrix} \underline{\bar{\psi}}_s$$

or

$$\begin{bmatrix} \bar{e}_d \\ \bar{e}_q \end{bmatrix} = - \begin{bmatrix} \bar{R}_a & \\ & \bar{R}_a \end{bmatrix} \begin{bmatrix} \bar{i}_d \\ \bar{i}_q \end{bmatrix} + \frac{1}{\omega_0} \frac{d}{dt} \begin{bmatrix} \bar{\psi}_d \\ \bar{\psi}_q \end{bmatrix} + \bar{\omega} \begin{bmatrix} -\bar{\psi}_q \\ \bar{\psi}_d \end{bmatrix}$$

(A-2.7)

Stator Flux Equations

From equation (A-1.11) the stator flux equations are,

$$\psi_d = - L_d\, i_d + \frac{3}{2}\, K_3\, L_{afd}\, i_{fd} + \frac{3}{2}\, K_3\, L_{akd}\, i_{kd}$$

and

$$\psi_q = - L_q\, i_q + \frac{3}{2}\, K_3\, L_{akq}\, i_{kq}$$

The per-unitized flux equations are:

$$\frac{\psi_d}{\psi_{dB}} = - \frac{L_d\, i_d}{L_{dB}\, I_{dB}} + \frac{3}{2} K_3 \frac{L_{afd}}{L_{dB}\, I_{dB}} \cdot i_{fd} \cdot \frac{I_{fdB}}{I_{fdB}}$$

$$+ \frac{3}{2} K_3 \frac{L_{akd}}{L_{dB}\, I_{dB}} \cdot i_{kd} \cdot \frac{I_{kdB}}{I_{kdB}}$$

and

$$\frac{\psi_q}{\psi_{qB}} = -\frac{L_q\, i_q}{L_{qB}\, I_{qB}} + \frac{3}{2} K_3 \frac{L_{akq}}{L_{qB}\, I_{qB}} \cdot i_{kq} \cdot \frac{I_{kqB}}{I_{kqB}} \qquad \text{(A-2.8)}$$

where I_{fdB} , I_{kdB} , I_{kqB} are assumed to be the rotor field, direct amortisseur and quadrature amortisseur base currents respectively, which are unknown for the time being.

From equations (A-2.8)

$$\begin{bmatrix} \bar{\psi}_d \\ \bar{\psi}_q \end{bmatrix} = \begin{bmatrix} -\bar{L}_d & \\ & -\bar{L}_q \end{bmatrix} \begin{bmatrix} \bar{i}_d \\ \bar{i}_q \end{bmatrix} + K_3 \begin{bmatrix} \bar{L}_{afd} & \bar{L}_{akd} & 0 \\ 0 & 0 & \bar{L}_{akq} \end{bmatrix} [\bar{i}_{fd} \quad \bar{i}_{kd} \quad i_{kq}]^T \qquad \text{(A-2.9)}$$

where

$$\begin{array}{|c|c|c|} \hline \bar{L}_{afd} & \bar{L}_{akd} & 0 \\ \hline 0 & 0 & \bar{L}_{akq} \\ \hline \end{array} = \begin{array}{|c|c|c|} \hline \dfrac{3\, L_{afd}\, I_{fdB}}{2\, L_{dB}\, I_{dB}} & \dfrac{3\, L_{akd}\, I_{kdB}}{2\, L_{dB}\, I_{dB}} & 0 \\ \hline 0 & 0 & \dfrac{3\, L_{akq}\, I_{kqB}}{2\, L_{qB}\, I_{qB}} \\ \hline \end{array} \qquad \text{(A-2.10)}$$

Rotor Voltage Equations

Assume that the rotor base voltages are,

$$\underline{E}_{rB} = [E_{fdB} \quad E_{kdB} \quad E_{kqB}]^T \qquad \text{(A-2.11)}$$

so

$$[Z_{rB}] = \begin{bmatrix} Z_{fdB} & & \\ & Z_{kdB} & \\ & & Z_{kqB} \end{bmatrix} = \begin{bmatrix} E_{fdB}/I_{fdB} & & \\ & E_{kdB}/I_{kdB} & \\ & & E_{kqB}/I_{kqB} \end{bmatrix}$$

(A-2.12)

$$\underline{\psi}_{rB} = \frac{1}{\omega_0} E_{rB} = [\psi_{fdB} \quad \psi_{kdB} \quad \psi_{kqB}]^T = [L_{rB}] \underline{I}_{rB} \qquad \text{(A-2.13)}$$

where

$$[L_{rB}] = \begin{bmatrix} L_{ffdB} & & \\ & L_{kkdB} & \\ & & L_{kkqB} \end{bmatrix}$$

From equation 2.13

$$\underline{e}_r = [R_r] \underline{i}_r + \frac{d}{dt} \underline{\psi}_r \qquad \text{(A-2.14)}$$

divide equation (A-2.14) by base values

$$\frac{\underline{e}_r}{\underline{E}_{rB}} = [Z_{rB}]^{-1} [R_r] \frac{\underline{i}_r}{\underline{I}_{rB}} + \frac{1}{\omega_0} \frac{d}{dt} \frac{\underline{\psi}_r}{\underline{\psi}_{rB}}$$

$$\underline{\bar{e}}_r = [\bar{R}_r]\,\underline{\bar{i}}_r + \frac{1}{\omega_0}\,\frac{d}{dt}\,\underline{\bar{\psi}}_r$$

or

$$\begin{bmatrix} \bar{e}_{fd} \\ 0 \\ 0 \end{bmatrix} = \begin{bmatrix} \bar{R}_{fd} & & \\ & \bar{R}_{kd} & \\ & & \bar{R}_{kq} \end{bmatrix} \begin{bmatrix} \bar{i}_{fd} \\ \bar{i}_{kd} \\ \bar{i}_{kq} \end{bmatrix} + \frac{1}{\omega_0}\,\frac{d}{dt} \begin{bmatrix} \bar{\psi}_{fd} \\ \bar{\psi}_{kd} \\ \bar{\psi}_{kq} \end{bmatrix} \qquad \text{(A-2.14)}$$

Rotor Flux Voltages

From equation (A-1.11)

$$\psi_{fd} = -\frac{2}{3\,K_3}\left(\frac{3}{2}\,L_{afd}\right) i_d + L_{ffd}\, i_{fd} + L_{fkd}\, i_{kd}$$

$$\psi_{kd} = -\frac{2}{3\,K_3}\left(\frac{3}{2}\,L_{akd}\right) i_d + L_{fkd}\, i_{fd} + L_{kkd}\, i_{kd} \qquad \text{(A-2.15)}$$

$$\psi_{kq} = -\frac{2}{3\,K_3}\left(\frac{3}{2}\,L_{akq}\right) i_q + L_{kkq}\, i_{kq}$$

divide equation (A-2.15) by base values,

$$\frac{\psi_{fd}}{\psi_{fdB}} = -\frac{2}{3K_3}\,\frac{3L_{afd}}{2L_{ffdB}I_{fdB}}\cdot i_d\cdot\frac{I_{dB}}{I_{dB}} + \frac{L_{ffd}\,i_{fd}}{L_{ffdB}I_{fdB}} + \frac{L_{fkd}}{L_{ffdB}I_{fdB}}\cdot i_{kd}\,\frac{I_{kdB}}{I_{kdB}}$$

$$\frac{\psi_{kd}}{\psi_{kdB}} = -\frac{2}{3K_3}\,\frac{3L_{akd}}{2L_{kkdB}I_{kdB}}\cdot i_d\cdot\frac{I_{dB}}{I_{dB}} + \frac{L_{kfd}\,i_{fd}}{L_{kkdB}I_{kdB}}\cdot\frac{I_{fdB}}{I_{fdB}} + \frac{L_{kkd}\,i_{kd}}{L_{kkd_B}I_{kdB}} \qquad \text{(A-2.16)}$$

$$\frac{\psi_{kq}}{\psi_{kqB}} = -\frac{2}{3K_3}\,\frac{3L_{akq}\,i_q}{2L_{kkqB}I_{kqB}}\cdot\frac{I_{qB}}{I_{qB}} + \frac{L_{kkq}\,i_{kq}}{L_{kkqB}I_{kqB}}$$

From equation (A-2.16) the per-unitized equations are,

$$\begin{bmatrix}\bar{\psi}_{fd}\\ \bar{\psi}_{kd}\\ \bar{\psi}_{kq}\end{bmatrix} = -\frac{2}{3K_3}\begin{bmatrix}\bar{L}_{afd} & 0\\ \bar{L}_{akd} & 0\\ 0 & \bar{L}_{akq}\end{bmatrix}\begin{bmatrix}\bar{i}_d\\ \bar{i}_q\end{bmatrix} + \begin{bmatrix}\bar{L}_{ffd} & \bar{L}_{fkd} & 0\\ \bar{L}_{kfd} & \bar{L}_{kkd} & 0\\ 0 & 0 & \bar{L}_{kkq}\end{bmatrix}\begin{bmatrix}\bar{i}_{fd}\\ \bar{i}_{kd}\\ \bar{i}_{kq}\end{bmatrix} \qquad \text{(A-2.17)}$$

where

$$\begin{bmatrix} \bar{L}_{afd} & 0 \\ \bar{L}_{akd} & 0 \\ 0 & \bar{L}_{akq} \end{bmatrix} = \begin{bmatrix} \frac{3\,L_{afd}\,I_{dB}}{2\,L_{ffdB}\,I_{fdB}} & 0 \\ \frac{3\,L_{akd}\,I_{dB}}{2\,L_{kkdB}\,I_{kdB}} & 0 \\ 0 & \frac{3\,L_{aq}\,I_{qB}}{2\,L_{kkqB}\,I_{kqB}} \end{bmatrix} \qquad \text{(A-2.18)}$$

and

$$\begin{bmatrix} \bar{L}_{ffd} & \bar{L}_{fkd} & 0 \\ \bar{L}_{kfd} & \bar{L}_{kkd} & 0 \\ 0 & 0 & \bar{L}_{kkq} \end{bmatrix} = \begin{bmatrix} \frac{L_{ffd}}{L_{ffdB}} & \frac{L_{fkd}\,I_{kdB}}{L_{ffdB}\,I_{fdB}} & 0 \\ \frac{L_{kfd}\,I_{fdB}}{L_{kkdB}\,I_{kdB}} & \frac{L_{kkd}}{L_{kkdB}} & 0 \\ 0 & 0 & \frac{L_{kkq}}{L_{kkqB}} \end{bmatrix} \qquad \text{(A-2.19)}$$

The condition of having $[\underline{L}_{rs}] = [\underline{L}_{sr}]^T$ is by comparing each term in equation (A-2.10) with those in equation (A-2.18) or

$$\begin{aligned} \frac{2}{3\,K_3}\,\frac{3\,L_{afd}\,I_{dB}}{2\,L_{ffdB}\,I_{fdB}} &= K_3\,\frac{3\,L_{afd}\,I_{fdB}}{2\,L_{dB}\,I_{dB}} \\ \frac{2}{3\,K_3}\,\frac{3\,L_{akd}\,I_{dB}}{2\,L_{kkdB}\,I_{kdB}} &= K_3\,\frac{3\,L_{akd}\,I_{kdB}}{2\,L_{dB}\,I_{dB}} \qquad \text{(A-2.20)} \\ \frac{2}{3\,K_3}\,\frac{3\,L_{akq}\,I_{qB}}{2\,L_{kkqB}\,I_{kqB}} &= K_3\,\frac{3\,L_{akq}\,I_{kqB}}{2\,L_{qB}\,I_{qB}} \end{aligned}$$

From equation (A-2.20) the following relations are obtained:

$$L_{ffdB}\, I_{fdB}^{2} = \frac{2}{3\, K_3^2}\, L_{dB}\, I_{dB}^{2} = L_{kkd}\, I_{kdB}^{2} \qquad \text{(A-2.21)}$$

and

$$L_{kkqB}\, I_{kqB}^{2} = \frac{2}{3\, K_3^2}\, L_{qB}\, I_{qB}^{2} \qquad \text{(A-2.22)}$$

Relations (A-2.21) and (A-2.22) indicate that the rotor volt-ampere $= \frac{2}{3\, K_3^2}$ the stator volt-ampere.

Note: For Park's transformation where $K_3 = 2/3$ the rotor volt-ampere $= \frac{3}{2}$ the stator volt-ampere and for orthogonal transformation where $K_3 = \sqrt{2}/3$ the rotor volt-ampere = the stator volt-ampere.

The condition for X_{ad} - base is to make all the mutual inductances between the stator and the rotor windings in one axis equal, i.e.

$$L_{afd} = L_{akd} = L_{ad} = L_d - \ell_d$$

and (A-2.23)

$$L_{akq} = L_{aq} = L_q - \ell_q$$

where ℓ_d and ℓ_q are leakage inductances.

Condition (A-2.23) can be derived by equating the mutual flux linkages in each winding.

$$L_{ad} I_{dB} = \frac{3}{2} K_3 L_{afd} I_{fdB} = \frac{3}{2} K_3 L_{akd} I_{kdB}$$

and (A-2.24)

$$L_{aq} I_{qB} = \frac{3}{2} K_3 L_{akq} I_{kqB}$$

From equation (A-2.24)

$$I_{fdB} = \frac{2}{3 K_3} \frac{L_{ad}}{L_{afd}} I_{dB}$$

$$I_{kdB} = \frac{2}{3 K_3} \frac{L_{ad}}{L_{akd}} I_{dB} \quad \text{(A-2.25)}$$

$$I_{kqB} = \frac{2}{3 K_3} \frac{L_{aq}}{L_{akq}} I_{qB}$$

where L_{ad}, L_{aq}, L_{akq}, L_{akd} and L_{afd} are constant inductances in Henries.

From equation (A-2.25) the rotor base currents necessary to satisfy the X_{ad} - base are obtained. As a summary the definitions of the base values can be divided into two parts.

(i) For the stator, the base voltage is usually defined from the knowledge of the transmission voltage. The base current can be obtained from the machine rating, which is usually known, and from the defined base voltage. Knowing the base voltage and the base current, then the stator base flux, impedances and the self inductances are calculated according to equations (A-2.3) and (A-2.4).

(ii) For the rotor, the base values are usually not known. By forcing the mutual inductances to be reciprocal ($[L_{sr}] = [L_{rs}]^T$), a relation between the stator and the rotor volt-amperes is found as in equations (A-2.21) and (A-2.22) Then by choosing another definition for rotor currents, which is X_{ad} - definition in this case, a relation between base stator and rotor currents can be obtained from which the base rotor currents are defined as in equation (A-2.25). Knowing the rotor base volt-ampere and the rotor base currents, the rotor base voltages, impedances and self inductances are automatically defined.

The per-unit equations obtained from the combination of equations (A-2.7), (A-2.14) and equations (A-2.8), (A-2.16) are,

$$\begin{bmatrix} \bar{e}_d \\ \bar{e}_q \\ \bar{e}_{fd} \\ 0 \\ 0 \end{bmatrix} = [r] \begin{bmatrix} \bar{i}_d \\ \bar{i}_q \\ \bar{i}_{fd} \\ \bar{i}_{kd} \\ \bar{i}_{kq} \end{bmatrix} + \frac{1}{\omega_0} \frac{d}{dt} \begin{bmatrix} \bar{\psi}_d \\ \bar{\psi}_q \\ \bar{\psi}_{fd} \\ \bar{\psi}_{kd} \\ \bar{\psi}_{kq} \end{bmatrix} + \bar{\omega} \begin{bmatrix} -\bar{\psi}_q \\ \bar{\psi}_d \\ 0 \\ 0 \\ 0 \end{bmatrix} \qquad \text{(A-2.26)}$$

where

$$\begin{bmatrix} \bar{\psi}_d \\ \bar{\psi}_q \\ \bar{\psi}_{fd} \\ \bar{\psi}_{kd} \\ \bar{\psi}_{kq} \end{bmatrix} = \begin{bmatrix} -X_d & 0 & X_{ad} & X_{ad} & 0 \\ 0 & -X_q & 0 & 0 & X_{aq} \\ -X_{ad} & 0 & X_{ffd} & X_{fkd} & 0 \\ -X_{ad} & 0 & X_{fkd} & X_{kkd} & 0 \\ 0 & -X_{aq} & 0 & 0 & X_{kkq} \end{bmatrix} \begin{bmatrix} \bar{i}_d \\ \bar{i}_q \\ \bar{i}_{fd} \\ \bar{i}_{kd} \\ \bar{i}_{kq} \end{bmatrix} \qquad \text{(A-2.27)}$$

and

$$[r] = \begin{bmatrix} -r_a & & & & \\ & -r_a & & & \\ & & r_{fd} & & \\ & & & r_{kd} & \\ & & & & r_{kq} \end{bmatrix} \qquad \text{(A-2.28)}$$

where X is used for per-unit inductances,

r is used for per-unit resistances,

and $\bar{\omega}$ is per-unit rotor speed.

APPENDIX B-1

LABORATORY MACHINE DATA [17]

30 KVA BASE

H	4.75 sec.	r_{fd}	0.00109
D	0.1	X_{fd}	0.185
r_a	0.0158	r_{kd}	0.0112
X_d	0.75	X_{kd}	0.094
X_q	0.238	X_{aq}	0.163
X_2	0.132	r_{kq}	0.0117
X_{ad}	0.675	X_{kq}	0.088

NETWORK PARAMETERS

r_E = 0.0229 , X_E = 0.0112 , X_C variable

NDS. Filter

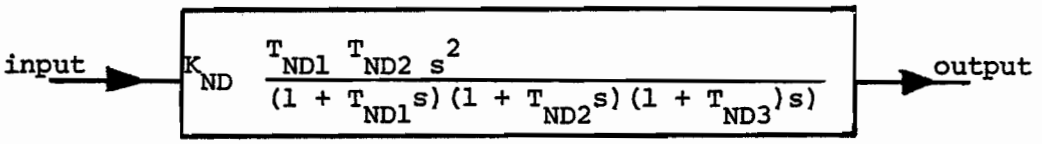

Figure B.1. NDS Filter transfer function [17] .

T_{ND1} = 0.033 sec.

T_{ND2} = 0.017 sec.

T_{ND3} = 0.01 sec.

K_{ND} variable.

APPENDIX B-2

STATE SPACE MODEL OF GENERAL TRANSFER FUNCTION [54]

The general transfer function is,

$$\frac{y(s)}{u(s)} = \frac{b_m s^m + \ldots + b_1 s + b_0}{a_n s^n + \ldots + a_1 s + a_0} \quad , \quad n > m > 0 \qquad \text{(B-2.1)}$$

or

$$\left(a_n \frac{d^n}{dt^n} + \ldots a_1 \frac{d}{dt} + a_0\right) y_{(t)} = \left(b_m \frac{d^m}{dt^m} + \ldots b_0\right) u(t) \qquad \text{(B.2.2)}$$

The state space model of this transfer function may be obtained by defining the state variables $x_1 \ldots x_n$ as,

$$\begin{aligned} x_1 &= a_n y - b_n u \\ x_2 &= \frac{d}{dt} x_1 + a_{n-1} y - b_{n-1} n \\ &\vdots \\ x_n &= \frac{d}{dt} x_{n-1} + a_1 y - b_1 u \end{aligned} \qquad \text{(B-2.3)}$$

combining equation B-2.2 with equation B-2.3 and eliminating y, the state equation will be,

$$\frac{d}{dt}\begin{bmatrix} x_1 \\ x_2 \\ \vdots \\ x_{n-1} \\ x_n \end{bmatrix} = \frac{1}{a_n}\begin{bmatrix} -a_{n-1} & a_n & 0 & \cdots & 0 \\ -a_{n-2} & 0 & a_n & 0 & \cdots & 0 \\ \vdots & \vdots & \vdots & \vdots & \vdots & \vdots \\ -a_1 & 0 & 0 & 0 & \cdots & a_n \\ -a_0 & 0 & \cdots & \cdots & \cdots & \cdots \end{bmatrix}\begin{bmatrix} x_1 \\ x_2 \\ \vdots \\ x_{n-1} \\ x_n \end{bmatrix}$$

$$+ \frac{1}{a_n}\begin{bmatrix} a_n b_{n-1} - a_{n-1} b_n \\ a_n b_{n-2} - a_{n-2} b_n \\ \vdots \\ a_n b_0 - a_0 b_n \end{bmatrix} u \qquad \text{(B-2.4)}$$

APPENDIX C

CALIBRATION OF THE NDS' FEEDBACK SCHEME

The proposed NDS' feedback scheme is calibrated against the feedback scheme used by [17] which was called the NDS feedback scheme and it is shown in Figure 5.3. The mathematical state space model of this scheme (NDS scheme) is obtained from Appendix B-2 as,

$$\frac{d}{dt}\begin{bmatrix} x_{D1} \\ x_{D2} \end{bmatrix} = \begin{bmatrix} -a_{D1} & 1 \\ -a_{D2} & 0 \end{bmatrix}\begin{bmatrix} x_{D1} \\ x_{D2} \end{bmatrix} + \begin{bmatrix} b_{D1} \\ b_{D2} \end{bmatrix} \mu \qquad (C.1)$$

where

$$a_{D1} = \frac{T_{ND1} + T_{ND2}}{T_{ND1}\, T_{ND2}}$$

$$a_{D2} = \frac{1}{T_{ND1}\, T_{ND2}}$$

and

$$b_{D1} = - K_{ND} \, (T_{ND1} + T_{ND2})$$

$$b_{D2} = - K_{ND}$$

The output of the NDS filter ν_D is

$$\nu_D = a_{D2} \, x_{D1} + K_{ND} \, \mu \qquad (C.2)$$

The values of the gain and the time constants are $K_{ND} = 100$, $T_{ND1} = 0.0200$ sec., $T_{ND2} = 0.0400$ sec.

The eignevalues shown in Table C.1 are for the following systems,

First row, for the basic system incorporated with HRE excitation system and the NDS feedback loop for the control angle $\phi = 0.0$, system model is the combination of equations 4.1, 5.1, and C.1 .

Second row, for the system of Figure 5.3(a) with the control angle $\phi = 0.0$, system model is the combination of the above model and equation 5.4 .

Third row, the same as in the second row but for $\phi = 30^{\circ}$.

Fourth row, the same as in the second row but for $\phi = 315^{\circ}$.

Fifth row, the same as in the second row but for $\phi = 240^{\circ}$.

The calibration of the NDS' feedback scheme with that used by [17] is achieved by comparing the eigenvalues in Table 5.3 and those in Table C.1 . The first row of both tables show that the above schemes are similar in their effect on the SSR positive sequence mode. The mechanical mode in both Tables is unstable, but it is better in case of the scheme of Reference [17] . However, the change in its damping is not large. The excitation system is still performing its normal function of fast regulation with both schemes. The last four rows of Tables 5.2

and C.1 show the direction of ϕ by which the SSR mode damping is improved. In both schemes the choice of ϕ in the first quadrant improve the SSR mode damping but reduces the damping of the PSS mode.

TABLE C.1

EIGENVALUES OF THE PRACTICAL SYSTEM WHEN THE NDS FEEDBACK SCHEME OF REFERENCE [17] IS CONSIDERED

	System Configuration	λ_{ssrn}	λ_{ssrp}	$\lambda_{mech.}$	$\lambda_{amort.}$	λ_{field}	λ_{EXC}		λ_{PSS}		λ_{NDS}
	Basic System	- 3.65	- 5.48	+ 1.21	- 58.3	- 2.53	- 70.8	- 2.53			- 16.5
$\phi = 0^{\circ}$	+	±	±	±		+	±	-			±
	NDS + HRE	j 705	j 52.3	j 8.04	- 10.8	j 5.0	j 109	j 5.0			j 21.5
	System	- 3.65	- 8.54	- 7.72	- 58.3	- 0.770	- 70.8	- 0.770	+ 4.48		- 20.8
$\phi = 0^{\circ}$	of	±	±	±		+	±	-	±	- 0.211	±
	Fig.5.3(a)	j 705	j 47.6	j 1.80	- 20.1	j 2.10	j 109	- j 2.10	j 31.3		j 14.6
	System	- 3.46	- 12.9	- 7.60	- 58.1	- .770	- 70.8	- .770	+ 9.34		- 20.3
$\phi = 30^{\circ}$	of	±	±	±		+	±	-	±	- .211	±
	Fig.5.3(a)	j 705	j 43.7	j 2.00	- 20.5	j 2.2	j 109	j 2.2	j 33.9		j 13.3
	System	- 4.20	- 2.06	- 7.70	- 57.0	- .770	- 70.8	- .770	- 1.04		- 25.6
$\phi=315^{\circ}$	of	±	±	±		+	±	-	±	- .211	±
	Fig.5.3(a)	j 705	j 51.2	j 1.43	- 20.1	j 2.1	j 109	j 2.1	j 25.7		j 15.2
	System	- 4.90	+ 8.5	- 7.50	- 55.7	- .730	- 70.8	- .730	- 4.7		- 21.3
$\phi=240^{\circ}$	of	±	±	±	±	+	±	-	±	- .211	±
	Fig.5.3(a)	j 705	j 50.1	j 1.23	j 14.6	j 2.14	j 109	j 2.14	j 21.2		j 3.54

Eigenvalues

X_C = 1.2 p.u., r_E = 0.0295 p.u., K_{ND} = 100 .

λ_{NDS} The eigenvalues associated with the NDS filter.

APPENDIX D

DERIVATION OF THE HYDRO-SYSTEM MECHANICAL EQUATIONS

The mechanical part of the hydro system is modeled by two inertias, one representing the generator H_G and the other representing the turbine, H_T. The two inertias are connected by a spring with stiffness K_{GT}, and shaft friction is modeled by a dash-pot connected between the two inertias. The model diagram is shown in Figure D.1.

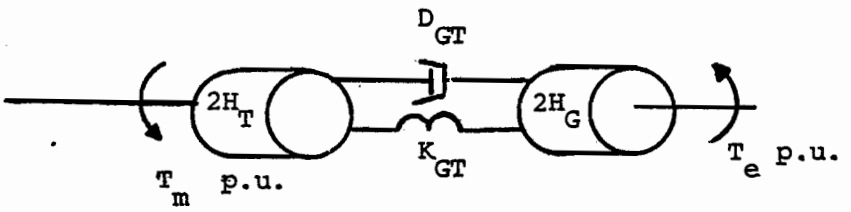

Figure D.1. Hydro-turbine inertia system model.

Since the quantities are in per-unit values, therefore 2H is used to represent J in Figure D.1.

The equations of motion of the system in Figure D.1 can be derived as follows,

The total kinetic energy of the system E_K is,

$$E_K = \frac{1}{2} 2 H_T \bar{\omega}_T^2 + \frac{1}{2} 2 H_G \bar{\omega}_G^2 \qquad (D.1)$$

$\bar{\omega}_T$, $\bar{\omega}_G$ are the per unit speeds of the turbine and the generator respectively.

The total potential energy of the system E_p is,

$$E_p = \frac{1}{2} K_{GT} (\delta_G - \delta_T)^2$$

where δ_G , δ_T are the angular positions of the turbine and the generator respectively.

$\frac{d}{dt}$ (Total energy) = Power supplied - Power dissipated.

$$2 H_T \bar{\omega}_T \frac{d}{dt} \bar{\omega}_T + 2 H_G \bar{\omega}_G \frac{d}{dt} \bar{\omega}_G + K_{GT} (\delta_G - \delta_T)(\bar{\omega}_G - \bar{\omega}_T) =$$

$$\bar{\omega}_T T_m - \bar{\omega}_G T_e - D_G \bar{\omega}_G^2 - D_T \bar{\omega}_T^2 - D_{GT} (\bar{\omega}_G - \bar{\omega}_T)^2$$

since the turbine and the generator speeds are different from zeros therefore,

$$2 H_T \frac{d \bar{\omega}_T}{dt} - K_{GT} (\delta_G - \delta_T) - T_m + D_T \bar{\omega}_T + D_{GT} (\bar{\omega}_T - \bar{\omega}_G) = 0$$

and

$$2 H_G \frac{d \bar{\omega}_G}{dt} + K_{GT} (\delta_G - \delta_T) + T_e + D_G \bar{\omega}_G + D_{GT} (\bar{\omega}_G - \bar{\omega}_T) = 0$$

$$\frac{d\,\delta_T}{dt} = \bar{\omega}_T - 1$$

$$\frac{d\,\delta_G}{dt} = \bar{\omega}_G - 1$$

in matrix form, the mechanical equations are,

$$\begin{bmatrix} 2H_G & & & \\ & 2H_T & & \\ & & 1 & \\ & & & 1 \end{bmatrix} \frac{d}{dt} \begin{bmatrix} \bar{\omega}_G \\ \bar{\omega}_T \\ \delta_G \\ \delta_T \end{bmatrix} = \begin{bmatrix} -D_G - D_{GT} & D_G & -K_{GT} & K_{GT} \\ D_T & -D_T - D_{GT} & K_{GT} & -K_{GT} \\ 1 & 0 & 0 & 0 \\ 0 & 1 & 0 & 0 \end{bmatrix} \cdot \begin{bmatrix} \bar{\omega}_G \\ \bar{\omega}_T \\ \delta_G \\ \delta_T \end{bmatrix} + \begin{bmatrix} -T_e \\ T_m \\ -1 \\ -1 \end{bmatrix} \qquad (D.2)$$

D_{GT} , D_G and D_T are the damping coefficients of the shaft, the generator and the turbine respectively.

APPENDIX E-1

CALCULATION OF SYNCHRONOUS GENERATOR PARAMETERS [81]

The machine p.u. parameters supplied by the manufacturer are usually given as

Base KVA = 2 GVA

Base Voltage = 735 KV

H = 4.00 sec.	X''_d = 0.200	X_ℓ = 0.150	T'_{d0} = 8 sec.
X_d = 1.00	X_q = 0.700	r_a = 0.00230	T''_{d0} = 0.07 sec.
X'_d = 0.300	X''_q = 0.300	T_a = 160 msec.	T''_{q0} = 0.09 sec.

The machine parameters necessary for theoretical analysis can be obtained from the above data as follows [83]

$$X_{ad} = X_d - X_\ell = \underline{0.85}$$

$$X_{aq} = X_q - X_\ell = \underline{0.55}$$

$$X_{fd} = X_{ad}\,[(X'_d - X_\ell) \,/\, (X_d - X'_d)] = \underline{0.182}$$

$$X_{ffd} = X_{ad} + X_{fd} = \underline{1.032}$$

$$X_{kd} = X_{ad}\,X_{fd}\,(X''_d - X_\ell) \,/\, [X_{ad}\,X_{fd} - X_{ffd}\,(X''_d - X_\ell)] = \underline{0.075}$$

$$X_{kkd} = X_{ad} + X_{kd} = \underline{.925}$$

$$X_{kq} = X_{aq}\,[(X''_q - X_\ell) / (X_q - X''_q)] = \underline{0.206}$$

$$X_{kkq} = X_{aq} + X_{kq} = \underline{0.756}$$

$$T'_{d0}\ (\text{rad.}) = \omega_0 * T'_{d0}\ (\text{sec.}) = 3016$$

$$r_{fd} = X_{ffd} / T'_{d0} = \underline{0.000342}$$

$$T''_d\ (\text{rad}) = T''_{d0}\ (\text{sec.}) * \omega_0 * X''_d / X'_d = 17.6$$

$$r_{kd} = [X_{kkd} * X_{ffd} - X^2_{ad}]\, X''_d / X_{ffd} * T''_d * X'_d = \underline{0.00852}$$

$$T''_{q0}\ (\text{rad}) = T''_{q0}\ (\text{sec.}) * \omega_0 = 33.93$$

$$r_{kq} = X_{kkq} / T''_{q0} = \underline{0.0223}$$

APPENDIX E-2

EXCITATION SYSTEM OF THE SYNCHRONOUS GENERATOR [81]

The leading circuit and the excitation system of the synchronous generator are:

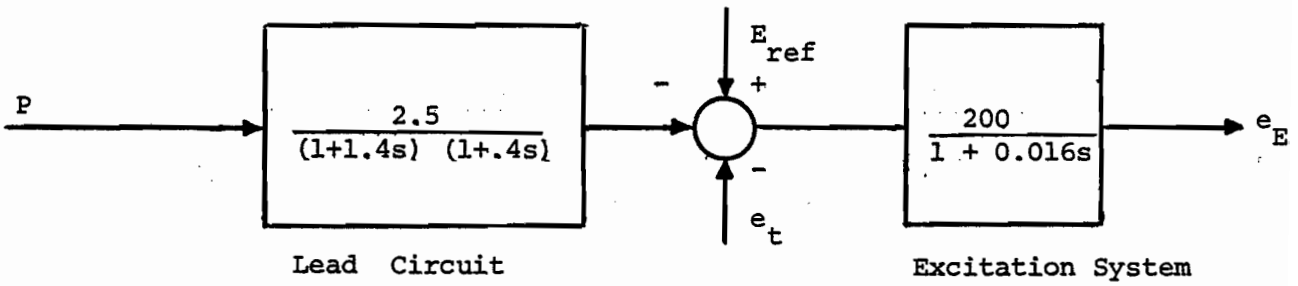

APPENDIX E-3

SYNCHRONOUS CAPACITOR PARAMETERS [81]

Manufacturer data

H	= 2.22 sec.	X''_d	= 0.197	X_ℓ	= 0.126	T'_{d0}	= 8.3-5 sec.
X_d	= 1.60	X_q	= 0.950	r_a	= 0.00274	T''_{d0}	= 0.0120 sec.
X'_d	= 0.300	X''_q	= 0.230	T_a	= 0.200 sec.	T''_{q0}	= 0.0370 sec.

The calculated data (see Appendix E-1)

X_{ad}	= 1.47	X_{ffd}	= 1.67	X_{kkq}	= 0.943	r_{kq}	= 0.0676
X_q	= 0.824	X_{kkd}	= 1.59	r_{fd}	= 0.000670	r_{kd}	= 0.0645

APPENDIX E-4 -

SYNCHRONOUS CAPACITOR EXCITATION SYSTEM [81]

The excitation system and the lead circuit transfer functions of the synchronous capacitor are,

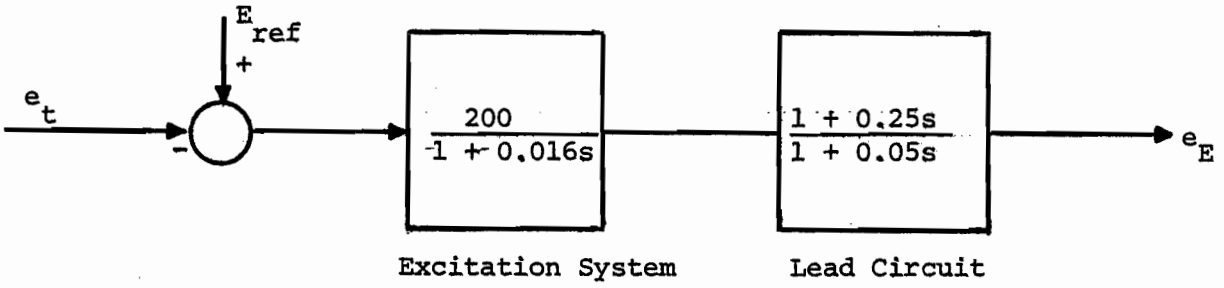

REFERENCES

[1] E.W. Kimbark, 'How To Improve System Stability Without Risking Subsynchronous Resonance', IEEE Trans., Vol. PAS-96, No. 5, September / October, pp. 1608-1619, 1977.

[2] E.W. Kimbark, 'Power System Stability', Vol. I, Chapter IV, John Wiley and Sons Inc., New York, Copyright 1948.

[3] R.T. Byerly, K.E. Kinbark, 'Stability of Large Electric Power Systems', IEEE Press, pp. 3-7, 1974.

[4] E.W. Kimbark, 'Improvement of Power System Stability by Changes in the Network', IEEE Trans., Vol. PAS-88, No. 5, May / June, pp. 773-781, 1969.

[5] J.W. Butler, C. Concordia, 'Analysis of Series-Capacitor Application Problems', AIEE Trans., Vol. 56, pp. 975-988, 1937.

[6] R.B. Bodine, C. Concordia, G. Kron, 'Self-Excited Oscillations of Capacitor Compensated Long Distance Transmission Systems', AIEE Trans., Vol. 62, pp. 41-44, 1943.

[7] C. Concordia, J.B. Tice, C.E.J. Bowler, 'Subsynchronous Torques on Generating Units Feeding Series Capacitor Compensated Lines', American Power Conference Proceedings, Vol. 35, pp. 1129-1136, 1973.

[8] R.H. Hartly, R.G. Farmer, L.A. Kilgore, D.G. Ramey, E.R. Taylor, 'EHV Series Capacitor Applications Considering SSR Oscillations', CIGRE 31-06, Session, 21-29 August, 1974.

[9] R.S. Seymour, E.C. Starr, 'Economic Aspects of Series Capacitors in High Voltage Transmission', AIEE Trans., Vol. 70, pp. 1663-1670, 1951.

[10] I.S. Benko, S.H. Gold, W.N. Rothenbuhler, L.E. Bock, I.B. Jonson, J.R. Stevenson, 'Internal Overvoltages and Protective Devices in EHV Compensated Systems, Series Capacitors and Shunt Reactors', CIGRE 33-05, Session, August 25 - September 2, 1976.

[11] J.A. Maneatis, E.J. Hubacher, W.N. Rothenbuhler, J. Sabath, '500 KV Series Capacitors Insulation in California', IEEE Trans., Vol. PAS-90, No. 3, May / June, pp. 1138-1149, 1971.

[12] G. Jancke, N. Fahlem, O. Nerf, 'Series Capacitors in Power Systems', IEEE Trans., Vol. PAS-94, No. 3, May / June, pp. 915-925, 1975.

[13] S.H. Gold, 'Power System Oscillations which Resulted in the Second Failure of generator Rotor at Mohave Generating Station Unit No. 1', A report of Southern California Edison Company, February 1972.

[14] M.C. Hall, D.A. Hodges, 'Experience with 500 KV Subsynchronous Resonance and Resulting Turbine Generator Shaft Damage at Mohave Generating Station', IEEE PES, 1976 Winter Meeting, ANP Tesla Symposium, 'Analysis and Control of Sunsynchronous Resonance', 76 CH1066-0-PWR, pp. 22-29.

[15] S.B. Crary, 'Power System Stability', Vol. I (Steady State Stability), p.9, General Electric Company Print, New York, Copyright 1945.

[16] L.A. Kilgore, R. Taylor, Jr., D.G. Ramey, R.G. Farmer, E. Katz, A.L. Schwalb, 'Solutions to the Problems of Series Capacitors', American Power Conference Proceedings, Vol. 35, pp. 1120-1128, 1973

[17] O. Saito, H. Mukae, K. Murotani, 'Suppression of Self-Excited Oscillations in Series-Compensated Transmission Lines by Excitation Control of Synchronous Machines', IEEE Trans., Vol. PAS-94, pp. 1770-1784, 1975.

[18] R.G. Farmer, A.L. Schwalb, 'Navajo Project Report on Subsynchronous Resonance Analysis and Solutions', IEEE Trans., Vol. PAS-96, No. 4, July / August, pp. 1226-1232, 1977.

[19] L.A. Kilgore, L.C. Elliott, E.R. Taylor, 'The Prediction and Control of Self-Excited Oscillations Due to Series Capacitors in Power Systems', IEEE Trans., Vol. PAS-90, pp. 1305-1311, 1971.

[20] J.W. Ballance, S. Goldberg, 'Subsynchronous Resonance in Series Compensated Transmission Lines', IEEE Trans., Vol. PAS-92, pp. 1649-1657, 1973.

[21] J.M. Undrill, T.E. Kostyniak, 'Subsynchronous Oscillations Part 1 - Comprehensive System Stability Analysis', IEEE Trans., Vol. PAS-95, No.4, July / August, pp. 1446-1455, 1976.

[22] S. Goldberg, W.R. Schmus, 'Subsynchronous Resonance and Torsional Stresses in Turbine Generator Shafts', C73 135-1, IEEE PES Winter Meeting, New York, January 28 - February 2, 1973.

[23] L.A. Kilgore, D.G. Ramey, W.H. South, 'Dynamic Filter and Other Solutions to the Subsynchronous Resonance Problem', American Power Conference, Chicago, April, 1975.

[24] C. Concordia, 'System Planning Considerations of Sub-Synchronous Resonance', IEEE PES, 1976 Winter Meeting, ANP Tesla Symposium, 'Analysis and Control of Subsynchronous Resonance', 76 CH1066-0-PWR, pp. 51-54.

[25] H.M. Rustebakke, C. Concordia, 'Self-Excited Oscillations in a Transmission System Using Series Capacitors', IEEE Trans., Vol. PAS-90, No. 7, September / October, PP. 1504-1512, 1970.

[26] M.C. Hall, R.L. Daniels, D.G. Ramey, 'A New Technique for Subsynchronous Resonance Analysis and an Application to the Kaiporowits System', IEEE Trans., Vol. PAS-96, No. 4, July / August, pp. 1251-1255, 1977.

[27] L.A. Kilgore, D.G. Ramey, M.C. Hall, 'Simplified Transmission and Generation System Analysis Procedures for Subsynchronous Resonance', IEEE Trans., Vol. PAS-96, No. 6, November / December, pp. 1840-1846, 1977.

[28] C.E.J. Bowler, 'Understanding Subsyncronous Resonance', IEEE, PES, 1976 Winter Meeting, ANP Tesla Symposium, 'Analysis and Control of Subsynchronous Resonance', 76 CH1066-0-PWR, pp. 66-73.

[29] R. Quary, R.J. Placek, 'Cyclic Fatigue of Turbine Generators Shafts', ibid, pp. 12-21.

[30] R.A. Hedin, R.C. Dancy, K.B. Stump, 'An Analysis of the Subsynchronous Interaction of Synchronous and Transmission Networks', American Power Conference Proceedings, Vol. 35, pp. 1112-1119, 1973.

[31] J.M. Undrill, F.P. deMello, 'Subsynchronous Oscillations Part 2 - Shaft-System Dynamic Interaction', IEEE Trans., Vol. PAS-95, No.4, July / August, pp. 1456-1464, 1976.

[32] C.J. Bowler, D.N. Ewart, C. Concordia, 'Self-Excited Torsional Frequency Oscillations with Series Capacitors', IEEE Trans., Vol. PAS-92, pp. 1688-1695, 1973.

[33] M.A. Badr, A.M. El-Serafi, 'Effect of Synchronous Generator Regulation on the Subsynchronous Resonance Phenomenon in Power Systems', IEEE Trans., Vol. PAS-92, No. 2, March / April, pp. 461-468, 1976.

[34] D.N. Walker, A.L. Schwalb, 'Results of Sub-Synchronous Resonance Test at Navajo', IEEE, PES, 1976 Winter Meeting, ANP Tesla Symposium, 'Analysis and Control of Subsynchronous Resonance', 76 CH1066-0-PWR, pp. 37-45.

[35] IEEE Subsynchronous Resonance Task Force, 'First Bench Mark Model for Computers Simulation of Subsynchronous Resonance' IEEE Trans., Vol. PAS-96, No. 5, pp. 1565-1572, 1977.

[36] C.E.J. Bowler, D.H. Baker, N.A. Mincer, P.R. Vandiveer, 'Operation and Test of Navajo SSR Protective Equipment', Paper F77 604-2, IEEE PES, Summer Meeting, Mexico City, July 17-22, 1977.

[37] J.B. Tice, C.E.J. Bowler, 'Control of the Phenomenon of Subsynchronous Resonance', American Power Conference, Chicago, April, 1975.

[38] A.A. Fouad, K.T. Khu, 'Damping of Torsional Oscillations in Power Systems with Series-Compensated Lines', IEEE Trans., Vol. PAS-97, No. 3, May / June, pp. 744-753, 1978.

[39] K. Murotani, M. Asano, 'Subsynchronous Resonance Oscillations of Series-Compensated Transmission System and Their Suppression', Electrical Engineering in Japan, Vol. 96, No. 6, pp. 113-121, 1976.

[40] A.L. Schwalb, 'Navajo Project Subsynchronous Resonance Monitor and Relaying Equipment, IEEE PES, 1976 Winter Meeting, ANP Tesla Symposium, 'Analysis and Control of Subsynchronous Resonance', 76 CH1066-0-PWR, pp. 77-80.

[41] T.S. Ning, 'Subsynchronous Overcurrent Relay for Generators Connected to a Series Compensated Power System', ibid, pp. 74-76.

[42] A.L. Courts, N.G. Hingorani, G.E. Stemler, 'A New Series Capacitor Protection Scheme Using Nonlinear Resistor', Paper F77 573-9, IEEE PES, Summer Meeting, Mexico City, July 17-22, 1977.

[43] C. Concordia, 'Subsynchronous Machines-Theory and Performance', General Electrical Company Press, Chapter II, Copyright 1951.

[44] E.W. Kimbark, 'Power System Stability, Synchronous Machines', Dover Publications, Inc., Chapter XII, New York, 1968.

[45] R.H. Park, 'Two-Reaction Theory of Synchronous Machines Generalized Method of Analysis Part-I', AIEE, Vol. 52, pp. 716-730, 1929.

[46] R.H. Park, 'Two-Reaction Theory of Synchronous Machines Part-II, 'AIEE, Vol. 52, pp. 352-355, 1933.

[47] J. Lemay, 'Modal Analysis of Power System Dynamics', Ph.D. Thesis, McGill University, 1972.

[48] M.R. Harris, P.J. Lawrenson, J.M. Stephenson, 'Per-Unit System', Cambridge University Press, 1970.

[49] A.W. Rankin, 'Per-Unit Impedances of Synchronous Machines', AIEE Trans., Vol. 64, pp. 569-573, 1945.

[50] A.W. Rankin, 'Per-Unit Impedances of Synchronous Machines - II', ibid, pp. 839-841.

[51] K. Prabhashankar, W. Janischewsyj, 'Digital Simulation of Multi Machine Power Systems for Stability Studies', IEEE, Vol. PAS-87, pp. 73-79, 1968.

[52] A.E. Fitzgerald, C. Kingsley, Jr., 'Electric Machinery', McGraw-Hill Book Company, Inc., 1952.

[53] A. Zadeh, C.A. Doser, 'Linear Systems Theory', McGraw-Hill Book Company, Inc., New York, 1963.

[54] E.L. Polak, E. Wong, 'Notes for a First Course on Linear System', Van Nostrand Reinhold, 1970.

[55] IEEE Committee Report, 'Computer Representation of Excitation Systems', IEEE Trans., Vol. PAS-87, No. 6, pp. 1460-1470, 1968.

[56] F.P. DeMeloo, C. Concordia, 'Concepts of Synchronous Machine Stability as Affected by Excitation Control', IEEE Trans., Vol. PAS-88, No. 4, pp. 316-329, 1969.

[57] P. Bingen, F.W. Keay, G.L. Landgren, C. Raczkowski, 'Dynamic Stability Tests on a 733 MVA Generator at Kincaid Station', IEEE Trans., Vol. PAS-93, pp. 1328-1334, 1974.

[58] F.W. Keay, C. Raczkowski, W.H. South, 'Excitation Control System Complex Compensation', ibid, pp. 1444-1448.

[59] F.W. Keay, W.H. South, 'Design of a Power System Stabilizer Sensing Frequency Deviation', IEEE Trans., Vol. PAS-90, No.2, pp. 707-713, 1971.

[60] C. Raczkowski, 'Complex Root Compensator, A New Concept for Dynamic Stability Improvement', IEEE Trans., Vol. PAS-93, pp. 1842-1848, 1974.

[61] C.E. Grund, 'Dynamic Stability Enhancement with Power System Stabilizer', Paper C74 123-6, IEEE PES, Winter Meeting, New York, January 27 - February 1, 1974.

[62] L. Ahlgren, K.E. Johansson, A. Gadhammar, 'Estimated Life Expenditure of Turbine-Generator Shafts at Network Faults and Risk for Subsynchronous Resonance in the Swedish 400 KV System', Paper F77 075-5, IEEE PES, Winter Meeting, New York, January 30 - February 4, 1977.

[63] A.J. Wood, 'Synchronizing Out of Phase', AIEE Trans., Vol. 76, pp. 1-10, 1957.

[64] T.J. Hammons, 'Effect of Three-Phase System Faults and Faulty Synchronization on the Mechanical Stressing of Large Turbine-Generator', Revue Generale d'Electricite, Vol. 86, No. 7/8, July / August, pp. 558-580, 1977.

[65] W.F. Ames, 'Mathematics in Science and Engineering', p. 220, Academic Press, Vol. 42, New York, 1968.

[66] A. Ralston, H.S. Wilf, 'Mathematical Methods for Digital Computers', New York, John Wiley and Sons, Inc. Vol. II, Part V, 1968.

[67] IBM System / 360, Scientific Subroutine Package (360A - CM - 03X) Version III.

[68] E.W. Kimbark, 'Power System Stability', Vol. III, Chapter XV, John Wiley and Sons Inc., New York, Copyright 1956.

[69] C.F. Wanger, R.D. Evans, 'Static Stability Limits and the Intermediate Condenser Station', AIEE Trans., Vol. 47, pp. 94-121, 1928.

[70] D.A. Woodford, M.Z. Tarnawecky, 'Compensation of Long Distance AC Transmission Lines by Shunt Connected Reactive Controllers', IEEE Trans., Vol. PAS-94, No. 2, pp. 655-664, 1975.

[71] J.D. Ainsworth, C.B. Cooper, F. Friedlander, H.L. Thanawala, 'Long Distance AC Transmission Using Static Stabilizers and Switch Linear Reactors', CIGRE 31-01, Session, 21-29 August, 1974.

[72] J.A. Koontz, 'Methods of Voltage Control of Long High-Voltage Lines by the Use of Synchronous Condenser', AIEE Trans., Vol. XLII, pp. 1054-1056, 1923.

[73] C. Concordia, L.G. Levoy, C.H. Thomas, 'Selection of Buffer Reactors and Synchronous Condensers on Power Systems Supplying Arc-Furnace Loads', AIEE Trans., Vol. 76, pp. 123-135, 1957.

[74] R. Elsliger, G. Lamontagne, J.C. Roy, 'Transmission of 16000 MW Over a Distance of 1200 KM from James Bay to Hydro-Quebec's Load Centers', CIGRE 32-07, Session, August 21-29, 1974.

[75] H. Becker, J. Dalzell, C.B. Cooper, H.B. Norman, C.A. Peixoto, K. Reichert, J.C. Roy, B. Thoren, 'Static Shunt Devices for Reactive Power Control', CIGRE 31-08, Session, August 21-29, 1974.

[76] K. Reichert, J. Kauferle, H. Glavitsch, 'Controllable Reactor Compensator for More Extensive Utilization of High Voltage Transmission Systems', CIGRE 31-04, Session, August 21-29, 1974.

[77] L. Gyugyi, R.A. Otto, T.H. Putman, 'Principles and Applications of Static Thyristor - Controlled Shunt Compensators', Paper F 78 096-0, IEEE PES, Winter Meeting, New York, January 29 - February 3, 1978.

[78] R.L. Hauth, T. Humann, R.J. Newell, 'Application of a Static VAR System to Regulate System Voltage in Western Nebraska', Paper F 78 097-8, ibid.

[79] H. Becker, D. Brandes, K. Gappa, 'Three Phase Shunt Reactors with Continuously Controlled Reactive Current', CIGRE 31-13, Session, August 28 - September 6, 1972.

[80] F. Friedlander, 'Transient Effects in Static Shunt Reactive Compensators for Long Distances', IEEE Trans., Vol. PAS-95, No. 5, pp. 1669-1680, 1976.

[81] Private Communication.

[82] J.M. Undrill, 'Dynamic Stability Calculations for an Arbitrary Number of Interconnected Synchronous Machines', IEEE Trans., Vol. PAS-87, No. 3, pp. 835-843, 1968.

[83] P.M. Anderson, A.A. Fouad, 'Power System Control and Stability', Iowa State University Press, AMES, Iowa, U. S. A., Chapter II, 1977.

[84] B.T. Ooi, M.M. Sartawi, 'Concepts on Field Excitation Control of Subsynchronous Resonance in Synchronous Machines', Paper F77 771-5, IEEE PES Summer Meeting, Mexico City, July 17-22, 1977.

[85] M.M. Sartawi, B.T. Ooi, 'Field Excitation Suppression by Real and Reactive Power Signal Feedback. Part I - A Small Perturbation Study', Paper A 78 293-3, IEEE PES Winter Meeting, New York, January 29 - February 3, 1978.

[86] M.M. Sartawi, B.T. Ooi, 'Field Excitation Suppression by Real and Reactive Power Signal Feedback. Part II - A Large Perturbation Study', Accepted for presentation at IEEE PES Summer Meeting July 16-21, Los Angeles, 1978.

[87] M.M. Sartawi, B.T. Ooi, 'Application and Limitation of Field Excitation Control of Subsynchronous Resonance in Synchronous Generators - Torsional Interaction', Accepted for presentation at the International Conference on Electrical Machines, September 11-13, Brussels, Belgium, 1978.